ABSTRACT

HEAVY METAL ADSORPTION ON IRON OXIDE AND IRON OXIDE-COATED SILICA: MACROSCOPIC, SPECTROSCOPIC, AND MODELING STUDIES

by
Ying Xu

To accurately model metal mobility and bioavailability in soils and sediments, systematic sorption studies are needed using representative and well-characterized minerals. Two important surfaces are iron oxide and silica, which are ubiquitous and associated with one another in the environment playing important roles in metal distribution. The objectives of this research are to develop models for predicting speciation and mobility of toxic trace metal ions in groundwater, soils, and sediments when competing ions are present. A model system for soils and sediments, iron oxide-coated silica, was synthesized; the degree of coatings was highly sensitive to the particle size of silica and ranged between 0.59 and 21.36 mg Fe g^{-1} solid. The iron oxide coatings increased surface area and introduced small pores. Surface charge distribution suggested that both silica and goethite surfaces are important for adsorption. The sub-micrometer-sized coatings exhibited a larger capacity for metals ions than discrete ones and, although in low concentration, they greatly affected metal affinity to the coated media. X-ray absorption spectroscopy (XAS) analysis revealed that both Ni(II) and Pb(II) ions form mononuclear bidentate edge-sharing surface complexes on FeO_6 octahedra. This mechanism appeared to be invariant of pH, ionic strength, metal loading, and reaction time. Constrained with spectroscopic information, the 2-pK triple layer model successfully predicted Ni or Zn adsorption in single adsorbate systems. The curvature in adsorption isotherms was accurately described using two types of sites – high affinity and low affinity ones. A

unique set of parameters was found for each metal ion that can successfully describe adsorption over a large range of experimental conditions, covering six or seven orders of magnitude in concentration, ionic strength from 10^{-3} to 10^{-2}, and an environmentally relevant pH range. Competition was also predicted quantitatively with parameters calibrated using single adsorbate data. Results of this work will assist in better understanding and predicting the mobility and bioavailability of trace metals in soils, sediments, and groundwater.

HEAVY METAL ADSORPTION ON IRON OXIDE AND IRON OXIDE-COATED SILICA: MACROSCOPIC, SPECTROSCOPIC, AND MODELING STUDIES

by
Ying Xu

A Dissertation
Submitted to the Faculty of
New Jersey Institute of Technology
in Partial Fulfillment of the Requirements for the Degree of
Doctor of Philosophy in Environmental Engineering

Department of Civil and Environmental Engineering

October 2005

APPROVAL PAGE

HEAVY METAL ADSORPTION ON IRON OXIDE AND IRON OXIDE-COATED SILICA: MACROSCOPIC, SPECTROSCOPIC, AND MODELING STUDIES

Ying Xu

Dr. Lisa Axe, Dissertation Advisor — Date
Associate Professor of Civil and Environmental Engineering, NJIT

Dr. Hsin-Neng Hsieh, Committee Member — Date
Professor of Civil and Environmental Engineering, NJIT

Dr. Trevor A. Tyson, Committee Member — Date
Professor of Physics, NJIT

Dr. Nathan Yee, Committee Member — Date
Assistant Professor of Earth and Environmental Science, Rutgers University

Dr. James A. Dyer, Committee Member — Date
Senior Consultant for DuPont Engineering Technology, Wilmington, DE

BIOGRAPHICAL SKETCH

Author: Ying Xu

Degree: Doctor of Philosophy

Date: October 2005

Undergraduate and Graduate Education:

- Doctor of Philosophy in Environmental Engineering,
  New Jersey Institute of Technology, Newark, NJ, 2005
- Master of Engineering in Chemical Engineering,
  China University of Petroleum, Beijing, P. R. China, 1995
- Bachelor of Engineering in Petroleum Refining Engineering,
  China University of Petroleum, Dongying, Shandong Province, P. R. China, 1992

Major: Environmental Engineering

Presentations and Publications:

Xu, Y.; Axe, L.; Yee, N. and J. A. Dyer (2005) Surface complexation modeling of heavy metal adsorption and competition on goethite *(submitted)*.

Xu, Y.; Axe, L.; Boonfueng, T.; Tyson, T.; Trivedi, P.; and Pandya K. (2005) Ni(II) complexation to amorphous hydrous ferric oxide: an x-ray absorption spectroscopy study *(submitted)*.

Xu, Y.; Boonfueng, T.; Axe, L.; Maeng, S.; and Tyson, T. (2005) Surface complexation of Pb(II) on amorphous iron oxide and manganese oxide: spectroscopic and time studies *(submitted)*.

Xu, Y. and Axe, L. (2005) Synthesis and characterization of iron oxide-coated silica and its effect on metal adsorption. *J. Colloid and Interface Sci.*, 282 (1) 11-19.

Boonfueng, T.; Axe, L.; and Xu, Y. (2005) Properties and structure of manganese oxide-coated clay. *J. Colloid and Interface Sci.*, 281 (1) 80-92.

Fan, M.; Boonfueng, T.; Xu, Y.; Axe, L.; and Tyson, T. A. (2005) Modeling Pb sorption to microporous amorphous oxides as discrete particles and coatings. *J. Colloid and Interface Sci.*, 281 (1) 39-48.

Xu, Y. and Axe, L. (2004) Characterization and Pb adsorption to iron oxide-coated silica. Proceedings of the Eleventh International Symposium on Water-Rock Interaction (Ed. Wanty, R.B. and Seal, R.R.II), Taylor & Francis Group plc, London, UK, 2004, 1425-1429.

Xu, Y.; Axe, L.; and Boonfueng, T. Iron Oxide Coatings and Heavy Metal Adsorption on Iron Oxide-Coated Silica: Macroscopic, Spectroscopic, and Modeling Studies. 2005 AEESP Research and Education Conference, Clarkson University, NY, July 24-27, 2005.

Xu, Y. and Axe, L. Goethite coated silica: synthesis, characterization, and its impact on Ni adsorption. 228th American Chemical Society (ACS) National Meeting, Symposium Honoring Professor Charles O'Melia, Philadelphia, PA, August 22-26, 2004.

Xu, Y. and Axe, L. Characterization and Pb adsorption to iron oxide-coated silica. 11th Water Rock Interaction Symposium, Saratoga Springs, NY, June 27-July 2, 2004.

Xu, Y.; Axe, L.; Maeng, S.; Trivedi, P.; Boonfueng, T.; Tyson, T. A.; and Pandya, K. Adsorption of heavy metals on iron oxide coated silica. 226 ACS National Meeting, New York, NY, United States, Sept. 7-11, 2003.

Fan, M.; Xu, Y.; Boonfueng, T.; Yuan, W.; Axe, L.; and Tyson, T. A. Intraparticle surface diffusion of lead in amorphous aluminum, iron, and manganese oxides. Extended Abstracts presented at the 226th ACS National Meeting, 43(2), 1119-1124, 2003.

Xu, Y. and Axe L. Heavy metal competition on iron oxide coated silica. ACS 77th Colloid and Surface Science Symposium, Georgia Institute of Technology, Atlanta, GA, Jun. 15-18, 2003.

To my husband,Yunhui Pu, and my parents, Ruixiang Xu and Peirong Xiao,
for their patience, understanding, support, and love.

ACKNOWLEDGMENT

I would like to express my deepest appreciation to Dr. Lisa Axe, who not only served as my research supervisor, providing valuable and countless resources, insight, and intuition, but also constantly gave me support, encouragement, and reassurance. Special thanks are given to Dr. Hsin-Neng Hsieh, Dr. Trevor A. Tyson, Dr. Nathan Yee and Dr. James A. Dyer for actively participating in my committee and providing valuable input from their own areas of expertise.

My appreciation to the DuPont Young Professor Grant and National Science Foundation Grant No. BES 0089903 for providing financial support for this research.

I would like to thank all my professors, laboratory staff, and the secretaries in the department of Civil and Environmental Engineering for constant guidance and help. I would also like to thank Dr. Kaumudi Pandya for her assistance in experiments over the years at X11A and X11B, National Synchrotron Light Source, Brookhaven National Laboratory.

All my fellow graduate students are deserving of recognition for their support. I've cherished their friendship for five years, and this will go on and be an asset in my life forever.

TABLE OF CONTENTS

TABLE OF CONTENTS
(Continued)

TABLE OF CONTENTS
(Continued)

TABLE OF CONTENTS
(Continued)

Chapter **Page**

LIST OF TABLES

LIST OF TABLES
(Continued)

LIST OF FIGURES

LIST OF FIGURES
(Continued)

LIST OF FIGURES
(Continued)

LIST OF FIGURES
(Continued)

Figure **Page**

LIST OF FIGURES
(Continued)

Figure **Page**

CHAPTER 1

INTRODUCTION

Heavy metals in natural aquatic and soil environments potentially impact the growth of plants and threaten the health of animals and humans even when present in trace amounts. Risk assessment and remediation require information on heavy metal speciation, mobility, and bioavailability to characterize their behavior and impact in the environment. Sorption is one of the most important processes that influences the distribution and transport of heavy metals in aquatic and/or soil environments (Benjamin and Leckie, 1981a; Siegel et al. 1992).

Heavy metal adsorption to hydrous iron, manganese, and aluminum oxides has been extensively investigated (e.g., Forbes et al. 1976; Swallow et al. 1980; Hsi and Langmuir, 1985; Hayes and Leckie, 1986; Johnson, 1990; Cowan et al. 1991; Müller and Sigg, 1992; Ainsworth et al. 1994; Manceau and Charlet, 1994; Coughlin and Stone, 1995; Fendorf et al. 1997; Green-Pedersen et al. 1997; Venema et al. 1998; Jenne, 1998; Villalobos et al. 2001; Peak and Sparks, 2002; Dyer et al. 2003; Wazne et al. 2003; O'Reilly and Hochella, 2003; Kanungo et al. 2004; Jeon et al. 2004). These minerals are prevalent in natural environments as particles or surface coatings, have high affinity and great capacity for metal ions (Schwertmann and Cornell, 1991), and therefore impact metal contaminant mobility (e.g., Anderson and Christensen, 1988; Jackson and Inch, 1989; Johnson, 1990; Coston et al. 1995; Fuller et al. 1996; Green-Pedersen et al. 1997; Dong et al. 2002). Although individual sorbents and contaminants have been investigated, the presence of competing ions is more frequently encountered (e.g.,

Anderson and Christensen, 1988; Cowan et al. 1991; Ryan and Gschwend, 1994; Coston et al. 1995; Jenne, 1998; Barnett et al. 2002). As a multicomponent-multiphase system, the natural aquatic environments can only be described properly when competitive reactions/processes are considered (Nilsson et al. 1996).

Adsorption of metal ions in aqueous solutions to mineral surfaces can be described in terms of surface complexation models (Hsi and Langmuir, 1985; Hayes and Leckie, 1986; Hiemstra et al. 1989; Dzombak and Morel, 1990; Katz and Hayes, 1995 a, b; Hiemstra and van Riemsdijk, 1996; Sahai and Sverjensky, 1997; Robertson and Leckie, 1997, 1998). For the description of metal binding on surfaces, a series of reaction equations need to be formulated (van Riemsdijk and Hiemstra, 1998). Sposito (1989) has summarized the principal mechanisms of adsorption as (1) inner-sphere complexation, (2) outer-sphere complexation, and (3) association with a diffuse layer; the role of these three mechanisms in diverse reactions as well as their contribution to surface charge development have also been reviewed (Sposito, 1989). The more accurate the model the more likely the prediction of metal/mineral interaction will be successful. However, describing ion binding on mineral surfaces in a way that is mechanistically reasonable is always a great challenge.

One common practice is to assume that the surface is chemically homogeneous and to invoke a two step protonation reaction as the basis for the charging of metal (hydr)oxides (van Riemsdijk and Hiemstra, 1998; Sahai and Sverjensky, 1997; Palmqvist et al. 1997; Davis et al. 1998); ion binding reactions are generally proposed based on information from adsorption edges, isotherms, and/or number of H^+ released (e.g., Forbes et al. 1976; Benjamin and Leckie, 1981a; Hayes et al. 1988; Lövgren et al. 1990; Müller

and Sigg, 1992; Gunneriusson et al. 1994; Nowack et al. 1996); the assumed surface complexes are checked by the goodness of fit (Goldberg, 1991). Although these approaches are usually successful, the surface species used may not be physically meaningful. Fortunately, recent advances in identification of sorbed species by in-situ spectroscopic techniques like X-ray absorption spectroscopy (XAS) and Fourier transform infrared spectroscopy (FTIR) have made it possible to overcome this drawback for many systems of interest (e.g., Chisholm-Brause et al. 1990; Charlet and Manceau, 1992; O'Day et al. 1994; Bargar et al. 1997a,b; Scheidegger et al. 1998; Manning et al. 1998; Sahai et al. 2000; Trainor et al. 2000; Nachtegaal and Sparks, 2003; Trivedi et al. 2003, 2004; Wazne et al. 2003). Qualitative and quantitative information from spectroscopy can be included in adsorption modeling, connecting molecular details to macroscopic measurements, and resulting in improved modeling of the solid/liquid interface (e.g., Katz and Hayes, 1995 a, b; Hayes and Katz, 1996; Dyer et al. 2003, 2004).

Overall, trace metal adsorption to mineral surfaces is an important phenomenon in many industrial applications as well as in the study of the natural environment. Development of better mechanistic adsorption models that describe the binding with physically meaningful species is not only of theoretical but also potentially of great practical interest (van Riemsdijk and Hiemstra, 1998). The objective of this proposed research is to understand the effect of iron oxides, as discrete particles and coatings, on contaminant adsorption. Surface complexation modeling constrained with XAS data is invoked for single and binary adsorbate studies. Results of this work assist in better understanding and predicting the mobility and bioavailability of trace metals in soils, sediments, and groundwater.

The following chapters include Chapter 2, a literature review on the importance of iron oxides and iron oxide coatings; Chapter 3, the objectives and hypotheses for this research; Chapter 4, Experimental Methods; Chapter 5, Characterization of Iron Oxide and Silica; Chapter 6, Synthesis and Characterization of Iron Oxide-Coated Silica; Chapter 7 and 8, mechanisms of heavy metal adsorption to iron oxide using Pb and Ni as examples, respectively; Chapter 9, surface complexation modeling of Ni and Zn adsorption and competition on goethite; Chapter 10, heavy metal adsorption on iron oxide-coated silica; and, lastly, Chapter 11, Conclusions and Future Work.

CHAPTER 2

OXIDES AND THEIR EFFECT ON SORPTION

Sorption of trace elements onto reactive mineral surfaces is an important process regulating contaminant mobility and bioavailability in natural systems (Forbes et al. 1976; Balistrieri and Murray, 1982; Anderson and Christensen, 1988; Jackson and Inch, 1989; Coston et al. 1995). This review focuses on the adsorption of solute(s) at the aqueous-mineral interfaces. Specifically in this chapter the following topics are discussed: (1) iron oxides and iron oxide coatings in environment, (2) macroscopic adsorption studies, (3) XAS studies, and (4) surface complexation modeling.

2.1 Iron Oxides and Iron Oxide Coatings in Environment

Iron oxides are prevalent in natural environments as particles or surface coatings, exhibiting a high affinity and great capacity for metal ions (Schwertmann and Cornell, 1991), and therefore impacting metal mobility significantly (e.g., Anderson and Christensen, 1988; Jackson and Inch, 1989; Johnson, 1990; Coston et al. 1995; Fuller et al. 1996; Green-Pedersen et al. 1997; Dong et al. 2002). These oxides in the environment are present as crystalline and amorphous forms including goethite, hematite, and ferrihydrite (also is referred to as hydrous ferric oxide, HFO). Goethite is the most common and thermodynamically stable iron oxide under most soil conditions (Schwertmann and Taylor, 1989; Ainsworth et al. 1989). Although metastable, ferrihydrite is also an important sorbent because of its abundance in the subsurface. Ferrihydrite conversion to goethite and hematite is slow at temperatures below 20 ^{o}C, and

is further retarded by adsorbed species (Scheinost et al. 2001; Schwertmann et al. 1985; Cornell, 1987; Cornell et al. 1987, 1992). Given localized increases in ferric concentrations, its precipitation is accompanied by a high partitioning of trace metals in soils (Manceau et al. 2003). Therefore, goethite and HFO have been widely used as model sorbents in adsorption studies (Cornell and Schwertmann, 1996). Dzombak and Morel (1990) comprehensively compiled and modeled metal adsorption on HFO using the diffuse double layer model. However, since 1990, spectroscopic evidence has proven to be critical in mechanistic model development.

In natural aquatic environments, many reactions such as dissolution, adsorption, precipitation, and colloidal adhesion result in multi-component solids with bulk and surface characteristics different from the original pure phases (Anderson and Benjamin, 1990). Specifically, oxide mineral coatings are often observed in soils and sediments (Ryan and Gschwend, 1994; Coston et al. 1995; Wang et al. 1993). For example, Ryan and Gschwend (1994) found that in oxic sediments, quartz grains are coated by colloidal kaolinite and microcrystalline iron (III) oxide, primarily goethite (α-FeOOH) at 39 $\pm$ 2 μmol Fe g^{-1} sediment (0.22% by weight). Coston et al. (1995) reported that in a shallow, unconfined aquifer of glacial outwash, sand and gravel were extensively coated with Al- and Fe-bearing minerals and that the iron concentrations ranged between 0.0736 and 4.96 mg Fe g^{-1} sand. Iron oxide coatings were also found on ped surfaces and pores of paddy and non-paddy soils at concentrations of 10 to 44 mg Fe g^{-1} soil and were characterized as ferrihydrite, lepidocrocite, and goethite (Wang et al. 1993). Many studies have shown the importance of these surface coatings in controlling metal distribution in soils and sediments (Edwards and Benjamin, 1989; Coston et al. 1995; Zachara et al. 1995; Fuller

et al. 1996; Green-Pedersen et al. 1997; Uygur and Rimmer, 2000;). In addition, coated minerals have been studied in recent years because of their potential application as effective sorbents (Coston et al. 1995; Zachara et al. 1995; Lo and Chen, 1997; Kuan et al. 1998; Khaodhiar et al. 2000; Meng and Letterman, 1993a).

Adsorption studies on both discrete iron oxide and iron oxide coatings are important for understanding and modeling heavy metal distribution and transport in the environment. While systematic studies are warranted in characterizing iron oxide-coated silica, an important representative surface in soil, methods and results of related studies are summarized in the following sections.

2.1.1 Oxide Coating Methods

Although iron oxide-coated media have been used to simulate natural systems or produce novel sorbents (Edwards and Benjamin, 1989; Zachara et al. 1995; Kuan et al. 1998; Khaodhiar et al. 2000; Meng and Letterman, 1993a; Lion et al. 1982; Dong et al. 2000; Lo et al. 1997; Szecsody et al. 1994; Joshi and Chaudhuri, 1996; Lai et al. 2000), little has been conducted in systematically evaluating factors that influence the degree of coating. Lo et al. (1997) found that higher coating temperatures enhanced the stability of the oxide coating. Furthermore, iron oxide coatings were amorphous at lower temperatures (60 ^{o}C), while goethite and hematite formed at 150 ^{o}C and hematite formed exclusively at temperatures greater than 300 ^{o}C. Lo and Chen (1997) found no significant difference between the amount of iron oxide coated at 105 and 200 ^{o}C, while Scheidegger et al. (1993) observed increases in goethite coating with increasing temperature (from 110 ^{o}C to 120 ^{o}C). In addition, coatings produced at pH 12 resulted in greater metal adsorption efficiency than those produced at circum neutral; however, the

coatings were less resistant to acid. Kuan et al. (1998) reported that at a higher coating pH (10.77-12.50), Al oxide coatings were more resistant to acidic and alkaline conditions and tended to be crystalline. Lo et al. (1997) found that the Fe concentration had less of an effect than pH on the degree of coating. Although the influence of substrate particle size has not been investigated systematically, Coston et al. (1995) showed that oxide concentration increased as particle size decreased in soils and sediments.

2.1.2 Coating Characterization

Many studies have been conducted to evaluate coating characteristics. Methods for mineral identification are based on specific properties of the minerals (de Kimpe, 1993). These properties include crystallographic, optical (microscopic), physical (cleavage, color, density), and chemical properties. Numerous researchers (Edwards and Benjamin, 1989; Zachara et al. 1995; Khaodhiar et al. 2000; Szecsody et al. 1994; Stahl and James, 1991 a, b; Marchetti et al. 1997) have produced Fe oxide coatings ranging between 0.7 and 50 mg Fe g^{-1} sand, while those of natural soils and sediments are in the range of 0.074 to 44.2 mg Fe g^{-1} sand (Ryan and Gschwend, 1994; Coston et al. 1995; Wang et al. 1993; Pieper et al. 1997). The oxide-silica interface has been investigated with x-ray photoelectron spectroscopy (XPS) and Fourier transform infrared spectroscopy (FTIR) (Scheidegger et al. 1993), where Fe-O-Si bonding was proposed. Liang et al. (2000) concluded that the quartz-ferrihydrite interface involves chemical interactions based on their observations that repulsive forces could not explain the results. Using Mössbauer spectroscopy, Marchetti et al. (1997) reported that the smaller the oxide particles the stronger the oxide-substrate interaction. X-ray diffraction (XRD), transmission electron microscopy (TEM), and scanning electron microscopy (SEM) have been used as well to

identify components, distribution, and structure of surface oxide coatings (Coston et al. 1995; Wang et al. 1993; Edwards and Benjamin, 1989; Kuan et al. 1998; Meng and Letterman, 1993b). Typically, oxides are non-uniform (Edwards and Benjamin, 1989) over the surface, as both the oxide and substrate have been observed (Anderson and Benjamin, 1990). Surface area combined with extractable Fe may be an effective geochemical 'indicator' of the potential variability of metal distribution in an aquifer (Fuller et al. 1996). The need to characterize the structure and behavior of sediments is clear.

2.1.3 Measurement of Coating

Iron concentration in coated silica is an important factor in evaluating the coating process and a number of researchers have used extraction (Kuan et al. 1998; Stahl and James, 1991a, b; Fan, 1996; Wang, 1995; Szecsody et al. 1994). These techniques have been developed by soil scientists, geologists, and oceanographers to enhance in clay mineral characterization (Ryan and Gschwend, 1991; Shuman, 1982; Furtado et al. 1990; Sequi et al. 1983; Borggaard, 1981; Geiger and Loeppert, 1986; Jackson et al. 1986; Kunze and Dixon, 1986; Leoppert and Inskeep, 1996). For example, Ross and Wang (1993) summarized five extraction methods that may be used to approximate the amounts and forms of Fe in soils (Table 2.1): dithionite citrate, acid ammonium oxalate, hydroxylamine, tiron (4, 5-dihydroxy-1, 3-benzene-disulfonic acid), and pyrophosphate. Other extraction methods for Fe include citrate-ascorbate (Reyes and Torrent, 1997), ethylenediaminetetraacetic acid (EDTA) (Borggaard, 1981), HCl, and $H_2C_2O_4$ (Chao and Zhou, 1983) for amorphous iron oxides; and, ascorbic acid-oxalate (Shuman, 1982) and titanium(III)-citrate-EDTA-HCO_3 (Ryan and Gschwend, 1991) for crystalline iron

Table 2.1 Extraction Methods for Oxides

Method	Extractants	Target forms of iron oxides	References
Dithionite-citrate method	Sodium hydrosulfite ($Na_2S_2O_4$) Sodium citrate ($Na_3C_6H_5O_7 \cdot 2H_2O$)	Crystalline, amorphous, and organic-complexed Fe, Mn, and Al	Ross and Wang (1993)
Acid ammonium oxalate method	Ammonium oxalate ($(NH_4)_2C_2O_4 \cdot H_2O$) Oxalic Acid ($H_2C_2O_4 \cdot 2H_2O$)	Amorphous and organic-complexed Fe, Mn, and Al	Ross and Wang (1993)
Hydroxylamine method	Hydroxylamine hydrochloride ($NH_2OH \cdot HCl$)-hydrochloric acid (HCl)	Amorphous and organic-complexed Fe and Al	Ross and Wang (1993)
Tiron method	4, 5-dihydroxy-1, 3-benzene-disulfonic acid	Amorphous and organic-complexed Fe and Al	Ross and Wang (1993)
Pyrophosphate method	Sodium pyrophosphate ($Na_4P_2O_7 \cdot 2H_2O$)	Organic-complexed Fe and Al	Ross and Wang (1993)
Citrate-ascorbate method	Sodium citrate ($Na_3C_6H_5O_7$) Sodium ascorbate	Amorphous Fe	Reyes and Torrent (1997)
EDTA method	Ethylenediaminetetraacetic acid (EDTA)	Amorphous Fe	Borggaard (1981)
Ti(III)-citrate-EDTA-HCO_3 method	Titanium (III) chloride ($TiCl_3$) Sodium citrate dehydrate ($(Na_3C_6H_5O_7)$ Tetrasodium EDTA (Na_4EDTA) Sodium bicarbonate ($NaHCO_3$)	Crystalline and amorphous Fe	Ryan and Gschwend (1991)
Ascorbic acid-oxalate method	Ascorbic acid ($C_6H_8O_6$) Ammonium oxalate ($(NH_4)_2C_2O_4 \cdot H_2O$)	Crystalline Fe	Shuman (1982)

oxides. Because extraction methods suggest the mineral form, dissolution data are commonly used for soil classification.

In this study, dithionite citrate will be used for extracting both crystalline and amorphous Fe oxide, and hydroxylamine will be employed for amorphous Fe oxide. The amount of crystalline Fe oxide is therefore the difference between the two.

2.1.4 Coating Factors

The amount of coating may be influenced by factors such as coating temperature, particle size, surface area, roughness, and other characteristics of the supporting media. Wang (1995) applied 0.04 g Fe g^{-1} GAC and Fan (1996) applied 0.055 g Mn g^{-1} GAC in their studies to achieve higher coating efficiencies. Metal concentrations initially applied by many researchers (Edwards and Benjamin, 1989; Stahl and James, 1991a, b; Wang, 1995; Fan, 1996; Khaodhiar et al. 2000; Kuan et al. 1998; Joshi and Chaudhuri, 1996; Stenkamp and Benjamin, 1994; Bailey et al. 1992) are usually in the order of 10^{-3} to 10^{-2} g metal g^{-1} media. A metal concentration of 0.05 g Fe g^{-1} silica will be applied in this research.

One important variable affecting the degree of coating is temperature. Fan (1996) obtained more Mn oxide coatings on granular activated carbon (GAC) at 160 ^{o}C than 105 ^{o}C, although the same concentration of Mn was applied. Edwards and Benjamin (1989) found that as Fe dose increased a much greater percentage of the surface was covered upon heating (110 $\pm$ 10 ^{o}C) as opposed to precipitation without heating. Also, the coatings produced with heating were observed to be more resistant to abrasion and exposure to mild acid solutions than those produced through alkaline precipitation (no heating). However, from their study it is not clear whether a difference in detachment

reflects kinetics or mineralogical form. A number of coating studies (Khaodhiar et al. 2000; Edwards and Benjamin, 1989; Stahl and James, 1991a, b; Wang, 1995; Fan, 1996) have shown that the degree of coating increased with increasing temperature.

Earlier studies (Table 2.2) have involved varying coating temperature, initial applied metal concentration, and silica (with different particle size, surface area, roughness and other characteristics). Although a relationship between the amount of coating and temperature was observed in earlier work, no such result was found with respect to particle size. Most likely, the degree of coating is a function of a number of factors. To systematically evaluate factors that influence the degree of coating, experiments will be designed using a three-level fractional factorial method (Anderson and Mclean, 1974) to reduce the number of studies and isolate effects. Factors investigated will include coating temperature (T), mean diameter of silica particle (D), Fe concentration initially applied (Fe_{ini}), and aging time (t, for adsorption method only).

In summary, adsorption studies on discrete iron oxides and iron oxide-coated silica are important in investigating heavy metal distribution in environment. However, for iron oxide-coated silica, factors affecting coating processes have not been fully evaluated.

2.2 Macroscopic Adsorption Studies

Metal sorption to hydrous oxides is affected by the solution pH (Gadde and Laitinen, 1974), ionic strength, (Swallow et al. 1980), inorganic and organic ligands present in the system (Forbes et al. 1974; Ali and Dzombak, 1996; Weng et al. 2002, Scheinost et al. 2001; Sauvé et al. 2000; Brooks and Herman, 1998; Düker et al. 1995; Ledin et al. 1994;

Table 2.2 Some Coating Work and Corresponding Coating Results

	Method	Metal coated	$Me_{applied}$ g Me/g sand	Me_{coated} g Me/g sand	Temp. °C	Sand size (mm)	Author
1	Natural Sediment	Fe oxide Al oxide	N.A.[1]	0.0022 0.0002	N.A.	0.25-1.0	Ryan and Gschwend (1994)
2	Natural aquifer	$Fe(OH)_3$	N.A.[1]	0.00005	N.A.	0.063-2 median 0.6	Martin and Kempton (2000)
3	Mix.[6]	FeOOH	NA[2]	0.003 -0.006	35	0.074 -0.21	Szecsody et al. (1994)
4	Mix.[6] Prcp.[3]	Fe oxide Mn oxide	NA[2]	0.00582 0.00195	35	0.21	Zachara et al. (1995)
5	Prcp.[3] Evp.[4]	Ferrihydrite	0.00336 0.0139	0.0007 0.01	25 110	0.59-0.84	Edwards and Benjamin (1989)
6	Prcp.[3]	FeOOH Fe_2O_3	0.00164	0.00125 -0.00132	105 500	NA[2]	Stahl and James (1991a)
7	Wet oxid.[5] Dry oxid.[5]	Birnessite Pyrolusite	0.00429 0.0277	0.00191 0.0269	44 105-160	NA[2]	Stahl and James (1991b)
8	Prcp.[3]	$Al(OH)_3$ $Fe(OH)_3$	0.00675	Assume 0.00675	22	0.000015 -0.00002	Meng and Letterman (1993a)
9	Prcp.[3]	$Al(OH)_3$	0.0135	0.00145 -0.00375	70	0.71-0.84	Kuan et al. (1998)
10	Prcp.[3]	Fe oxide	0.0448	NA[2]	110	0.49	Joshi and Chaudhuri (1996)
11	Prcp.[3]	Ferrihydrite	0.0228	NA[2]	110	0.297 -0.42	Stenkamp and Benjamin (1994)
12	Prcp.[3]	Ferrihydrite	0.0169 -0.0209	NA[2]	110	0.65-0.85	Bailey et al. (1992)
13	Prcp.[3]	Fe oxide	0.04-0.12	0.035 -0.072	90-105	0.42-0.841	Wang (1995)
14	Prcp.[3]	Mn oxide	0.0146 -0.055	0.0021 -0.035	60-160	0.5	Fan (1996)
15	Prcp.[3]	Fe_2O_3	0.0039	0.0074	110	0.6-0.85	Khaodhiar et al. (2000)

[1] N.A.-not applicable;
[2] NA-not available;
[3] Prcp.-precipitation;
[4] Evp.-evaporation;
[5] oxid.-oxidation;
[6] Mix.-Mixing.

Ephraim et al. 1991; Bar-Tal et al. 1988; Lion et al. 1982; Baccini et al. 1982; Buerge-Weirich et al. 2002), sorbate/sorbent ratio (Gadde and Laitinen, 1974; Hayes and Leckie, 1986; Weesner and Bleam, 1998; Webster et al. 1998), and competing metal ions (Benjamin and Leckie, 1981b; Voegelin et al. 2001; Christl and Kretzschmar, 1999; Christophi, 1998; Christophi and Axe, 2000; Gadde and Laitinen, 1974; Palmqvist, et al. 1999; Swallow et al. 1980; Trivedi et al. 2001b; Vulava et al. 2000). Other factors involve redox, temperature, supersaturated solutions of metal ions, and microbial effects. Generally, metal cation adsorption increases with increasing pH as the surface charge becomes more negative. Ionic strength affects metal adsorption by influencing adsorbate activity as well as the surface charge and double-layer capacitance and thickness. However, the effect of ionic strength is often relatively minor compared to pH. Complexing ligands may decrease or increase adsorbate uptake. Adsorption competition occurs when multiple species are present and compete for a limited number of surface sites.

Macroscopic studies include adsorption edges and isotherms. The former addresses pH and ionic strength dependence of adsorption, while the latter describes metal concentration dependence. In the following, both adsorption edges and isotherms as well as metal competition studies are introduced.

2.2.1 Adsorption Edge

A plot of cation adsorption to iron oxides vs. pH is usually sigmoidal with percent metal sorbed increasing from 0 to 100% over a narrow pH range (Cornell and Schwertmann, 1996; Hayes and Leckie, 1986). Sorbate/solid ratio influences the position of edge jump. Adding more solid causes the edge jump to shift to a lower pH; on the other hand,

increasing the sorbate concentration will cause either no shift at very low coverage or a shift to higher pH values becoming less steep with increasing coverage (Hayes and Katz, 1996). Temperature has also been observed to affect cation uptake; adsorption edges of Zn, Cu, Pb, and Cd on goethite (Johnson, 1990; Rodda et al. 1993) and Ni, Gd, and Y on alumina (Kosmulski, 1997) shifted to lower pH values as temperature rose from 10-70 and 15-35 ^{o}C, respectively. The relative affinity of a metal is reflected by the position of the edge jump. Dzombak and Morel (1990) reported the following trend for metal affinity to HFO Ca < Ni < Zn < Cd < Pb < Cr and Cornell and Schwertmann (1996) discussed a trend of Mn < Ni < Co < Cd < Zn < Pb< Cu.

The effect of ionic strength on the adsorption edge although suggestive, is not concrete. Nonspecific adsorption of cations (such as alkali cations) is dependent on ionic strength, where specific adsorption is typically absent ionic strength effects (Cornell and Schwertmann, 1996). Hayes and Leckie (1987) observed little ionic strength (IS = 10^{-2}-10^{0}) effect on Pb and Cd adsorption on goethite, the results were best modeled as an inner-sphere surface reaction. In modeling, the absence or presence of an ionic strength effect on metal adsorption is usually interpreted as inner-sphere or outer-sphere adsorption, respectively. Additionally, cation adsorption is often accompanied by proton release. The number in the past has been attributed to mononuclear or binuclear complexes and typically restricted to one or two (Cornell and Schwertmann, 1996). Intermediate values (Forbes et al. 1976; Hayes and Leckie, 1986; Müller and Sigg, 1992; Kooner, 1993; Gunneriusson et al. 1994; Trainor et al. 2000) may be caused by hydrolysis of the cation and/or occurrence of two types of sites or surface species (Cornell and Schwertmann, 1996). Benjamin and Leckie (1981a) observed 3.2 protons

released from Zn sorption to HFO; the authors explained their results as formation of multinuclear species. Although these approaches are usually successful in modeling, the surface species may not be unique or physically meaningful.

2.2.2 Adsorption Isotherm

Isotherms exhibit several types of shapes depending on metal concentration and/or surface coverage (Hayes and Katz, 1996). At low concentration and low surface coverage, isotherms are often linear, the slope of which is referred to as distribution coefficient (K_d). K_d has been used extensively to describe the partitioning of ions at the solid/liquid interface and is often found to be a function of pH, solution composition, and solid/liquid ratio (Jackson and Inch, 1989; Kooner, 1993; Lee et al. 1996; Larsen and Postma, 1997). Therefore, one condition may not be applicable to another. When an isotherm is conducted over a wider concentration range, it often becomes highly nonlinear and may level off at relatively high metal concentration. This type of isotherm can be described by the Langmuir model using two parameters, K for the equilibrium constant and C_t for site density. The Langmuir isotherm has been applied in a variety of adsorption studies (Pierce and Moore, 1980; Kanungo, 1994; Lee et al. 1996; Gupta, 1998; Small et al. 2001; Christophi and Axe, 2000; Trivedi et al. 2001b; Dong et al. 2001; Vaishya and Gupta, 2002, 2004; Delolme et al. 2004; Juang and Chung, 2004). The Freundlich isotherm has been used often for metal adsorption on oxides or soil samples (Barrow et al. 1989; Gupta, 1998; Sen et al. 2002; Vaishya and Gupta, 2002, 2004), and suggests the existence of more than one type of site.

Isotherms may be more complicated than discussed above. Robertson and Leckie (1998) observed three regions in the isotherm for Cu adsorption to goethite: below ~10^{-5}

mole Cu g^{-1} goethite (~1-7% of the total sites), between ~10^{-5} and ~$10^{-4.3}$ mole Cu g^{-1} goethite (~3-30% of the total sites), and above ~$10^{-4.3}$ mole Cu g^{-1} goethite. Similar trends for isotherms were found in other studies on Cd/HFO (Dzombak and Morel, 1986; Spadini et al. 2003), Cr/HFO (Charlet and Manceau, 1992), Zn/HFO (Kinniburgh and Jackson, 1982), and Co/Al_2O_3 (Katz and Hayes, 1995a). Homogeneous precipitation may occur if the metal ion is supersaturated resulting in an abrupt increase in the isotherm slope (Hayes and Katz, 1996). Gradual increases in the slope at high metal concentrations were modeled as surface polymers or surface precipitation (Katz and Hayes, 1995b; Dzombak and Morel, 1986; Charlet and Manceau, 1992) and have been supported by XAS for Cr/HFO system (Charlet and Manceau, 1992). Similar features in Cd/goethite isotherm (Robertson and Leckie, 1998) were successfully modeled using the triple layer model assuming several surface species. Based on wet chemical, spectroscopic, and crystallographic considerations, Spadini et al. (2003) proposed a low-affinity site for modeling isotherms at high surface coverage.

Although many studies have been conducted with single sorbate systems, metal ions may co-exist in the environment resulting in competition, which is discussed in the following section.

2.2.3 Competition Studies

Many researchers have investigated competition, for example, Gadde and Laitinen (1974) concluded that Pb sorbed more strongly than other ions, Zn, Cd, and Ti, on HFO and HMO. Adsorption of trace metals (Cu, Pb, Zn, Ni, and Cd) tends to be suppressed by high levels of weakly adsorbing alkaline earth ions (Balistrieri and Murray, 1982; Cowan et al. 1991; Trivedi et al. 2001b). Christophi and Axe (2000) observed that goethite has a

greater affinity for Pb than Cu. Cd adsorption is strongly influenced by the presence of competing cations such as divalent Ca and Zn (Benjamin and Leckie, 1981a; Bradl (2004). Kanungo et al. (2004) found in a study on Co, Ni, Cu, and Zn sorption to HMO that Ni experienced the greatest degree of displacement. Crawford et al. (1993) observed Zn and Ni in equal concentrations adsorb independently of each other on ferrihydrite; it's likely that the site density was not limited in this study. However, Zn was observed to have higher affinity than Ni on goethite (Tiller et al. 1984; Crawford et al. 1993; Gupta, 1998; Dube et al. 2001; Trivedi et al. 2001b; Jeon et al. 2003). Nevertheless, competition between trace metals may be difficult to demonstrate when site density is not limiting (Swallow et al. 1980; Benjamin and Leckie, 1981a; Palmqvist et al. 1999).

For soil samples, Gomes et al. (2001) found Cr, Pb, and Cu were the most strongly sorbed heavy metal cations, whereas Cd, Ni, and Zn were the least competitive. They also found that for metals of the same valence, sequences did not exactly follow the order of electronegativity. Stefanova (2001) observed a high selectivity of Cu and Pb over Zn and Cd ions by Keramzite sand. Khaodhiar et al. (2000) found Cu(II) adsorption increased slightly in the presence of arsenate but was not affected by chromate. Arsenate adsorption was not affected by either copper or chromate, while chromate adsorption increased in the presence of Cu(II) and decreased in the presence of arsenate. The authors modeled the single-sorbate behavior successfully with the triple layer model, but could not predict adsorption for multi-sorbate systems with surface complexation constants from single-sorbate systems. The local structure of the sorbed species is needed to constrain surface complexation modeling.

Overall, macroscopic adsorption studies are just a starting point for investigating metal partitioning at the solid/liquid interfaces. Efforts to further describe and predict their behavior are restricted by poor understanding of the adsorption mechanism. Recent advances in addressing speciation using in situ spectroscopic techniques such as XAS have made it possible to overcome this drawback (Brown, 1990; Brown and Sturchio, 2002; Hayes and Katz, 1996). Spectroscopic studies are introduced in the next section.

2.3 Adsorption on Oxides – Spectroscopic Studies

XAS and its derivatives XANES (X-ray absorption near edge structure) and EXAFS (extended X-ray absorption fine structure) spectroscopy are powerful tools for ascertaining the speciation of trace metals in natural soils and sediments (O'Day et al. 1998). Many researchers have used EXAFS to study the speciation of metal ions in natural sediments. O'Day et al. (1998) found that as sphalerite (ZnS) weathers, Zn is scavenged primarily as zinc hydroxide and/or zinc-iron oxyhydroxide phases, depending on the total amount of iron in the system. Similarly, Pb sorbed to iron oxyhydroxides at low pH (<7) when oxides were present in significant amounts. Pb sorption onto iron oxyhydroxides and precipitation of lead carbonate may occur at higher pH (>7) depending on the lead and iron concentrations in the system. Cd released from sphalerite weathering is preferentially partitioned into the aqueous phase. Scheinost et al. (2002) studied Zn speciation in soils near a former sphalerite smelter. They found that in the topsoil, Zn exists as franklinite ($ZnFe_2O_4$) (60%), sphalerite (30%), and aqueous or outer-sphere Zn^{2+}; in the subsoil, aqueous or outer-sphere Zn^{2+} prevailed (55%) and the remaining 45% was incorporated by hydroxyl-Al interlayers of phyllosilicates. The

authors concluded that hydroxyl-Al interlayered phyllosilicates act as a potential sink for Zn in acidic soils. Furrer et al. (2001) proposed a similar binding mechanism for Ni. EXAFS studies helped to isolate the sorption mechanism where hydroxyl-Al interlayers of phyllosilicates may be important for the retention of 3d metals (Scheinost et al. 2002).

EXAFS has been extensively used to probe the local structure of adsorbed species on model soil surfaces. From such studies, Axe et al. (1998) concluded that the strontium ion remains hydrated thus physically adsorbed to HFO surface. Sahai et al. (2000) observed that strontium sorbed to kaolinite, amorphous silica gel, and goethite surfaces by forming hydrated surface complexes and this structure did not change up to 57 days. Concomitant with a maximum of dissolved CO_2, the authors observed an increase of Sr sorption at approximately pH 8.5 where the local structure was consistent with $SrCO_3$(s). Sahai et al. (2000) suggested that sorption of carbonate may nucleate the precipitation of $SrCO_3$ in the pH range in which carbonate species sorption on goethite is near a maximum. Additionally, Zn(II) was found to form bidentate surface complex on 2-lineferrihydrite (Waychunas et al. 2002, 2003; Trivedi et al. 2004), aluminum oxide (Trainor et al. 2000), and goethite (Schlegel et al. 1997; Trivedi et al. 2001a).

Many studies have been conducted on Pb(II) adsorption mechanisms on crystalline iron and aluminum oxides (e.g., Chisholm-Brause et al. 1989, 1990; Roe et al. 1991; Bargar et al. 1997b; Strawn et al. 1998; Ostergren et al. 1999a, b, 2000a; Elzinga et al. 2001; Templeton et al. 2003). To construct an accurate description of Pb(II)-oxide surface, Bargar et al. (1997b) studied Pb(II) sorption products and surface functional groups on iron oxides. They found that Pb(II) ions sorbed as mononuclear bidentate complexes to edges of FeO_6 octahedra on both goethite (up to 4.2 μmol Pb m^{-2}) and

hematite (up to 9.9 μmol Pb m^{-2}). Combined with bond-valence determination, the authors proposed that Pb(II) adsorption occurred primarily at [$Fe^{Fe}_{Fe}\rightarrow O^{-1/2}$] and [$Fe\text{-}OH_2^{+1/2}$] sites. Similar surface complexes have been observed for Al oxides (Bargar et al. 1997a; Strawn et al. 1998). However, Pb binding has been found to change with increasing sorption density: surface complexes on goethite shifted from bidentate corner-sharing to bidentate edge-sharing as the loading increased from 0.83 to 4.9 μmol Pb m^{-2} (Templeton et al. 2003). On the other hand, Pb(II) polynuclear complexes were observed on γ-Al_2O_3 (1.3 μmol Pb m^{-2}, Chisholm-Brause et al. 1990), α-Al_2O_3 (> 3.4 μmol Pb m^{-2}, Bargar et al. 1997a), and goethite (9.6-19.2 μmol Pb m^{-2}, Roe et al. 1991). Interestingly, Trivedi et al. (2003) found a mixture of bidentate edge- and monodentate corner-sharing Pb(II) complexes on 2-line ferrihydrite at pH 4.5 above which only the former was observed despite the extent of surface coverage.

Pb(II) uptake by goethite in the presence of various anions has also been investigated. Bargar et al. (1998) proposed that the presence of Cl^- has little effect on the Pb(II)/goethite and Pb(II)/γ-alumina surface complexes at pH 7, while Pb(II)-Cl^--goethite ternary complexes were formed at pH $\leq$ 6. Recent studies (Elzinga et al. 2001; Ostergren et al. 2000 a, b) indicate that first and second-shell distances for Pb sorption to goethite are essentially unchanged ($\Delta R < 0.03$ Å) by the presence of carbonate or sulfate. While much work has been conducted with crystalline oxide surfaces, limited EXAFS studies have been reported on amorphous iron oxides. Manceau et al. (1992) observed that Pb(II) was adsorbed on HFO as mononuclear bidentate complexes on edges of FeO_6 octahedra based on a short-term contact time of three hours. Scheinost et al. (2001) found that Cu and Pb formed similar edge-sharing inner-sphere sorption complexes when

sorbed to 2-line ferrihydrite, this structure did not change as a function of time (up to 2 months), ferrihydrite morphology (with and without freeze-drying), and competing ions (Cu^{2+}). In their analysis, Cu and Pb were expected to bind to the same types of sites. However, competition was not observed. Again as discussed above, Trivedi et al. (2003) observed inner-sphere bidentate edge- and monodentate corner-sharing Pb(II) complexes, at constant pH, the configuration of the sorption complex was observed to be independent of the adsorbate concentration thus suggesting one average type of mechanism.

Ni has also been studied extensively using EXAFS. Much of the existing work has focused on its sorption to aluminum oxides, silica, or related minerals (Clause et al. 1992; Paulhiac and Clause, 1993; Scheidegger et al. 1996, 1998; Ford et al. 1999; Roberts et al. 1999; Nachtegaal and Sparks, 2003; Voegelin and Kretzschmar, 2005), where the formation of layered double hydroxide (LDH) precipitates were observed. Elzinga and Sparks (1999) reported that adsorption and surface precipitation are consecutive mechanisms involving nonspecific or specific adsorption followed by dissolution of Al and nucleation of a mixed Ni/Al phase. In the process, Al dissolution has been found to be the rate limiting mechanism based on rates of Ni uptake and Al dissolution (Scheidegger et al. 1998). EXAFS analysis reveals that formation of Ni-Al LDH is characterized by increased second shell contributions as the structure grows (Scheidegger et al. 1998). Also, as pH decreased from 7.5 to 6, the rate of formation decreased from 15 min to 72 hours (Roberts et al. 1999). Recently, however, Strathmann and Myneni (2005) found that Ni(II) forms inner-sphere mononuclear bidentate complexes with aluminol groups on boehmite (γ-AlOOH), where contact times ranged from 1 to 31 days with loadings between 7.0×10^{-6} and 4.11×10^{-5} mol g^{-1}. The total Ni(II)

concentration in their system was about one order of magnitude lower than in other studies where LDH precipitates were observed (Scheidegger et al. 1996, 1998; Scheinost et al. 1999; Elzinga and Sparks, 1999; Roberts et al. 1999; Nachtegaal and Sparks, 2003). Previous work with Ni and iron oxides has been limited to coprecipitation with goethite and hematite; Ni^{2+} was found to substitute for Fe^{3+} at 3% and 6% (molar ratio) loadings, respectively (Manceau et al. 2000; Singh et al. 2000). Little has been reported on Ni adsorption to iron oxide surfaces. Although a number of researchers (Dzombak and Morel, 1990; Coughlin and Stone, 1995; Buerge-Weirich et al. 2002) have modeled Ni adsorption on goethite using SOM^{+} surface species, molecular-scale analyses are needed to corroborate this mechanism.

Overall, the mobility, bioavailability, and toxicity of heavy metals are greatly controlled by adsorption reactions taking place at the oxide/water interfaces. XAS analysis is an effective tool in deciphering mechanisms at the surface. These investigations demonstrate how the structure of sorbent, through the nature of the reactive surface sites, may control the mobility and speciation of metals in the environment (Manceau et al. 1992). Macroscopic observations can be more confidently explained, and as is shown by Trivedi (2001) and Dyer et al. (2003), XAS derived structural information may be combined with macroscopic studies to predict heavy metal mobility in aquatic/soil environments.

2.4 Adsorption Modeling – Surface Complexation Models

Many researchers used traditional Langmuir (e.g., Pierce and Moore 1980; Padmanabham, 1983; Jackson and Inch, 1989; Miller et al. 1989; Kooner, 1993;

Kanungo, 1994; Lee et al. 1996, 1998; Sauvé et al. 2000) and empirical Freundlich models (Dzombak and Morel, 1986; Mishra and Tiwary, 1995, 1998; Nakahara, 1996; Mishra et al. 1997; Gupta, 1998; Christophi and Axe, 2000, Vaishya and Gupta, 2004) to describe equilibrium adsorption. However, a good fit using the Langmuir equation, or any other model without complementary molecular information, does not necessarily support the proposed mechanism (Schulthess and Sparks, 1991). For the Freundlich model, generally, if data can be fit with this isotherm, surface site heterogeneity is likely (Trapnell, 1955; Adamson, 1982). There are two limitations however in using the Freundlich equation (Schulthess and Sparks, 1991): first, it is only applicable to dilute solutions, adsorption at high aqueous concentrations is generally overestimated and no maximum adsorption is predicted; and, secondly, it does not explain the adsorption mechanism.

The distribution coefficient, K_d, has been used extensively to describe the partitioning of ions at the solid/liquid interface even though it is a function of pH, solution composition, solid/liquid ratio, and time (Lee et al. 1996; Jackson and Inch, 1989; Kooner, 1993; Larsen and Postma, 1997). Misak et al. (1996) concluded that the erroneous $\log K_d$-pH plots in their study was caused by changes in the activity coefficients of surface species even at sufficiently low surface coverages. Sauvé et al. (2000) studied Cd partitioning in 64 contaminated soil samples, where K_d varied over a range from 10 to 100,000. Therefore, partitioning parameters achieved from one situation may not be applied to another; adsorption modeling using a single parameter, K_d, has significant limitations in the sense of adsorption prediction.

Surface complexation modeling (SCM) has been demonstrated to be one of the most promising methods in modeling sorption. It offers a distinct advantage by representing surface chemical reactions with a set of quasi-thermodynamic constants, which are independent of changes in solution conditions (Hayes, 1987). A number of studies have shown that adsorption can be described in terms of SCMs accounting for the effect of pH, ionic strength, and surface-coverage (Hsi and Langmuir, 1985; Hayes and Leckie, 1986; Hiemstra et al. 1989; Dzombak and Morel, 1990; Katz and Hayes, 1995 a, b; Hayes and Katz, 1996; Hiemstra and Riemsdijk, 1996; Sahai and Sverjensky, 1997; Robertson and Leckie, 1997, 1998). One requirement of using SCMs is that controlling reactions and surface species must be known or assumed. The more accurate the surface complex, the more likely the model can predict surface interactions successfully. However, describing ion binding on mineral surfaces in a way that is mechanistically reasonable is always a great challenge and discussed below.

2.4.1 Surface Reactions and Species

In a review, Sposito (1989) summarized that regardless of the molecular structure, polymeric constituents of natural aqueous colloidal systems present reactive functional groups of two kinds: siloxane ditrigonal cavities and inorganic or organic hydroxyl groups. One common practice is to assume that the surface is chemically homogeneous and a two-step protonation reaction accounts for the charging of metal (hydr)oxides (Palmqvist et al. 1997; Sahai and Sverjensky, 1997; Davis et al. 1998; van Riemsdijk and Hiemstra, 1998). Adsorbate reactions are generally proposed based on adsorption edges, isotherms, and/or the number of H^+ released (e.g., Forbes et al. 1976; Benjamin and Leckie, 1981a; Hayes and Leckie, 1987; Hayes et al. 1988; Lövgren et al. 1990; Müller

and Sigg, 1992; Gunneriusson et al. 1994; Nowack et al. 1996). Assumed surface complexes are checked by the goodness of the model fit (Goldberg, 1991). For example, shifts in the adsorption edge at very low coverage are usually attributed to the presence of a small number of high affinity sites (Honeyman, 1984). Dzombak and Morel (1990) used two types of sites, a high affinity and a low affinity one, to describe the pH dependence of adsorption data. Although these approaches are usually successful, the surface species selected may not be unique or physically meaningful.

Fortunately, recent advances in addressing speciation using in situ spectroscopic techniques such as XAS and FTIR spectroscopy have made it possible to overcome this drawback (Hayes and Katz, 1996; Brown, 1990). Especially from XAS analysis, inner-sphere versus outer-sphere complexation, mononuclear versus multinuclear, or solid solution formation can be distinguished through a local structure analysis (e.g., Chisholm-Brause et al. 1990; Charlet and Manceau, 1992; O'Day et al. 1994; Bargar et al. 1997a, b; Scheidegger et al. 1998; Manning et al. 1998; Sahai et al. 2000; Trainor et al. 2000; Nachtegaal and Sparks, 2002; Trivedi et al. 2003, 2004; Wazne et al. 2003). For example, vanadium (V) adsorption on goethite at pH 1.5 to 12 could be better modeled with two monodentate surface complexes as compared to two bidentate species; however, based on XAS, only inner-sphere bidentate surface complexes formed (Peacock and Sherman, 2004). Also, SCM modeling was found to under-predict Co(II) adsorption on α-Al_2O_3 at high surface coverage (> 10%) using mononuclear complexes; while based on XAS results, Katz and Hayes (1995b) successfully modeled this adsorption using polymer complexes.

Overall, surface complexation modeling is heavily dependent on the accurate chemical and physical representation of surface complexes and the oxide surface (Hayes and Leckie, 1987; Cowan et al. 1991). Spectroscopic studies can provide qualitative and quantitative information on adsorption modeling, connecting molecular details to macroscopic measurements and significantly improving the ability to model the solid/liquid interface (e.g., Katz and Hayes, 1995 a, b; Hayes and Katz, 1996; Dyer et al. 2003, 2004).

2.4.2 Surface Complexation Models and Their Applications

A variety of SCMs have been used for predicting sorption of metal ions and other species on minerals (Westall and Hohl, 1980; Hayes and Katz, 1996; Lützenkirchen, 2002). Although these models may be expressed with similar mass law and material balance equations, they involve different descriptions of the electrical double layer (Westall and Hohl, 1980). The non-electrostatic model (NEM) neglects the electrostatic effects; the diffuse layer model (DLM) uses the Gouy-Chapman equation for the relationship between surface charge and potential in the interfacial region; the constant capacitance model (CCM) has one sorption plane with an inner-layer capacitance, C_1; and the triple layer model (TLM) incorporates the full Gouy-Chapman-Stern-Grahame equation for the interfacial region with two planes for surface complexation, an inner- and outer-layer capacitance, C_1 and C_2 (Westall and Hohl, 1980; Hayes and Katz, 1996). The DLM and CCM are often limited to lower and higher (>0.01 M and constant) ionic strength conditions, respectively. The TLM can be applied to a wide range of ionic strengths with an upper limit of applicability being that for the Davies Equation (Davies, 1962), which is employed to account for activity corrections (Hayes et al. 1991).

Surface complexation models have successfully described acid-base properties of oxides (Hayes et al. 1991; Sahai and Sverjensky, 1997) and metal binding with various mineral surfaces (Robertson et al. 1997, 1998; Katz and Hayes, 1995 a, b). For example, Dzombak and Morel (1990) used a two-site DLM and Hiemstra and van Riemsdijk (1996, 1999) used a charge distribution multi-site complexation (CD-MUSIC) model to describe metal sorption to HFO and goethite successfully. Hayes et al. (1991) used CCM, DLM, and TLM to fit goethite titration data and found that many combinations of parameters can successfully replicate acid-base behavior. A unique set of parameters is still difficult to achieve. Although a set of averaged parameters were used to predict adsorption behavior of complex assemblages of different bacterial types (Yee and Fein, 2001, 2003), few studies have addressed both isotherm and edge data over a large range of conditions with the same model (e.g., Müller and Sigg, 1992; Waite et al. 1994; Heidmann et al. 2005). Furthermore, most models have been derived from adsorption edges (Dyer et al. 2003). The applicability of these models may be questionable in the event there is an effect of adsorbate concentration with more than one type of site (Rodda et al. 1993; Dyer et al. 2003). Even with both edge and isotherm data, a single set of SCM parameters could not predict Pb(II) sorption onto ferrihydrite over a wide range of conditions, the equilibrium "constant" was adjusted with pH to fit the isotherm data (Dyer et al. 2003). Robertson and Leckie (1998) also could not apply a unique model for Cu adsorption isotherms with goethite, covering three pH values (4-6) and two ionic strengths (10^{-2}-10^{-1}).

To summarize, surface complexation models can be used to describe adsorption data in a thermodynamically consistent way using physically realistic surface species.

Spectroscopic techniques, especially XAS, provide mechanistic information about metal adsorption to mineral surfaces, thus significantly improving the predictive ability of SCMs. A unique set of parameters that is capable of describing various conditions is difficult to achieve, models must be calibrated using experimental data covering a wide range of conditions.

2.5 Summary

In summary, adsorption studies on discrete iron oxides and iron oxide-coated silica are important in investigating heavy metal mobility, bioavailability, and toxicity in the environment. Factors affecting coating processes have not been fully evaluated for iron oxide-coated silica and a systematic investigation is warranted. XAS analysis is an effective tool in deciphering metal adsorption mechanisms at the oxide/water interfaces. Coupled with macroscopic observations surface complexation models can describe adsorption data in a thermodynamically consistent way using physically realistic surface species. However, a unique set of parameters that is capable of describing various situations is difficult to achieve, models must be calibrated using experimental data covering a significant and relevant range of conditions.

In the next chapter, objectives and hypotheses are presented and followed by the associated methods.

CHAPTER 3

OBJECTIVES AND HYPOTHESES

As discussed in the review, sorption of trace elements onto reactive mineral surfaces is an important process regulating contaminant mobility and bioavailability in natural systems. Iron oxide is an important phase (Fuller et al. 1996; Green-Pedersen et al. 1997) that exists both discretely and as surface coatings. Although many studies have been conducted on heavy metal adsorption to discrete iron oxides and/or iron oxide-coated media, the coating process has not been systematically investigated. Furthermore, in modeling adsorption mechanisms, physically realistic surface species based on spectroscopic analyses are needed (e.g., Hsi and Langmuir, 1985; Gunneriusson et al. 1994; Robertson and Leckie, 1997, 1998; Sahai and Sverjensky, 1997).

In an effort to model heavy metal distribution and transport in soils and sediments, the objectives of this proposed research are as follows:

- Synthesize and characterize iron oxide-coated silica, which serves as a model system for soils and sediments. A systematic investigation will be conducted to address the factors influencing goethite coating to silica. Also, a variety of analyses will be applied to characterize the goethite-coated silica.

- Elucidate mechanistic interactions between heavy metal ions and the mineral surfaces. XAS analysis will be performed on heavy metal adsorption to iron oxide samples under varying conditions relevant to the subsurface in an effort to elucidate sorption mechanisms.

- Develop mechanistic models for heavy metal adsorption to mineral surfaces based on macroscopic and spectroscopic information. Various types of adsorption data (including titration, adsorption isotherm, and adsorption edge) covering a wide range of experimental conditions will be used to calibrate the surface complexation model.

- Understand the effect of competing ions on heavy metal adsorption to iron oxides. The ability of models developed in this research to predict heavy metal competition on iron oxide will be tested.

Specific hypotheses for this research include:

First, surface functional groups and reactions are similar between crystalline and amorphous iron oxides (Davis and Leckie, 1978; Charlet and Manceau, 1993; Bargar et al. 1997b; Villalobos et al. 2001; Dixit and Hering, 2003). Therefore, XAS results for metal ions sorbed on HFO may be applied to that on goethite. Bargar et al. (1997a, b) reported that iron oxides and aluminum oxides have fundamentally similar crystal chemistry – both form FeO_6 or AlO_6 octahedra with very similar average Al-O and Fe-O bond lengths, therefore, they may exhibit comparable surface structures and functional groups. Bargar et al. (1997a, b) found that Pb(II) ions sorbed as mononuclear bidentate complexes to edges of FeO_6 or AlO_6 octahedra on goethite, hematite, and aluminum oxide. Also, Pb adsorption to HFO (three hours contact time) and 2-line ferrihydrite (Manceau et al. 1992; Scheinost et al. 2001; Trivedi et al. 2003 [for pH > 4.5]) were dominated by similar surface complexes. The first hypothesis will be tested by analyzing Pb/HFO sorption samples (4 hours contact time) with XAS and comparing to that of Pb/goethite.

Secondly, coupled with XAS data, intrinsic surface complexation constants can be achieved by calibrating the SCM with a variety of adsorption data including titration, isotherm, and edge data covering a wide range of conditions. SCMs offer the advantage of representing surface chemical reactions with a set of quasi-thermodynamic constants, which are independent of changes in solution conditions (Hayes, 1987). However, few studies have addressed both isotherm and edge data over a large range of conditions with the same model (e.g. Müller and Sigg, 1992; Waite et al. 1994; Heidmann et al. 2005);

this may be due to the fact that most models have been derived only from adsorption edges (Dyer et al. 2003) or that the surface reaction products may not be physically meaningful. To obtain a unique set of parameters describing the oxide/water interfaces, this study will use XAS derived surface complexes and calibrate models with data covering a broad range of experimental conditions.

The third hypothesis is that mechanistic SCM parameters for a single solute can be applied to multi-solute systems. As discussed in the first hypothesis, adsorption sites are highly related to surface functional groups and surface structures; metal ions will then occupy the same types of sites in the presence of other metal ions. The mechanistic modeling parameters from single sorbate systems are thus expected to describe the multisorbate system. Although no direct XAS support was found, there are studies showing some success in modeling metal competition based on single sorbate parameters. Ali and Dzombak (1996) predicted sulfate and organic acids adsorption reasonably well based on single-sorbate data over a wide range of conditions. Palmqvist et al. (1999) showed single adsorbate modeling predicted adsorption competition for Cu and Zn but underestimated Pb(II) adsorption. In this study, metal competition will be predicted using SCMs from single sorbate systems. These models are based on XAS derived mechanistic information and calibrated using data covering a significant range of conditions.

Finally, goethite is selected as the representative iron oxide sorbent in soils and sediments for this research. Goethite and hematite are thermodynamically the most stable Fe oxides under aerobic surface conditions and therefore, the most widespread crystalline Fe oxides in soils and sediments (Schwertmann and Cornell, 1991). However,

existing in almost all soils and other surface formations (e.g. lakes, streams), goethite is predominant under cool to temperate, humid climates and associated with hematite in warmer regions. Soil goethite can be formed in two ways (Cornell and Schwertmann, 1996): Ferrous iron can be released from iron silicates, carbonates, and sulfides, for example, or reduced through microbial respiration. The ferrous ion is then oxidized under aerobic conditions and precipitates via a nucleation-crystal growth process. Alternatively, ferrihydrite precipitation undergoes dissolution/reprecipitation and converts to goethite. The transformation is slow at neutral pH (months to years), but can be greatly accelerated (in days) by organic reducing agents such as cysteine (Schwertmann and Cornell, 1991). In the laboratory, goethite formation is favored by raising or lowering the pH away from the PZC of ferrihydrite (pH 7-8, Schwertmann and Cornell, 1991) which promotes dissolution of ferrihydrite (Schwertmann and Murad, 1983).

Because its surface chemistry and crystal morphology are well characterized and because its widespread in natural environments, goethite has been extensively used as a model component for soils and sediments in a variety of investigations (e.g. Tiller et al. 1984; Hayes and Leckie, 1987; Crawford et al. 1993; Bargar et al. 1998; Sahai et al. 2000; Trivedi et al. 2001b; Templeton et al. 2003). For the same reasons, adsorption to goethite will be the focus of this research and goethite will be synthesized through ferrihydrite transformation under basic conditions (pH>12). Considering that the pH for natural aquatic environments ranges between six and eight and becomes acidic with for example the introduction of acid mine drainage or historically poor waste management practices, adsorption studies will be investigated covering an environmentally relevant

pH range of 4 to 7. Heavy metals may exist at trace level in natural aquatic systems (10^{-11}-10^{-7} M, Buerge-Weirich et al. 2002; Nolan et al. 2002) and may be at much higher concentrations in industrial wastewater discharge and contanimated sites. To develop models that can be widely applicable, adsorption data will be collected over as broad a metal concentration range as possible from approximately 10^{-11} M up to less than its solubility limit.

In the following chapters, methods to achieve the objectives and corresponding results are presented.

CHAPTER 4

EXPERIMENTAL METHODS

In this section, methods used for synthesis, characterization, adsorption, XAS, and modeling are presented. All chemicals used are of reagent grade unless otherwise stated. Quality assurance / quality control (QA/QC) was conducted in accordance with standard methods (Clesceri et al. 1998) and the associated procedure is presented in Appendix A. For all experiments, Milli-Q Type 1 deionized (DI) water was used; all containers were washed, soaked in 10% HNO_3 overnight, and then rinsed with DI water before use.

4.1 Synthesis of Iron Oxides

Amorphous hydrous ferric oxide (HFO) used in this study was synthesized following the method described by Dzombak and Morel (1986). HFO was always freshly synthesized for each adsorption study in a 1 g L^{-1} batch using $Fe(NO_3)_3 \cdot 9H_2O$ (99.99%+, Aldrich) and DI water. Precipitation was conducted under a N_2 environment (N_2 flowrate = 1~2 L min^{-1}, N_2 pressure = 2.27 atm) and turbulence (Re $\geq 1.0 \times 10^4$) maintained by a motorized stirrer with polyethylene coated impeller. The ferric nitrate solution was adjusted to pH 7~7.5 by dropwise addition of 10 N NaOH solution and aged for 4 hours before adsorption studies.

Goethite was synthesized based on the Atkinson et al. (1967) method and characterized in earlier work (Trivedi and Axe, 2001b); its characteristics are discussed along with that of the coating in Chapter 5 and 6. The procedure is similar to that for HFO except that the ferric nitrate solution was adjusted to pH 12. After aging for 4

hours, goethite suspensions were centrifuged at 12000 RPM for 20 minutes using the Sorvall® RC-28S centrifuge. The paste was re-suspended and centrifuged again to remove the background electrolyte (Na^+ and NO_3^- ions). The cleaning process was repeated until the conductivity of the supernatant after centrifugation reached background. The goethite paste after cleaning was freeze-dried and stored for future use. Goethite was re-suspended and aged for 4 hours before use in adsorption studies to ensure a stable particle size distribution (Trivedi, 2001).

4.2 Pretreatment of Silica

All silica samples were quartz, based on XRD analysis. The 0.2 mm (mean) silica was of 99.995% (metals basis) purity and purchased from Alfa Aesar (Alfa Aesar silica). The 0.9 mm and 1.4 mm (mean) silica samples were provided courtesy of U.S. Silica Company (US silica). All silica samples were initially acid-washed (2 ml acid g^{-1} silica) with 10^{-1} N HNO_3 for 24 hours. After decanting the solution, the remaining silica was rinsed repeatedly with DI water and then dried at 105 °C for 24 hours before storing in Nalgene® containers for future use.

4.3 Coating Methods

Two methods were used for producing goethite-coated silica, a modified adsorption method based on Szecsody et al. (1994) and a modified precipitation method based on Meng and Letterman (1993a). To evaluate factors that influence the degree of coating, experiments were designed using a three-level fractional factorial method (Anderson and Mclean, 1974) to reduce the number of studies and isolate effects. Factors investigated

included coating temperature (T), mean diameter of silica particle (D), Fe concentration initially applied (Fe_{ini}), and aging time (t, for adsorption method only).

In the modified adsorption method, discrete goethite was mixed with the silica suspension at pH 7.5 and the factors varied according to the factorial design of experiment. The suspension was subsequently dried in the oven for 6 days, rinsed with DI water, and dried again for another 6 days. The drying temperature was varied from 35 to 110 ^{o}C based on the design of an experiment.

In the second method, goethite was synthesized under identical chemical and physical conditions as discrete goethite except in the presence of silica. Ferric nitrate was dissolved in a silica suspension, completely mixed, and purged with N_2 gas. The system pH was raised to 12 by drop-wise addition of 10 N NaOH and aged for 4 hours. Subsequently, the suspension was aged for two weeks and rinsed with DI water. The coated silica was then dried for 3 days. In this method, temperature during aging ranged from 60 to 110 ^{o}C.

To avoid inclusion of loosely attached oxide in characterization, abrasion studies were performed on the coated silica at $Re > 10^4$ for 4 hours. The total Fe_{conc} was determined with a modified dithionite-citrate method based on Ross and Wang (1993) where the supernatant was then analyzed by atomic absorption spectrophotometry (AA) analysis (Clesceri et al. 1998). Amorphous Fe oxide was extracted with hydroxylamine hydrochloride-hydrochloric acid solution (0.25 M $NH_2OH{\cdot}HCl$, 0.25 M HCl) (Ross and Wang, 1993). Crystalline Fe oxide is the difference between the total and amorphous Fe concentration.

4.4 Extraction Methods

In this study, the total Fe oxide concentration was determined with a modified dithionite-citrate method based on Ross and Wang (1993), dissolving the ferric oxide via shaking samples at ambient temperature overnight in a reducing and complexing solution of 0.68 M sodium citrate solution and dithionite (sodium hydrosulfite). The supernatant was then analyzed with atomic absorption spectrophotometry (AA) (Ross and Wang, 1993).

Amorphous Fe oxide was extracted with hydroxylamine hydrochloride-hydrochloric acid solution (0.25 M $NH_2OH{\cdot}HCl$, 0.25 M HCl) following the same procedure as for total Fe content (Ross and Wang, 1993). The crystalline Fe oxide concentration is the difference between the total and amorphous Fe oxide.

4.5 Characterization of Uncoated and Coated Silica

Studies have shown that the adsorption of trace elements by mixed solids is related to the content and interaction of the component minerals; limited knowledge of the physical-chemical characteristics of the system has restricted our ability to predict the distribution of trace elements in aquatic and soil environments (Meng and Letterman, 1993a). The information obtained from X-ray analysis, particle size analysis, electron microscopy, surface area, and the point of zero charge are helpful in explaining adsorption.

4.5.1 X-Ray Diffraction (XRD)

Mineralogy was assessed with a PW3040-MPD XRD (Philips Electronic Instruments Company). The silica particles were placed in the sample holder with the back filling technique. Diffraction data were obtained by step-scans using Cu K-α radiation

generated at 45 kV and 40 mA, scanning from 10^{o} to 120^{o} 2θ. The (hkl) values corresponding to various peaks were calculated and compared with the standard powder diffraction file (PDF) (JCPDS, 1998).

4.5.2 X-Ray Fluorescence (XRF)

Elemental analysis was performed with a sequential X-ray spectrometer system (PW2400R, Philips Electronic Instruments Company). The PW2592/15 Rh tube and goniometer detector were used and the X-ray path was in Helium. The results were analyzed with the Philips SemiQ program and were normalized to 100.0%.

4.5.3 Particle Size Analysis (PSA)

Particle size distribution (PSD) was evaluated with a Beckman-Coulter LS 230 analyzer as a function of ionic strength and pH. Laser diffraction technique sizes particles by utilizing the diffraction pattern of scattered light over a range of 0.04 μm to 2 mm. Sodium nitrate ($NaNO_3$) was added to adjust the ionic strength and pH was adjusted with 10^{-1} N sodium hydroxide (NaOH) or 10^{-1} N nitric acid (HNO_3). The system was completely mixed in a 1 L beaker with a stir bar for at least 3 hours at room temperature before the particle size analysis. Reynolds number was calculated based on the characteristic length using the stir bar (Perry and Green, 1984).

4.5.4 Scanning Electron Microscopy (SEM)

Environmental scanning electron microscopy (ESEM, Model 2020, ElectroScan Corporation) and LEO 1530 field emission (FE)-SEM were utilized to study the surface

morphology. Samples were fixed on the aluminum sample holder with double-stick conductive carbon substrate.

4.5.5 Surface Area, Porosity, and Pore Size Distribution

Surface area (BET method) was measured with a NOVA 3000 series unit as well as by the Gas Technology Institute (GTI, 2002). Porosity (mercury porosimetry) and pore size distribution (mercury porosimetry) analyses were performed by GTI (2002).

4.5.6 Fourier Transform Infrared Spectroscopy (FTIR)

To study the interfacial bonding mechanism between goethite and silica, Fourier transform infrared (FTIR) spectra were obtained on an ATI Mattson Research Series 1 FTIR Spectrometer. Goethite, silica, and goethite-coated silica samples were dispersed homogeneously in KBr matrices and pressed into discs. Five hundred scans of resolution 4 cm^{-1} were averaged to improve signal to noise ratio. The instrument was continually purged with dry air. Spectra were obtained over the range of 400-4000 cm^{-1}.

4.5.7 Surface Charge Distribution

Surface charge distribution varies depending on the degree of hydration, contamination of the surface by other ions, and method of determination. The point of zero charge (pH_{PZC}) of a system of any complexity is the condition of no net charge on the surface (Parks, 1967; Westall et al. 1976); others may prefer to designate this the common intersection point, pH_{CIP}, for mixed systems. The PZC can be measured from a wide variety of experiments in which pH is a master variable (Parks, 1967). Methods used to determine

PZC include electrophoretic mobility, potentiometric titrations, streaming potential, and cation and anion adsorption.

Potentiometric titrations were conducted with 1 g L^{-1} sorbent at three ionic strengths (IS, 10^{-3}, 10^{-2}, and 10^{-1}) adjusted with $NaNO_3$. The suspension was purged with high purity (99.999%) nitrogen gas to remove CO_2. Titrations were conducted from pH 2 to 10 for silica and coated silica and 4 to 10 for goethite with stepwise addition of 0.1 ml titrant (10^{-1} and/or 10^{-2} N HNO_3 or NaOH); pH values were recorded after an equilibration time of 2 minutes per step (Trivedi and Axe, 2001b).

4.6 Adsorption Studies

In all adsorption studies, bulk aqueous phase concentrations of metals were used below their solubility limit with respect to the thermodynamically stable form (Appendix B). Ionic strength, pH, and metal ion concentrations were adjusted with $NaNO_3$, HNO_3 and NaOH, and metal nitrate, respectively. Turbulence (Re $\geq 1.0\times10^4$) was maintained to eliminate resistance due to external mass transfer. All macroscopic adsorption studies were conducted in Nalgene® containers with a contact time of 4 hours using a shaker (C-1 Platform Shaker, New Brunswick Scientific) at room temperature (~22 °C) and open to the atmosphere.

The amount of metal adsorbed was calculated from a mass balance by subtracting final aqueous concentration from initial concentration. Metal concentrations were analyzed with either Beckman Liquid Scintillation System (model LS6500) or graphite furnace atomic absorption spectrophotometer (AA, Perkin Elmer 4110 ZL). When using

the liquid scintillation counter, an isotope-tagged (i.e., Ni^{63}, Zn^{65}, Pb^{210}) metal-nitrate stock solution was used to adjust metal concentration.

Constant boundary condition (CBC) experiments were conducted to study the transient sorption process. In these studies, the bulk aqueous concentration of metal ions was maintained approximately constant by monitoring and adding adsorbate as necessary. CBC studies were performed in 1 L Nalgene® bottles using the isotope-tagged stock solution to adjust metal concentration.

4.7 X-ray Absorption Spectroscopy (XAS) Analysis

Samples for XAS studies were prepared similar to macroscopic adsorption studies. The suspension was separated by centrifugation and stored wet for XAS analysis. The metal loading was obtained from the simultaneously prepared tagged sample using scintillation counting (Trivedi, 2001).

The XAS data were collected at beamline X-11A and X-11B at the National Synchrotron Light Source (NSLS), Brookhaven National Laboratory. The storage ring was operated at 2.81 GeV beam energy with a beam current in the range of 100-300 mA. Silicon (111) double-crystal monochromators were used for both beamlines. The incident beam (I_0) was detuned by 30% to reject high-energy harmonics. Data were collected in both transmission and fluorescence modes. The I_0 ion chamber was filled with $N_2(g)$ and the fluorescence signal (I_f) was collected using a Lytle detector filled with Ar gas. The transmission signal (I_t) was measured with a $N_2(g)$ and Ar(g) mixture-filled ion chamber and the gas composition was adjusted to absorb approximately 60% of the incoming X-rays. EXAFS spectra were collected from 12,855 to 13,602 eV over the Pb

L_{III}-edge, from 8,133 to 8,884 eV over the Ni K-edge, and from 6,912 to 7,857 eV over the Fe K-edge. Pb, Ni, and Fe foils were used as references for energy calibration. At least five scans for Fe and typically ~20 scans for Pb and Ni were collected. The analysis was carried out on the averaged data to improve signal statistics. All EXAFS data were collected at room temperature. XAS data for reference compounds were collected in transmission mode. Both transmission and fluorescence data were collected for the hydrated ion in a metal nitrate solution in order to address self-absorption (Tröger et al. 1992).

The XAS data were analyzed with WinXAS 2.3 (Ressler, 1998) and followed standard procedures (Bunker and Sayers, 1988). For each scan, the background was fitted with a linear polynomial through the pre-edge region and subtracted. The edge jump of the background-corrected XAS spectra was then normalized to one by refining 100-200 eV above the edge with a zero order polynomial and normalizing the spectra to the ordinate value of this polynomial. The energy threshold (E_0) of the absorption spectrum was determined from the first inflection point of the edge region and was used to convert the absorption spectrum from energy to k space. A cubic spline function was applied to account for the isolated atomic absorption $\mu_0(E)$. EXAFS function ($\chi(k)$) was obtained after subtracting $\mu_0(E)$ from the absorption of the atom in condensed matter. The $\chi(k)$ data were weighted by k^3 to enhance the higher k-space data and then Fourier transformed using the Bessel window function to produce the radial structural function (RSF). The RSF was not corrected for phase shift. EXAFS fitting of the RSF was conducted using theoretical phase shift and amplitude functions calculated by FEFF 7

(Zabinsky et al. 1995). Fits were optimized by minimizing the residuals and errors were assessed by fitting the spectra averaged over subgroups of scans.

4.8 Surface Complexation Modeling

The nonlinear least-square fitting program, FITEQL Version 4.0 (Herbelin and Westall, 1999) was used for fitting parameters from titration and adsorption data. This program solves the equilibrium model at each data point and optimizes adjustable parameters until the sum of the squares of the residuals (SOS/DF term in FITEQL) between the measured data and the calculated values is minimized (Herbelin and Westall, 1999). The TLM has the flexibility in placing electrolyte and metal ions along the interface and therefore is selected for modeling the goethite titration and adsorption data. In distinguishing inner- and outer-sphere adsorption, the TLM has been demonstrated to accurately cover a large range of conditions (Cowan et al. 1991; Hayes and Katz, 1996; Dyer et al. 2004). Parameters calibrated from the titration data were further applied in modeling adsorption.

In the following chapters, results are discussed: Chapter 5, Characterization of Iron Oxides and Silica; Chapter 6, Synthesis and Characterization of Iron Oxide-Coated Silica; Chapter 7, Surface Complexation of Pb(II) on Amorphous Iron Oxide: Spectroscopic and Time Studies; Chapter 8, Ni(II) Complexation to Amorphous Hydrous Ferric Oxide: An X-ray Absorption Spectroscopy Study; Chapter 9, Surface Complexation Modeling of Heavy Metal Adsorption and Competition on Goethite; and Chapter 10, Ni and Zn Sorption to Iron Oxide-Coated Silica.

CHAPTER 5

CHARACTERIZATION OF IRON OXIDES AND SILICA

In this section, results are presented for characterizing iron oxide and silica. Goethite was produced in earlier work (Trivedi, et al. 2001a); HFO is synthesized following the same method as of Axe and Anderson (1995). Characterization analyses are conducted in corresponding studies and are summarized below.

5.1 Characterization of Iron Oxides

XRD analysis reveals that goethite is highly crystalline; the ESEM micrograph shows needle shaped or acicular crystals of 0.5 to 1 μm in length. In the particle size analysis, the goethite powder is re-suspended for 4 hours and the stabilized particles range from 0.2 to 84 μm. The BET surface area of the goethite is 31 m^2 g^{-1}; the pore size ranges from 2 to 220 nm and the porosity of goethite is 0.3%.

Potentiometric titrations were performed to evaluate the PZC of goethite; the result, 8.78 ± 0.97 (Figure 5.1), suggests slight drifting to a higher pH compared to that found earlier 7.8 ± 0.4 (Trivedi and Axe, 2000). Possible reasons for this difference may be that potentiometric titrations were performed on different batches of goethite. Studies (Schwertmann et al. 1985; Villalobos et al. 2003) have shown that crystalline shape, size of particles, and the resulting reactivity of goethite depended on experimental conditions such as rate of addition and total base added, presence of sorbing ions, and aging time. Small variances between different batches may exists and influence the PZC. Previous studies (Evans et al. 1979; Zeltner and Anderson, 1988) have shown that when the goethite suspension was purged for 2 months, the PZC increased from 8.1 to 9.1 as

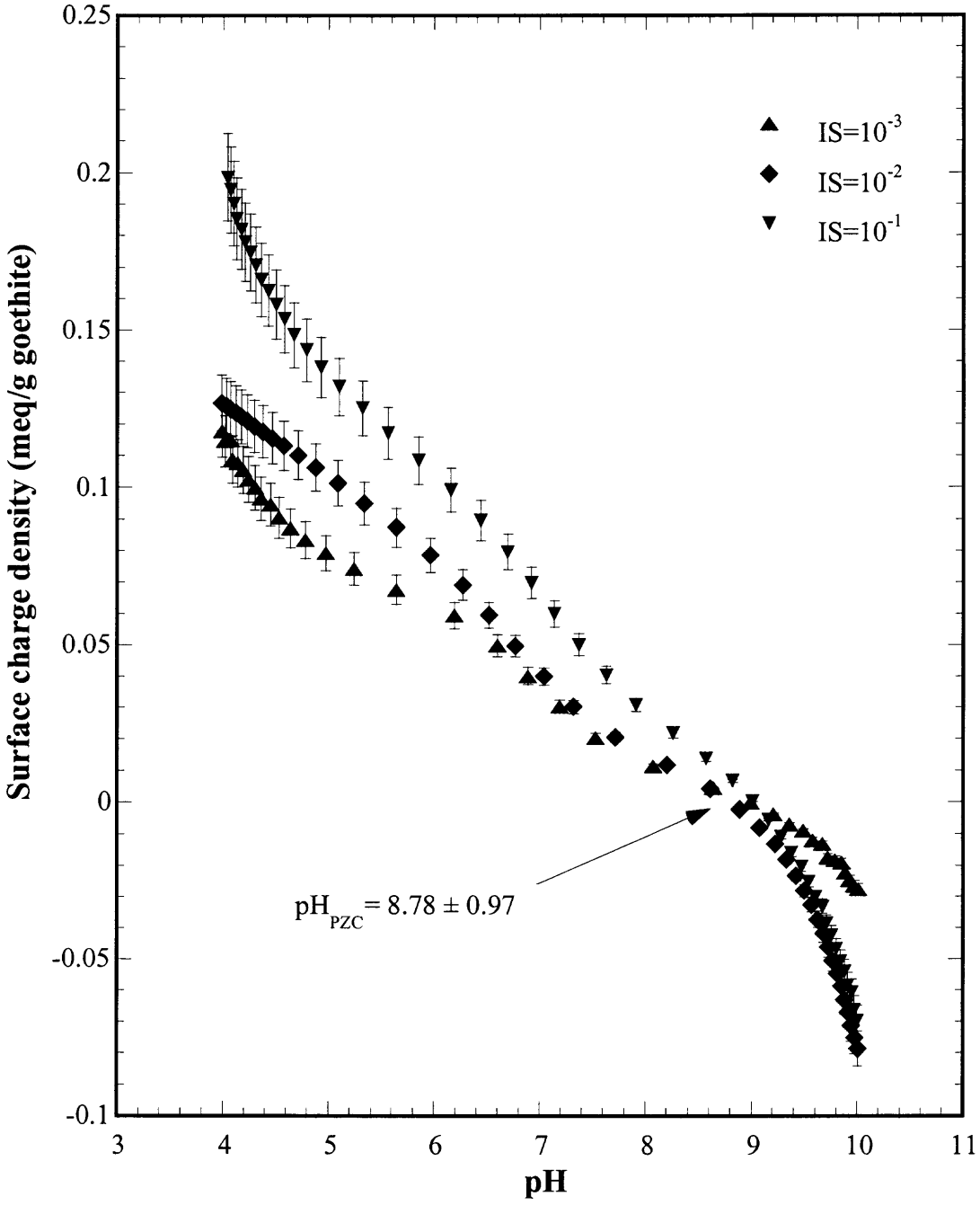

Figure 5.1 Potentiometric titration of goethite (1 g L^{-1}) at room temperature.

measured by potentiometric titration (Zeltner and Anderson, 1988). The authors explained the changes in PZC by CO_2 adsorption and desorption. However, aging impacts crystallization, which would significantly affect the PZC. Reported PZC values of goethite (Table 5.1) range from 7.5 to 9.38. The PZC for goethite (8.78 ± 0.97) observed in this study is consistent with this range.

Characterization of HFO was conducted earlier by Axe and Anderson (1995) and is used as a reference for the HFO used in this study. For freeze-dried HFO, the surface area and mean pore size radius measured with N_2 adsorption and desorption were 36.6 m^2 g^{-1} and 3.8 nm, respectively. The porosity was 0.5 and the pore size distribution from Hg porosimetry showed a mean pore size of less than 5 nm. The particle size distribution of HFO in the aqueous phase revealed particle diameters ranging between 1 and 200 μm with a mode of approximately 90 μm.

5.2 Characterization of Silica

Acid washed silica samples were analyzed with XRD, XRF, particle size analysis (PSA), ESEM, and surface charge distribution.

5.2.1 XRD

XRD analyses were conducted on Alfa Aesar silica and US silica samples and showed patterns consistent with that of α-quartz (Powder Diffraction File (PDF) #33-1161) published by International Center for Diffraction Data (ICDD). The diffraction patterns of these two silica samples with the (hkl) planes (Figure 5.2 and Table 5.2) showed that relative intensities were equivalent for the 100% peak, but there was deviation for the

Table 5.1 PZC Values of Goethite in Some Studies

	PZC of goethite	Reference
1	9.38	Yoon et al. (1979)
2	9.20	Evans et al. (1979)
3	9.0	Zeltner and Anderson (1988)
4	8.50	Hsi and Langmuir (1985)
5	8.45	Hayes and Leckie (1987)
6	8.00	Hingston et al. (1972)
8	7.60	Forbes et al. (1974)
9	7.55	Atkinson et al. (1967)
10	7.50	Yates and Healy (1975)

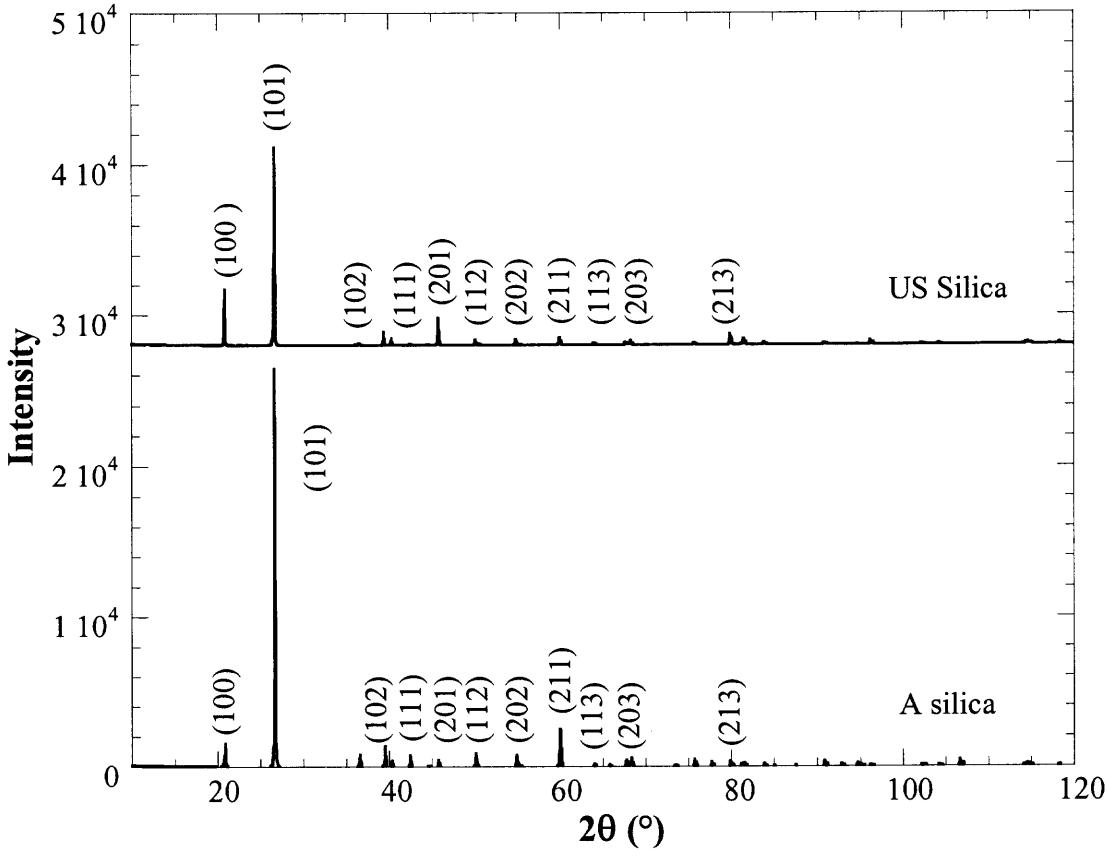

Figure 5.2 X-Ray diffraction patterns of US silica and Alfa Aesar silica (the number sets identify the crystal planes).

Table 5.2 XRD Data of Alfa Aesar (A) and US Silica Compared with the Standard Powder Diffraction Database File

2θ (°)			d-spacing (nm)			Relative Intensities			hkl planes			WHH (°2θ)	
A silica	US silica	PDF	A silica	US silica	PDF	A silica	US silica	PDF	h	k	l	A silica	US silica
20.89	20.84	20.85	4.25	4.26	4.26	5.2	29.3	22	1	0	0	0.1350	0.0892
26.65	26.65	26.65	3.34	3.34	3.34	100.0	100.0	100	1	0	1	0.1233	0.1362
39.50	39.37	39.46	2.28	2.29	2.28	5.0	7.7	8	1	0	2	0.1337	0.0485
50.16	50.13	50.14	1.82	1.82	1.82	3.4	3.1	14	1	1	2	0.1361	0.0938
60.00	59.99	59.95	1.54	1.54	1.54	9.4	3.9	9	2	1	1	0.1078	0.2182

22% peak. The differences between the sample and the PDF may be attributed to preferred orientation. The width at the half height (WHH) (Figure 5.2) for the most intense peak of US and Alfa Aesar silica are 0.14 and 0.12 $^{o}2\theta$, respectively.

5.2.2 X-Ray Fluorescence (XRF)

XRF was performed on silica samples to determine composition. Two original and eight acid-washed US silica samples were analyzed, while only one Alfa Aesar silica sample was taken because the measured SiO_2 content (100%) conformed to the reported 99.995% purity. Alfa Aesar silica shows 100% purity (Table 5.3), while the original US silica was 95.883% of SiO_2 with some impurities of Al, Fe, and S. Retention of trace elements is reported to be related to their Al and Fe content (Meng and Letterman, 1993a), and therefore, these Al and Fe impurities may influence adsorption. However, after acid-wash treatment of silica samples, the SiO_2 content increased to 98.759% for all US silica samples. Therefore, based on XRF analysis, Alfa Aesar silica may be the most appropriate for adsorption studies. US silica requires pretreatment.

5.2.3 Particle Size Analysis (PSA)

Results of the particle size analysis for Alfa Aesar silica show that ionic strength and pH do not influence the particle size distribution. Alfa Aesar silica has a mode of 0.22 mm (Figure 5.3), US silica has a mode of 0.99 mm (Figure 5.4), and again both ionic strength and pH do not affect the particle size distribution. Considering that the silica particles may be applied in column studies for adsorption, Alfa Aesar silica, which has a much smaller particle size, may promote clogging when coated with iron oxide. Therefore, based on the particle size analysis, US silica is more suitable for adsorption studies.

Table 5.3 XRF Results for Alfa Aesar (A) and US Silica

Silica	Components	Concentration with XRF (%)		Concentration reported (%)
A	SiO_2	100		99.995
US		Original	Acid-washed	Original
	Al_2O_3	2.513	0.471	<0.8
	SiO_2	95.883	98.759	99.0-99.9
	SO_3	0.245	Not detected	Not reported
	K	0.208	0.049	Not reported
	FeOOH	0.9205	0.107	<0.1
	TiO_2	0.1425	0.615	<0.1
	Cl	0.089	Not detected	Not reported

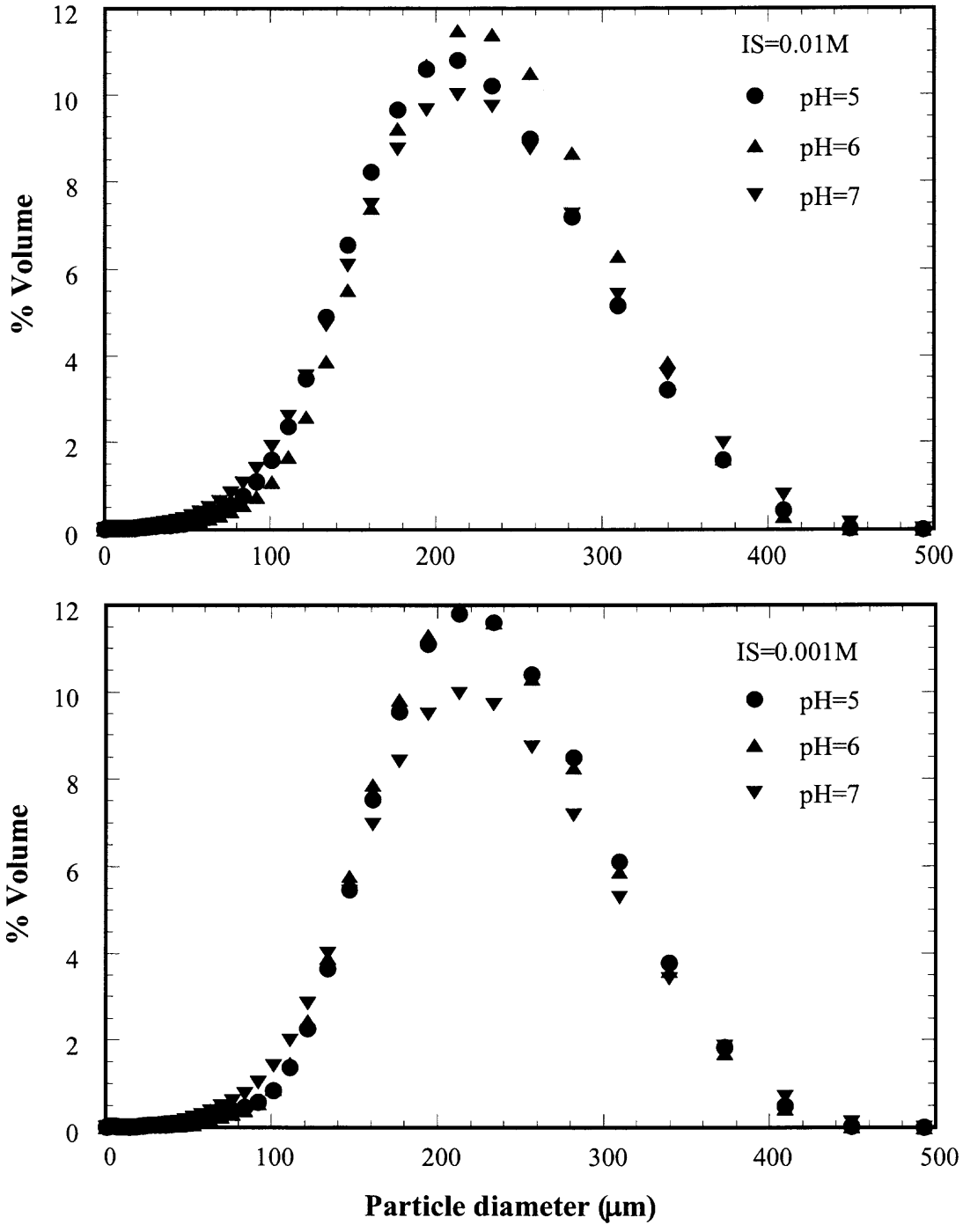

Figure 5.3 Particle size distribution for Alfa Aesar silica as a function of pH and ionic strengths.

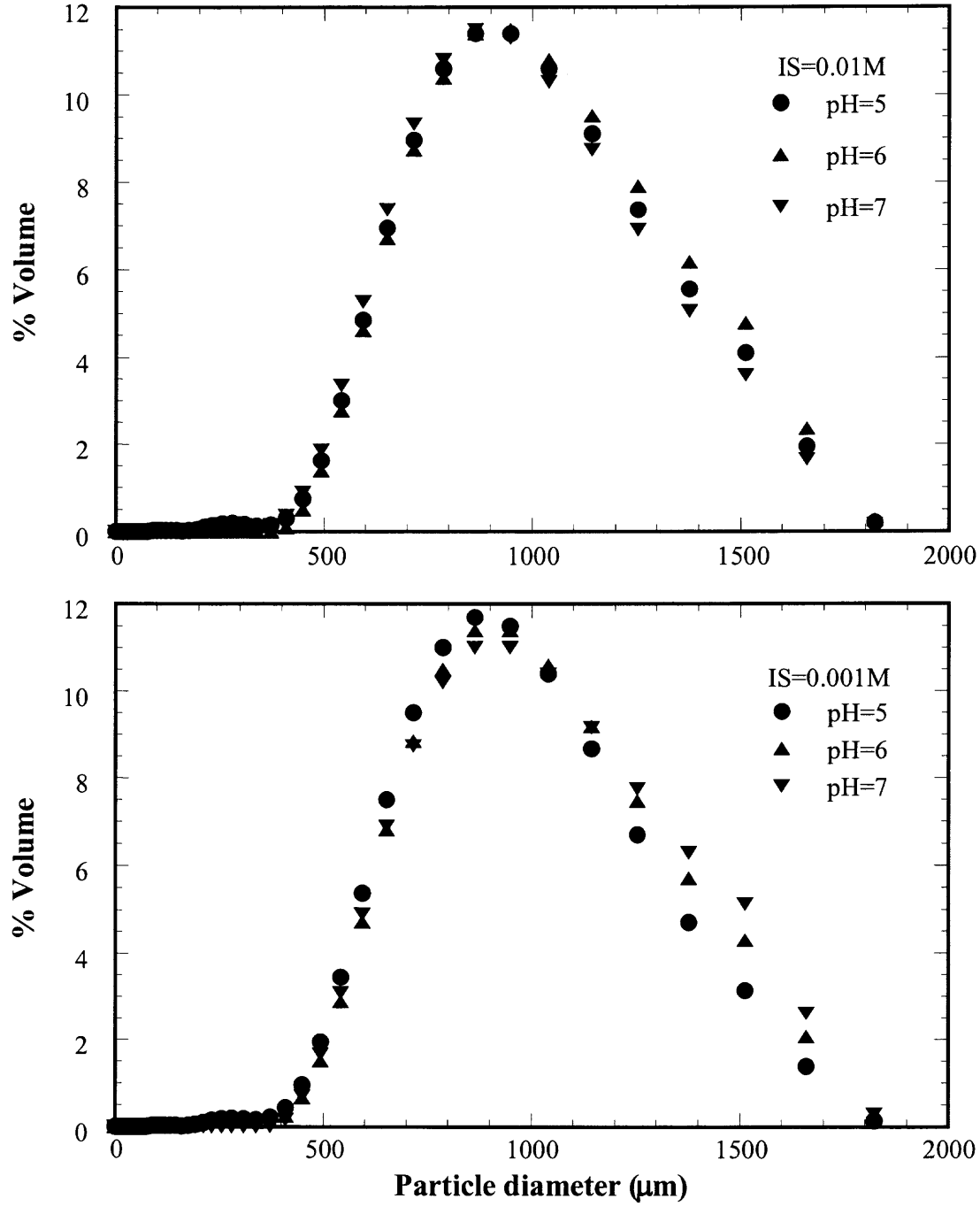

Figure 5.4 Particle size distribution for US silica as a function of pH and ionic strength.

5.2.4 Environmental Scanning Electron Microscopy (ESEM)

The ESEM micrographs of US and Alfa Aesar silica are taken at similar magnification. Considering that Alfa Aesar silica has an average particle size of 220 μm, while that of US silica is 900 μm, Figure 5.5 and Figure 5.6 were collected at lower magnification to show the relative roughness of these two particles at larger scale. Both have relatively smooth and rough areas on the surface. Figure 5.7 and Figure 5.8 show the surface of Alfa Aesar and US silica particles at 1500×, respectively; similarly, both rough and smooth parts of the surfaces. The surface roughness of Alfa Aesar and US silica particles are comparable.

Trivedi (2001) found that the goethite crystals are needle-shaped or acicular, approximately 0.5 to 1 μm in length, and goethite crystals aggregate into somewhat spherical particles. At a lower ionic strength of 10^{-3}, the largest particles were approximately 10 to 20 μm. The upper two figures in Figure 5.9 show the size and shape of the goethite particles that will be used in this research, and the lower two figures reveal the 0.5-1.0 μm, needle-shaped goethite crystals at higher magnification. The ESEM results are in agreement with Trivedi's (2001).

From the ESEM analysis of the surface roughness of silica particles and the size of goethite particles, both Alfa Aesar and US silica are suitable for goethite coating.

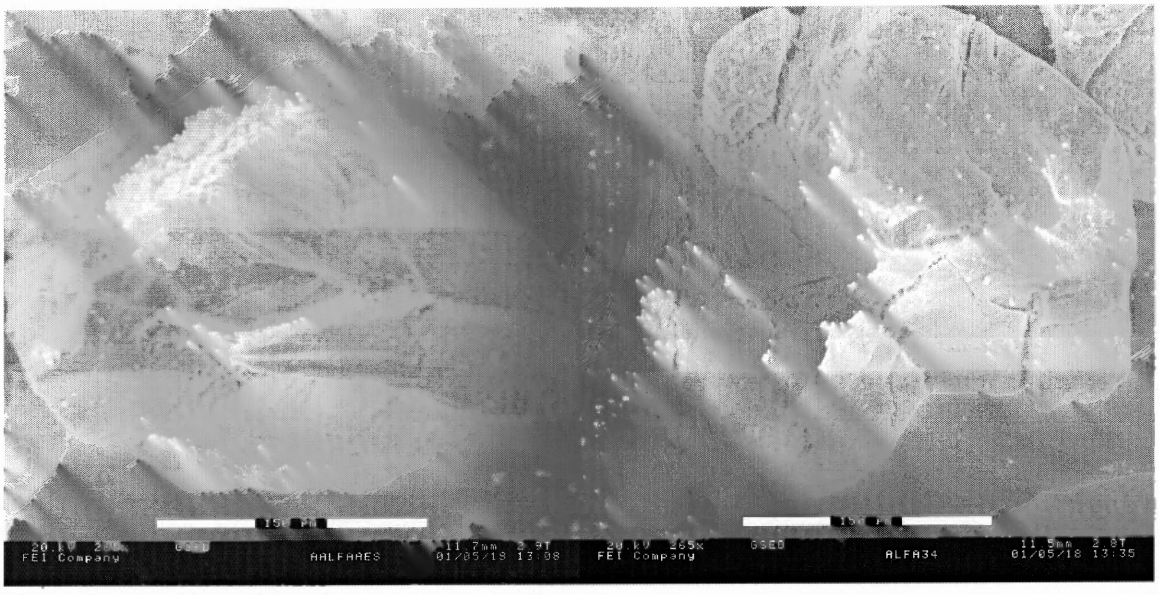

Figure 5.5 ESEM micrograph for Alfa Aesar silica.

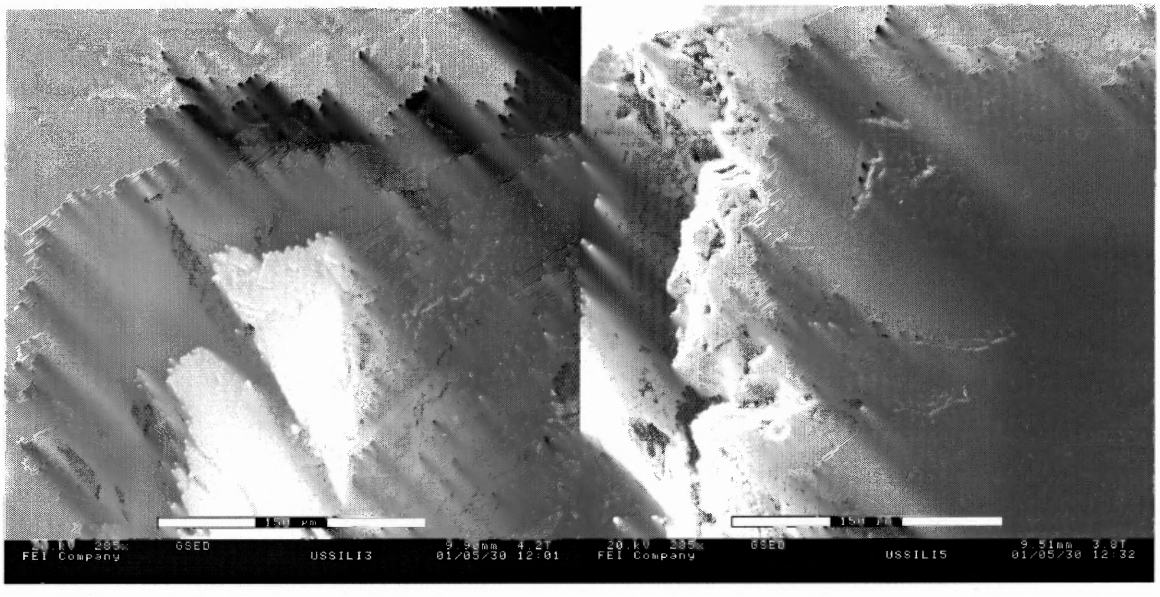

Figure 5.6 ESEM micrograph for US silica.

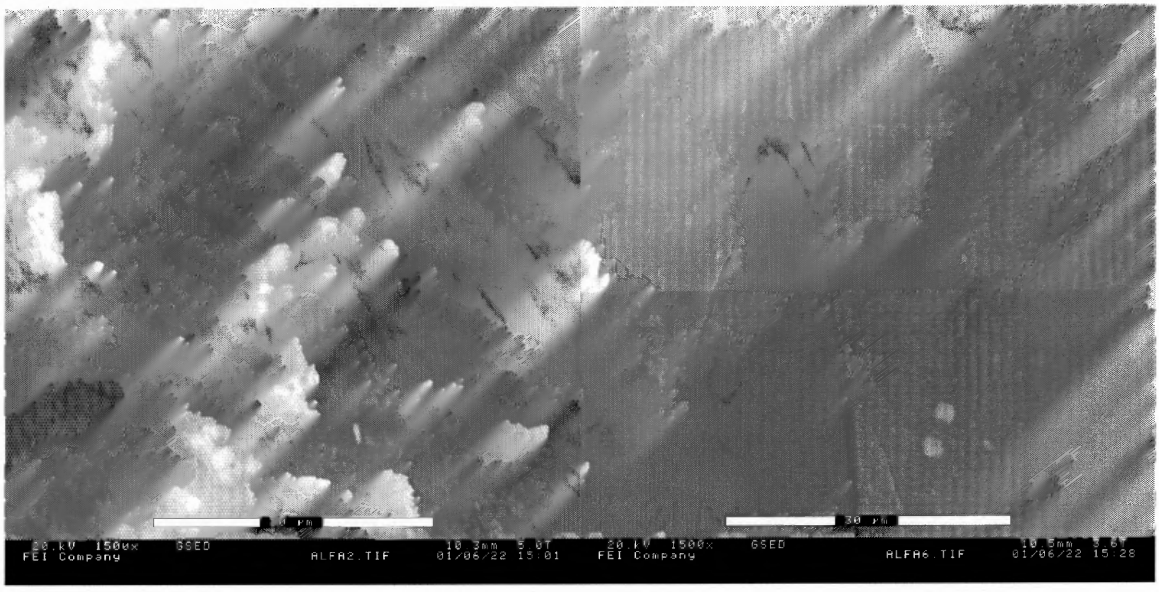

Figure 5.7 Micrograph of Alfa Aesar silica.

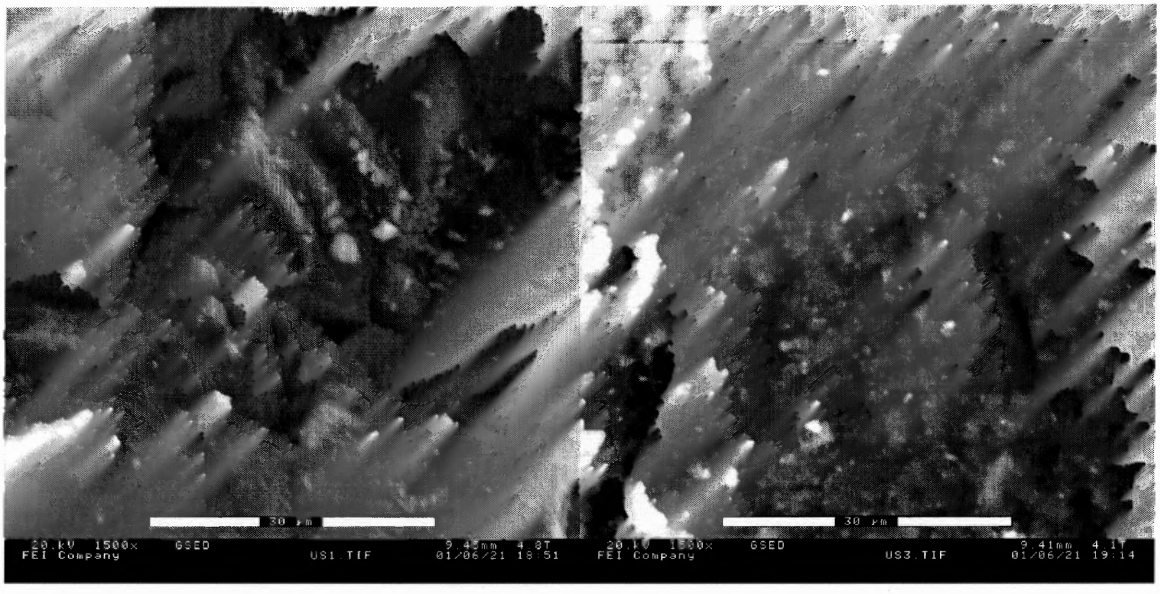

Figure 5.8 Micrograph of US silica.

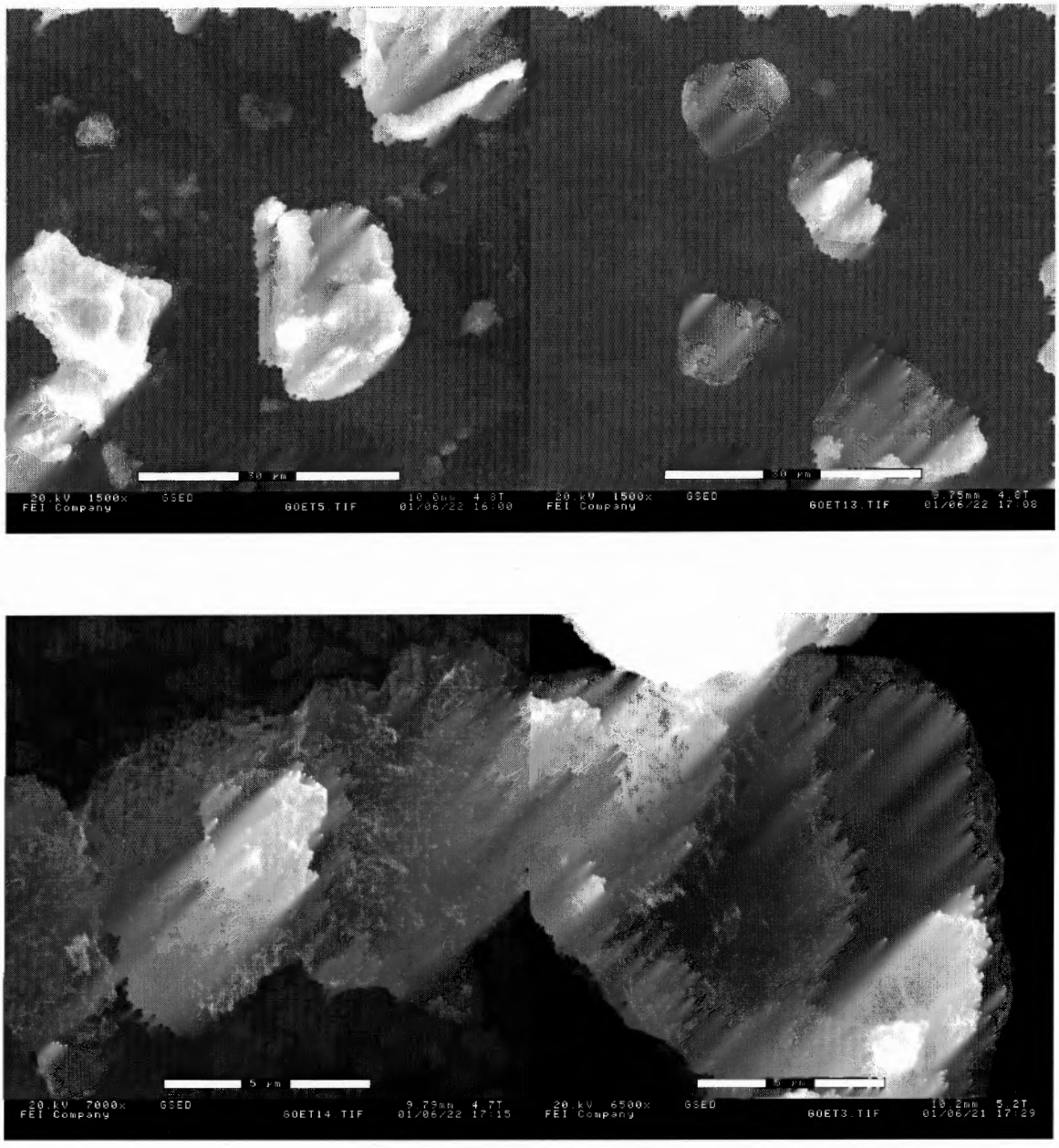

Figure 5.9 Micrograph of goethite.

5.2.5 Surface Charge Distribution

Potentiometric titrations were conducted to verify the PZC of Alfa Aesar and US silica. Usually titrations can be performed with either acid or base. In acid titrations, the silica suspension needs to be adjusted to a higher pH and is then titrated with an acid. This process is reversed when the titration is conducted with base.

In this study, titration of silica was initially performed with acid (HNO_3). The resulting PZC of Alfa Aesar and US silica was about 5.0 and 4.9, respectively, and are higher than that of other studies listed in Table 5.4. These differences which may be caused by the dissolution of silica. Yates (1975) studied the influence of oxide solubility during a titration in determining oxide surface charge. He found that the dissolution does not affect titrations below pH 7, because the neutral species $Si(OH)_4^0$ predominates. However, the hydrolysis of $Si(OH)_4^0$ occurs above this pH consuming OH^- (has a buffer effect around its pK_{a1}, 9.46, Yates, 1975) and thus affecting the titration procedure. When the effect of dissolution is not corrected in the calculation, the surface charge increases. Therefore, the consumption of OH^- should be considered when performing titrations with acid, especially when the silica concentration in the suspension is low and surface dissolution is potentially a significant fraction of the total silica present (2 g L^{-1} in this study).

Ultimately, base titrations were used to determine the surface charge distribution of silica samples. The PZC value of silica samples in this study is 2.85 (Figure 5.10) and is consistent with other studies. The acid-washed US silica sample has less than 1.5% (mass) impurities as seen in Table 5.3; nevertheless, these impurities are likely on the surface affecting the surface charge.

Table 5.4 Isoelectric Points of SiO_2

IEP	Description		Investigator	Reference
1.5 1.8	Brazilian crystal, mep Crystals-Harding Mine, NM, mep.		Bhappu	Parks (1965)
2.5±0.2	Natural crystals, mep		Iwasaki, Cooke, and Choi	
2.2-2.8	Quartz-beach sand, sp		Flaningham	
2.3 2.0 1-2 2.7-3	ads. sp. in HCl only sp in 10^{-4} M NaCl pt	Brazilian crystal	Li	
<3	Quartz, mep.		O'Connor and Buchaman	
3.7	Brazilian crystal, sp.		Gaudin and Fuerstenau	
2-3	pH of min. gelation rate		Moulik and Ghosh	
1-2 1-1.5 2	Sols synthetic: IEP-location of viscosity minima 1% SiO_2 sols, mep pH-min. gelation rate		DeBoer, Linsen, and Okkerse	
1.3	pH-min. gelation rate		Sen and Ghosh	
2.8-3	PH-min. gelation rate		Hückel	
~0.5	IEP by eo		Michaelis	
4.1	PZC-potentiometric titrations		Schwarz et al.	Schwarz et al. (1984)
1.8				Stumm and Morgan (1996)
3.5	Commercial sol "Ludox" with spherical SiO_2 particles		Bolt	Bolt (1957)
3.5 3.5 3.5 3.5	Degussa Aerosil amorphous silica, pt Degussa Aerosil amorphous silica, pt Pyrogenic CAB-O-SIL am. silica, pt BDH precipitated amorphous silica, pt		Casey Brady Abendroth Yates	Sahai and Sverjensky (1997)

ads.: IEP estimated as pH at which adsorption of indifferent positive ions equals that of negative ions;
eo.: electroendoosmosis or electroosmosis;
pt.: IEP estimated by potentiometric titration.
sp.: IEP estimated as pH of zero streaming potential or current;
mep.: microelectrophoresis;

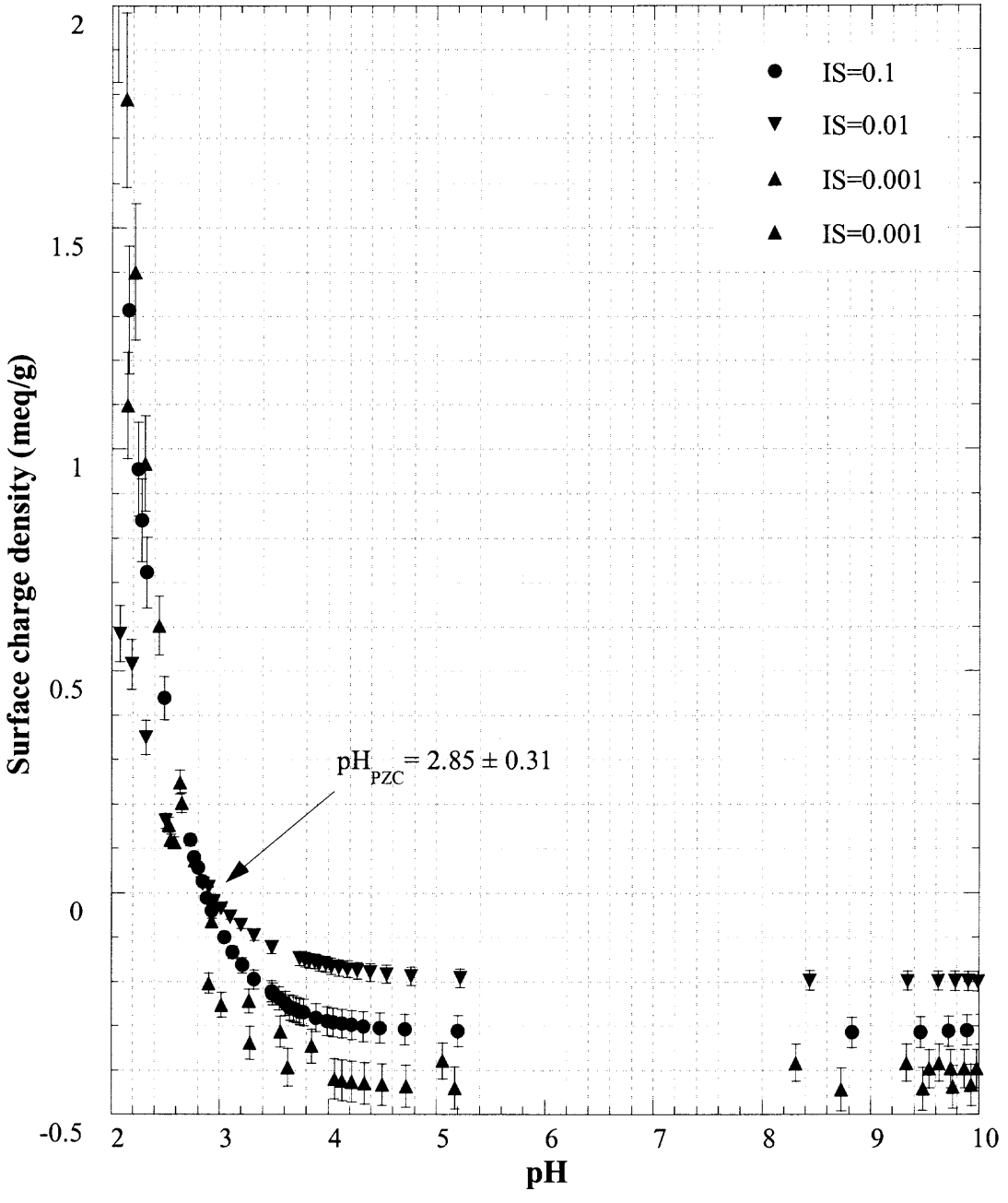

Figure 5.10 Potentiometric titration of 2 g L^{-1} acid-washed US silica with 0.1, 1, and 10 N NaOH where 1 N HNO_3 was used to adjust initial pH. Titration was conducted under a N_2 pressure of 35 psi.

5.3 Summary

From the results of XRD analysis, Alfa Aesar and US silica have XRD patterns that are similar with the standard PDF of α-quartz. Based on XRF the purity was 100% for Alfa Aesar silica and 98.759% for US silica. The modes of the size distributions revealed 220 μm for Alfa Aesar silica and 900 μm for US silica. From ESEM micrographs, Alfa Aesar and US silica show comparable surface roughness, both are potentially suitable for goethite coating with respect to column works. Because a pH greater than 9 may change the silica surface permanently and influence the surface charge determination further, titrations of silica were conducted with base in which the initial pH is low. The PZC of US silica is about 2.85 and is consistent with other studies.

In the next chapter, characterization results on iron oxide-coated silica are discussed, where US silica is applied.

CHAPTER 6

SYNTHESIS AND CHARACTERIZATION OF IRON OXIDE-COATED SILICA AND ITS EFFECT ON METAL ADSORPTION

Two methods were used for producing goethite-coated silica, a modified adsorption method based on Szecsody et al. (1994) and a modified precipitation method based on Meng and Letterman (1993a). To evaluate factors that influence the degree of coating, experiments were designed using a three-level fractional factorial method (Anderson and Mclean, 1974) to reduce the number of studies and isolate effects (Table 6.1). Factors investigated include coating temperature (T), mean diameter of silica particle (D), Fe concentration initially applied (Fe_{ini}), and aging time (t, for adsorption method only).

6.1 Synthesis of Goethite-Coated Silica

The Fe_{conc} before and after the abrasion study (Figure 6.1) demonstrated that approximately 0.5 to 11 mg Fe g^{-1} silica detached from the coating constituting as much as 80% of the initial loading. Scheidegger et al. (1993) separated coated sand with strongly bound goethite from weakly attached goethite aggregates by washing the system in a 1 M $NaNO_3$ solution. Stenkamp and Benjamin (1994) and Khaodhiar et al. (2000) washed the iron oxide-coated sand with DI water until the supernatant pH was about 7. Others (Edwards and Benjamin. 1989; Zachara et al. 1995; Kuan et al. 1998; Joshi and Chaudhuri, 1996) have rinsed until the runoff was visually clear. Abrasion is necessary before quantifying the degree of coating, and coating characteristics discussed below are those measured after the process.

Table 6.1 Experimental Conditions for Adsorption and Precipitation Coating Processes Based on the Fractional Factorial Experimental Design

Coating method	Experiment Run #	T (°C)	D (mm)	Fe_{ini} (% wt)	t (day)
Adsorption method	1	35	0.2	1	1
	2	35	0.9	3	2
	3	35	1.5	5	3
	4	60	0.2	3	3
	5	60	0.9	5	1
	6	60	1.5	1	2
	7	110	0.2	5	2
	8	110	0.9	1	3
	9	110	1.5	3	1
Precipitation method	10	60	0.2	1	N.A.*
	11	60	0.9	3	
	12	60	1.5	5	
	13	90	0.2	3	
	14	90	0.9	5	
	15	90	1.5	1	
	16	110	0.2	5	
	17	110	0.9	1	
	18	110	1.5	3	

* N.A.: not applicable.

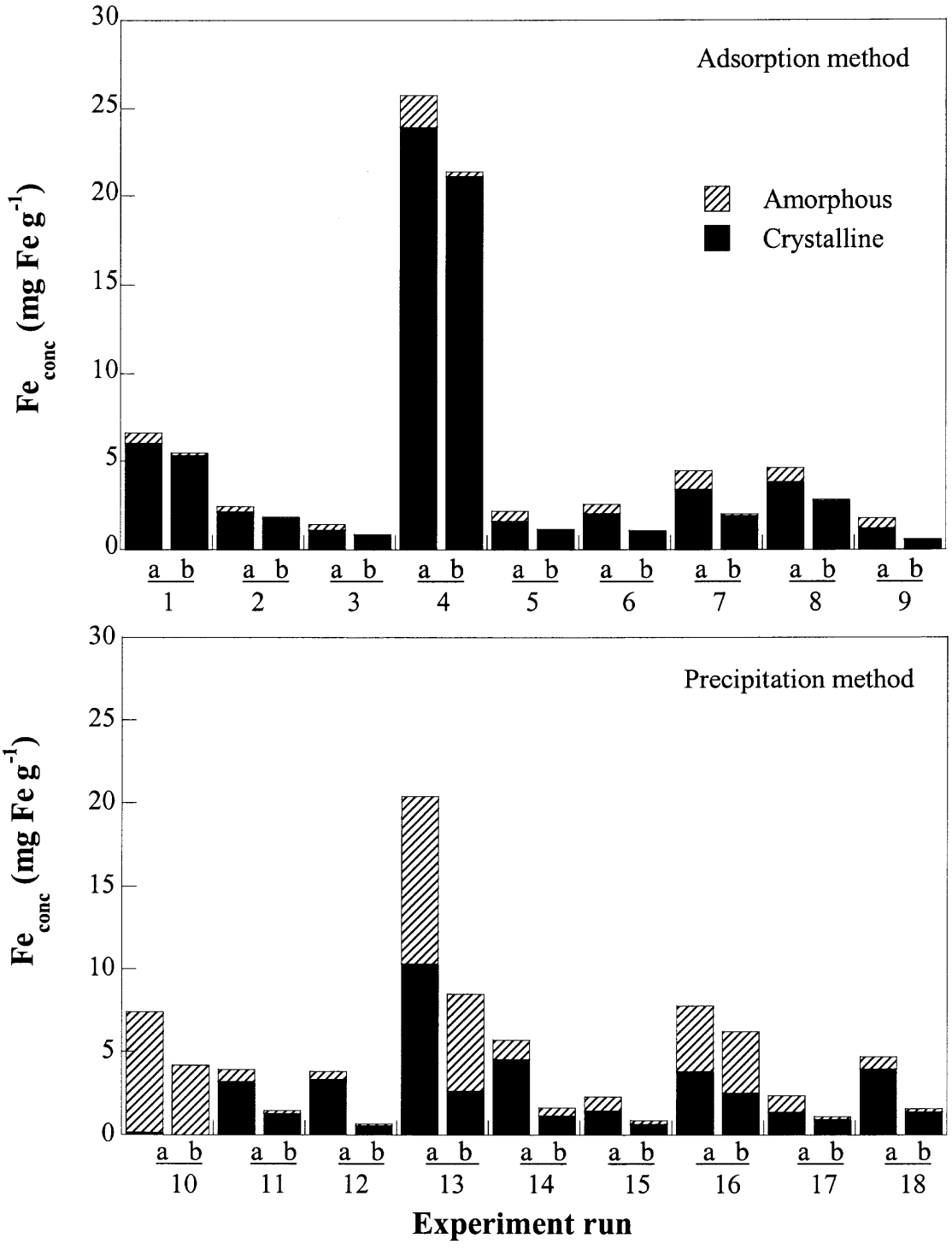

Figure 6.1 Comparison between Fe_{conc} before and after abrasion studies. Experiments 1 through 9 are based on the adsorption method, and 10 through 18 the precipitation method; column (a) represents Fe_{conc} before abrasion, and column (b) is that after abrasion.

Extraction results after abrasion showed the degree of coating was in the range of 0.59 to 21.36 mg Fe g^{-1} sand for adsorption and 0.67 to 8.5 mg Fe g^{-1} sand for precipitation (Figure 6.1). These results are consistent with those observed in soils and sediments (Ryan and Gschwend, 1994; Coston et al. 1995; Wang et al. 1993; Pieper et al. 1997). From the adsorption process, goethite constitutes greater than 95% (average 96.8%) of the oxide, while it is less than 89% (average 62.9%) employing precipitation. This difference may be explained by silica solubility evaluated with MINEQL+ (version 5.0) (Westall et al. 1976), where the dissolved $Si(OH)_4^0$ concentration is about 3×10^{-2} M at pH 12 and 25 °C; these conditions represent those used for the aqueous coating application (precipitation). Therefore, dissolved $Si(OH)_4^0$ may be incorporated into the iron oxide structure during precipitation. The resulting less crystalline form of iron oxide may be due to the presence of the substrate as well as silica dissolution, and has been observed by others (e.g., Anderson and Benjamin, 1985; Cornell et al. 1987) to inhibit crystallization. In the adsorption method, dissolution is not relevant as goethite was prepared before coating. Subsequently, in re-suspending the two minerals at pH 7.5 and 25 °C, dissolved $Si(OH)_4^0$ is approximately 10^{-4} M; however, the suspension is repeatedly rinsed after aging.

Given the observed oxide loadings, only silica was observed in the XRD patterns (Figure 6.2). Generally, the patterns of silica are similar to those of coated silica; the differences in the relative intensities may be attributed to the variability in preferred orientation of the silica sample. Nevertheless, powder residuals produced in the precipitation process at 110°C were confirmed to be goethite (Figure 6.2, and enlarged in Figure 6.3 for detailed planes). As discussed earlier, Lo et al. (1997) found amorphous

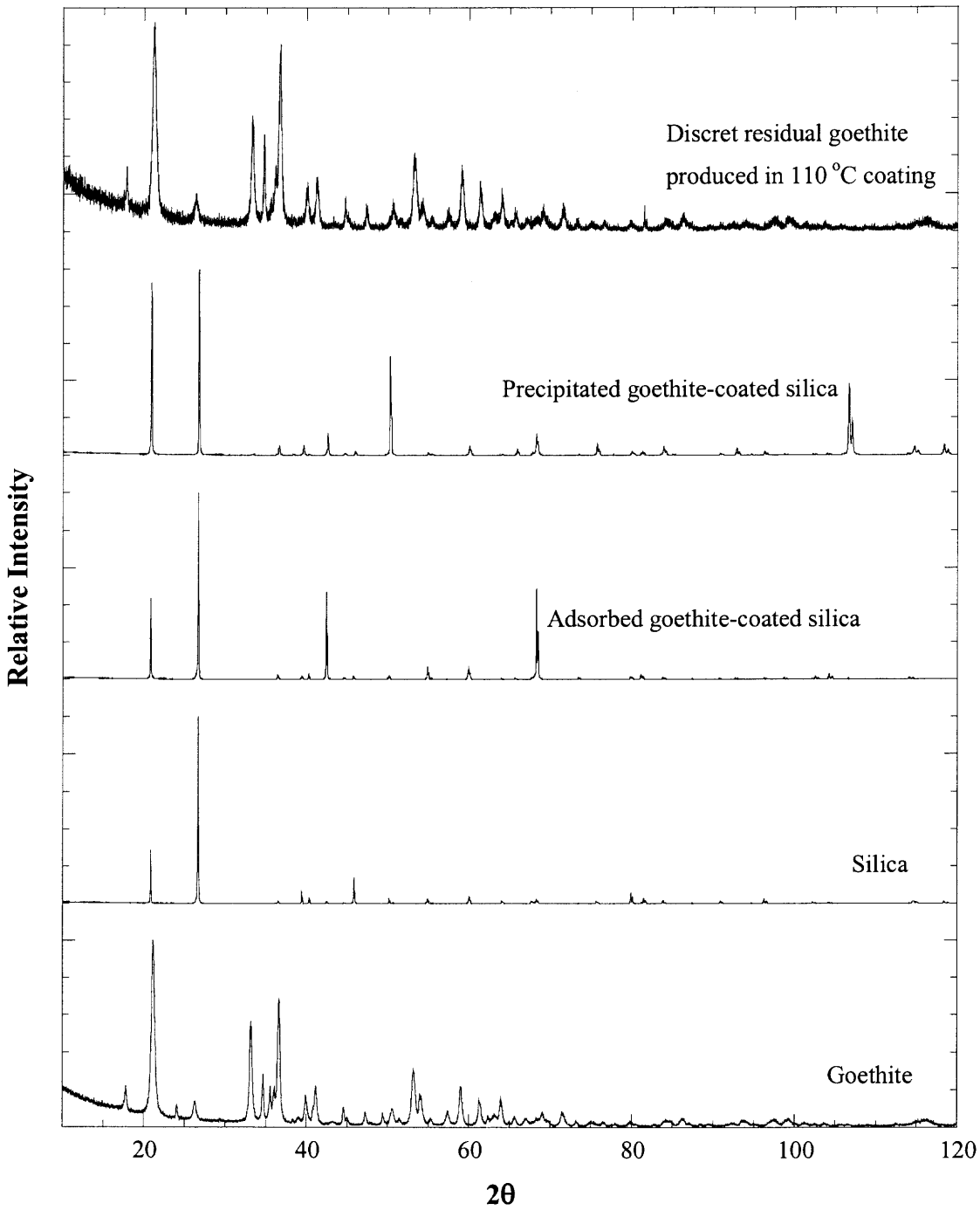

Figure 6.2 XRD patterns for goethite, silica, goethite-coated silica, and residual goethite produced in the coating process.

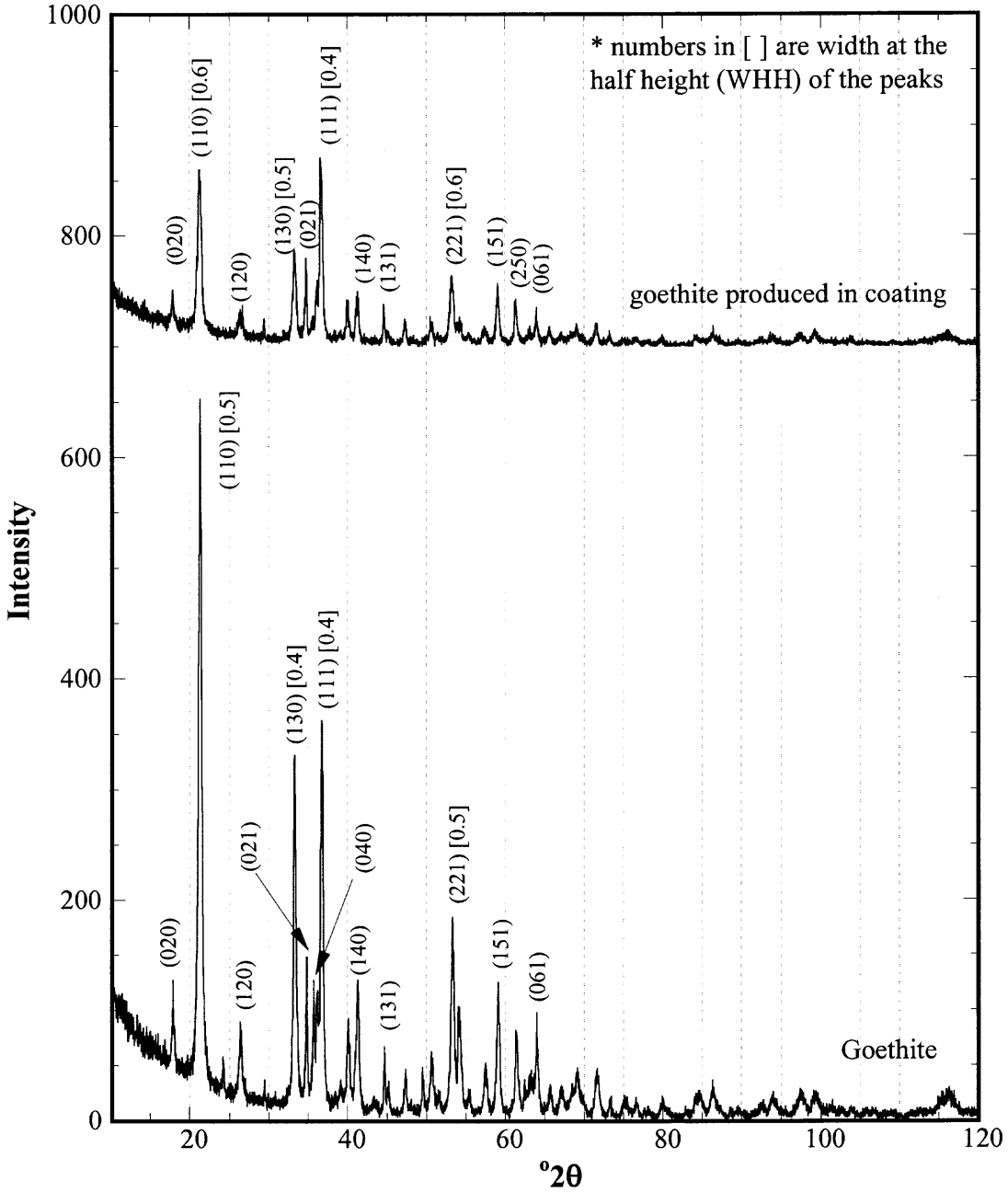

Figure 6.3 XRD analysis of goethite produced in coating.

iron oxide coatings at 60°C, goethite and hematite at 150 °C, and hematite above 300 °C. Zhong et al. (1999) observed amorphous iron oxide coatings transformed to γ-Fe_2O_3 (maghemite) after heating oxide-coated alumina at 400 °C. In this study, hematite was not observed even at the most elevated temperatures.

However, temperature was observed to affect the degree of coating (Figure 6.4), which was greater at 60 °C than 35 °C in adsorption and again greater at 90 °C than 60 °C in precipitation. The oxide coating decreased at the highest temperature (110 °C), which is similar to that observed by Stahl and James (1991a) where iron oxide coating decreased as the temperature increased from 105 °C to 500 °C. Nevertheless, increased oxide coating at greater temperatures has also been achieved (Edwards and Benjamin, 1989; Scheidegger et al. 1993). For example, Edwards and Benjamin (1989) and Scheidegger et al. (1993) observed greater coating at higher temperatures (110 and 120 °C, respectively) than lower ones (room temperature and 110 °C, respectively). Interestingly, Lo and Chen (1997) found no significant difference between the amount of iron oxide coated at 105 and 200 °C. Also, a number of researchers (Edwards and Benjamin, 1989; Lo et al. 1997; Bailey et al. 1992) have reported that higher coating temperatures enhanced attachment. Therefore, the effect of temperature on coatings may require further investigation with respect to oxide concentration and mineralogy. Overall, based on the results of the experimental design (Figure 6.4), the most significant factor in the coating process is particle size (D) where coating increased as the substrate particle size decreased; other factors (T, Fe_{ini}, and t) are of less importance. Optimal coating factors are a temperature of 60 °C for adsorption and 90 °C for precipitation, a

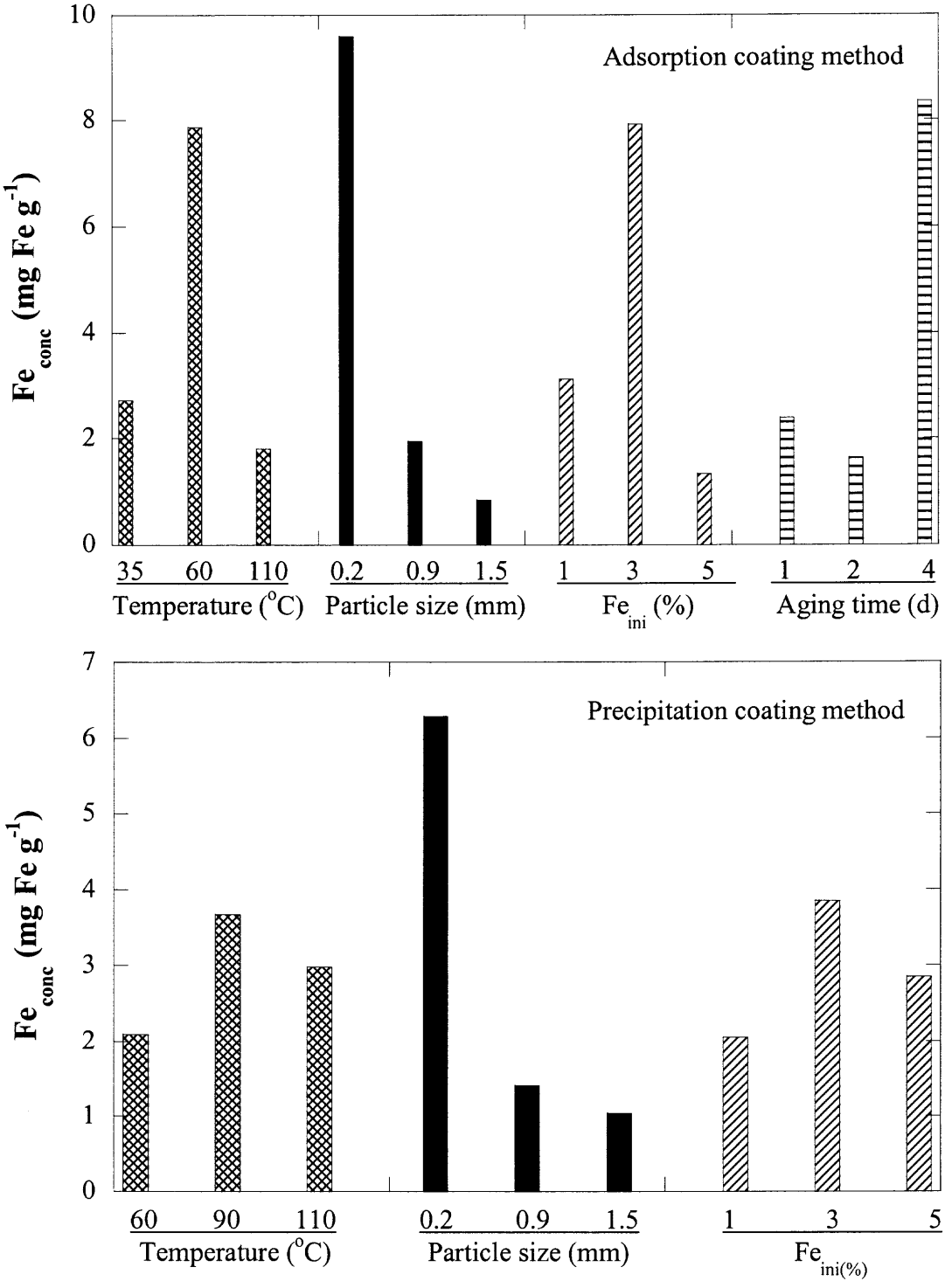

Figure 6.4 Effect of coating conditions from the fractional factorial study.

substrate diameter of 0.2 mm, an initial Fe concentration of 3% (by weight as Fe), and for adsorption an aging time of 4 days (Figure 6.4).

6.2 Characterization of Iron Oxide-Coated Silica

The coated silica with the highest iron concentration (21.36 mg Fe g^{-1} solid, coated by adsorption method at pH 7.5 and 60 °C) was analyzed with FTIR to investigate interactions between the substrate and coating. Overall, the spectrum of goethite-coated silica is very similar to that of silica (Figure 6.5); therefore a difference spectrum was calculated based on the approach described by Scheidegger et al. (1993). Despite the weak signal as a result of the low iron concentration, the difference spectrum showed characteristic goethite absorption bands at 892, 795, and 455 cm^{-1}, suggesting unambiguously that goethite was coated on the silica surface. The appearance of the 1080 cm^{-1} peak in the difference spectrum may indicate enhanced asymmetric stretching of SiO_4. The Fe-O stretching band was found to shift from 640 to 620 cm^{-1} and an absorption band at 825 cm^{-1} appeared in the difference spectrum as well (Figure 6.5). Interestingly, absorption bands at similar positions, 580 and 825 cm^{-1} (olivine, Christensen et al. 2000), 612 and 848 cm^{-1} (olivine, Gadsden, 1975), and 566 and 828 cm^{-1} (fayalite, Gadsden, 1975; Fabian et al. 2001) have been observed for iron silicate minerals. Additionally, other researchers have reported that substitution of Fe^{3+} for Si^{4+} caused a substantial shift of the Si-O-Si stretching band (1080 cm^{-1}) to lower frequencies, for example, a shift to 750 cm^{-1} for a lignitic coal ash slag (Nowok et al. 1993) and 940 cm^{-1} for a ferrihydrite sample precipitated with 4.35% Si by weight (Schwertmann and Thalmann, 1976). Comparing the coating spectrum to that of the physically mixed

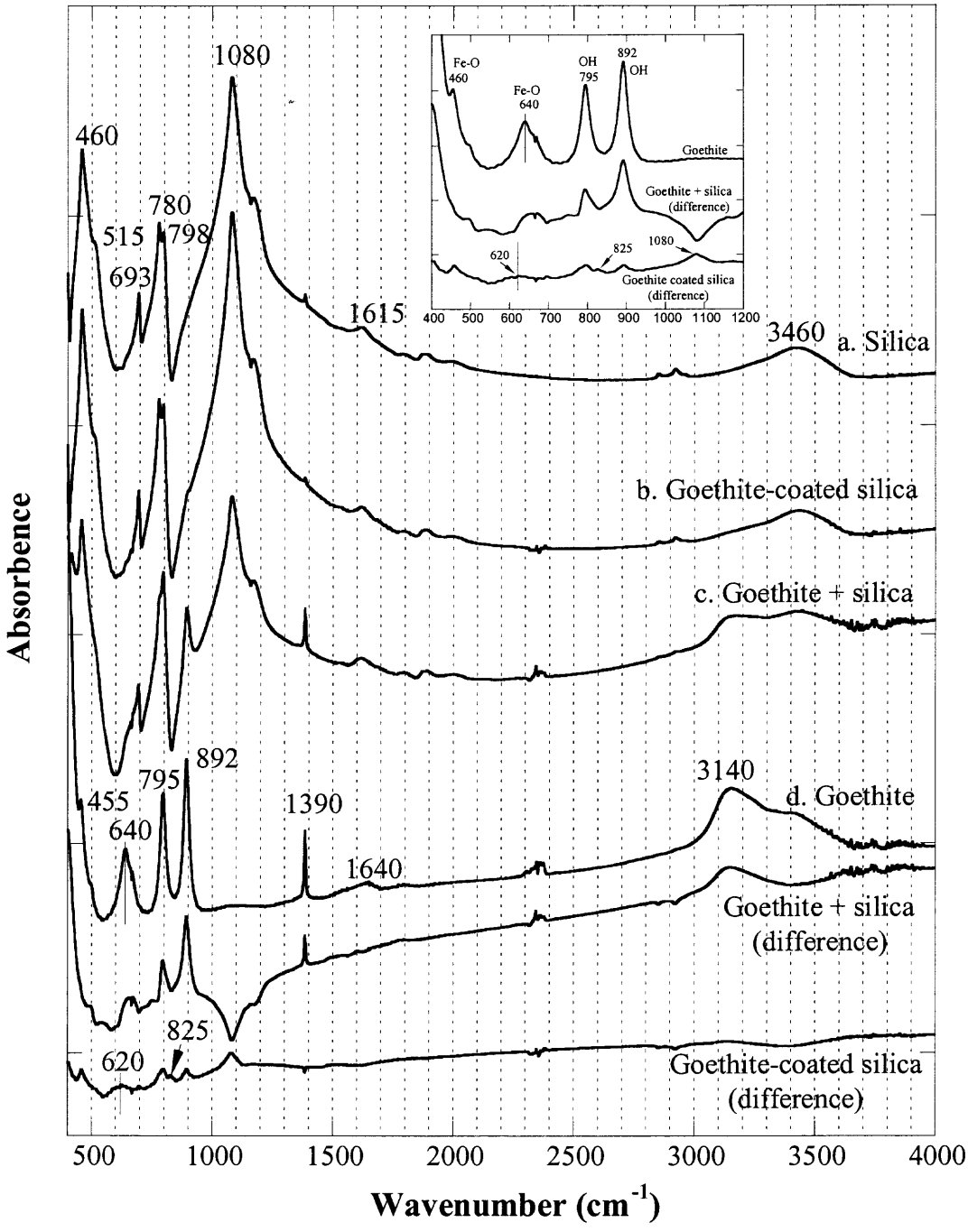

Figure 6.5 FTIR spectra of a. silica; b. goethite-coated silica (21.36 mg Fe g^{-1} solid, coated with adsorption method at pH 7.5 and 60 °C); c. physically mixed goethite and silica (20.76 mg Fe g^{-1} solid); and d. goethite. The 1390 cm^{-1} peak reveals existence of the NO_3^- impurity in the goethite sample.

goethite and silica results in only the two distinct spectra (Figure 6.5). In attempt to understand the oxide-silica interfacial interactions, other samples coated by precipitation (pH 12) or with differing temperature (i.e., 35, 90, and 110 °C) were evaluated; because of the lower iron concentrations, however, only one goethite band was discernible in the difference spectra. Interactions between silica and the oxide coatings potentially involve electrostatic, van der Waals, and/or chemical bonds. Goethite was coated at pH 12 (as in precipitation method), where both goethite and silica are negatively charged, suggesting electrostatic repulsion. Furthermore, fluid shear from the abrasion study is approximately one to two orders of magnitude greater than van der Waals forces. Therefore, these results along with FTIR suggest the iron oxide-silica interaction may involve chemical forces.

Optically, red-brown goethite coatings were observed to be non-uniform and mostly located in concave rough areas (even before abrasion) (Figure 6.6), indicating that rougher areas of silica may result in higher loadings of coating material. ESEM images (Figure 6.7) reveal needle-shaped goethite crystals located mostly in rough areas as well. The precipitation method produced smaller crystals of goethite (< 150 nm) than the adsorption method (100-1000 nm) (Figure 6.7), and is somewhat consistent with the extraction analysis in that ferrihydrite was present suggesting the presence of silica may inhibit crystal growth. Elemental mapping from EDX analysis (Figure 6.8) shows Fe concentrating in rough areas, and the relative distribution of Fe and Si demonstrates a non-uniform coating on the silica surface, which is in agreement with others (Edwards and Benjamin, 1989; Scheidegger et al. 1993).

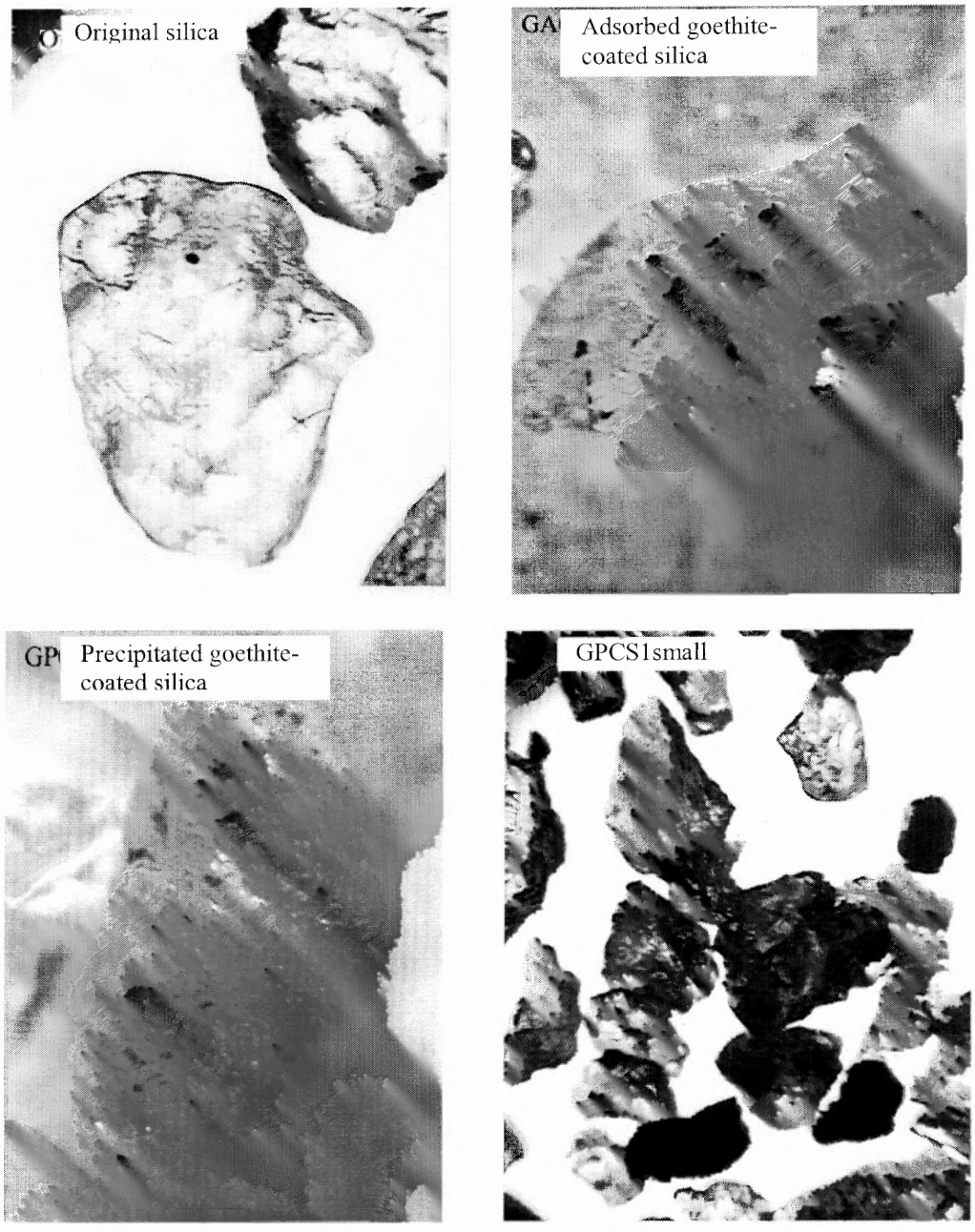

Figure 6.6 Optical micrograph of uncoated and coated US silica (1 cm in photograph represents 0.2 mm of real size).

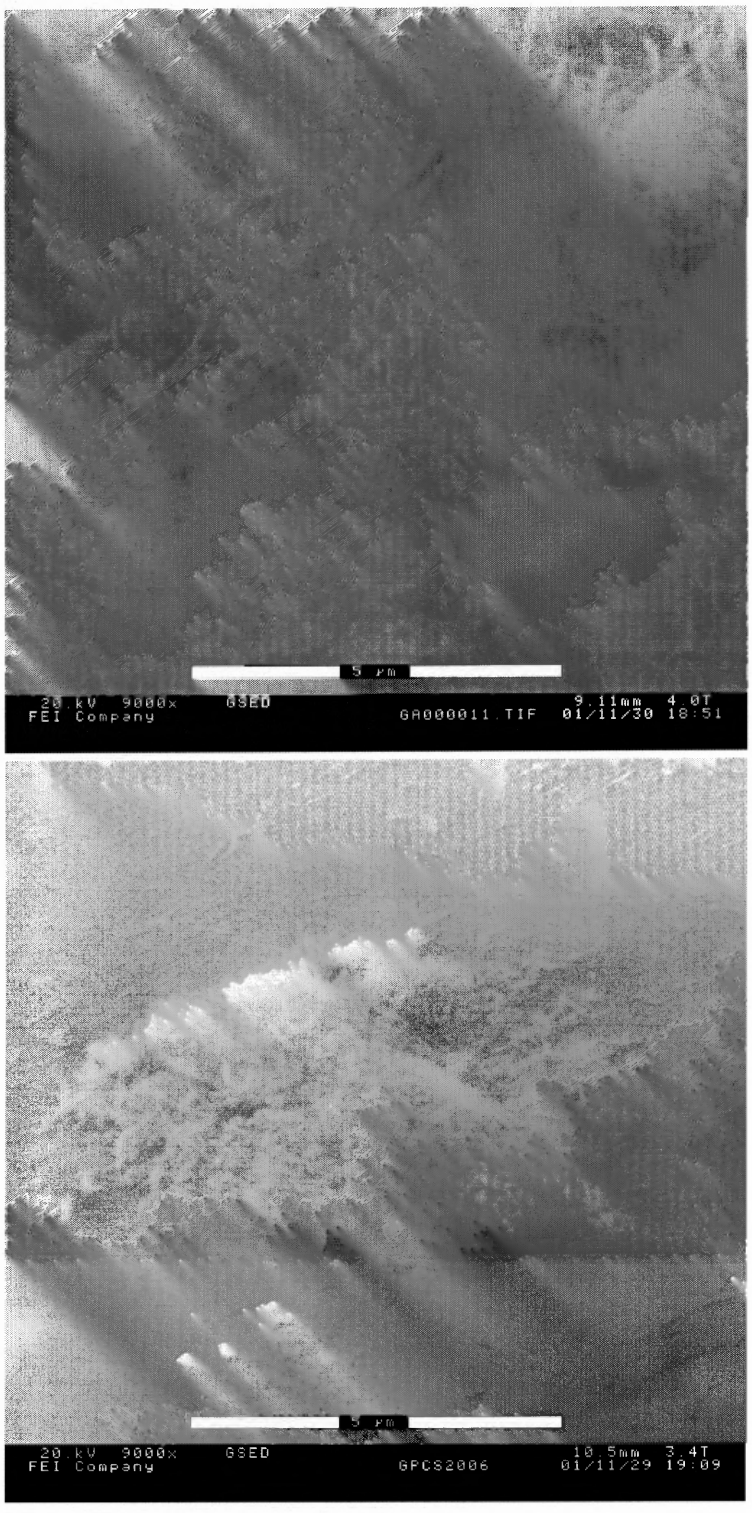

Figure 6.7 ESEM micrograph (9000×) of goethite-coated silica (after abrasion): upper figure is a rough area of goethite-coated silica using the adsorption method; lower figure is a smooth area of goethite-coated silica employing the precipitation approach.

1000×

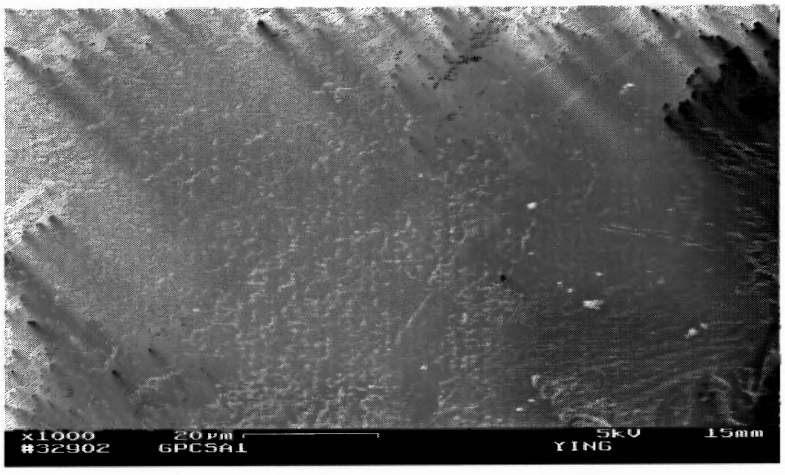

Fe mapping

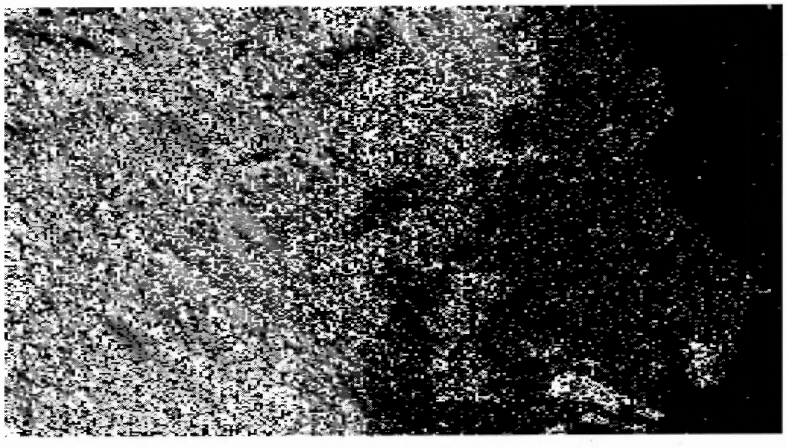

Si mapping

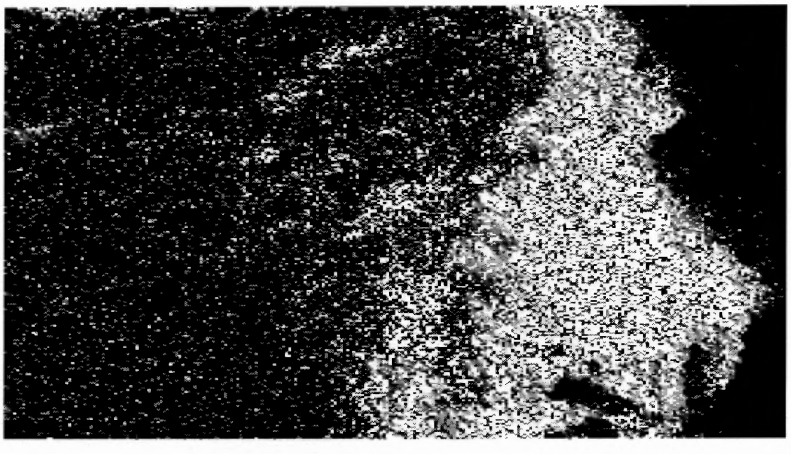

Figure 6.8 EDX results of goethite-coated silica (white images in mapping represent the corresponding element).

Furthermore, because discrete goethite particles are much smaller (0.2~100 μm, Trivedi and Axe, 2001a) than silica (average 900 μm) and the coatings accumulate in rough concave areas, the coating does not appear to impact the particle size distribution (Figure 6.9). However, the surface area of the coated systems increased by one to two orders of magnitude (Table 6.2) due to the attachment of fine iron oxide particles. Scheidegger et al. (1993) reported that the surface area of the goethite-coated sand is consistent with the theoretical sum of the surface areas of the pure silica and the corresponding weight fraction of goethite. The surface areas of goethite coatings were back calculated and resulted in 40 m^2 g^{-1} for the adsorbed and 78 m^2 g^{-1} for the precipitated forms. As observed in ESEM images the goethite coating is composed of sub-micrometer crystals (Figure 6.7) and is not comparable with aqueous aggregates (Trivedi and Axe, 2001a). In this study, although porosity is equivalent for all systems (about 8 ~ 9%, Table 2), smaller pores were observed with the coated silica versus the uncoated system (Figure 6.9). Intraparticle diffusion is an important process in metal sorption to amorphous hydrous ferric oxide (Trivedi and Axe, 2001a), however, with 8% porosity, this phenomenon is not expected to be significant for the goethite-coated silica.

Nevertheless, many studies have demonstrated the importance of Fe-oxide coatings in sequestrating metals (Uygur and Rimmer, 2000; Fuller et al. 1996; Lo and Chen, 1997; Khaodhiar et al. 2000; Stenkamp and Benjamin, 1994; Lo et al. 1997). Surface charge characteristics impact adsorption capacities (Scheidegger et al. 1993). Therefore, potentiometric titrations were conducted to investigate the surface charge distribution of uncoated and goethite-coated silica. The pH_{PZC} for the silica shifts to a higher pH with iron oxide coatings and is between that of pure silica and goethite

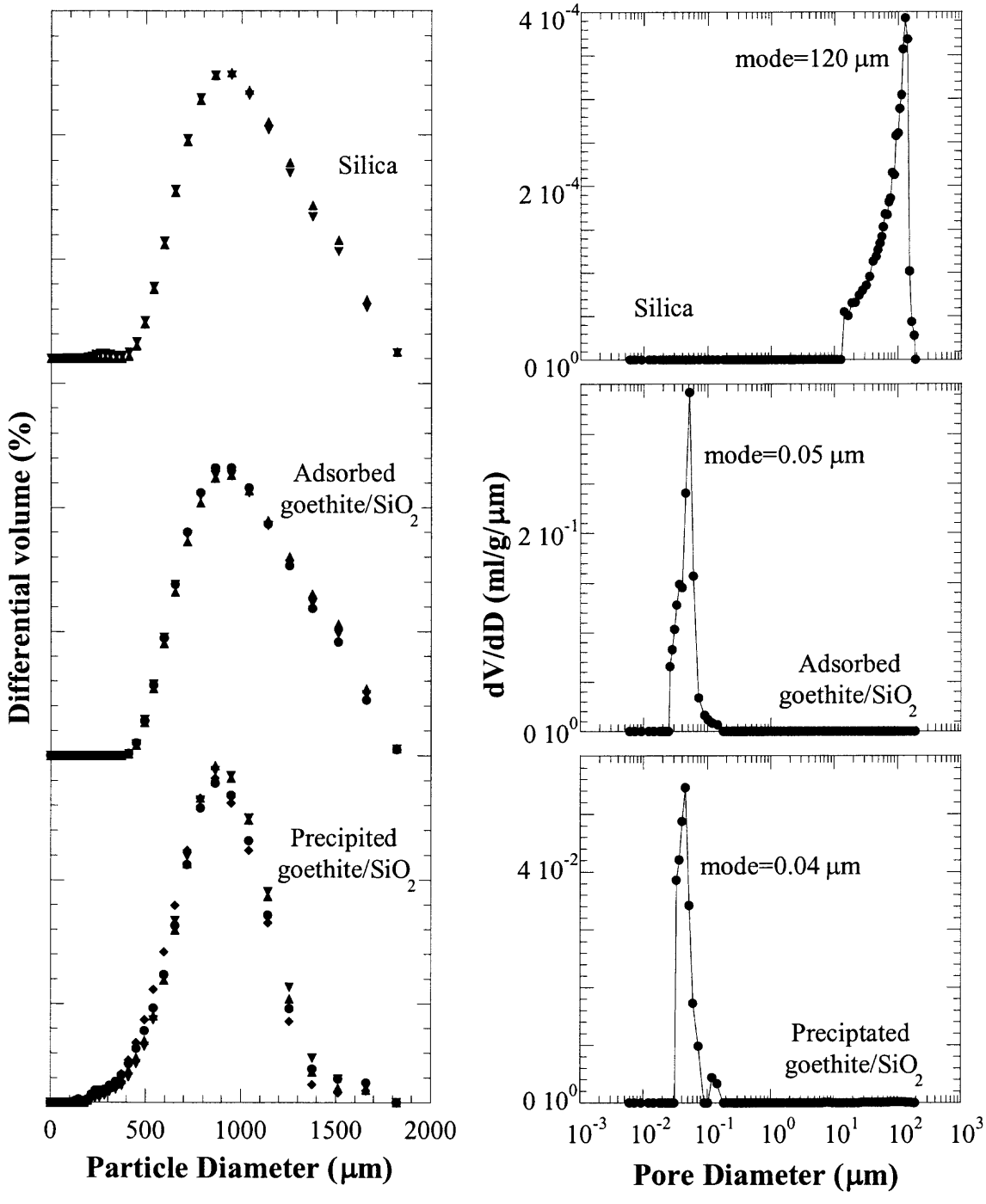

Figure 6.9 Pore size distribution (right) and particle size distribution (left) of uncoated and coated silica. (For particle size distribution: • IS=0.1, ▲ IS=0.01, ▼ IS=0.001 using $NaNO_3$, pH 6, average size of silica sample is 0.9 mm, 0.3 g L^{-1}).

Table 6.2 Surface Area and Porosity of Silica and Coated Silica

Sample	Silica	Adsorbed goethite coated silica*	Precipitated goethite coated silica*
Fe_{conc} (mg Fe g^{-1})	0.31	17.64	3.43
Porosity (%)	8.3315	8.9695	7.8814
Measured Surface area[1] (m^2 g^{-1})	0.0757	1.2092	0.5021
Calculated surface area of goethite coatings (m^2 g^{-1}) [2]	N.A.[3]	40	78

[1] Data from GTI (2002).
[2] Calculation based on the theoretical sum of the surface areas of silica and corresponding weight fraction of goethite is set equal to the measured value (Scheidegger et al. 1993).
[3] N.A. – not applicable.
* Measured before abrasion studies.

(Figure 6.10). Schwarz et al. (1984) had similar observations for a silica-alumina oxide mixture. Stenkamp and Benjamin (1994) found a pH_{PZC} close to 7.5 for an iron oxide-coated sand while those for sand and iron oxide are 3 and between 8 and 9, respectively. One study (Meng and Letterman, 1993a) showed that the ζ potential of the $Al(OH)_3/SiO_2$ suspension increased as the $Al(OH)_3/SiO_2$ ratio increased until uniform coverage was obtained and the isoelectric pH was equivalent to that of pure $Al(OH)_3$. Schwarz et al. (1984) demonstrated that a simple mass weighting model, originally proposed by Parks (1967), allows for an accurate determination of the pH_{PZC} of a silica-alumina oxide mixture. Using the Fe_{conc} and the theoretical surface area of goethite coatings (Table 6.3), the predicted values of the pH_{PZC} are 4.29 and 6.55 for adsorbed and precipitated oxide-coated silica, respectively, and are comparable to the measured values (Table 6.3) given the significant uncertainty.

Preliminary adsorption edges (Figure 6.11) show Ni adsorption on goethite-coated silica is greater than that of pure silica. Anderson and Benjamin (1990) reported that Cd^{2+} uptake by an $Al(OH)_3/SiO_2$ suspension was indistinguishable from that of $Al(OH)_3$ suggesting uniform coverage of the oxide. Meng and Letterman (1993a) observed that Cd^{2+} adsorption on an $Fe(OH)_3/SiO_2$ mixed oxide was consistent with discrete $Fe(OH)_3$, however, for the coated system discrete $Fe(OH)_3$ was present. In this study, the silica surface is partially coated and discrete goethite was not present during adsorption. The surface charge distribution reveals that both silica and goethite surfaces are available for adsorption. Assuming Ni adsorption occurs on both surfaces, overall adsorption may be explained as the sum of the two. However, the estimated adsorption is much less than that observed (Figure 6.11). To further understand the increase in sorption, Ni adsorption

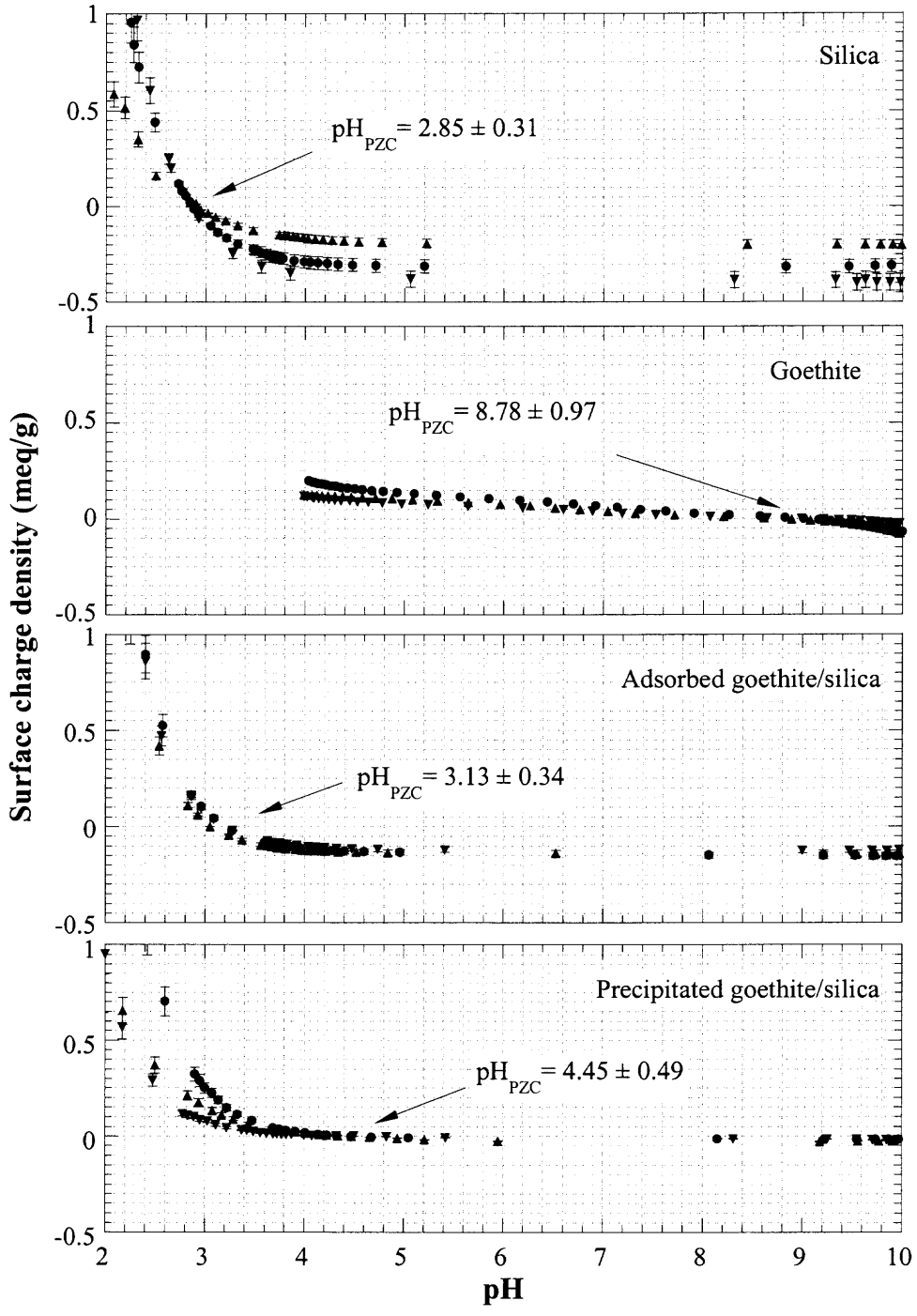

Figure 6.10 Surface charge distribution of silica, goethite, and goethite-coated silica (1 g L^{-1} solid). Ionic strength adjusted with $NaNO_3$: • IS=0.1, ▲ IS=0.01, ▼ IS=0.001. The PZC of the adsorbed goethite-coated silica is based on the crossover of two titration curves and the average pH at which zero charge occurred under each ionic strength. All other PZCs were determined by the crossover of three titration curves.

Table 6.3 PZC Measured and Calculated for Coated Silica (after Abrasion)

Sample	Silica	Adsorbed goethite-coated silica	Precipitated goethite-coated silica
Fe_{conc} (mg Fe g^{-1}):	-	0.47	0.59
Surface area of goethite coatings (m^2 g^{-1}):	-	33[1]	133[1]
pH_{PZC}:			
Measured:	2.85	3.13	4.45
Calculated[2]:	-	4.29	6.55

[1] Calculation based on Fe_{conc} and measured surface areas (GTI, 2002): silica 0.0757 m^2 g^{-1}; adsorbed goethite-coated silica 0.1 m^2 g^{-1}; precipitated goethite-coated silica 0.2 m^2 g^{-1}.

[2] pH_{PZC} calculated based on surface area-weighted average of two components – silica and goethite coating.

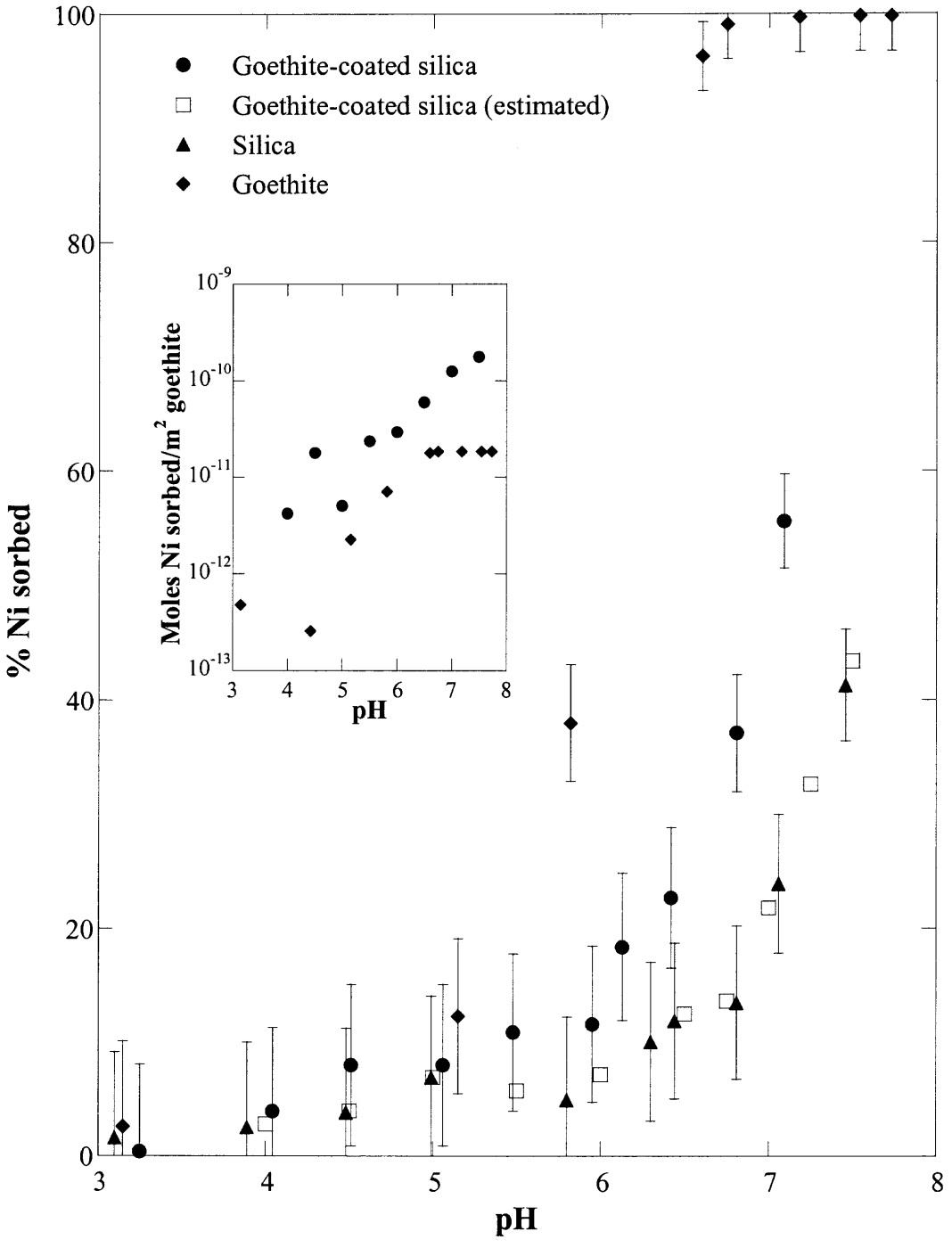

Figure 6.11 Ni adsorption edges on silica (5 g L^{-1}), goethite-coated silica (5 g L^{-1}, Fe concentration 4.01 mg Fe g^{-1} silica), and goethite (1 g L^{-1}), at ionic strength 0.01 ($NaNO_3$), $[Ni]_0=5\times10^{-10}$ M, and 25°C with 4 hours equilibration time. Estimated adsorption on coated silica was calculated based on weight fraction present of each surface.

to silica was deducted from that sorbed on the goethite-coated one and normalized to the theoretical surface area of the coating. Comparing adsorption to discrete goethite, Ni sorbed on coatings was approximately one order of magnitude greater (Figure 6.11 insert), suggesting a larger specific adsorption capacity. Uygur and Rimmer (2000) reached similar conclusions for Zn adsorption on iron oxide-coated calcite. These observations may suggest that the surface properties of discrete oxides may not be applicable when modeling the oxide-coated system. In summary, the complementary suite of analyses used in this research demonstrates that the presence of sub-micrometer iron oxide coatings at the mineral-water interface increased the adsorption capacity as compared to the discrete oxide.

6.3 Summary

In summary, a model system – iron oxide-coated silica was synthesized and characterized. Adsorption and precipitation methods were used for producing goethite coatings, which ranged between 0.59 and 21.36 mg Fe g^{-1} solid. A more crystalline form of iron oxide was achieved in adsorption than in precipitation potentially due to the effect of the substrate inhibiting crystallization. The degree of coating was highly sensitive to the particle size of silica. Abrasion studies were found to be necessary in removing the loosely attached goethite particles and the interaction between goethite and silica potentially involves chemical forces. The iron oxide coatings on the silica surface are non-uniform increasing surface area and introducing small pores. The pH_{PZC} of coated silica is between that of pure silica and iron oxide suggesting both silica and goethite surfaces are important for adsorption. Ni adsorption on the coated silica is greater than

that for pure silica, and the goethite coating exhibited a larger capacity than the discrete goethite system. Both characterization and adsorption studies reveal that sub-micrometer iron oxide coatings are produced; these coatings significantly increased adsorption capacity impacting interactions at the aqueous interface.

In the following chapters, mechanisms of heavy metal adsorption to iron oxide are investigated using XAS and are followed by surface complexation modeling and sorption to coated silica.

CHAPTER 7

SURFACE COMPLEXATION OF PB(II) ON AMORPHOUS IRON OXIDE: SPECTROSCOPIC AND TIME STUDIES

As discussed earlier in the hypothesis of this research, HFO is the precursor of goethite, and because they may have similar surface functional groups and surface structures, sorbed Pb(II) surface complexes are expected to be alike. This similarity was recently demonstrated in other studies (Manceau et al. 1992; Bargar et al. 1997b; Scheinost et al. 2001; Trivedi et al. 2003) where mononuclear bidentate complexes to edges of FeO_6 were observed. In this chapter, Pb/HFO sorption samples are analyzed with XAS. Because HFO is metastable and can transform into more crystalline form, Pb adsorption on HFO as a function of time is also studied and analyzed at both Pb L_{III}-edge and Fe K-edge.

7.1 Pb EXAFS of Pb/HFO Samples

Pb adsorption mechanisms on freshly precipitated HFO samples as a function of pH, ionic strength, Pb loading, and time have been studied (Table 7.1). The EXAFS spectra collected for Pb standards (PbO, $PbCO_3$, and aqueous $Pb(NO_3)_2$) are compared to Pb/HFO adsorption samples (Figure 7.1 and Figure 7.2). The $\chi(k)\cdot k^3$ spectra of PbO and $PbCO_3$ are similar to that observed by others (Bargar et al. 1997a; O'Day et al. 1998; Ostergren et al. 1999b) and the fitting results (Table 7.2) are consistent with XRD. The $\chi(k)\cdot k^3$ spectra of aqueous $Pb(NO_3)_2$ solution is characterized by a backscattering envelope dominated by a first-shell of oxygen atoms around the central Pb atom (Figure 7.1). The RSF clearly demonstrates this Pb-O contribution showing one peak at approximately 1.9 Å (Figure 7.3), which was fitted with 6.97 ± 0.43 O atoms at 2.5 ±

Table 7.1 Sample Preparation Conditions

Sample	pH	IS	Solid (g L^{-1})	$[Pb]_0$ (M)	$[Pb]_{eq}$ (M)	Pb_{ads} (mol g^{-1})	Reaction time
Pb/HFO 10^{-3} mol/g, pH6, IS 10^{-3}	6	2.8×10^{-3}	0.1	4×10^{-4}	5.9×10^{-5}	3.41×10^{-3}	4 hours
Pb/HFO 10^{-4} mol/g, pH6, IS 10^{-3}	6	5.6×10^{-3}	0.2	5×10^{-5}	9.0×10^{-6}	2.04×10^{-4}	4 hours
Pb/HFO 10^{-4} mol/g, pH5, IS 10^{-3}	5	5.6×10^{-3}	0.2	5×10^{-5}	9.4×10^{-6}	2.03×10^{-4}	4 hours
Pb/HFO 10^{-3} mol/g, pH5, IS 10^{-3}	5	5.6×10^{-3}	0.2	4×10^{-4}	1.6×10^{-5}	1.92×10^{-3}	4 hours
Pb/HFO 10^{-3} mol/g, pH5, IS 10^{-2}	5	5.6×10^{-2}	0.2	4×10^{-4}	1.8×10^{-5}	1.91×10^{-3}	4 hours
Pb/HFO, 1 month 10^{-3} mol/g, pH5, IS 10^{-2}	5	1.4×10^{-2}	0.3	5×10^{-4}	1.1×10^{-4}	1.75×10^{-3}	1 month
Pb/HFO, 4 month 10^{-3} mol/g, pH5, IS 10^{-2}	5	1.4×10^{-2}	0.3	5×10^{-4}	9.7×10^{-5}	1.80×10^{-3}	4 months
Pb/HFO, 9 month 10^{-3} mol/g, pH5, IS 10^{-2}	5	1.4×10^{-2}	0.3	5×10^{-4}	1.2×10^{-4}	1.72×10^{-3}	9 months
Pb/HFO, 14 month 10^{-3} mol/g, pH5, IS 10^{-2}	5	1.4×10^{-2}	0.3	5×10^{-4}	1.2×10^{-4}	1.73×10^{-3}*	14 months
Pb/HFO, 21 month 10^{-3} mol/g, pH5, IS 10^{-2}	5	1.4×10^{-2}	0.3	5×10^{-4}	1.2×10^{-4}	1.73×10^{-3}*	21 months

*: Data measured on the 392nd day. System was kept in turbulence and XAS samples were taken in the 14th and 21st month.

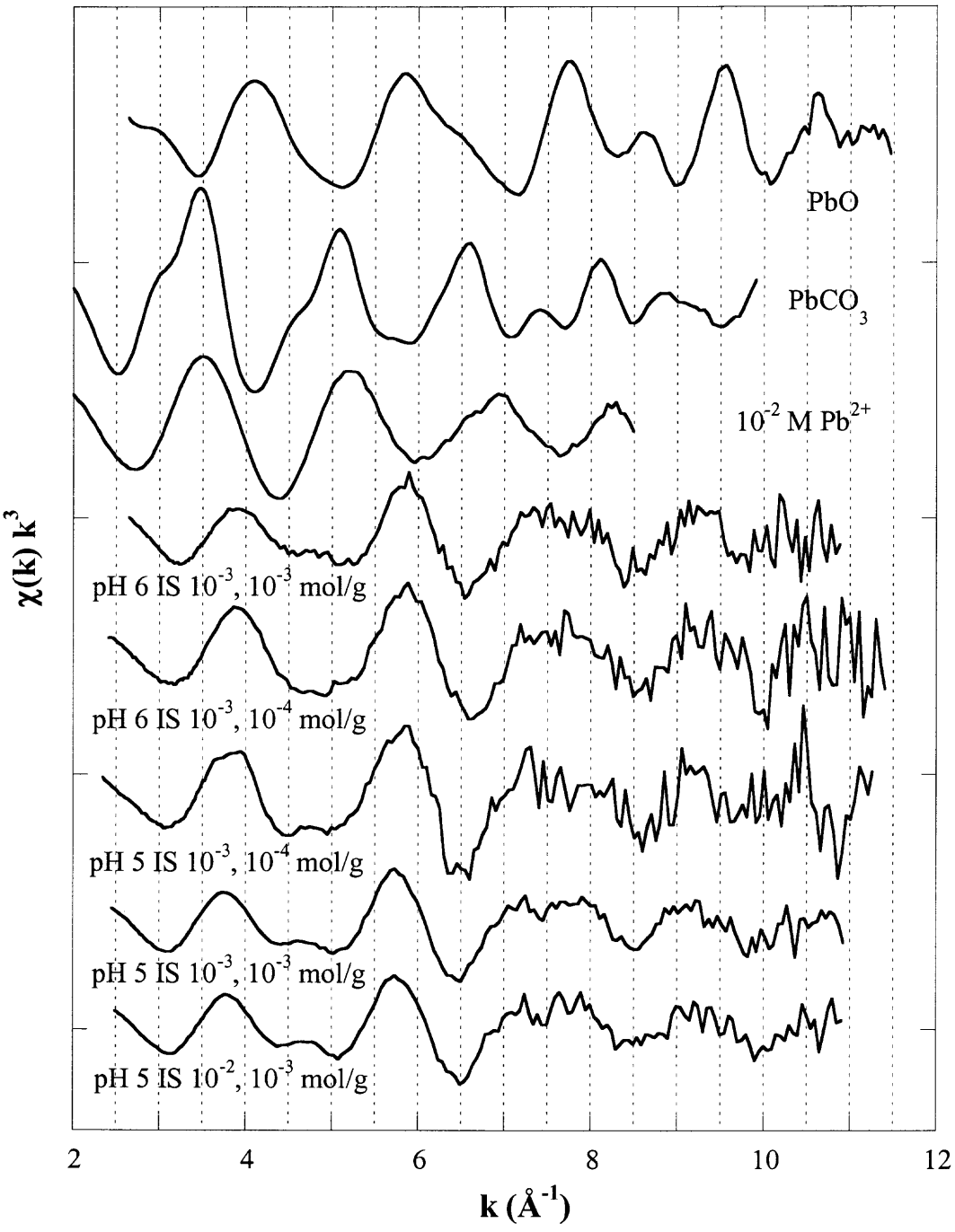

Figure 7.1 EXAFS spectra of Pb standards and 4-hour Pb/HFO sample at Pb L_{III}-edge.

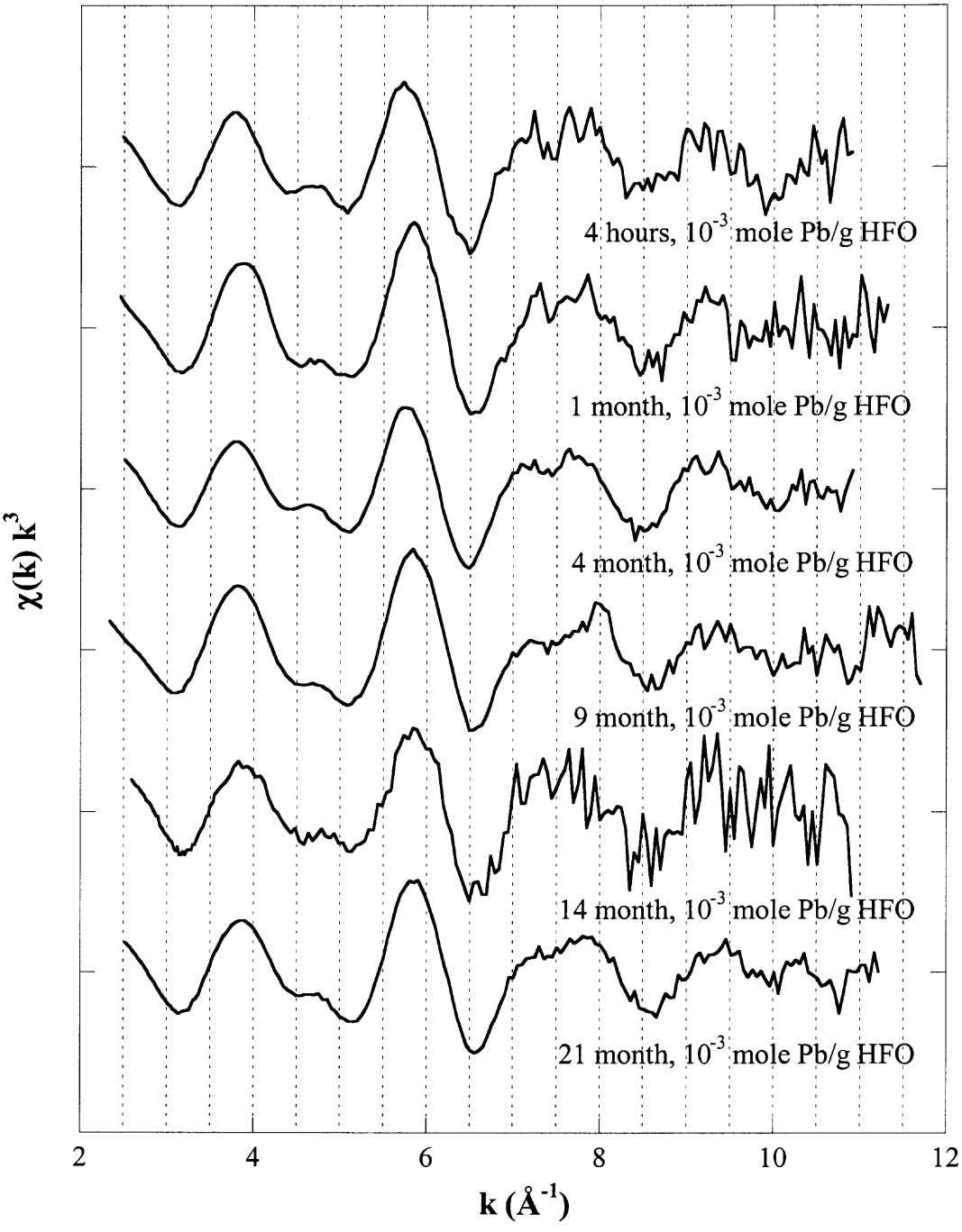

Figure 7.2 EXAFS spectra of Pb/HFO samples at pH 5 and IS 10^{-2} as a function of time at Pb L_{III}-edge.

Table 7.2 EXAFS Results of Pb Standards at Pb L_{III} Edge

Sample	Atom	N	R (Å)	σ^2 (Å^2)	ΔE_0 (eV)	Residual
β-PbO (XRD)[1]	O	2	2.24			
	O	2	2.48			
	Pb	4	3.54			
$PbCO_3$ (XRD)[2]	O	1	2.62			
	O	2	2.66			
	O	2	2.68			
	O	2	2.71			
	O	2	2.77			
	Pb	6	4.13			
	Pb	6	4.18			
PbO	O	1.87 ± 0.11	2.23 ± 0.01	0.006 ± 0.001	-11.68 ± 1.09	11.78
	Pb	1.41 ± 0.13	3.53 ± 0.01	0.005 ± 0.001		
$PbCO_3$	O	11.20 ± 2.60	2.60 ± 0.01	0.025 ± 0.003	-1.09 ± 2.27	15.54
	Pb	9.64 ± 0.27	4.15 ± 0.02	0.018 ± 0.001		
$Pb(NO_3)_2$	O	6.97 ± 0.43	2.50 ± 0.08	0.023 ± 0.001	-7.48 ± 0.44	6.64

Fourier transform was performed over range: PbO 3.0-10.8 Å^{-1}, $PbCO_3$ 2.08-9.79 Å^{-1}, Pb^{2+} 2.26-8.48 Å^{-1}; PbO was fitted over 0.74-3.95 Å, $PbCO_3$ 0.46-4.69 Å, and Pb^{2+} 0.42-3.0 Å.

N, coordination number; R, interatomic distance; σ^2, Debye–Waller factor; ΔE_0, edge shift

[1]: Hill (1985)

[2]: Sahl (1974)

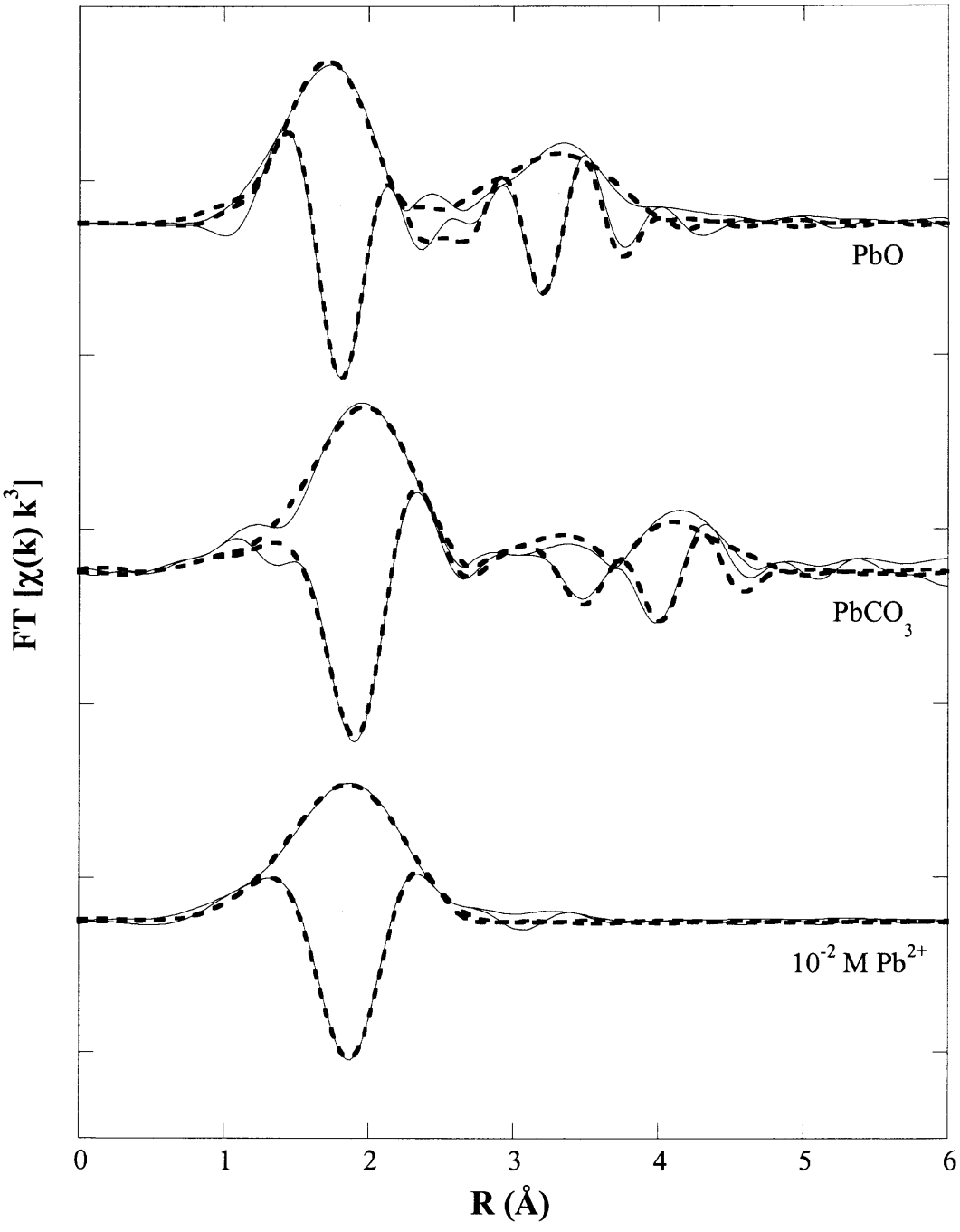

Figure 7.3 Fourier transform and fit of Pb standards spectra at Pb L_{III} edge. FT was performed over range: PbO 3.0-10.8 $Å^{-1}$, $PbCO_3$ 2.08-9.79 $Å^{-1}$, Pb^{2+} 2.26-8.48 $Å^{-1}$; PbO was fitted over 0.74-3.95 Å, $PbCO_3$ 0.46-4.69 Å, and Pb^{2+} 0.42-3.0 Å. Lines represent data, dashed lines represent fit.

0.08 Å. This octahedral structure represents that of fully hydrated Pb(II), as greater than 99% of the total Pb exists as Pb^{2+} in this aqueous sample. This result is consistent with other studies (Bargar et al. 1997a; Elzinga and Sparks, 2002).

All spectra of Pb/HFO sorption samples are different from those of PbO, $PbCO_3$, and aqueous $Pb(NO_3)_2$ (Figure 7.1 and Figure 7.2), suggesting unique structures from these standards. Overall, the spectra are dominated by the backscattering from a first shell of O atoms and beat features at 4.5 – 5.0 $Å^{-1}$ and 6.5 – 8.5 $Å^{-1}$ indicative of a heavier backscatter from second shell contributions. The $\chi(k)\cdot k^3$ spectra were Fourier transformed over the range 2.8 – 9.5 $Å^{-1}$ and fitted over the range 0.45 – 3.58 Å with a Fe-substituted PbO model generated theoretically using FEFF7 (Zabinsky et al. 1995). The RSFs show two peaks at ~1.9 Å and ~2.9 Å (Figure 7.4 and Figure 7.5), and fitting (Table 7.3) reveals 1.27 – 2.92 O atoms at 2.25 – 2.30 Å for the first shell. The second shell could only be fit with Fe atoms and resulted in 0.92 – 2.05 Fe atoms at 3.29 – 3.34 Å. The experimental amplitude and phase were reproduced by the fitting (Figure 7.4 and Figure 7.5). However, the larger Debye-Waller factor for the second shell (Table 7.3) suggests greater variation in the Pb-Fe distances than those for Pb-O.

The absence of Pb backscatters around the central atom suggests that the adsorbed Pb(II) ions on HFO are isolated mononuclear complexes. The absence of O as a second shell and the tighter Pb-O distances as compared to the hydrated form observed indicate that the waters of hydration were lost upon adsorption to HFO. Other EXAFS investigations (Manceau et al. 1992; Scheinost et al. 2001; Trivedi et al. 2003) reported that the adsorbed Pb(II) on ferrihydrite results in two O atoms at 2.3 Å and less than one to two Fe atoms at around 3.3 Å. The fitting results of this study are similar with those

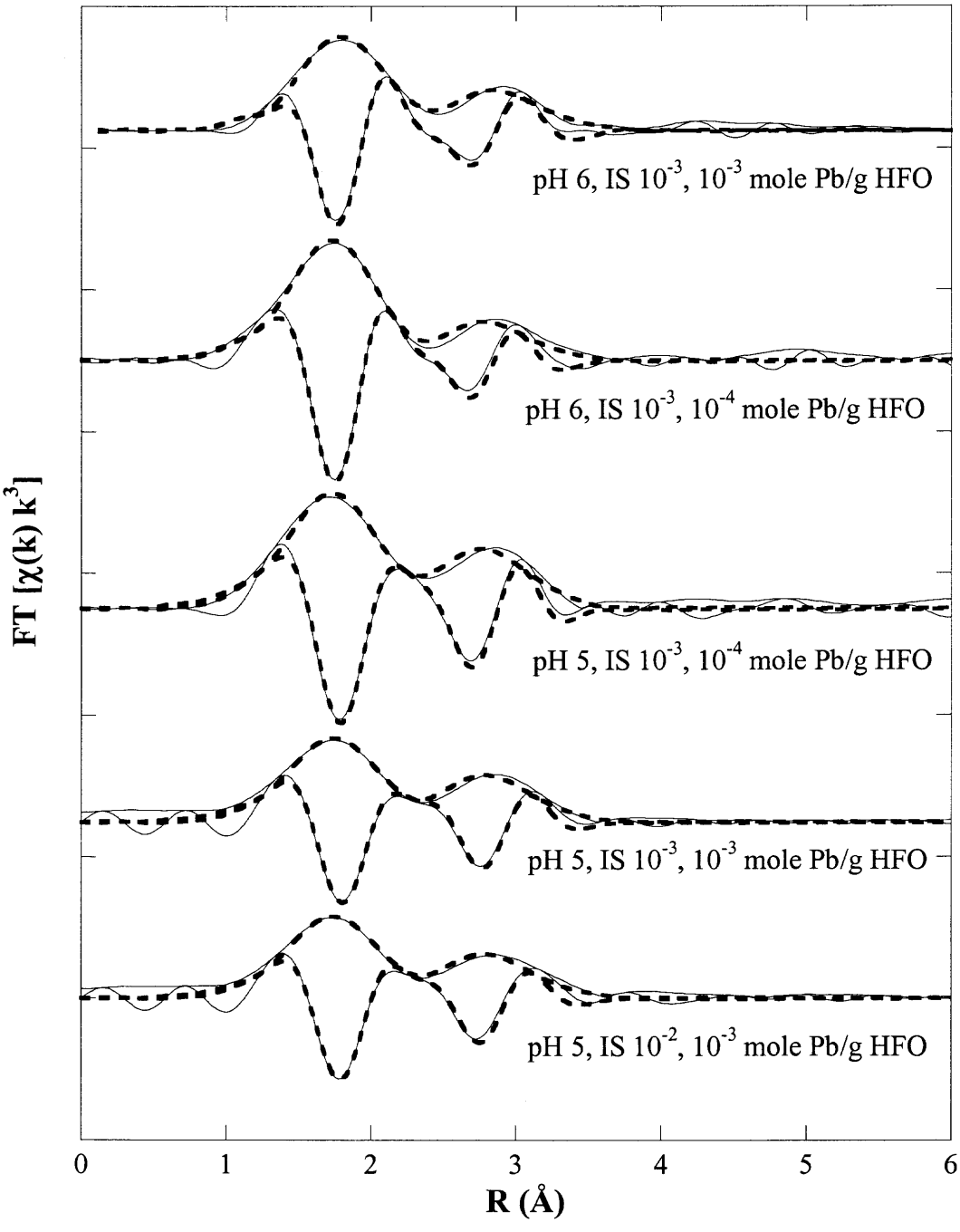

Figure 7.4 Fourier transform and fit of 4-hour Pb/HFO adsorption samples at Pb L_{III} edge. FT was performed over range 2.8-9.5 $Å^{-1}$, fitted over 0.45-3.58 Å.

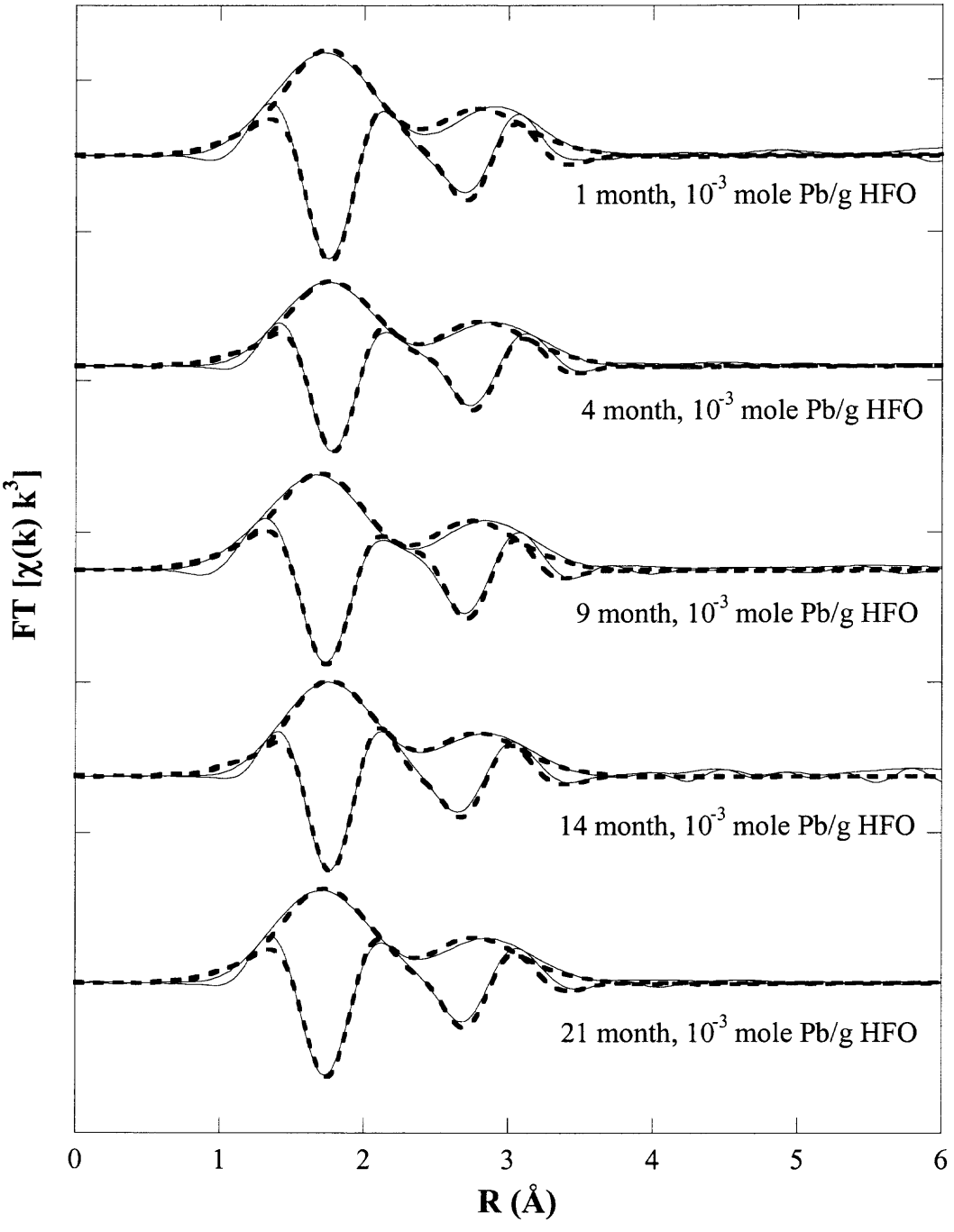

Figure 7.5 Fourier transform and fit of Pb/HFO adsorption samples at pH 5 and 10^{-2} ionic strength as a function of time at Pb L_{III} edge. FT was performed over range 2.8-9.5 $Å^{-1}$, fitted over 0.45-3.58 Å.

Table 7.3 EXAFS Results of Pb/HFO Samples at Pb L_{III} Edge

Sample	Atom	N	R (Å)	σ^2 (Å^2)	ΔE_0 (eV)	Residual
Pb-HFO 10^{-3} mol/g, pH6, IS 10^{-3}	O Fe	1.27 ± 0.06 2.22 ± 0.90	2.30 ± 0.01 3.34 ± 0.02	0.003 ± 0.001 0.019 ± 0.005	-8.84 ± 2.47	7.40
Pb-HFO 10^{-4} mol/g, pH6, IS 10^{-3}	O Fe	2.34 ± 0.80 0.92 ± 1.21	2.27 ± 0.03 3.29 ± 0.06	0.007 ± 0.002 0.010 ± 0.008	-13.86 ± 2.93	10.40
Pb-HFO 10^{-4} mol/g, pH5, IS 10^{-3}	O Fe	2.92 ± 0.41 1.40 ± 1.11	2.29 ± 0.02 3.29 ± 0.02	0.009 ± 0.002 0.011 ± 0.007	-14.98 ± 1.97	9.76
Pb-HFO 10^{-3} mol/g, pH5, IS 10^{-3}	O Fe	1.87 ± 0.29 1.57 ± 0.45	2.29 ± 0.01 3.33 ± 0.02	0.007 ± 0.025 0.013 ± 0.003	-15.43 ± 1.31	11.60
Pb-HFO 10^{-3} mol/g, pH5, IS 10^{-2}	O Fe	1.82 ± 0.31 1.76 ± 0.62	2.29 ±0.02 3.34 ± 0.02	0.008 ± 0.003 0.015 ± 0.007	-14.80 ± 2.98	12.23
Pb-HFO, 1 month 10^{-3} mol/g, pH5, IS 10^{-2}	O Fe	2.23 ± 0.12 1.97 ± 0.47	2.28 ± 0.02 3.32 ± 0.02	0.008 ± 0.055 0.016 ± 0.003	-12.22 ± 0.65	10.95
Pb-HFO, 4 month 10^{-3} mol/g, pH5, IS 10^{-2}	O Fe	1.43 ± 0.06 2.05 ± 0.39	2.30 ± 0.02 3.36 ± 0.01	0.005 ± 0.001 0.017 ± 0.003	-12.14 ± 0.27	9.21
Pb-HFO, 9 month 10^{-3} mol/g, pH5, IS 10^{-2}	O Fe	2.51 ± 0.15 1.27 ± 0.13	2.25 ± 0.02 3.30 ± 0.02	0.010 ± 0.001 0.011 ± 0.001	-15.86 ± 0.65	11.60
Pb-HFO, 14 month 10^{-3} mol/g, pH5, IS 10^{-2}	O Fe	1.34 ± 0.15 1.92 ± 2.09	2.29 ± 0.04 3.31 ± 0.05	0.004 ±0.002 0.017 ± 0.009	-11.16 ± 4.88	7.64
Pb-HFO, 21 month 10^{-3} mol/g, pH5, IS 10^{-2}	O Fe	1.76 ± 0.23 2.08 ± 0.21	2.27 ± 0.03 3.32 ± 0.04	0.007 ± 0.002 0.017 ± 0.001	-12.99 ± 4.10	9.46

Fourier transform was performed over range 2.8-9.5 Å^{-1}, fitted over 0.45-3.58 Å.
An S_0^2 of 0.91 was used to account for self-absorption based on the ratio of fluorescence to transmission data for aqueous Pb^{2+}.
N, coordination number; R, interatomic distance; σ^2, Debye–Waller factor; ΔE_0, edge shift

previous studies. Bargar et al. (1997b) proposed that the expected Pb-Fe distances are 2.91-3.49 Å for bidentate adsorption to edges of FeO_6 octahedra. Therefore, EXAFS analysis of Pb/HFO samples suggests that upon adsorption, Pb ions lose their waters of hydration and form mononuclear bidentate complexes at the edges of FeO_6 octahedra.

Pb/HFO sorption samples were prepared at pH 5 and 6, ionic strength from 10^{-3} to 10^{-2}, loading from 10^{-4} to 10^{-3} mole Pb g^{-1} HFO, and reaction time of 4 hours to 21 months; the similarity in $\chi(k)\cdot k^3$ spectra and the fitting results of all these samples indicate similar local structures. Therefore Pb adsorption to HFO may be described with one average type of mechanism under the experimental conditions tested. This result also suggests that Pb(II) forms similar surface complexes on the micropore walls as on the external particle surface as 23% of additional sites were occupied during intraparticle diffusion. In other words, internal and external adsorption sites are approximately equivalent. One assumption in earlier modeling efforts (Axe and Anderson, 1995, 1997; Trivedi and Axe, 2001a; Fan et al. 2005) was that the adsorption sites located along the micropore walls are no different from ones on the external surface; this assumption is verified in this current Pb/amorphous HFO EXAFS study.

The conversion of HFO to goethite and hematite has been reported to be slow at temperatures below 20 °C, and is further retarded by adsorbed species (Schwertmann et al. 1985; Cornell, 1987; Cornell et al. 1987). The effect of Pb(II) on the transformation of HFO to goethite or hematite during the long-term CBC studies is addressed in the following section.

7.2 Fe XAS of Iron Oxides and Pb/HFO Samples

Three iron oxides, freshly prepared HFO, goethite (α-FeOOH), and hematite (α-Fe_2O_3), and two Pb/HFO samples (reacted for 4 hours and 21 months respectively) were analyzed with XAS to study the crystallization of HFO. In the XANES analysis (Figure 7.6), the spectra of HFO and goethite were adjusted to correct for energy calibration at the Fe K-edge. All samples (Figure 7.6) have a similar pre-edge feature suggesting existence of defective FeO_6 octahedra (Combes et al. 1989). The more pronounced pre-edge structure for HFO samples indicates a greater degree of defects. Tetrahedrally coordinated Fe atoms produce a well-resolved shoulder (at about three fifths of the edge height) before maximum edge peak (Combes et al. 1989). The absence of such a feature in the spectra of HFO and its similarity to that of goethite, which exhibits octahedral (FeO_6) structure (Szytula et al. 1968), suggest HFO and Pb/HFO samples too have octahedral structure. This result is consistent with other studies (Manceau and Combes, 1988; Combes et al. 1989, 1990; Manceau et al. 1992; Charlet and Manceau, 1992; Manceau and Drits, 1993; Waychunas et al. 1993). Compared to hematite, goethite and HFO appear to have less features in the XANES spectra. Although relatively low in intensity, the shape of the edge crest of HFO is closer to that of goethite suggesting similarities. Also, similar edge crests were observed for HFO and Pb-sorbed HFO samples (aged for 4 hours and 21 months) indicating a similar local structure even as a function of reaction time.

The EXAFS spectra (Figure 7.7) of hematite and goethite reveal backscattering from multiple Fe atoms at different distances. The first two RSF peaks of each spectrum (Figure 7.8) can be fitted with O and two subshells of Fe atoms, respectively, for which the coordination numbers were fixed based on XRD results (Blake et al. 1966; Gualtieri

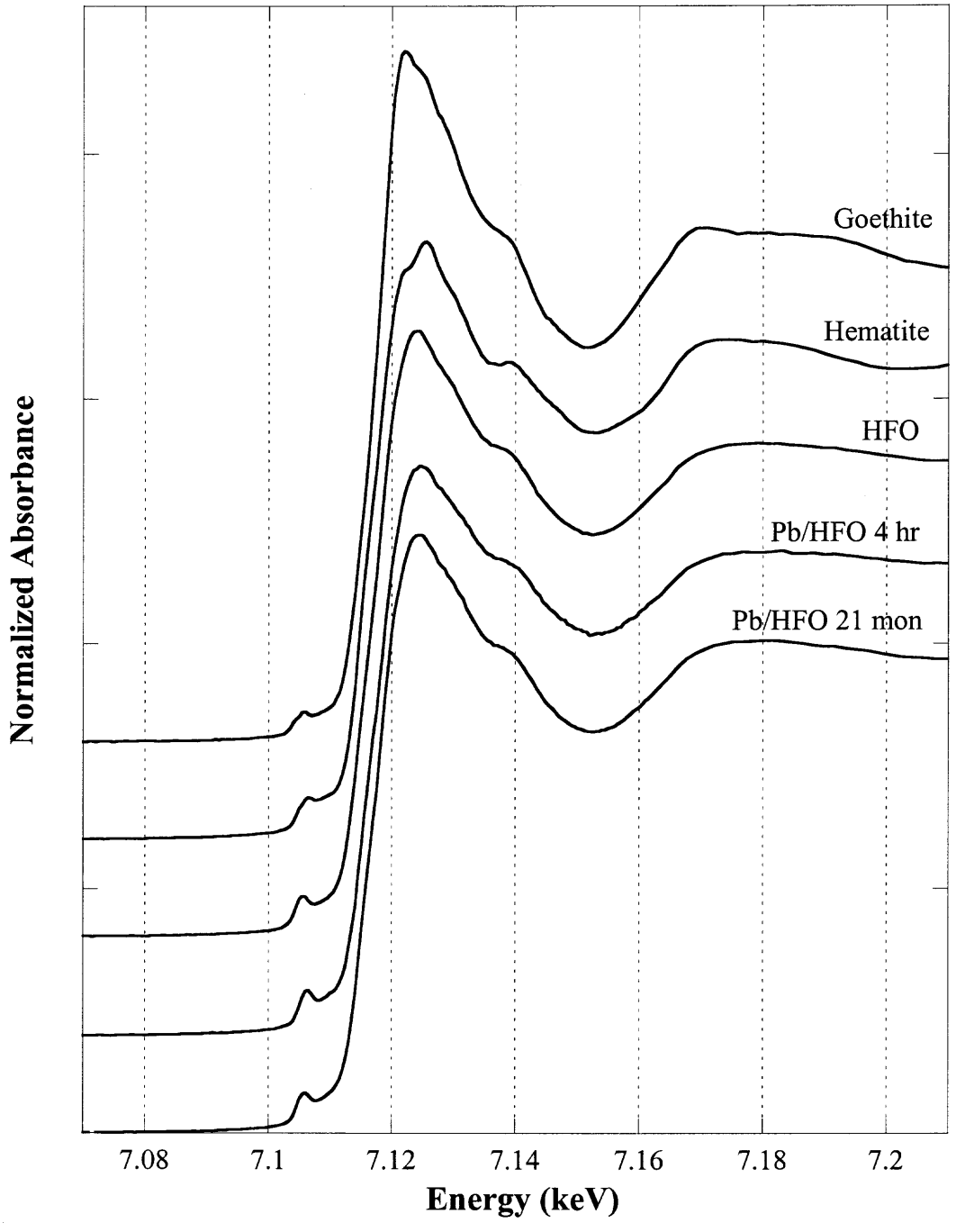

Figure 7.6 Fe K-edge XANES spectra of iron oxides.

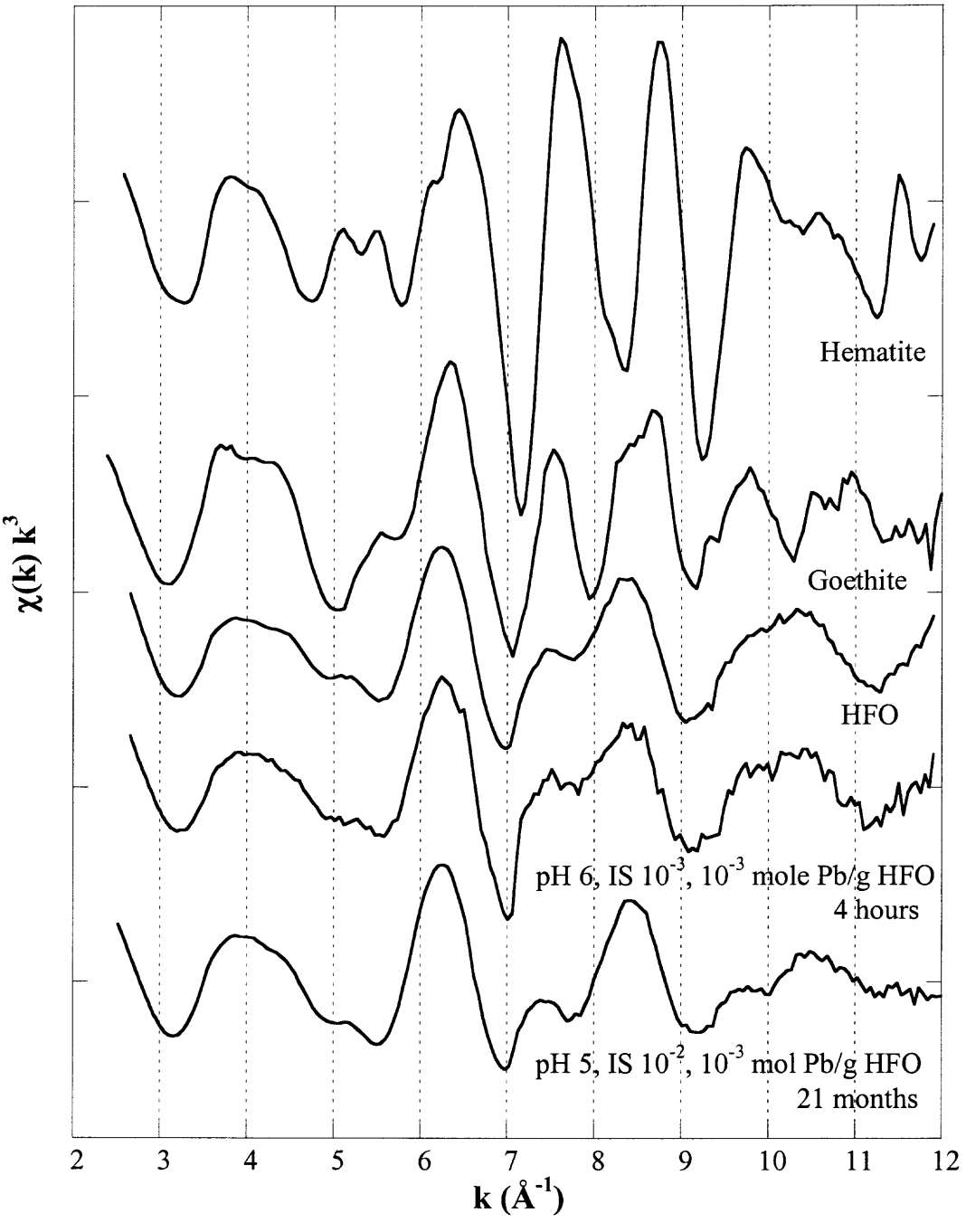

Figure 7.7 EXAFS spectra of iron oxides and Pb/HFO samples at Fe K-edge.

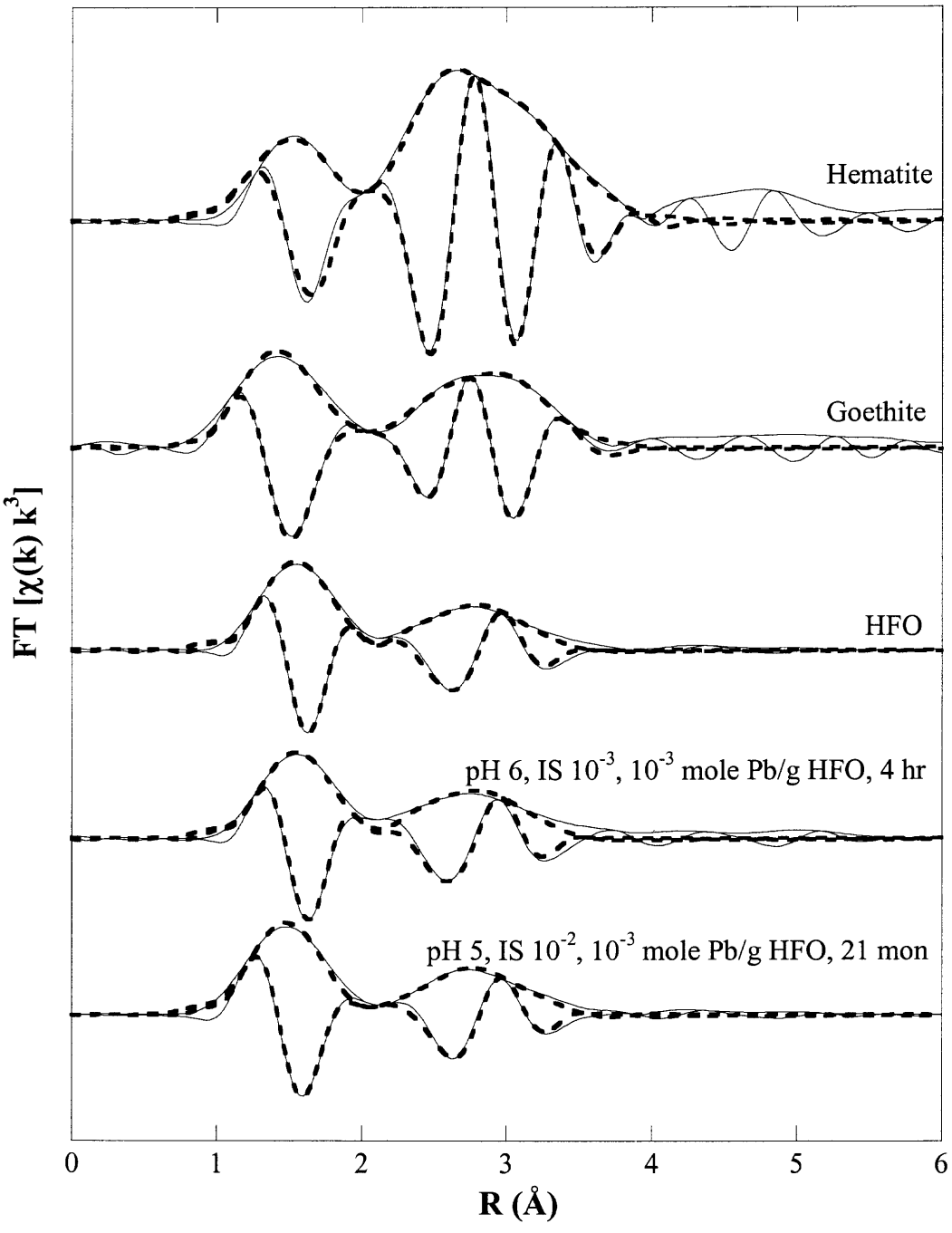

Figure 7.8 Fourier transform and fit of Pb/HFO adsorption samples at Fe K-edge. FT was performed over range: hematite 2.83-11.42 $Å^{-1}$, goethite 2.63-11.19 $Å^{-1}$, HFO and Pb-HFO sorption samples 2.86-11.77 $Å^{-1}$.

and Venturelli, 1999). Overall the fitting results are consistent with XRD data (Table 7.4), except the distance of the second Fe subshell for hematite is about 0.18 Å shorter than the theoretical value (3.36 Å). There are multiple Fe-Fe distances for hematite and goethite (Table 4); the fitting results represent an averaged local structure. The beat features in the $\chi(k)\cdot k^3$ data at about 5-5.6, 6.2, and 8.2 $Å^{-1}$ in the hematite spectrum and 3.8-4.4, 8.3-8.7, and 10.4-11.2 $Å^{-1}$ in the goethite spectrum represent contributions from Fe atoms beyond the second shell (Fe shell located at 2.93-3.29 Å). For hematite and goethite, the edge-sharing of FeO_6 octahedra produces Fe-Fe distances of 2.97-3.28 Å and that for double corner-sharing is 3.37-3.70 Å (Charlet and Manceau, 1992). Therefore, the beat features in the spectra suggest the presence of double corner-sharing between FeO_6 octahedra, which is necessary for crystal growth.

For HFO, many studies have reported an octahedral coordination environment (Manceau and Combes, 1988; Combes et al. 1989, 1990; Manceau et al. 1992; Charlet and Manceau, 1992; Waychunas et al. 1993). In this study, the spectra (Figure 7.7) of HFO show beats at 4.5, 5.2, 7.5, and 9.2-9.9 $Å^{-1}$ indicative of Fe atoms around the central one. The RSF (Figure 7.8) reveals two well-defined peaks that can be fitted with O and Fe atoms, respectively. Considering error, the fitted Fe-O distance is similar to those of hematite and goethite (Table 7.4). The Fe-Fe distance is in between those of hematite and goethite indicating existence of face-sharing octahedra, which produces the shortest Fe-Fe distance of 2.90 Å in hematite while there is no such sharing in goethite (Charlet and Manceau, 1992). Manceau and Combes (1988) also observed the presence of face-sharing $Fe(O,OH)_6$ octahedra in HFO which necessitates the dissolution-reprecipitation mechanism in the transformation from HFO to goethite. In crystalline iron oxides

Table 7.4 EXAFS Results of Iron Oxides and Pb/HFO Samples at Fe K-edge

Sample	Atom	N	R (Å)	σ^2 (Å^2)	C_3 (Å^3)	ΔE_0 (eV)	Residual
Hematite (XRD[1])	O	6	1.95-2.12**				
	Fe	1	2.90				
	Fe	3	2.97				
	Fe	3	3.36				
	Fe	6	3.71				
Goethite (XRD[2])	O	6	1.93-2.10***				
	Fe	6	3.01				
	Fe	6	3.29				
	Fe	12	3.43				
Hematite	O	6*	2.03 ± 0.02	0.011 ± 0.0001	0.0004 ± 0.0001	-7.02 ± 0.09	10.48
	Fe	4*	2.93 ± 0.02	0.005 ± 0.0001	-0.003 ± 0.0001		
	Fe	3*	3.18 ± 0.02	0.003 ± 0.0001	-0.0027 ± 0.0001		
Goethite	O	6*	2.08 ± 0.04	0.010 ± 0.001	0.0022 ± 0.0008	-1.30 ± 3.59	6.77
	Fe	6*	3.01 ± 0.02	0.012 ± 0.001	-0.0006 ± 0.0001		
	Fe	17 ± 15	3.29 ± 0.03	0.025 ± 0.011	-0.0021 ± 0.0003		
HFO	O	2.42 ± 0.03	2.03 ± 0.02	0.002 ± 0.0001	0.0006 ± 0.0001	-1.37 ± 0.33	11.09
	Fe	3.76 ± 0.13	2.95 ± 0.02	0.014 ± 0.0003	-0.0025 ± 0.0002		
Pb-HFO 10^{-3} mol/g, pH6, IS 10^{-3}	O	2.68 ± 0.21	2.03 ± 0.02	0.003 ± 0.001	0.0004 ± 0.0003	-2.40 ± 2.03	15.09
	Fe	4.32 ± 0.34	2.92 ± 0.04	0.014 ± 0.001	-0.0029 ± 0.0005		
Pb-HFO, 21 month 10^{-3} mol/g, pH5, IS 10^{-2}	O	3.79 ± 0.07	2.03 ± 0.02	0.005 ± 0.0001	0.0010 ± 0.0001	-3.26 ± 0.70	10.30
	Fe	3.36 ± 0.06	2.94 ± 0.02	0.012 ± 0.0003	-0.0026 ± 0.0001		

Fourier transform was performed over range: hematite 2.83-11.42 Å^{-1}, goethite 2.63-11.19 Å^{-1}, HFO and Pb-HFO sorption samples 2.86-11.77 Å^{-1}.
Hematite was fitted over 0.53-3.95 Å, goethite 0.63-3.76 Å, HFO and Pb-HFO samples 0.52-3.91 Å.
N, coordination number; R, interatomic distance; σ^2, Debye–Waller factor; C_3, third cumulant; ΔE_0, edge shift.
*: Fixed N numbers in hematite and goethite fitting; **: 3 O at 1.95 Å, 3 O at 2.12 Å; ***: 2 O at 1.93 Å; 1 O at 1.95 Å; 1 O at 2.07 Å; 2O at 2.10 Å.
[1]: Blake et al. 1966; [2]: Gualtieri and Venturelli, 1999.

(hematite, goethite, akaganeite, and lepidocrocite), edge-sharing and corner-sharing octahedra produce an Fe-Fe distance ranging 2.97-3.28 Å and 3.37-3.87 Å, respectively (Charlet and Manceau, 1992). The 2.95 Å Fe-Fe distance for HFO sample (Table 7.4) suggests the presence of face and edge-sharing polymer in HFO without corner-sharing.

The $\chi(k)\cdot k^3$ spectra (Figure 7.7), RSF (Figure 7.8), and the fitting results (Table 7.4) of 4-hour and 21-month Pb/HFO samples are similar to those of HFO. Fits were not obtained with Pb in the second shell, therefore Pb(II) ions do not appear to substitute into Fe positions in freshly prepared HFO even with Pb/Fe molar ratio of 0.37 (corresponding to 3.41×10^{-3} mole Pb g^{-1} HFO) or aged for 21 months. The similarity in EXAFS results of 4-hour and 21-month Pb/HFO with pure HFO suggests that HFO does not transform into a more crystalline form in the presence of Pb(II) during aging up to 21 months. The adsorbed Pb(II) ions binding to the edges of HFO polymers may block the edge and corner-sharing between HFO polymers thus inhibiting crystal growth. This observation is important for situations where adsorption occurs not long after ferric oxide precipitation (possibly in wastewater treatment), the large binding capacity of the amorphous oxide is maintained resulting in more effective removal of Pb (II).

7.3 Intraparticle Surface Diffusion Modeling

Results for Pb/HFO adsorption at pH 5 (Figure 7.9) show that approximately 72% sorbed within 30 min (Figure 7.9 insert). This fraction represents that sorbed to the external surface. The remaining Pb was sorbed through a much slower process. As discussed earlier, this second step was observed by maintaining a constant boundary condition with the Pb(II) in the bulk aqueous phase and therefore on the external surface. This slow

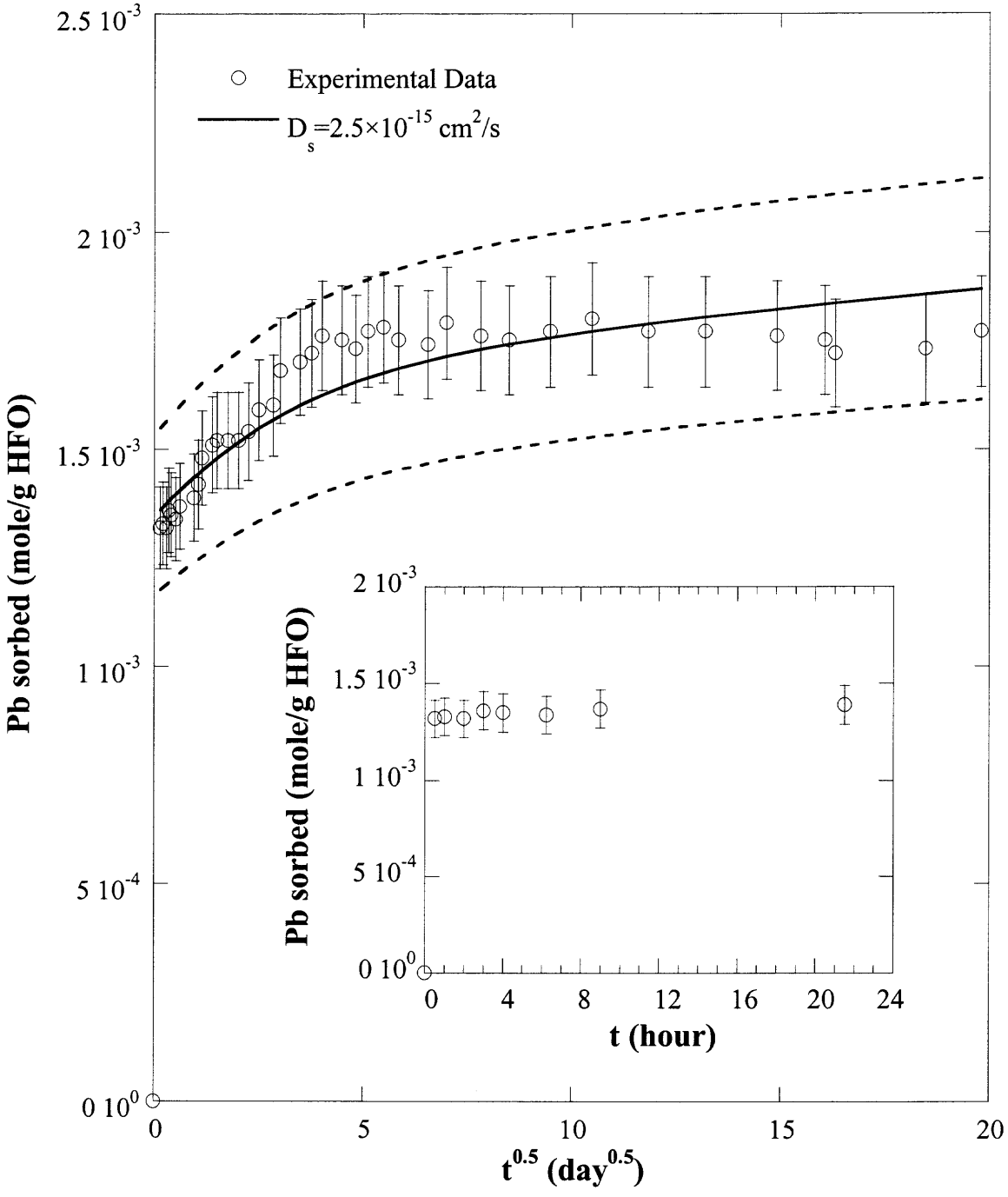

Figure 7.9 Pb/HFO CBC study on 0.3 g L^{-1} HFO at IS = 1.4×10^{-2}, pH = 5, and $[Pb]_e$ = 1×10^{-4} M. Dashed lines represent the error (± two standard deviations) of the model.

adsorption process was observed for over 10 months.

The above XAS results suggest that, in the presence of Pb(II), HFO remains in amorphous form for up to 21 months; Pb adsorption is invariant as a function of time. These conclusions support the assumption in modeling sorption to microporous amorphous oxides (Axe and Anderson, 1995, 1997; Trivedi and Axe, 2001a; Fan et al. 2005) that Pb adsorption sites located on the micropore walls are no different from ones on the external surface. Therefore, integrating the analytical solution over a spherical particle results in the amount of Pb sorbed to the internal surface of a single particle at a given time (Axe and Anderson, 1995, 1997; Trivedi and Axe, 2001a; Fan et al. 2005). The moles (M) sorbed internally is expressed below:

$$M = 4\pi C_S \frac{R^3}{3}\left[1 - \frac{6}{\pi^2}\sum_{n=1}^{\infty}\frac{1}{n^2}\exp\left(-\frac{Dn^2\pi^2 t}{R^2}\right)\right]$$

$$D = \frac{D_s}{1+\left(\frac{\varepsilon}{\rho K_i}\right)}$$

where C_s is the metal concentration sorbed on the oxide external surface, R is the radius of the particle, ϵ is the oxide porosity, ρ is the bulk density, K_i is the distribution coefficient representing the equilibrium constant times the internal site density, and D_s is the surface diffusivity.

The amount of Pb sorbed along the micropores times the number of particles with that radius was summed over the entire particle size distribution to obtain the total Pb concentration sorbed internally. The summation of Pb sorbed internally and externally provides the theoretical value of the total Pb sorbed. D_s is the only fitting parameter in the modeling process. The best-fit D_s is obtained by minimizing the variance between that

theoretically sorbed and the experimental data. Modeling results for Pb/HFO CBC experiment are shown as an example (Figure 7.9). The experimental data fall within two standard deviations of the model suggesting that the diffusion model fits data reasonably well. The best-fit D_s was 2.5×10^{-15} cm^2 s^{-1} suggesting a slow and rate-limiting process for Pb sorption to HFO. Results from many studies support that intraparticle diffusion is the rate-limiting step in metal sorption to microporous oxides (Waychunas et al. 1993; Theis et al. 1994; Axe and Anderson, 1995, 1997; Papelis et al. 1995; Strawn et al. 1998; Scheinost et al. 2001; Trivedi and Axe, 2001a; Strathmann and Myneni, 2005; Fan et al. 2005). The D_s of this study (2.5×10^{-15} cm^2 s^{-1}) is consistent with the range obtained by Fan et al. (2005) for Pb sorption in HAO, HMO, and HFO (10^{-16} to 10^{-14} cm^2 s^{-1}). Based on this surface diffusivity and boundary condition, it will take more than 20 years for Pb sorption to approach equilibrium where the internal sites account for ~ 46% of the total uptake.

7.4 Summary

Pb(II) adsorption mechanisms on freshly precipitated HFO as a function of time have been studied. XAS results reveal that the freshly precipitated HFO exhibits short-range order possibly forming edge and face-sharing polymers. The sorbed Pb(II) ions do not substitute for Fe in the polymer structure. However, by binding to the edges of octahedra polymers, Pb(II) ions inhibit crystallization of HFO, which is stable up to 21 months of aging, thus maintaining its large capacity for Pb(II). EXAFS analysis of Pb(II)-sorbed amorphous HFO samples suggests that Pb(II) ions form mononuclear bidentate edge-sharing surface complexes on FeO_6 octahedra. This mechanism appears to be invariant

of pH, ionic strength, Pb loading, and reaction time. Pb adsorption on HFO is a two-step process – a fast initial uptake followed by a slow surface diffusion step. The adsorption mechanism does not appear to change with reaction time (as long as 21 months) suggesting that internal sites on micropore walls are no different than the external ones. Intraparticle diffusion modeling based on this observation described the Pb/HFO long-term sorption data reasonably well. The surface diffusivity obtained from the modeling verifies a slow and rate-limiting diffusion process, which may occur for decades accounting for approximately 46% of total Pb uptake.

XAS results suggest Pb(II) forms similar surface complexes on a series of iron oxides exhibiting comparable surface structures and functional groups – amorphous HFO (this study and Manceau et al. 1992 for difference contact time), 2-line ferrihydrite (Scheinost et al. 2001; Trivedi et al. 2003 [for pH > 4.5]), goethite, and hematite (Bargar et al. 1997b). It is possible that sorption mechanisms of other heavy metals also are controlled by the sorbent surface structures and similar surface complexes will form on HFO and goethite. Therefore, in the next chapter, XAS analysis on Ni/HFO sorption samples is presented and is followed by Ni/goethite modeling.

CHAPTER 8

NI(II) COMPLEXATION TO AMORPHOUS HYDROUS FERRIC OXIDE: AN X-RAY ABSORPTION SPECTROSCOPY STUDY

In this chapter, Ni/HFO sorption samples are analyzed with XAS at the Ni K-edge and Fe K-edge. Macroscopic adsorption studies are performed first to prepare XAS samples.

8.1 Ni/HFO Adsorption Studies

Ni adsorption studies were conducted to investigate the effect of ionic strength, pH, and Ni concentration. The characteristic sigmoid shape of the edges (Figure 8.1) shows 50% adsorption at pH 6. Consistent with others (Green-Pedersen et al. 1997; Hayes and Leckie, 1987; Dzombak and Morel, 1990), ionic strength did not affect adsorption potentially suggesting that Ni ions form inner-sphere complexes on the HFO surface. From isotherms (Figure 8.2), the sorbed concentration is linearly related to the bulk aqueous one over a large concentration range (10^{-11}~10^{-3} M), potentially indicative of one average type of adsorption site. This linear relationship was also observed in a study conducted by Trivedi and Axe (2001b). The molecular level EXAFS analysis further addresses adsorption mechanisms.

8.2 EXAFS Analysis of Ni

The measurement of EXAFS spectra at energies just greater than the Fe K-edge (i.e. Co, Ni, and Cu) is difficult because the fluorescence signal from trace elements is typically two orders of magnitude less intense (1:100) than the Fe fluorescence from the matrix (Manceau et al. 2000). To overcome this difficulty, either a high flux X-ray beam or

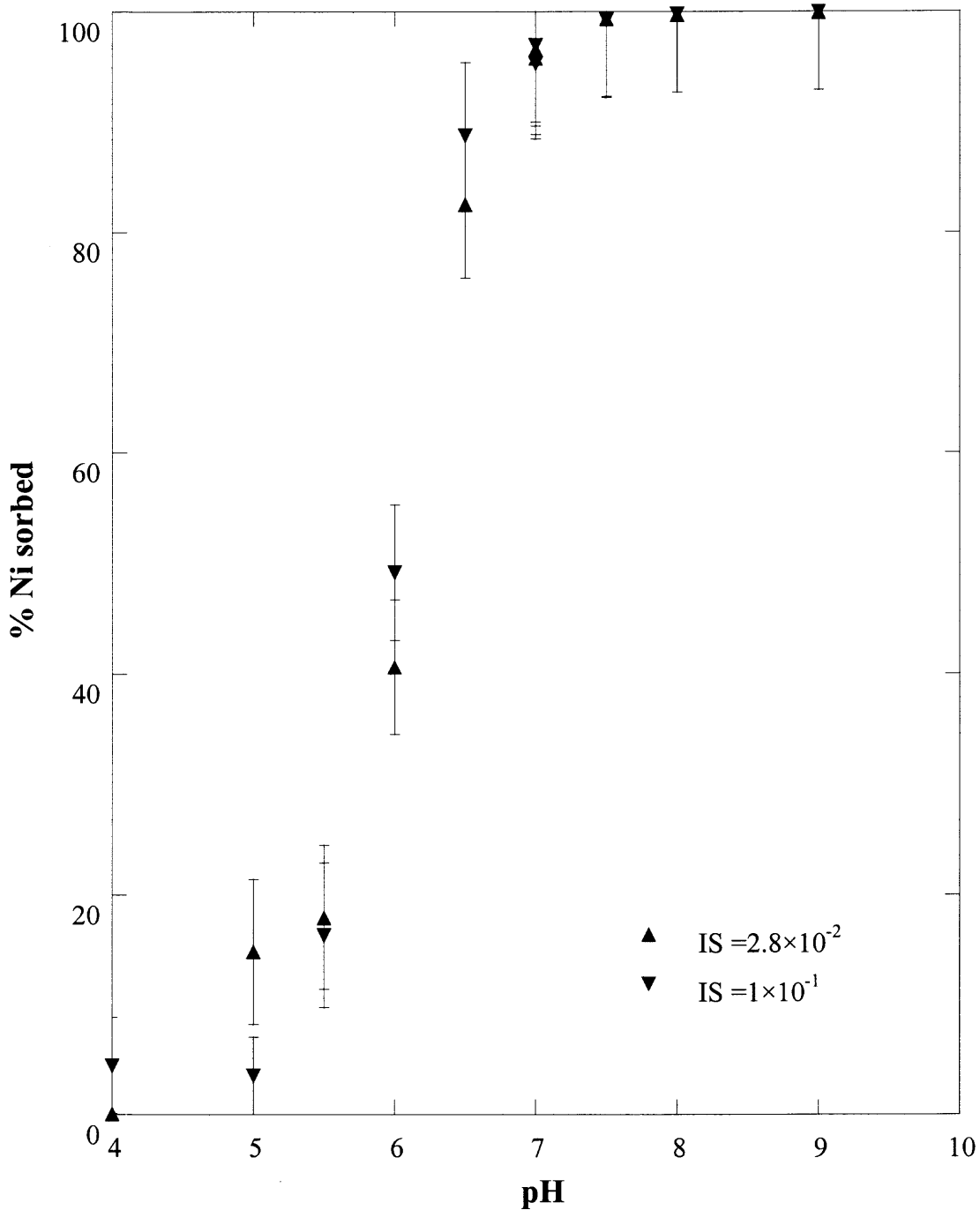

Figure 8.1 Ni adsorption edge on 1 g L^{-1} HFO at initial $[Ni]_0 = 5\times10^{-9}$ M, $NaNO_3$ based electrolyte, and 25 °C.

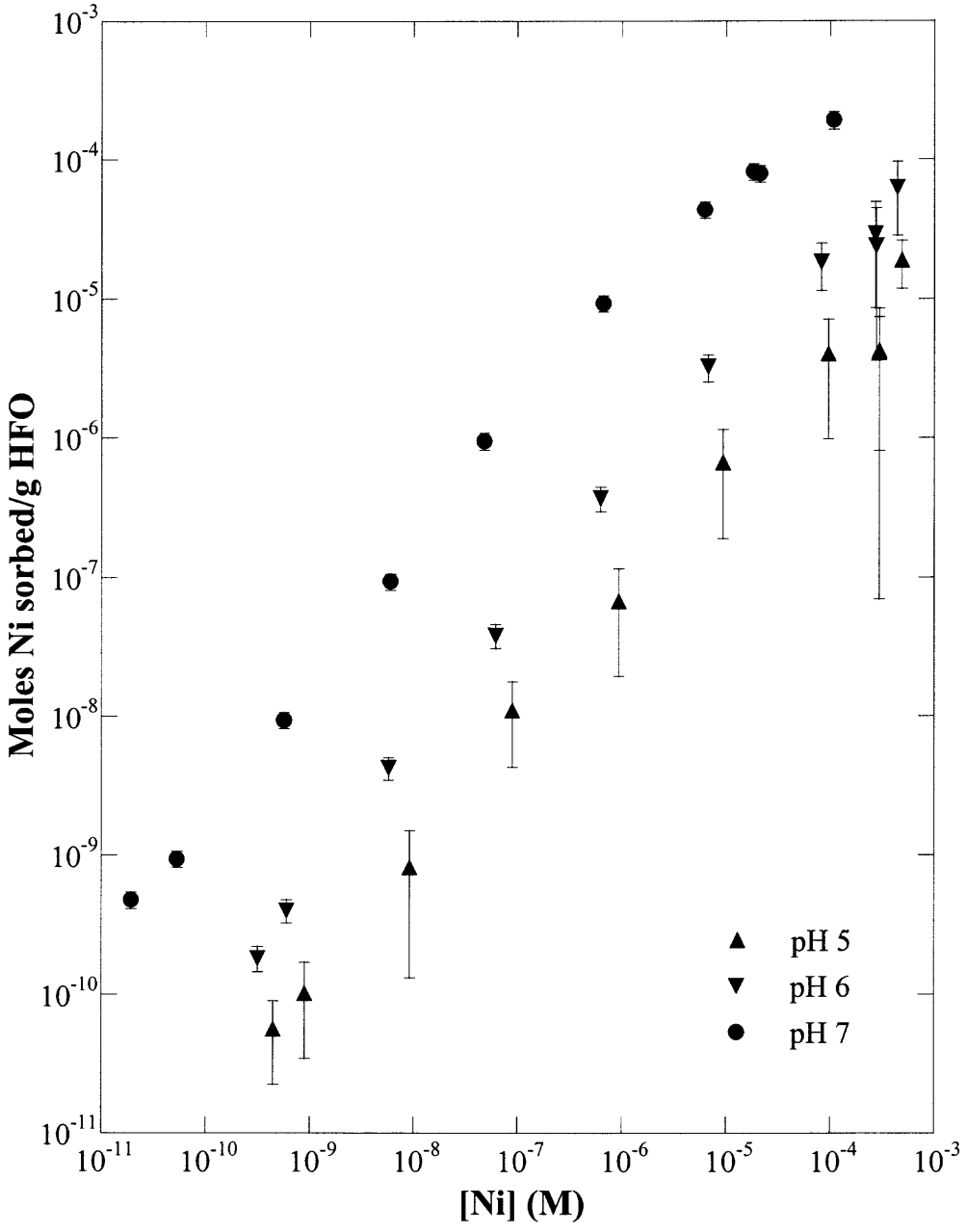

Figure 8.2 Ni adsorption isotherm on 1 g L^{-1} HFO as a function of pH at ionic strength 2.8×10^{-2} ($NaNO_3$) and room temperature.

high metal loading is needed. Because the flux at the beamline was fixed, loadings were maximized (Table 8.1) given the solubility of Ni(II).

In EXAFS analysis of standards (Figure 8.3), the $\chi(k)\cdot k^3$ spectra of aqueous Ni^{2+} ions are dominated by the backscattering from oxygen atoms, resulting in one shell and consistent with $[Ni(OH_2)_6]^{2+}$ octahedra (Table 8.2). Richens (1997) reported that solutions of $[Ni(OH_2)_6]^{2+}$ are immediately generated upon dissolution of simple Ni^{2+} salts in water containing non- or weakly-coordinating counter-anions. Spectra of the $NiCO_3\cdot nH_2O$ and NiO references reveal backscattering from heavier (Ni) atoms (Figure 8.3), which represent a second shell in the Fourier transform. For $NiCO_3\cdot nH_2O$, the first shell was fit with 5-6 O atoms at 2.05 ± 0.02 Å and two subshells, a carbon shell with 4-5 atoms at 2.77 ± 0.02 Å and a Ni shell with 7-8 atoms at 3.67 ± 0.02 Å. The two-shell fitting for NiO resulted in 5-6 O atoms at 2.07 ± 0.02 Å and 12-13 Ni atoms at 2.95 ± 0.02 Å. Overall, these results are consistent with XRD data (Pertlik, 1986; Wyckoff, 1988).

EXAFS samples were prepared addressing the effect of ionic strength from 2.8×10^{-3} to 10^{-1}, pH 6 to 7, loading from 8×10^{-4} to 8.1×10^{-3} mole Ni g^{-1} HFO, and reaction time from 4 hours to 8 months; a coprecipitation sample (3.5×10^{-3} mole Ni g^{-1} HFO) was also prepared for comparison. These spectra (Figure 8.4) are unique from that of NiO (Figure 8.3) and appear to exhibit a similar envelope as in the Ni^{2+} spectrum (Figure 8.3 and Figure 8.4) except for beat features observed at approximately 5, 7, 8.3, and 9 $Å^{-1}$. The difference suggests backscattering of heavier atoms (Ni or Fe) beyond the first oxygen shell and the loss of some waters of hydration upon binding to the HFO

Table 8.1 Preparation Conditions for Ni XAS Samples

Sample	pH	IS	Solid (g/L)	$[Ni]_0$ (M)	$[Ni]_{eq}$ (M)	Ni_{ads} (mol/g)	Reaction time
Ni-HFO, coppt* 3.5×10^{-3} mol/g, pH7, IS 10^{-2}	7	1.4×10^{-2}	0.2	10^{-2}	9.3×10^{-3}	3.5×10^{-3}	4 hr
Ni-HFO 8.1×10^{-3} mol/g, pH6, IS 10^{-3}	6	2.8×10^{-3}	0.1	10^{-2}	9.19×10^{-3}	8.1×10^{-3}	4 hr
Ni-HFO 4×10^{-3} mol/g, pH7, IS 10^{-2}	7	1.4×10^{-2}	0.2	10^{-2}	9.2×10^{-3}	4.0×10^{-3}	4 hr
Ni-HFO 1×10^{-3} mol/g, pH7, IS 10^{-2}	7	1.4×10^{-2}	0.5	5×10^{-3}	4.5×10^{-3}	1.0×10^{-3}	4 hr
Ni-HFO 3.7×10^{-3} mol/g, pH7, IS 10^{-1}	7	1.0×10^{-1}	0.2	10^{-2}	9.26×10^{-3}	3.7×10^{-3}	4 hr
Ni-HFO, 5 days 8.0×10^{-4} mol/g, pH7, IS 10^{-2}	7	1.4×10^{-2}	1.0	2×10^{-3}	1.2×10^{-3}	8.0×10^{-4}	5 days
Ni-HFO, 42 days** 8.6×10^{-4} mol/g, pH7, IS 10^{-2}	7	1.1×10^{-2}	0.1	10^{-4}	1.4×10^{-5}	8.6×10^{-4}	42 days
Ni-HFO, 8 months** 8.7×10^{-4} mol/g, pH7, IS 10^{-2}	7	1.1×10^{-2}	0.1	10^{-4}	1.3×10^{-5}	8.7×10^{-4}	8 months

* coppt: coprecipitation;
** Samples prepared by Paras Trivedi.

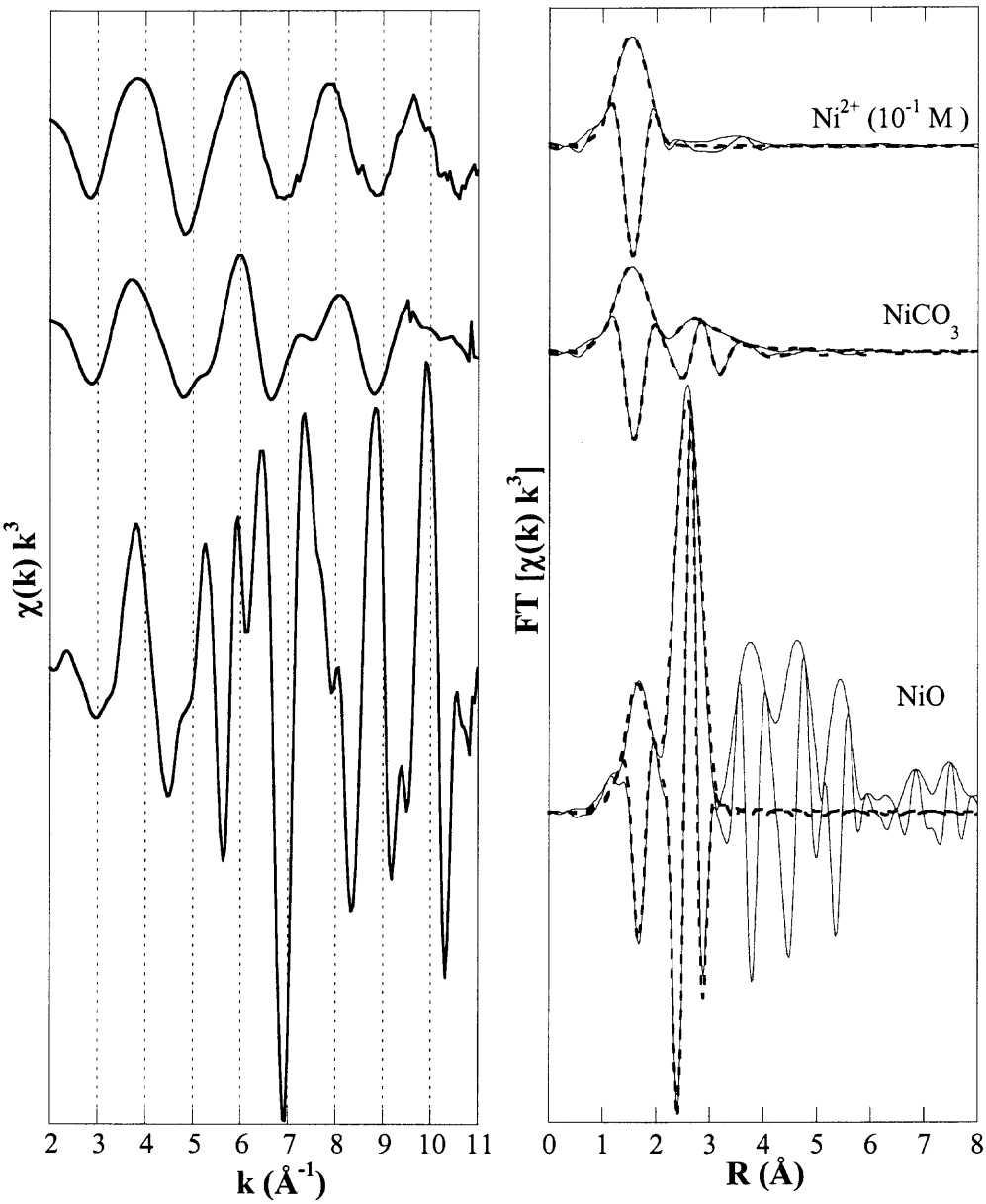

Figure 8.3 $\chi(k)\cdot k^3$ spectra and Fourier transform of Ni standards at the Ni K-edge at room temperature. Fourier transform was performed over range, NiO 2.50-10.99 $Å^{-1}$, $NiCO_3 \cdot nH_2O$ 2.4-9.3 $Å^{-1}$, Ni^{2+} (aq) 2.36-9.27 $Å^{-1}$.

Table 8.2 EXAFS Results of Ni Standards at Ni K Edge

Sample	Atom	N	R (Å)	σ^2 (Å^2)	C_3 (Å^3)	ΔE_0 (eV)	Residual
NiO (XRD)[1]	O	6	2.08				
	Ni	12	2.94				
$NiCO_3$ (XRD)[2]	O	6	2.08				
	C	6	2.93				
	Ni	6	3.62				
NiO	O	5.67 ± 0.19	2.07 ± 0.02	0.006 ± 0.001		-3.61 ± 0.08	5.62
	Ni	12.70 ± 0.07	2.95 ± 0.02	0.007 ± 0.001			
$NiCO_3 \cdot nH_2O$	O	5.29 ± 0.06	2.05 ± 0.02	0.008 ± 0.001			
	C	4.50 ± 0.34	2.77 ± 0.02	0.018± 0.004	-0.035 ± 0.001	0.77 ± 0.07	4. 80
	Ni	7.15 ± 0.17	3.67 ± 0.02	0.014 ± 0.001	0.004 ± 0.001		
Ni^{2+} (aq)	O	7.61 ± 0.37	2.09 ± 0.02	0.007 ± 0.001	0.001 ± 0.001	-1.64 ± 0.54	7.14

Fourier transform was performed over range, NiO 2.50-10.99 Å^{-1}, $NiCO_3 \cdot nH_2O$ 2.4-9.3 Å^{-1}, Ni^{2+} (aq) 2.36-9.27 Å^{-1}; NiO was fitted over 0.73-3.18 Å, $NiCO_3 \cdot nH_2O$ 0.65-4.3 Å, and Ni^{2+} (aq) 0.27-2.23 Å.
N, coordination number; R, interatomic distance; σ^2, Debye–Waller factor; ΔE_0, edge shift.
An S_0^2 of 0.8 was used to account for self-absorption based on the ratio of fluorescence to transmission data for aqueous Ni^{2+}.
[1] Wyckoff (1988)
[2] Pertlik (1986)

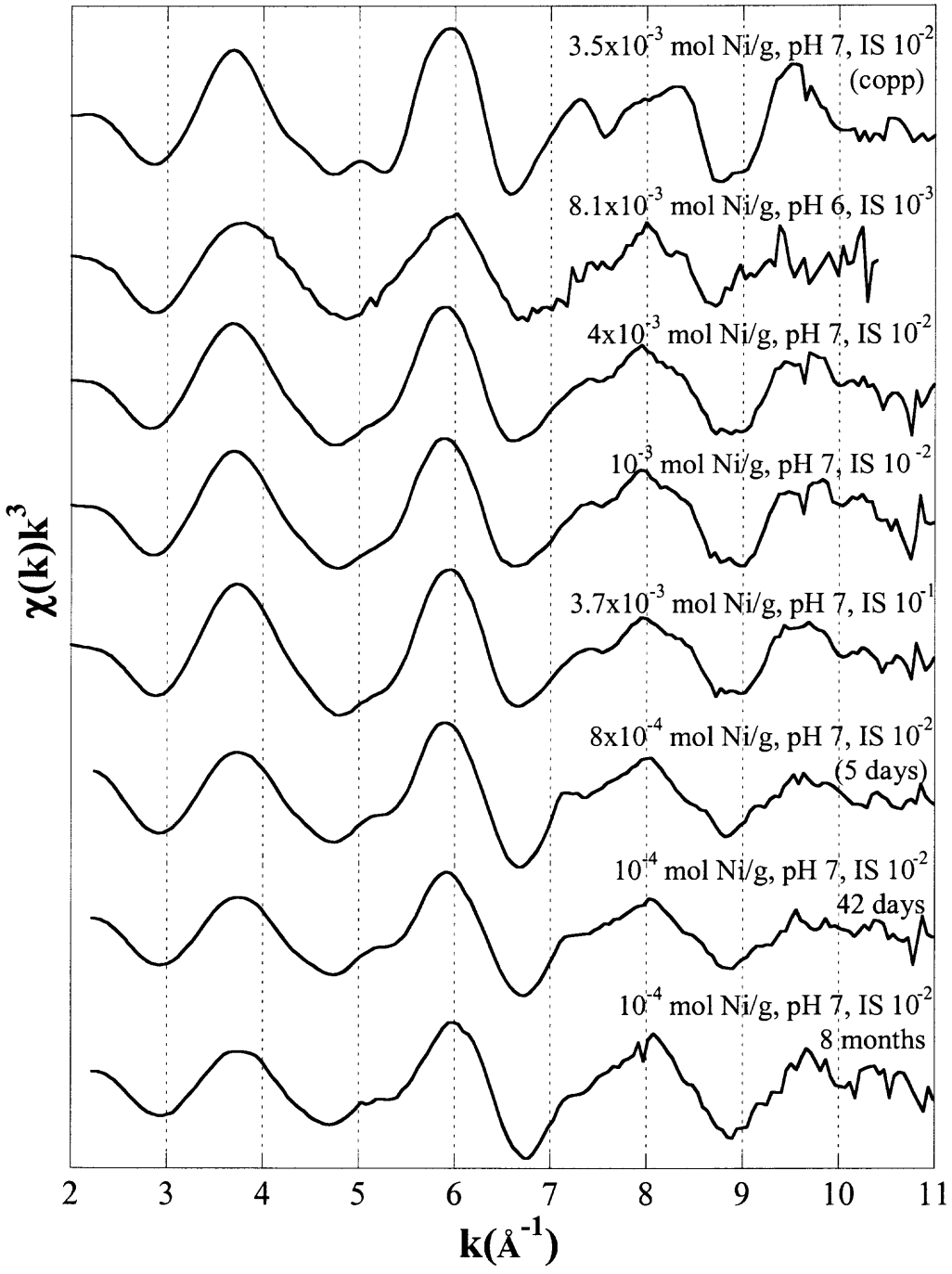

Figure 8.4 $\chi(k)\cdot k^3$ spectra of Ni-HFO sorption complexes as a function of pH, IS, and adsorbate loading studied at the Ni K-edge at room temperature.

surface. Although the spectra are similar to that of $NiCO_3 \cdot nH_2O$ (Figure 8.3 and Figure 8.4), the peak at 6 $Å^{-1}$ shifts slightly to lower k and the shoulder at about 7 $Å^{-1}$ shifts slightly to higher k for the samples. These shifts suggest $NiCO_3 \cdot nH_2O$ does not precipitate and is consistent with thermodynamic calculations using MINEQL+ (Westall et al. 1976) where Ni^{2+} is the dominant species at pH less than 7.7 in an aqueous system open to the atmosphere.

The spectrum of Ni/HFO coprecipitation sample stands out from those of the sorption ones with unique features including a shoulder at about 4.4 $Å^{-1}$ and a discrete peak at 5 $Å^{-1}$ (Figure 8.4). This spectrum is identical to that of poorly crystallized hydrated α-$Ni(OH)_2$ obtained by Pandya et al. (1990). The most thermodynamically stable form of nickel hydroxide is β-$Ni(OH)_2$ (theophrastite) (Wallner and Gatterer, 2002; Baes and Mesmer, 1976), which belongs to the trigonal system with P-3m1 space group (Wallner and Gatterer, 2002). The structure of α-$Ni(OH)_2$ is similar to that of β-$Ni(OH)_2$ except that between the (001) planes the presence of water layers results in an increase in the c-axis spacing (Pandya et al. 1990). The α-$Ni(OH)_2$ is labile and easily transforms to β-$Ni(OH)_2$ (Bode et al. 1966). Therefore metastable α-$Ni(OH)_2$ may have coprecipitated with HFO. The Fourier transform of the $\chi(k) \cdot k^3$ spectra (Figure 8.5) show two shells fit with 4-5 O atoms at 2.04 ± 0.02 Å and about 4 Ni atoms at 3.02 ± 0.02 Å (Table 8.3). Considering the error, fitting results are consistent with that of Pandya et al. (1990) where 6 O atoms at 2.04 Å and 5-6 Ni atoms at 3.07 Å were found.

The $\chi(k) \cdot k^3$ spectra of adsorption samples are very similar (Figure 8.4) with one another suggesting similar local structure. The Fourier transforms (Figure 8.5) identify two shells fit with 3-7 O atoms at about 2.05 Å (Table 8.3) and a second shell that could

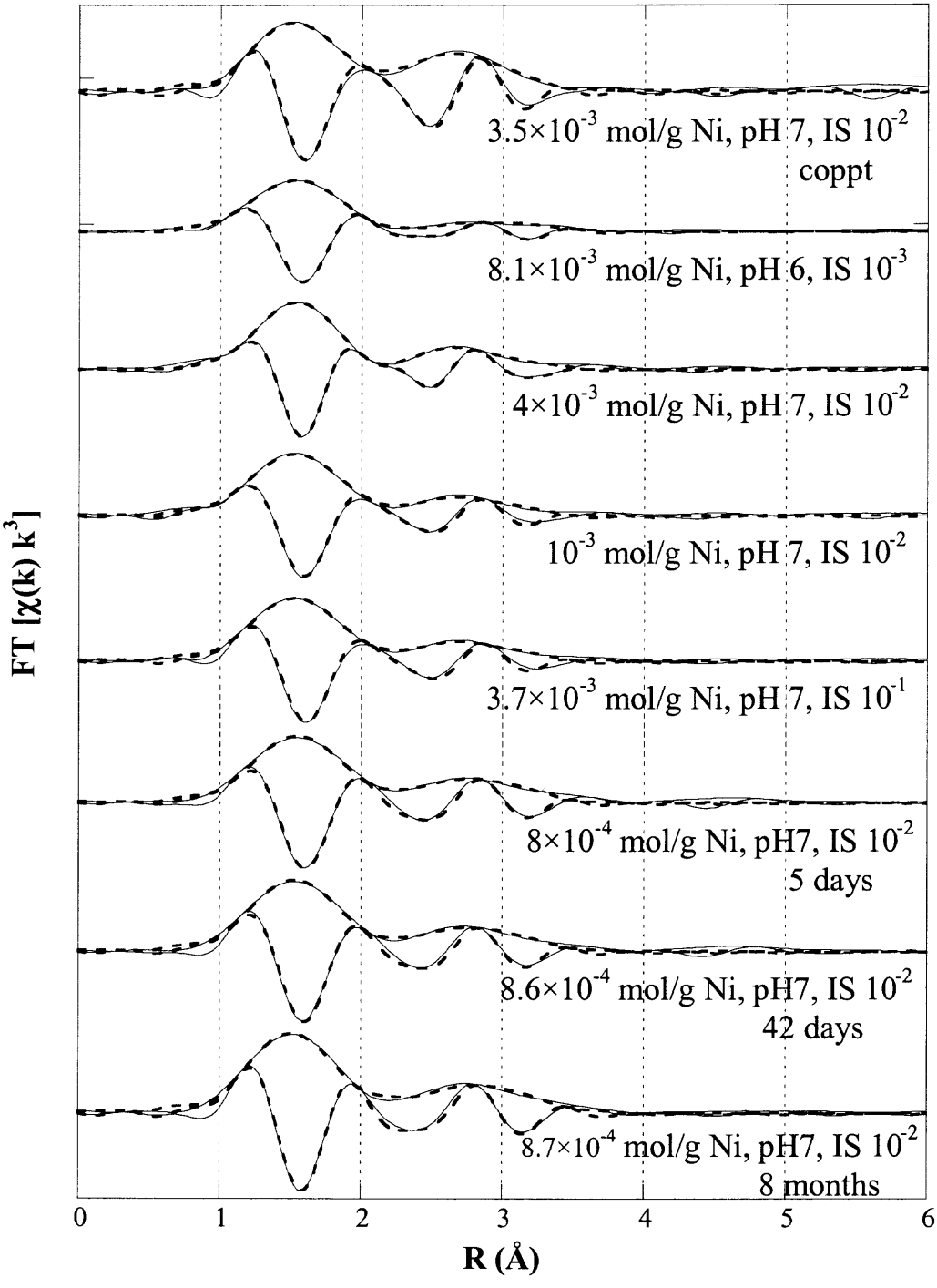

Figure 8.5 Fourier transforms (magnitude and imaginary part) of Ni K-edge XAS spectra of Ni-HFO sorption complexes (Fourier transformed and fitted over ranges: 2.4-9.3 $Å^{-1}$ and 0.84-3.80 Å).

Table 8.3 EXAFS Results of Ni/HFO Samples at Ni K-Edge

Sample	Atom	N	R (Å)	σ^2 (Å^2)	C_3 (Å^3)	ΔE_0 (eV)	Residual
Ni-HFO, coppt 3.5×10^{-3} mol/g, pH7, IS 10^{-2}	O Ni	4.41 ± 0.05 4.00 ± 0.03	2.04 ± 0.02 3.02 ± 0.02	0.002 ± 0.001 0.007 ± 0.001	-0.0009 ± 0.0001	-9.91 ± 0.22	9.02
Ni-HFO 8.1×10^{-3} mol/g, pH6, IS 10^{-3}	O Fe	4.38 ± 0.13 0.67 ± 0.06	2.05 ± 0.02 2.93 ± 0.02	0.006 ± 0.002 0.005 ± 0.002	-0.0045 ± 0.0003	-5.77 ± 0.33	5.74
Ni-HFO 4×10^{-3} mol/g, pH7, IS 10^{-2}	O Fe	6.74 ± 0.21 2.83 ± 0.21	2.05 ± 0.02 3.01 ± 0.02	0.009 ± 0.001 0.012 ± 0.002	-0.0023 ± 0.0001	-7.45 ± 0.21	6.08
Ni-HFO 1×10^{-3} mol/g, pH7, IS 10^{-2}	O Fe	5.61 ± 0.57 1.75 ± 0.66	2.05 ± 0.02 3.05 ± 0.02	0.007 ± 0.002 0.007 ± 0.005	-0.0013 ± 0.0007	-7.20 ± 0.32	7.96
Ni-HFO 3.7×10^{-3} mol/g, pH7, IS 10^{-1}	O Fe	4.93 ± 0.61 1.79 ± 0.22	2.04 ± 0.02 3.02 ± 0.02	0.004 ± 0.002 0.006 ± 0.002	-0.0015 ± 0.0003	-7.72 ± 1.64	9.03
Ni-HFO, 5 days 8×10^{-4} mol/g, pH7, IS 10^{-2}	O Fe	4.56 ± 0.16 2.77 ± 0.20	2.06 ±0.02 2.99 ± 0.02	0.005 ± 0.001 0.011 ± 0.001	-0.0029 ± 0.0004	-5.97 ± 0.31	8.41
Ni-HFO, 42 days 8.6×10^{-4} mol/g, pH7, IS 10^{-2}	O Fe	4.80 ± 0.32 2.44 ± 0.13	2.05 ±0.02 2.95 ± 0.02	0.004 ± 0.001 0.009 ± 0.001	-0.0032 ± 0.0002	-7.79 ± 0.67	8.97
Ni-HFO, 8 months 8.7×10^{-4} mol/g, pH7, IS 10^{-2}	O Fe	3.36 ± 0.70 2.75 ± 0.77	2.03 ±0.02 2.92 ± 0.04	0.001 ± 0.002 0.011 ± 0.003	-0.0041 ± 0.0009	-5.97 ± 1.17	8.85

Fourier transform was performed over range 2.4-9.3 Å^{-1}, fitted over 0.84-3.8 Å.
N, coordination number; R, interatomic distance; σ^2, Debye–Waller factor; ΔE_0, edge shift.

be fit using either Fe or Ni atoms. Distinguishing between Fe and Ni atoms solely based on EXAFS fitting is difficult, because of the difference in atomic number, because they have similar ionic radii (0.65 vs. 0.69 Å, Richens, 1997), and because they form similar local structures – octahedral (Combes et al. 1989; Pandya et al. 1990; Scheidegger et al. 1996). The Ni/HFO coprecipitation sample provides a good comparison. The differences in $\chi(k)\cdot k^3$ spectra between the sorption and coprecipitation samples (Figure 8.4) suggest that the second shell in the former may be composed of Fe atoms. Also, as the Ni loading increases, the (potential) number of Ni atoms does not (Table 8.3); these results are not self consistent for polymers or precipitates where the Ni coordination number would increase as the structure grows. Therefore, the second shell is most likely an Fe shell and the formation of a Ni polymer or $Ni(OH)_2$ is ruled out.

Using Fe in the second shell resulted in 3-7 O atoms at 2.03-2.06 Å and 1-3 Fe atoms at 2.92-3.05 Å. These results are consistent with two-shell fitting of a coprecipitated Ni/goethite sample (Manceau et al. 2000), where 5.3 O atoms at 2.07 Å and 2.1 Fe atoms at 3.00 Å were obtained. However, two outer shells were also observed by Manceau et al. (2000) of 1.4 Fe atoms at 3.18 Å and 2.5 Fe atoms at 3.62 Å, suggesting substitution of Ni^{2+} for Fe^{3+} in the goethite matrix. The absence of multiple Fe shells in our study indicates Ni(II) ions form surface complexes with HFO. Although the coordination number of the 8-month sample (3.36) may suggest tetrahedral structure for Ni, the Ni-O distance of 2.03 Å is consistent with octahedral structure. Additionally, the Ni-Fe distance of 2.92-3.05 Å suggests formation of bidentate edge-sharing complexes. A more recent study (Strathmann and Myneni, 2005) reported similar surface species (mononuclear bidentate edge-sharing surface complexes) for Ni^{2+} sorption on

pure boehmite (γ-AlOOH). Fundamentally, aluminum and iron oxides exhibit similar octahedral structural units with comparable Al-O and Fe-O bond lengths (Bargar et al. 1997a, b); therefore they may have similar surface structures and functional groups. Bargar et al. (1997a, b) found Pb(II) surface complexes on iron and aluminum oxides well consistent with on another. Therefore, it is not surprising that Ni forms similar surface complexes on iron oxide (this study) and aluminum oxide (Strathmann and Myneni, 2005).

EXAFS results (Table 8.3, Figure 8.4 and Figure 8.5) suggest that Ni(II) forms inner-sphere mononuclear bidentate complexes along edges of FeO_6 octahedra. This surface complex was observed for ionic strengths 2.8×10^{-3} to 10^{-1}, pH 6 to 7, loadings 8×10^{-4} to 8.1×10^{-3} mole Ni g^{-1} HFO, and reaction times of 4 hours to 8 months. Through a constant boundary condition study conducted over 8 days, Trivedi and Axe (2001b) found as much as 40% of the total sites were located on micropore walls of HFO samples; they successfully modeled the sorption data assuming similar internal and external sites. Results of our study further corroborate that sorption to internal and external surfaces potentially involve the same mechanism up to eight months. Because only one Fe shell was observed, Ni^{2+} does not appear to substitute for Fe^{3+}.

Previous studies (Combes et al. 1989, 1990; Manceau and Drits, 1993) have shown that HFO exhibits short-range structure and transforms to crystalline forms through progressive long-range ordering. The effect of Ni(II) on the formation and transformation of HFO is addressed in the following section.

8.3 EXAFS Analysis of Fe

The $\chi(k)\cdot k^3$ spectra of discrete, sorbed, and co-precipitated samples (Figure 8.6) reveal similar structures. Fitting resulted in (Table 8.4) 2-3 O atoms at 2.03-2.04 Å and 3-4 Fe atoms at 2.95 to 2.98 Å suggesting edge-sharing FeO_6 polymers. Double corner- or single corner-sharing with Fe-Fe distances longer than 2.98 Å are characteristic of crystalline iron oxides (Charlet and Manceau, 1992) but were not observed. Even at the highest loading of 8.1×10^{-3} mole Ni g^{-1} HFO, no evidence of crystallization was seen with XRD after aging the sample for 1 year. Ni(II) ions bound to surfaces or coprecipitated with HFO may have inhibited crystallization of the amorphous iron oxide. Similar results have been observed for the Pb/HFO system (Chapter 7).

In studying crystal chemistry of Ni(II) in synthetic goethite (Manceau et al. 2000; Carvalho-E-Silva et al. 2003) and hematite (Singh et al. 2000), Ni(II) was coprecipitated with amorphous iron oxides and went through an aging process (3, 14, and 93 days) under elevated temperatures (70-90 °C) and pH (7.5 to ~13). Subsequent EXAFS analysis revealed Ni^{2+} substitution for Fe^{3+}. However, the transformation of HFO to goethite and hematite has been reported to be slow at temperatures below 20 °C, and is further retarded by adsorbed species (Schwertmann et al. 1976; Cornell et al. 1987; Cornell and Giovanoli, 1988; Paige et al. 1997; Martínez and McBride, 1998). In this study, the HFO samples sorbed or coprecipitated with Ni(II) were maintained under room temperature at pH less than or equal to 7. Ni^{2+} was not observed to substitute for Fe^{3+} possibly because HFO did not undergo long range ordering and therefore the Ni(II) complexes were stable up to 8 months. In other words, Ni^{2+} substitution for Fe^{3+} may require crystal growth of iron oxides. In soils and sediments, trace metals could be

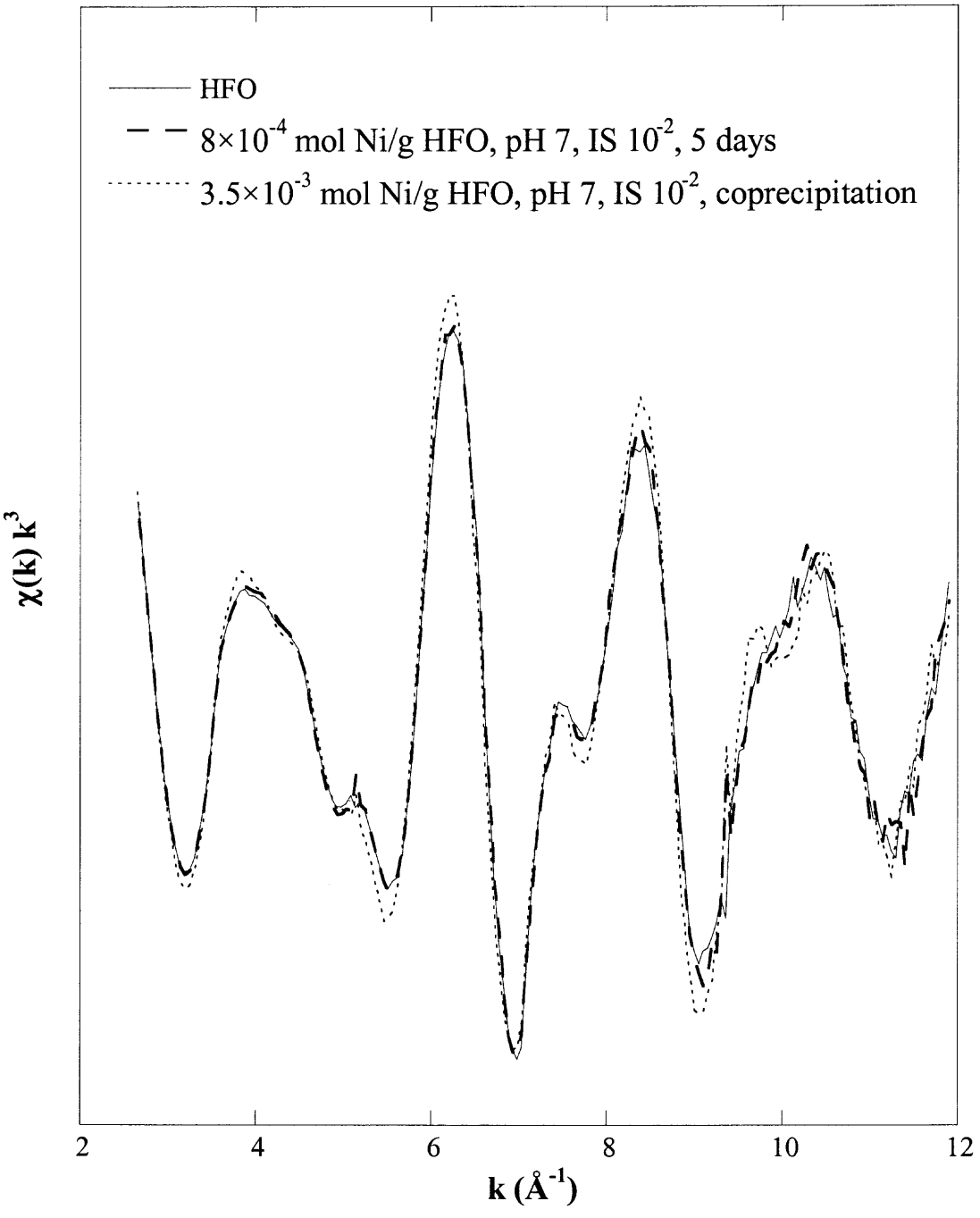

Figure 8.6 $\chi(k)\cdot k^3$ spectra of HFO, Ni/HFO 5-day sorption sample, and coprecipitated Ni/HFO sample.

Table 8.4 EXAFS Results of HFO and Ni/HFO Samples at Fe K-Edge

Sample	Atom	N	R (Å)	σ^2 (Å^2)	C_3 (Å^3)	ΔE_0 (eV)	Residual
HFO	O	2.42 ± 0.03	2.03 ± 0.02	0.002 ± 0.001	0.0006 ± 0.0001	-1.37 ± 0.33	11.09
	Fe	3.76 ± 0.13	2.95 ± 0.02	0.014 ± 0.001	-0.0025 ± 0.0002		
Ni-HFO, 5 days 8×10^{-4} mol/g, pH7, IS 10^{-2}	O	2.42 ± 0.04	2.04 ± 0.02	0.002 ± 0.001	0.0007 ± 0.0001	-1.29 ± 0.47	10.26
	Fe	3.39 ± 0.16	2.95 ± 0.02	0.013 ± 0.001	-0.0026 ± 0.0001		
Ni-HFO, coppt 3.5×10^{-3} mol/g, pH7, IS 10^{-2}	O	2.69 ± 0.07	2.04 ± 0.02	0.002 ± 0.001	0.0006 ± 0.0001	-0.74 ± 0.41	9.84
	Fe	3.18 ± 0.19	2.98 ± 0.02	0.010 ± 0.001	-0.0019 ± 0.0002		

Fourier transform was performed over range 2.86-11.77 Å^{-1} and fitted over 0.52-3.91 Å.
N, coordination number; R, interatomic distance; σ^2, Debye–Waller factor; C_3, third cumulant; ΔE_0, edge shift.

stabilized by incorporating into the structure of goethite and hematite, which may occur over long periods of time (in terms of years) under varying environmental conditions.

8.4 Summary

Overall, results suggest that Ni(II) forms mononuclear bidentate edge-sharing surface complexes upon adsorption to HFO. This mechanism was observed as a function of ionic strength 2.8×10^{-3} to 10^{-1}, pH 6 to 7, loading 8×10^{-4} to 8.1×10^{-3} mole Ni g^{-1} HFO, and reaction time 4 hours to 8 months. The presence of Ni(II) potentially inhibited HFO transformation into a more crystalline iron oxide; therefore the large sorption capacity of HFO was maintained. Metastable α-$Ni(OH)_2$ appears to have formed when coprecipitated with HFO. Ni^{2+} was not found to substitute for Fe^{3+} up to 8 months at room temperature possibly because HFO did not undergo phase transformation into a more crystalline form. This study is among the first in systematically addressing Ni(II) adsorption mechanisms to amorphous iron oxides. The experimentally defined surface complexes can be used to constrain surface complexation modeling for improved description and prediction of Ni distribution at the iron oxide/aqueous interfaces, which will be introduced in the next chapter.

CHAPTER 9

SURFACE COMPLEXATION MODELING OF HEAVY METAL ADSORPTION AND COMPETITION ON GOETHITE

This chapter focuses on constraining surface complexation modeling with XAS results to develop one unique set of SCM parameters for the description of both adsorption edge and isotherm data. Data represent those covering a broad range of conditions, including pH, ionic strength, metal concentration, and the presence of a competing ion. Ni(II) and Zn(II) are two common metal contaminants that may coexist due to release from historically poor waste management practices including industries such as electroplating. Ni and Zn adsorption and competition at the goethite/water interface are investigated in this chapter.

First, the adsorption mechanism needs to be defined. Based on the last chapter Ni forms mononuclear bidentate edge-sharing complexes on HFO with loadings up to 8.1×10^{-3} mole Ni g^{-1} and similar surface species may form on goethite. Zn(II) was found to form bidentate surface complexes on both 2-line ferrihydrite (Waychunas et al. 2002, 2003; Trivedi et al. 2004) and goethite (Schlegel et al. 1997; Trivedi et al. 2001a). Schlegel et al. (1997) reported that Zn(II) formed inner-sphere mononuclear edge- and corner-sharing complexes upon adsorption to goethite at 10% proton site coverage (total [Zn] = 2×10^{-4} M). Trivedi et al. (2001a) also observed inner-sphere surface complexes up to a loading of 2×10^{-5} mol Zn g^{-1}. For these reasons, bidentate surface complexes are assumed in this study, where SOH represents a surface hydroxyl group and the surface reaction for either Ni or Zn (Me) on goethite is the following:

$$2SOH + Me^{2+} = (SO)_2Me + 2H^+ \qquad \log K_{Me}$$

This reaction is also consistent with the reported proton release for Zn adsorption on goethite (Forbes et al. 1976; Kooner, 1993; Trainor et al. 2000). Although the systems were open to the atmosphere, there was no evidence of structural contributions from carbonate in XAS analyses (Chapter 8; Trivedi et al. 2001a). Carbonate species have not been reported to affect adsorption of Zn, Ni, Cd, and Pb under atmospheric conditions (Balistrieri and Murray, 1982; Lützenkirchen and Behra, 1994; Green-Pedersen et al. 1997; Villalobos et al. 2001; Strathmann and Myneni, 2005).

9.1 Potentiometric Titration Data

Titration results (Figure 9.1) reveal that the point of zero charge (PZC) for goethite is at pH 8.8 ± 0.97 (pH_{PZC}). This value is consistent with reported ones, which range from 7.5 to 9.5 (Lumsdon and Evans, 1994; Robertson and Leckie, 1998; Peacock and Sherman, 2004). The variation in the reactivity of goethite is caused by the synthetic conditions such as total base added, rate of addition, the presence of sorbing ions, and aging time (Schwertmann et al. 1985; Villalobos et al. 2003). Each crystal plane has a distinct site density (Hiemstra et al. 1989); the pH_{PZC} may also be a function of the particle shape, size, and surface area. Sverjensky (2005) reported that pH_{PZC} may be lower without sufficient purging to remove carbon dioxide compared to otherwise obtained values. Previous studies (Evans et al. 1979; Zeltner and Anderson, 1988) have shown that when the goethite suspension was purged for 2 months, the PZC increased from 8.1 to 9.1; in their interpretation, changes in PZC were due to CO_2 adsorption and desorption. However, aging also affects crystallinity, which would impact the PZC as well.

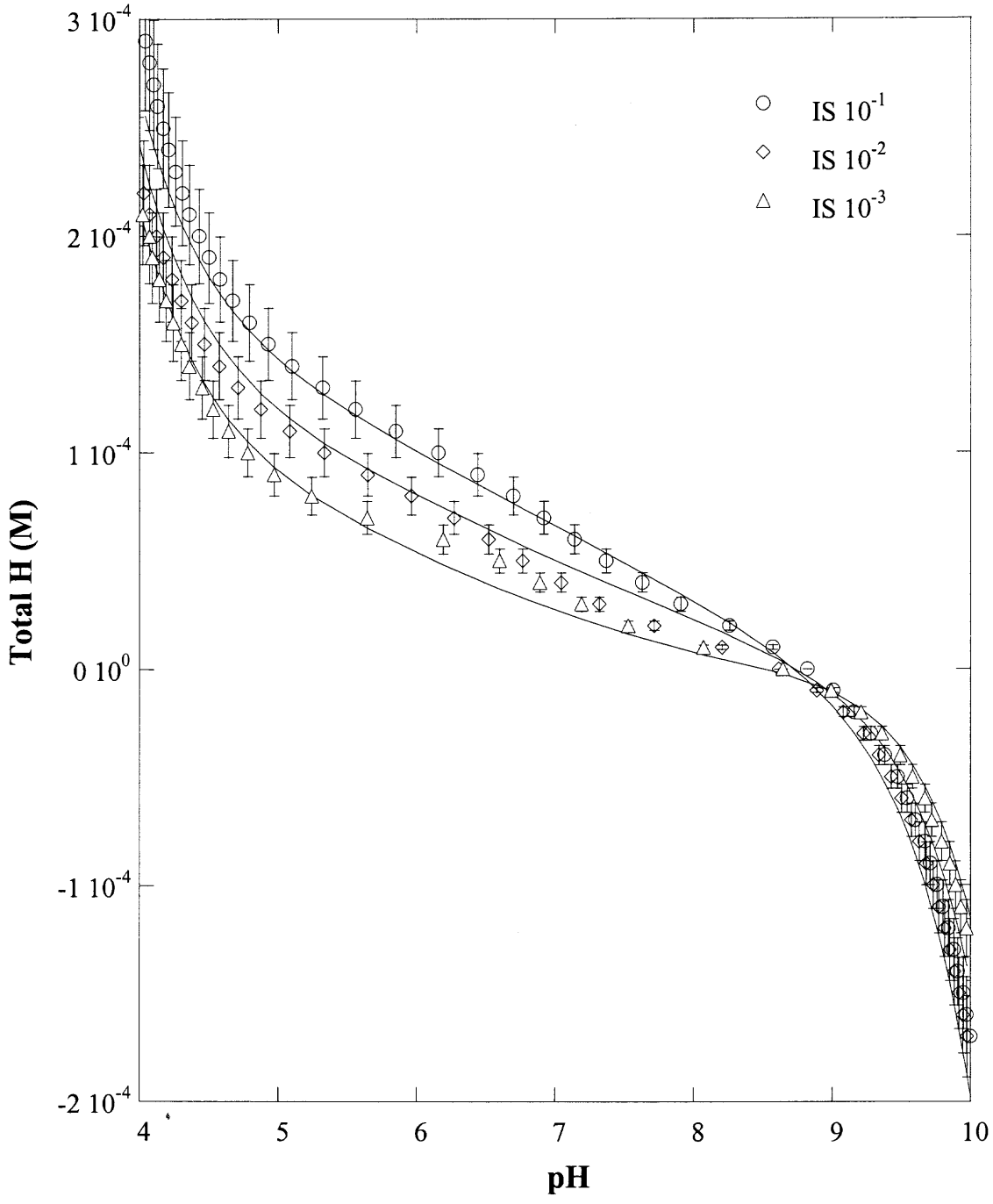

Figure 9.1 Potentiometric titration of 1 g L^{-1} goethite in $NaNO_3$-based electrolyte at room temperature (lines represent TLM results using parameters corresponding to $\Delta pK_a = 1$).

Goethite titration data were used to calibrate the TLM. Because FITEQL is unlikely to converge if the protolysis constants ($\log K_{a1}$ and $\log K_{a2}$) and electrolyte binding constants ($\log K_{cat}$ and $\log K_{an}$) are simultaneously set as adjustable parameters (Hayes et al. 1991). The former was constrained based on the relationship that pH_{PZC} is equal to $(\log K_{a1}+\log K_{a2})/2$. As a result, ΔpK_a as well as the inner-layer capacitance (C_1) were optimized outside of the FITEQL program. The outer-layer capacitance (C_2) is traditionally set at 0.2 F/m^2 (Hayes et al. 1991). For the total site density (N_s) of goethite, a value of ~6 sites nm^{-2} was calculated (Tadanier and Eick, 2002; Peacock and Sherman, 2004) based on a crystallographic consideration proposed by Hiemstra and van Riemsdijk (1996). This value was adopted for our work. Similar values for site density have been used in other studies and proved reasonable in describing these systems (Hayes and Leckie, 1986; Müller and Sigg, 1992; Coughlin and Stone, 1995; Kooner et al. 1995; Venema et al. 1996; Robertson and Leckie, 1998; Liu and Huang, 2001). In summary, the TLM parameters optimized in FITEQL in this study were $\log K_{cat}$ and $\log K_{an}$. Ionic strength effects are accounted for in FITEQL using activity coefficients calculated with the Davies equation (Davies, 1962).

The TLM results for ΔpK_a values varying from 1 to 5 (Table 9.1) show that, although the protolysis constants systematically decreased by 0.5 log units, the maximum change in either $\log K_{cat}$ or $\log K_{an}$ is only approximately 0.14 log units. Therefore, the electrolyte binding constants reflect little sensitivity to changes in ΔpK_a. In addition, the summation of the absolute values of $\log K_{cat}$ and $\log K_{an}$ is approximately equal to $2pH_{PZC}$. This relationship was used by Kosmulski (1996) to reduce the number of adjustable parameters. The optimum C_1 value was found to be 2.0 F m^{-2} for all ΔpK_a values and

Table 9.1 Surface Reactions and TLM Parameters for the Goethite-Water Interface

Reactions for the goethite-water interface	
Surface protolysis reactions:	
$SOH_2^+ = SOH + H^+$	$\log K_{a1}$
$SOH = SO^- + H^+$	$\log K_{a2}$
Electrolyte binding reactions:	
$SOH + Na^+ = SO^-\text{-}Na^+ + H^+$	$\log K_{cat}$
$SOH + NO_3^- + H^+ = SOH_2^+\text{-}NO_3^-$	$\log K_{an}$
Surface site density:	$N_s = 3.09 \times 10^{-4}$ mol g^{-1} (6 site nm^{-2})
Inner layer capacitance:	C_1 (F m^{-2})
Outer layer capacitance:	$C_2 = 0.2$ F m^{-2}

TLM parameters for the goethite-water interface:

ΔpK_a	$\log K_{a1}$	$\log K_{a2}$	$\log K_{cat}$	$\log K_{an}$	C_1 (F m^{-2})	SOS/DF
1	-8.3	-9.3	9.94	-8.25	2.0	21.14
2	-7.8	-9.8	9.80	-8.38	2.0	21.14
3	-7.3	-10.3	9.75	-8.43	2.0	21.14
4	-6.8	-10.8	9.74	-8.45	2.0	21.15
5	-6.3	-11.3	9.73	-8.44	2.0	21.19

was highly correlated to site density. Based on residuals, all five sets provide equivalent fits to the titration data. Hayes et al. (1991) also found multiple solutions that successfully replicated acid-base behavior of α-FeOOH, α-Al_2O_3, and TiO_2. Koopal et al. (1987) suggested that for crystalline oxides with few defects small ΔpK_a values are needed. Also molecular statics calculations have been performed to estimate stability constants for proton binding to goethite (Rustad et al. 1996); 19 out of 26 intrinsic $logK_a$ values were found to range between 7.7 and 9.4 where the pH_{PZC} was calculated to be 8.9. A ΔpK_a value of one was chosen in this study. The model described the experimental titration data between pH 4 and 10 very well (Figure 9.1). This set of parameters was therefore used in modeling adsorption.

9.2 Ni Adsorption on Goethite

In this work, the objective was to model both adsorption edges and isotherms. Studies (Balistrieri and Murray, 1982; Rodda et al. 1993) have shown that parameters derived from edge (pH dependence) modeling failed to account for the concentration dependence of sorption; Palmqvist et al. (1997) and Dyer et al. (2003) also strongly emphasize the importance of evaluating surface complexation models from data reflecting concentration ranges as wide as possible.

Ni adsorption isotherms on goethite were conducted from pH 4 to 7 (Figure 9.2). Although adsorption increases with pH, isotherms between pH 4 and 5 are almost equivalent and within the experimental error. This result may be due to very low adsorption and thus the error is large. Overall, Ni adsorption increases significantly between pH 5.5 and 6.5. These isotherms also show that below 10^{-6} M, the sorbed

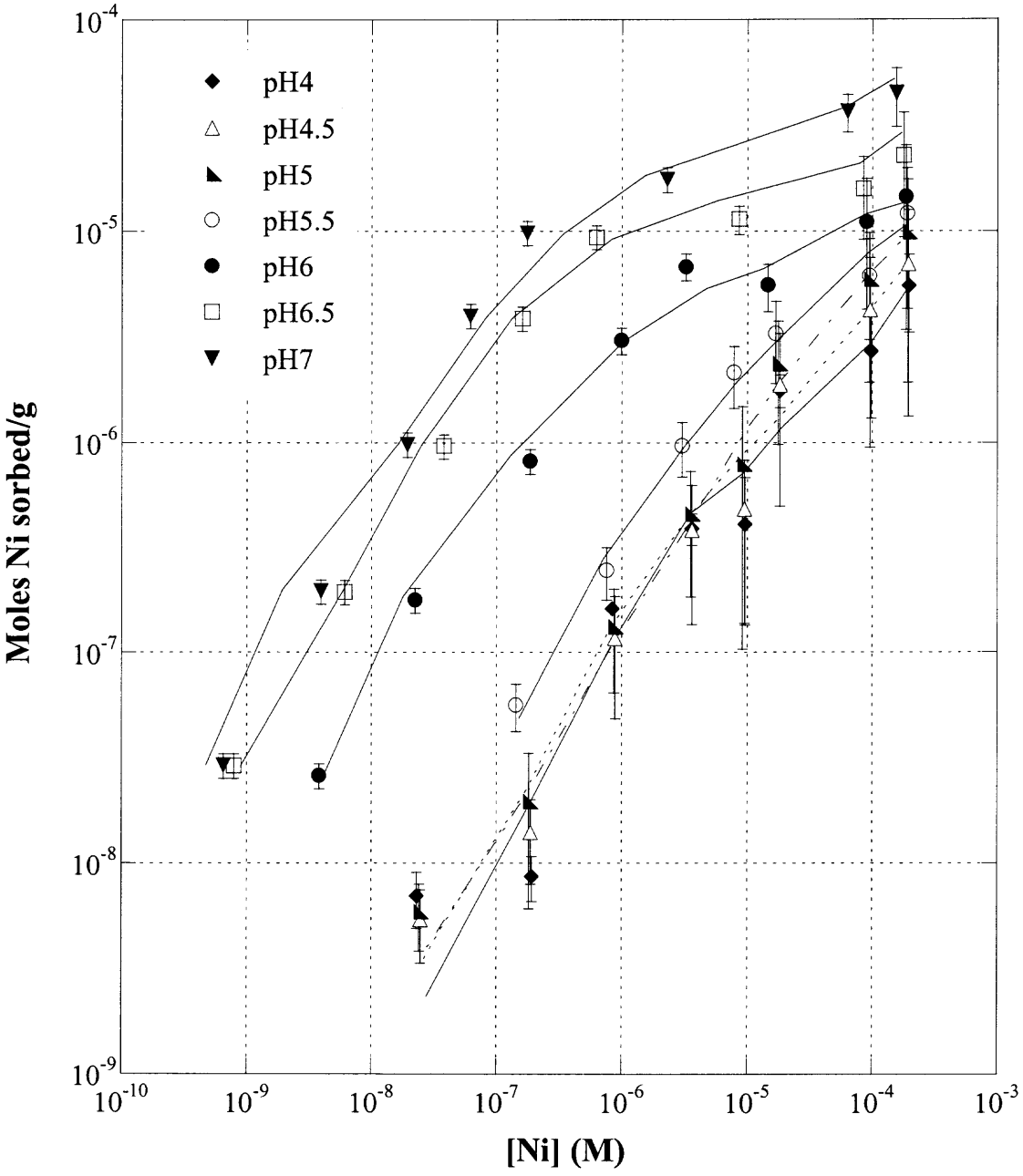

Figure 9.2 Ni adsorption isotherms for an open system at room temperature using 1 g L^{-1} goethite and 10^{-3} ionic strength (adjusted with $NaNO_3$). Solid lines represent TLM predictions.

concentration is linearly related to the bulk aqueous concentration suggesting one type of site. Palmqvist et al. (1997) did not observe a set of "high-affinity" surface sites in the sorption of Pb, Cd, Zn, and Cu onto goethite below a concentration of ~10^{-6} M. However, the slope of the isotherms became less than one for Ni concentrations greater than 10^{-6} M, suggesting surface site heterogeneity (Robertson and Leckie, 1997). The slight curvature seen in this same range of the isotherm may indicate an approach to saturation of the stronger binding sites. These asymptotes may correspond to site density varying with pH. Trivedi et al. (2001b) also observed that site density is a function of pH.

Surface heterogeneity has to be taken into account in modeling isotherms over the entire range of Ni concentrations tested. However, as discussed earlier, only one type of site was observed in XAS analysis. Because XAS data are averaged over the entire surface, there may be a small fraction of other site types present, which are not detected in the analysis. Benjamin and Leckie (1980, 1981b) proposed that the oxide surface exhibits a spectrum of binding energies; as the surface binds more ions, the higher energy sites may become limiting and the overall binding energy of the surface decreases. Although different binding energies exist on the goethite surface, the reaction stoichiometry proposed may still reflect an equivalent surface complex. A two-site model was used as employed by Dzombak and Morel (1990). XAS derived $(SO)_2Ni$ complexes were applied for both high affinity (K_H) and low affinity (K_L) sites.

Surface complexation modeling resulted in seven best-fit sets of parameters (Table 9.2), which correspond to each constant-pH Ni adsorption isotherm. The site density of high affinity sites (N_{sH}) increased with pH to attain convergence; these were constrained from the isotherm studies. Overall, the TLM accurately reproduced the

Table 9.2 Model Parameters for Ni and Zn Adsorption Isotherms for Goethite at Different pH Values

$$2SO_LH + Me^{2+} = (SO_L)_2Me + 2H^+ \qquad \log K_L$$

$$2SO_HH + Me^{2+} = (SO_H)_2Me + 2H^+ \qquad \log K_H$$

pH	Log K_L	Log K_H	N_{sH} (mol/g)
Parameters for Ni adsorption			
4	-1.93	3.73	2.5×10^{-6}
4.5	-2.62	2.18	2.5×10^{-6}
5	-3.34	0.39	2.5×10^{-6}
5.5	-4.42	-0.42	5.0×10^{-6}
6	-5.34	-1.15	2.0×10^{-5}
6.5	-6.63	-2.45	3.5×10^{-5}
7	-6.89	-3.04	6.0×10^{-5}
Parameters for Zn adsorption			
4	-2.10	4.18	5.0×10^{-7}
4.5	-2.66	3.29	1.0×10^{-6}
5	-3.56	2.34	3.1×10^{-6}
5.5	-3.92	2.14	3.1×10^{-6}
6	-4.36	0.86	7.3×10^{-6}
6.5	-4.60	0.41	7.3×10^{-6}
7	-5.00	-0.29	7.3×10^{-6}

isotherm data (Figure 9.2). The results suggest that although polynuclear surface complexes and/or precipitation can account for isotherms with slopes not equal to one (Lützenkirchen and Behra, 1994; Katz and Hayes, 1996), multisite adsorption is applicable when supported by spectroscopic data. More than one type of surface site has been experimentally observed on ferric oxyhydroxide (Bottero et al. 1993) and supported in crystallographic analysis (van Riemsdijk and Hiemstra, 1999). As Robertson and Leckie (1997) note, even when slopes equal one, this does not guarantee that only one type of site is present; it is more likely that several site types exist.

Even if site density is a function of pH, it appears that at least in this study, the high affinity site density falls within an order of magnitude of each other. Therefore, in terms of applying the TLM, a single set of parameters describing both adsorption edge and isotherm data would be more practical. Adsorption edges (Figure 9.3) are consistent with isotherm data, the % Ni sorbed increased significantly from pH 5 to 6.5 at low Ni concentrations (Figure 9.3); however, at the highest $[Ni]_0$ (Fig. 3a) the typical sigmoid curve is not observed potentially due to site saturation. All seven sets of TLM parameters derived from isotherms were used to predict edge data (Figure 9.3). Overall, only the pH 6.5 set of parameters was found to predict all edge data reasonably well (represented by the solid line in each edge plot in Figure 9.3). These parameters were further tested on the isotherms, and results (Figure 9.4) indicate that this one set of parameters successfully modeled adsorption. Therefore, a single set of TLM parameters was found to describe Ni adsorption on goethite over a broad range of conditions, covering almost seven orders of magnitude in concentration (10^{-10} to 10^{-3} M), ionic strength from 10^{-3} to 10^{-2}, and an environmentally relevant pH range from 5 to 6.5.

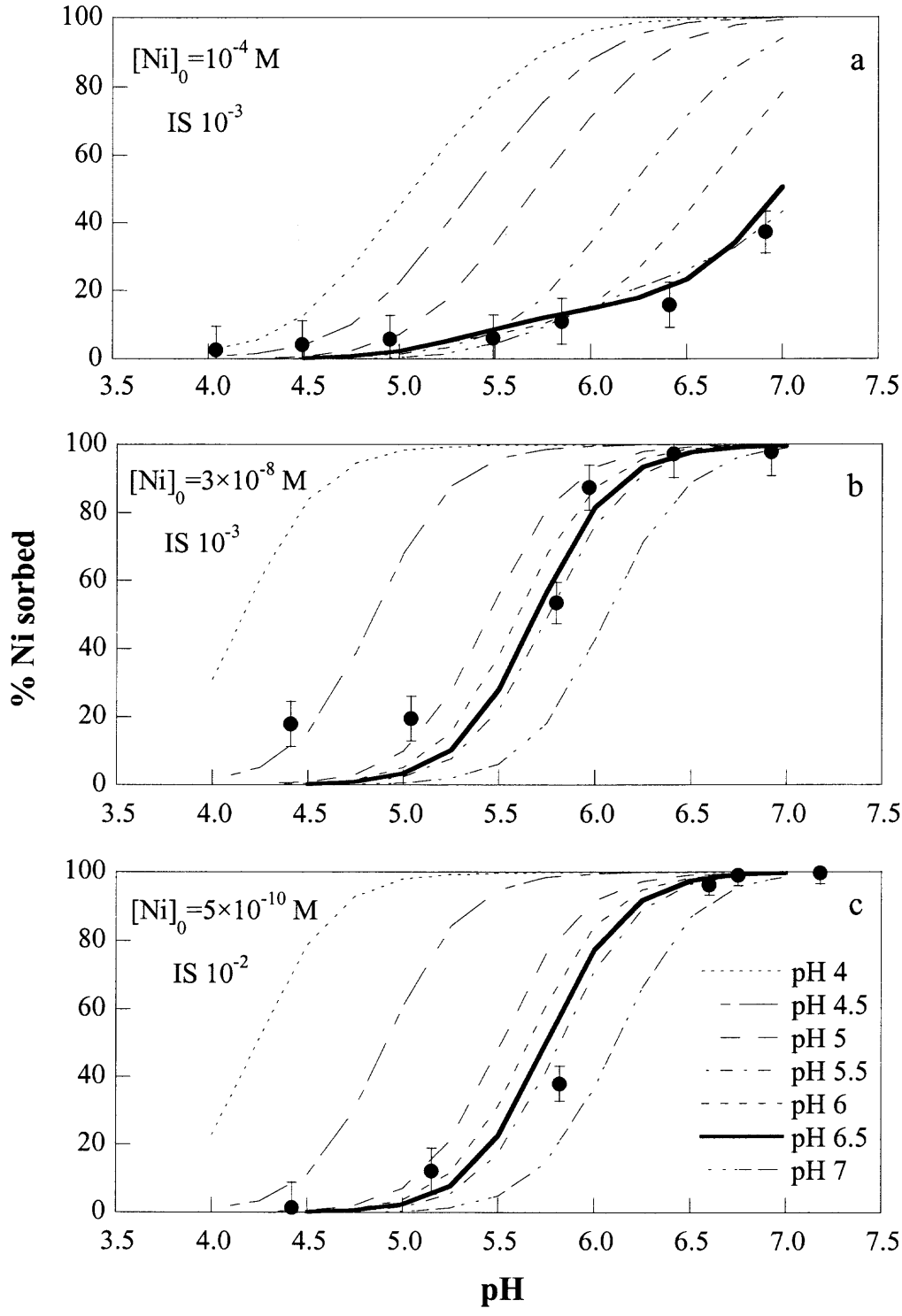

Figure 9.3 Ni adsorption edges for 1 g L^{-1} goethite conducted in air at room temperature; ionic strength adjusted with $NaNO_3$ (dots represent experimental data, lines represent TLM modeling using best-fit parameters obtained from modeling the isotherm data at different pH values).

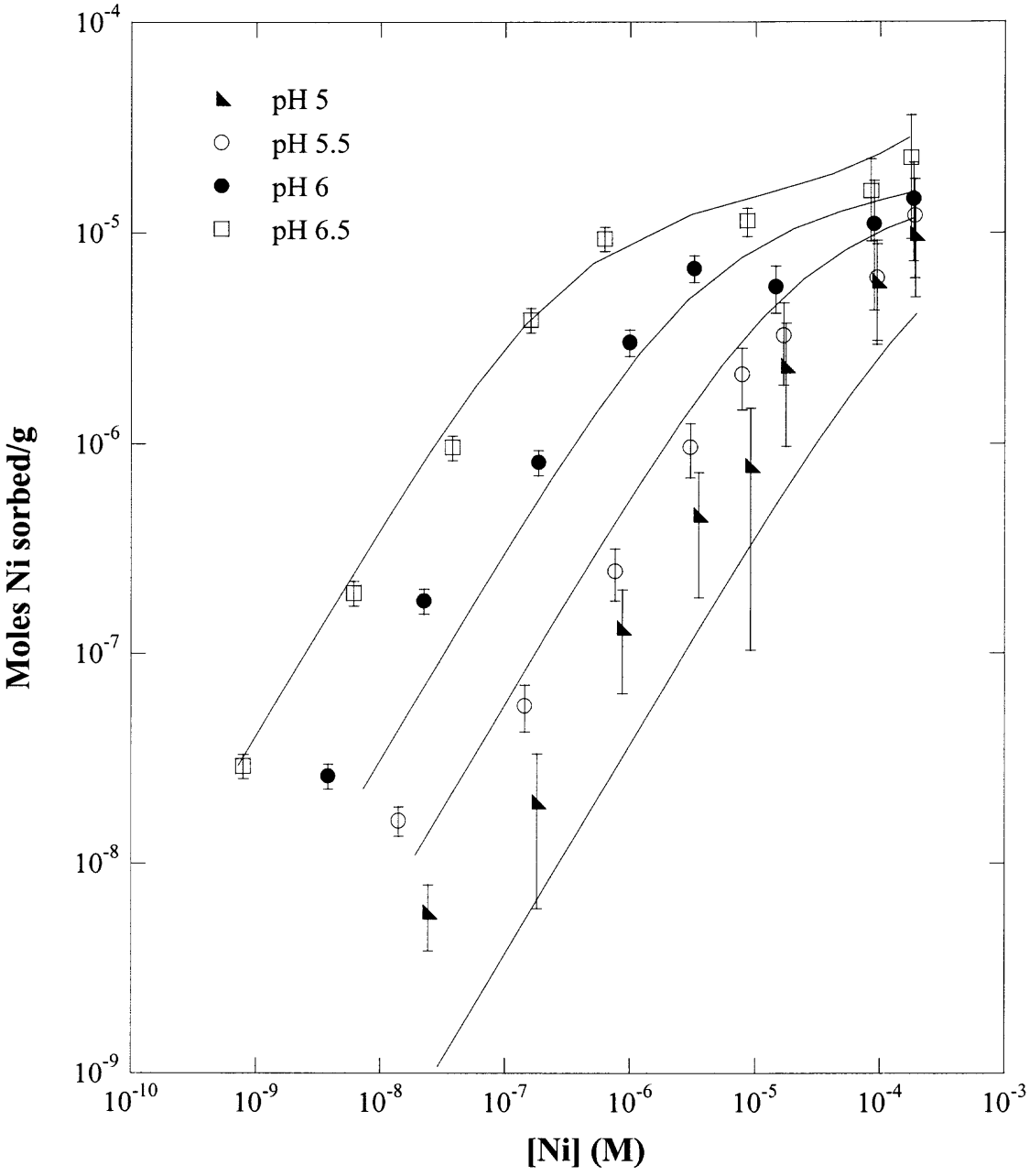

Figure 9.4 Ni adsorption isotherms for an open system at room temperature using 1 g L^{-1} goethite and 10^{-3} ionic strength (adjusted with $NaNO_3$). Solid lines represent TLM predictions using the parameters obtained from modeling isotherm at pH 6.5.

9.3 Zn Adsorption on Goethite

Regression of the Zn-goethite adsorption data using the TLM involved the same procedure applied in modeling Ni adsorption onto goethite. Adsorption isotherms (Figure 9.5) also reveal decreasing slopes as concentration approaches 10^{-5} M, necessitating the use of high and low affinity sites for modeling. Seven sets of parameters were obtained (Table 9.2) from modeling (Figure 9.5) and tested with edge data (Figure 9.6). For Zn, the pH 5.5 parameter set was observed to provide a reasonable fit of both the edge (solid line in each edge plot in Figure 9.6) and isotherm data (Figure 9.7) given uncertainties in both the data and model. Therefore, this unique set of parameters was found to describe Zn adsorption on goethite over a large range of conditions, covering six orders of magnitude in concentration (10^{-10} to 10^{-4} M), ionic strength from 10^{-3} to 10^{-2}, and an environmentally relevant pH range from 4 to 6.

Palmqvist et al. (1997) found no evidence of high-affinity surface sites on goethite; however, their study was conducted at low concentrations (~ 10^{-6} M). For Zn sorption on ferrihydrite, Dzombak and Morel (1990) obtained a group of $\log K_H$ and $\log K_L$ parameters by modeling a variety of edge and isotherm data; weighted averages of these logKs were determined to be the best estimates. Although reasonable fits were achieved using the best estimates, the surface complexes used in modeling were not spectroscopically supported. Dyer et al. (2004) used an XAS-derived surface complex $[(FeO)_2Zn]$ to fit Zn adsorption on 2-line ferrihydrite data over a pH range of 4-8 and a loading of 10^{-5} to 5×10^{-1} moles Zn $mole^{-1}$ Fe. Both the site density and best-fit equilibrium "constant" had to be adjusted with pH to adequately fit the isotherm data. In this study, a two-site TLM resulted in improved predictions of the Ni and Zn adsorption

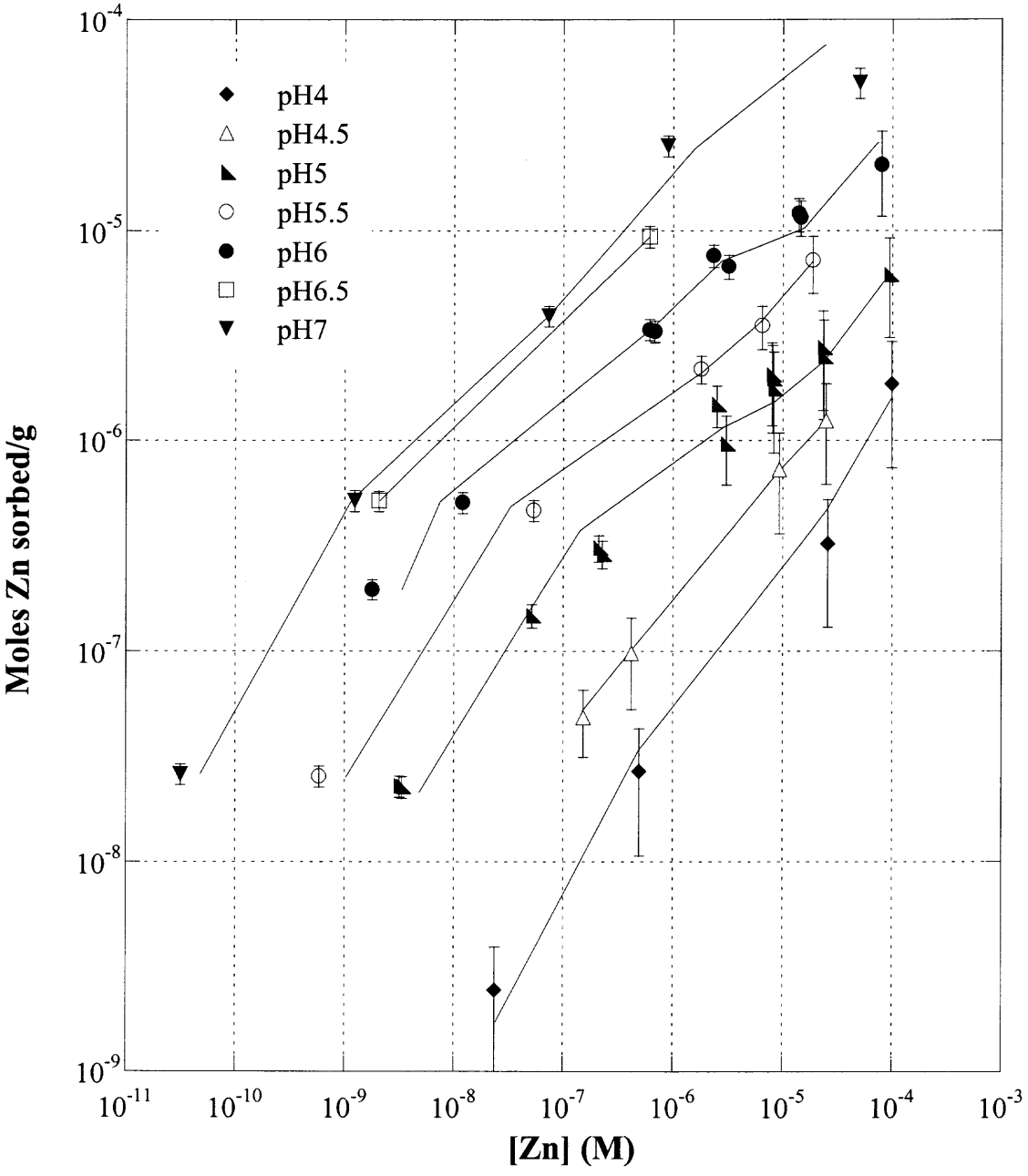

Figure 9.5 Zn adsorption isotherms for an open system at room temperature using 1 g L^{-1} goethite and 10^{-3} ionic strength (adjusted with $NaNO_3$). Solid lines represent TLM predictions.

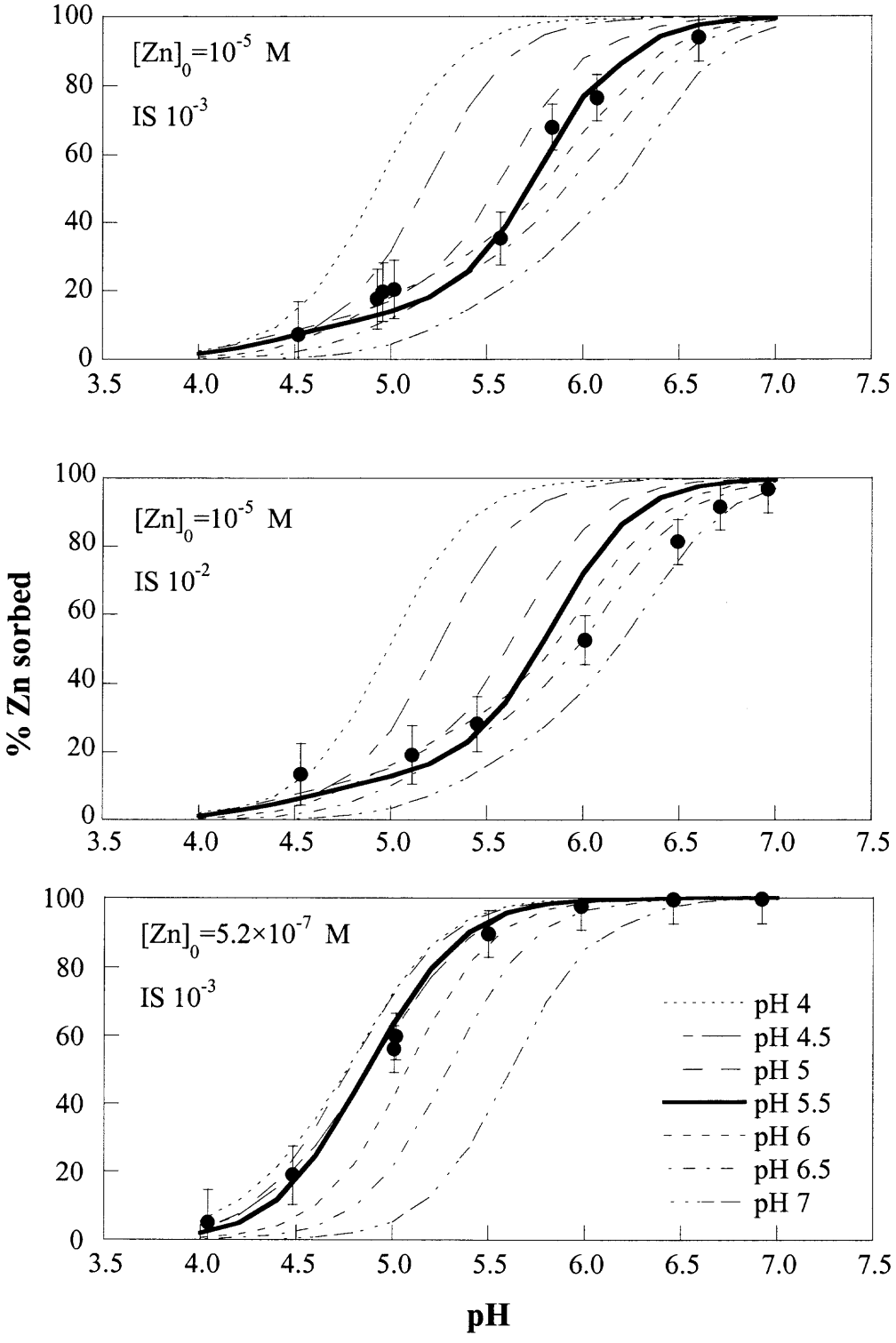

Figure 9.6 Zn adsorption edges for 1 g L^{-1} goethite conducted in air at room temperature; ionic strength adjusted with $NaNO_3$ (dots represent experimental data, lines represent TLM modeling using best-fit parameters obtained from modeling the isotherm data at different pH values).

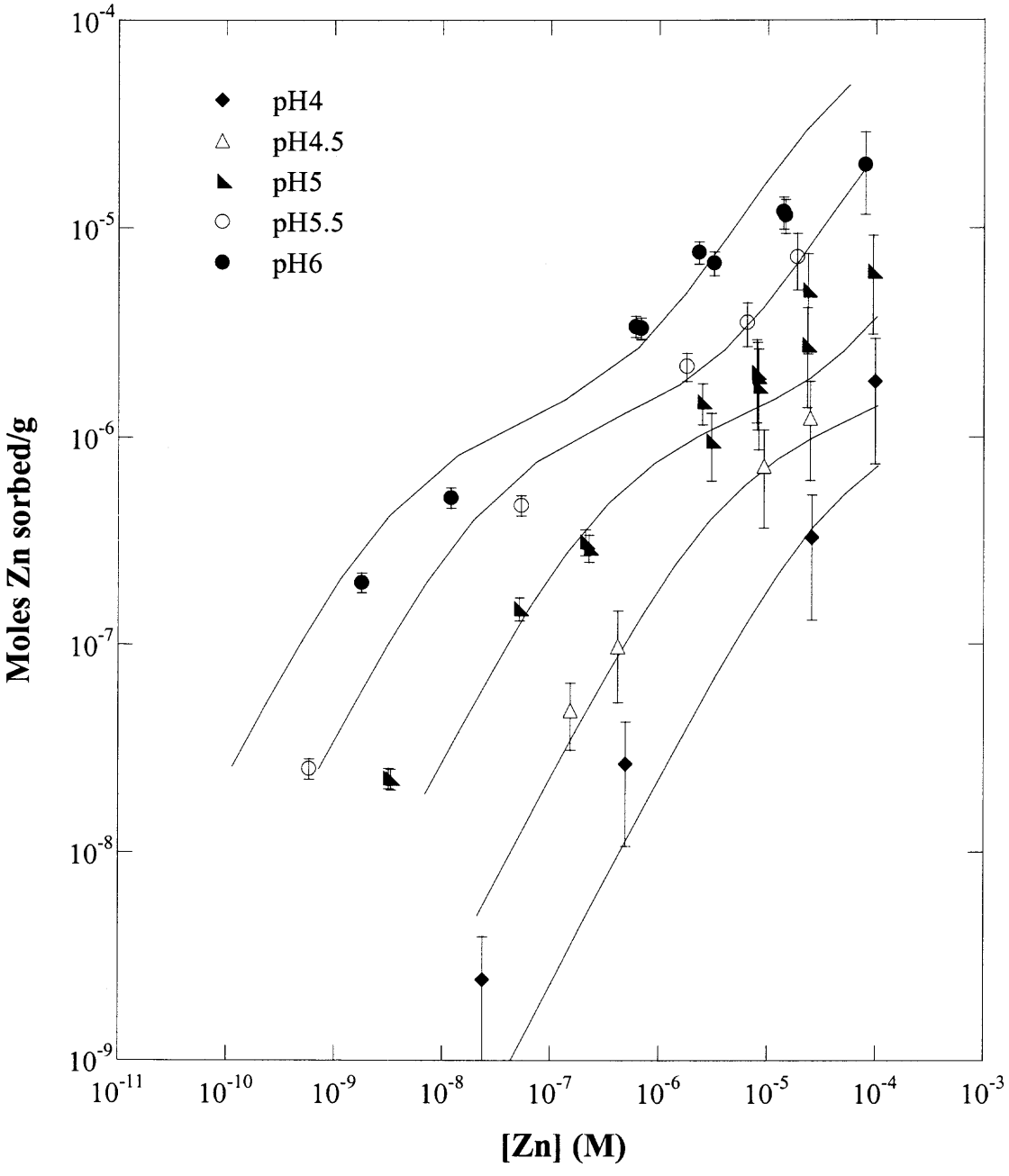

Figure 9.7 Zn adsorption isotherms for an open system at room temperature using 1 g L^{-1} goethite and 10^{-3} ionic strength (adjusted with $NaNO_3$). Solid lines represent TLM predictions using the parameters obtained from modeling isotherm at pH 5.5.

data over a broad range of conditions when using a single set of model parameters.

9.4 Ni and Zn Competition

The modeling results for single adsorbate systems (Table 9.2) indicate that the reaction constants for Zn(II) adsorption are greater than that for Ni(II), suggesting Zn ions exhibit a higher affinity than Ni ions for the goethite surface. This observation is in agreement with other studies (Tiller et al. 1984; Crawford et al. 1993; Gupta, 1998; Dube et al. 2001; Trivedi et al. 2001b; Jeon et al. 2003). Therefore, competition is expected when both ions are present and the site density is limited. Competition has been investigated by many researchers. For example, Gadde and Laitinen (1974) concluded that Pb sorbed more strongly than other ions (Zn, Cd, and Ti) on HFO and HMO surfaces; Balistrieri and Murray (1982) found that Mg(II) tends to suppress the adsorption of trace metals (Cu, Pb, Zn, and Cd) on goethite; Christophi and Axe (2000) observed that goethite has a greater affinity for Pb than Cu; Trivedi et al. (2001b) found that Zn and Ni bind more strongly than Ca to goethite; Bradl (2004) observed that Cd adsorption is strongly influenced by the presence of competing cations, such as divalent Ca and Zn; and Kanungo et al. (2004) found in a study on Co, Ni, Cu, and Zn sorption onto HMO that Ni experienced the greatest degree of displacement (Kanungo et al. 2004). However, competition between trace metals in other studies may have been difficult to demonstrate, because site density may not have been limiting (Swallow et al. 1980; Palmqvist et al. 1999).

The competition experiments were performed at pH 6. Compared to single adsorbate systems, Ni(II) adsorption decreased by approximately 23% due to presence of

Zn(II) (Figure 9.8). With a higher affinity for goethite surfaces, Zn(II) competes with Ni(II) in occupying sites available for both metals. Ni(II) and Zn(II) competition was predicted using both sets of parameters for Ni (pH 6.5 set) and Zn (pH 5.5 set) and results were within the data and model error (Figure 9.8), predictions were within the data error.

Although SCMs have been employed to simulate multisolute adsorption competition, success has been mixed. Using a generalized two-layer model, Ali and Dzombak (1996) predicted adsorption of sulfate and organic acids reasonably well based on single-adsorbate data over a wide range of conditions. Underprediction for the weaker adsorbate was explained by adsorbate-specific surface site heterogeneity and/or by inaccurate representation of Coulombic effects in the model. Gao and Mucci (2001) predicted the shape of the competitive adsorption data for phosphate and arsenate on goethite, but failed to reproduce it quantitatively. Heidmann et al. (2005) were able to predict Cu and Pb competition on kaolinite successfully using the combination of a 1-pK Basic Stern model for edge sites and an extended Basic Stern model for face sites; nevertheless the surface complexes were simply assumptions without spectroscopic support. Hayes and Katz (1996) pointed out that non-electrostatic, diffuse layer, and constant capacitance models are likely to be less successful in modeling competition data, because they do not account for differences in the affinity of inner- and outer-sphere complexes. Christl and Kretzschmar (1999) demonstrated that surface site density is a key parameter in applying SCMs to multicomponent environments and they obtained best predictions with site densities between 5 and 10 sites nm^{-2} for hematite. Palmqvist et al. (1999) showed that single-adsorbate modeling predicted adsorption competition for Cu and Zn, but underestimated Pb(II) adsorption. Both the TLM and NEM predicted Cd and

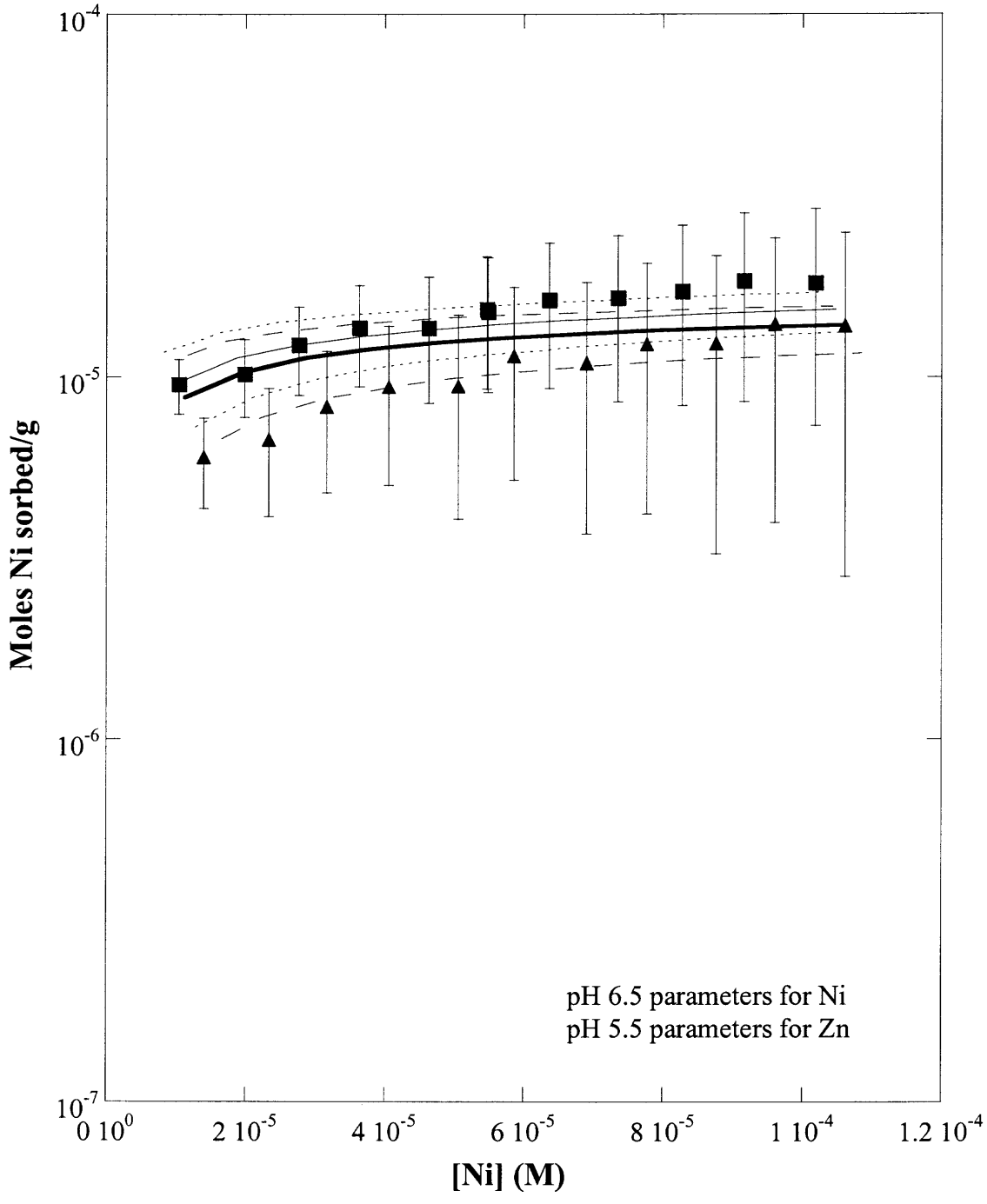

Figure 9.8 Ni adsorption in Zn-Ni bisolute systems at 1 g L^{-1} goethite, pH 6, 10^{-3} ionic strength (symbols represent experimental data; solid lines represent TLM predictions using log K_{a1}=-8.3, log K_{a2}=-9.3, log K_{anion}=9.94, log K_{cation}=-8.25 and fitting parameters obtained from single adsorbate modeling; dotted and dashed lines represent +/- two standard deviations).

Ca competition on HFO; however, the model failed at the lowest ionic strength (0.005) studied (Cowan et al. 1991). Results of this study indicate that, when coupled with spectroscopic data, parameters derived from single-adsorbate systems can be used to predict adsorption competition within reasonable uncertainty limits.

9.5 Summary

A triple-layer surface complexation model has been used to simulate metal adsorption onto goethite surfaces. Constrained with spectroscopic information, a 2-pK, 2-site TLM successfully predicted Ni and Zn adsorption in single-adsorbate systems. Curvature in the constant-pH adsorption isotherms was accurately described using both high-affinity and low-affinity type sites. A unique set of parameters was found for each metal ion that successfully describes adsorption over a wide range of experimental conditions (six to seven orders of magnitude in adsorbate concentration, ionic strength ranging from 10^{-3} to 10^{-2}, and an environmentally relevant pH range). Competition was also predicted with parameters calibrated using single adsorbate data. Results of this study suggest that accurate chemical and physical representations of the complexes at the interfacial region assist in developing mechanistically based predictive models. As a result, these unique sets of parameters for Ni and Zn may inherently provide a more comprehensive depiction of surface interactions over a broad range of conditions.

Although adsorption and competition on discrete oxide have been successfully described using surface complexation models, to predict metal distribution and transport in soils and sediments these models needs to be tested using metal adsorption to iron

oxide-coated silica. Ni and Zn sorption to iron oxide-coated silica is discussed in the next chapter.

CHAPTER 10

NI AND ZN SORPTION TO IRON OXIDE-COATED SILICA

Iron oxide-coated silica represents an important surface in soils and sediments. The effect of iron oxide coatings on adsorption needs to be addressed for better understanding of heavy metal distribution in the environment. Macroscopic adsorption studies have been conducted on goethite-coated silica and compared with those on discrete silica and goethite. Results are discussed below.

10.1 Ni and Zn Adsorption Edges

Ni adsorption edges on 5 g L^{-1} goethite-coated silica (GACS) and silica were performed over the pH range from 2 to 8 as a function of ionic strength (IS, 10^{-3} to 10^{-2}). The sigmoid-shaped edge was not found for silica, possibly due to site saturation, and was only observed for GACS at IS 10^{-3} (Figure 10.1). The edge jump begins at pH 6 for silica and covers a range of 4-8 for GACS. Compared to silica, 50% adsorption for the GACS system occurred 1.4 pH units lower at IS 10^{-3} and 0.6 pH units lower at IS 10^{-2}. The GACS surface clearly shows a greater affinity for Ni. Ionic strength effects are observed for the silica surface (Figure 10.1) potentially suggesting Ni sorbed as outer-sphere complexes. Although inner-sphere Ni complexes were found on discrete HFO and goethite, as presented in Chapter 7, the distinct edges at ionic strength 10^{-3} and 10^{-2} for Ni/GACS system suggest that the silica surface significantly impact the electrostatic character of coated silica. This observation is consistent with the small amount of goethite coatings, which are non-uniformly distributed (Figure 6.6 and Figure 6.7). However, the significant increase in % Ni sorbed for GACS (Figure 10.1) suggests that

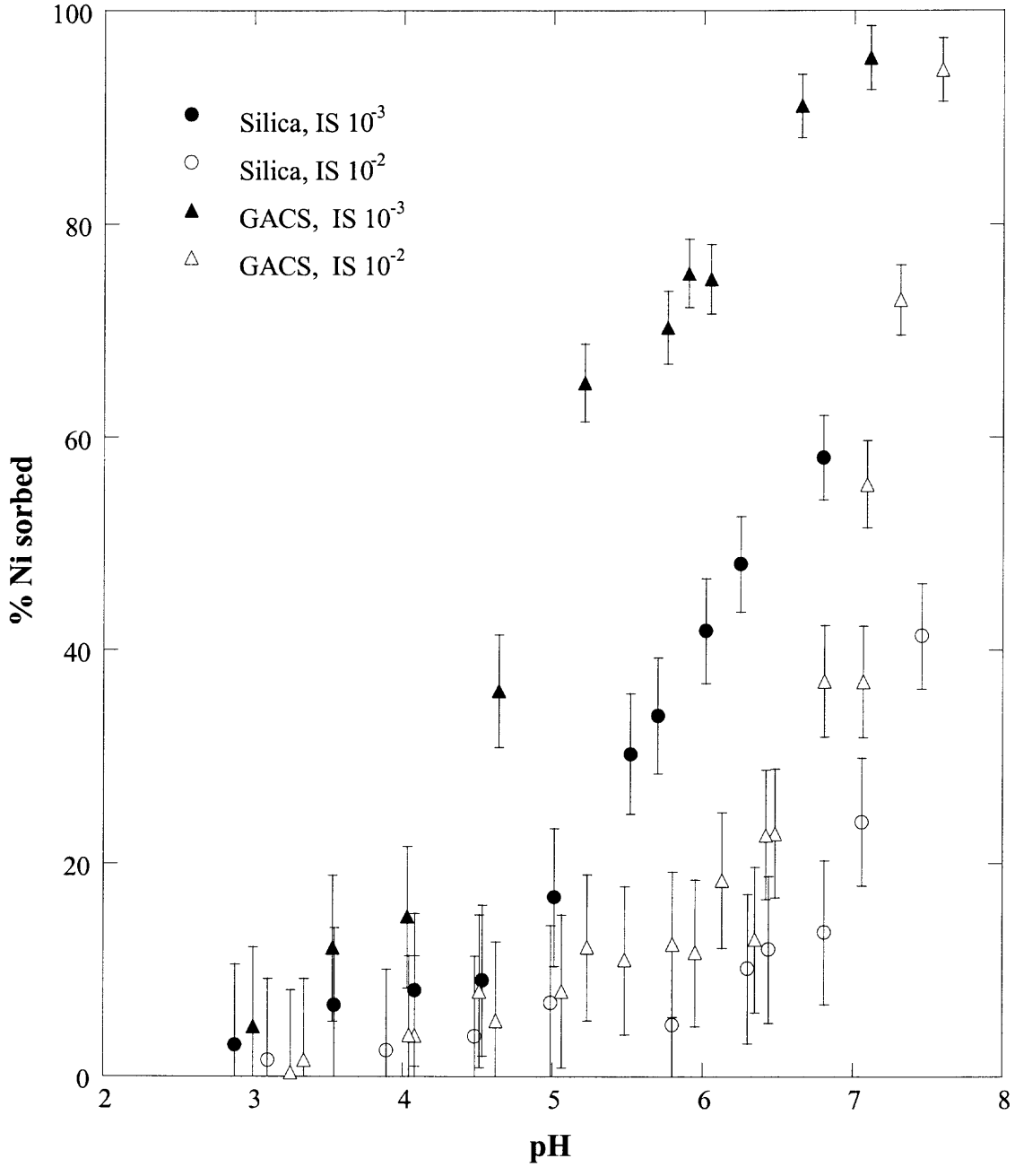

Figure 10.1 Ni adsorption edges on 5 g L^{-1} silica and goethite-coated silica (GACS, 4.01 mg Fe g^{-1} solid) with $[Ni]_0 = 5\times10^{-10}$ M as a function of ionic strength (IS).

adsorption affinity of the coated media is strongly influenced by goethite coatings.

Similar results were observed in Zn adsorption edges (Figure 10.2). Percent Zn sorbed increases after pH 5 for silica and the edge jump was over a broad pH range from 4 to 8 for GACS. The goethite coatings present a higher affinity for Zn than silica and the pH values at which 50% adsorption occurs lowered by 1.7 pH units at IS 10^{-3} and 1.4 pH units at IS 10^{-2}. Both systems show ionic strength effects on Zn sorption; therefore, silica again appears to dominate electrostatic interactions of the coated media.

Overall, similar to proton adsorption, both components of the coated silica affect Ni and Zn adsorption. By distinguishing inner- and outer-sphere adsorption with XAS, the triple layer model is expected to be more advantageous in modeling than other models such as CCM, DLM, and Stern model. This modeling work along with XAS is recommended in future research.

10.2 Ni and Zn Adsorption Isotherms

Ni adsorption isotherms with silica, GACS, and goethite were conducted from pH 4 to 7 under ionic strength 10^{-3}. Results (Figure 10.3) indicate that Ni adsorption to these sorbents increases in the order of silica < GACS < goethite. For silica (Figure 10.4a), pH 4 and 5 isotherms have slopes approximately equal to one below a Ni concentration of 10^{-7} M and less than one between 10^{-7}-10^{-6} M. Saturation of the higher affinity sites (approximately 5×10^{-9} mole Ni g^{-1} silica) may have occurred. The shape of the pH 4 and 5 isotherms at Ni concentrations greater than 10^{-6} M is consistent with presence of a lower affinity site and/or formation of Ni polymer (Dzombak and Morel, 1990; Katz and Hayes, 1995b; Hayes and Katz, 1996). However, there was no indication of low affinity

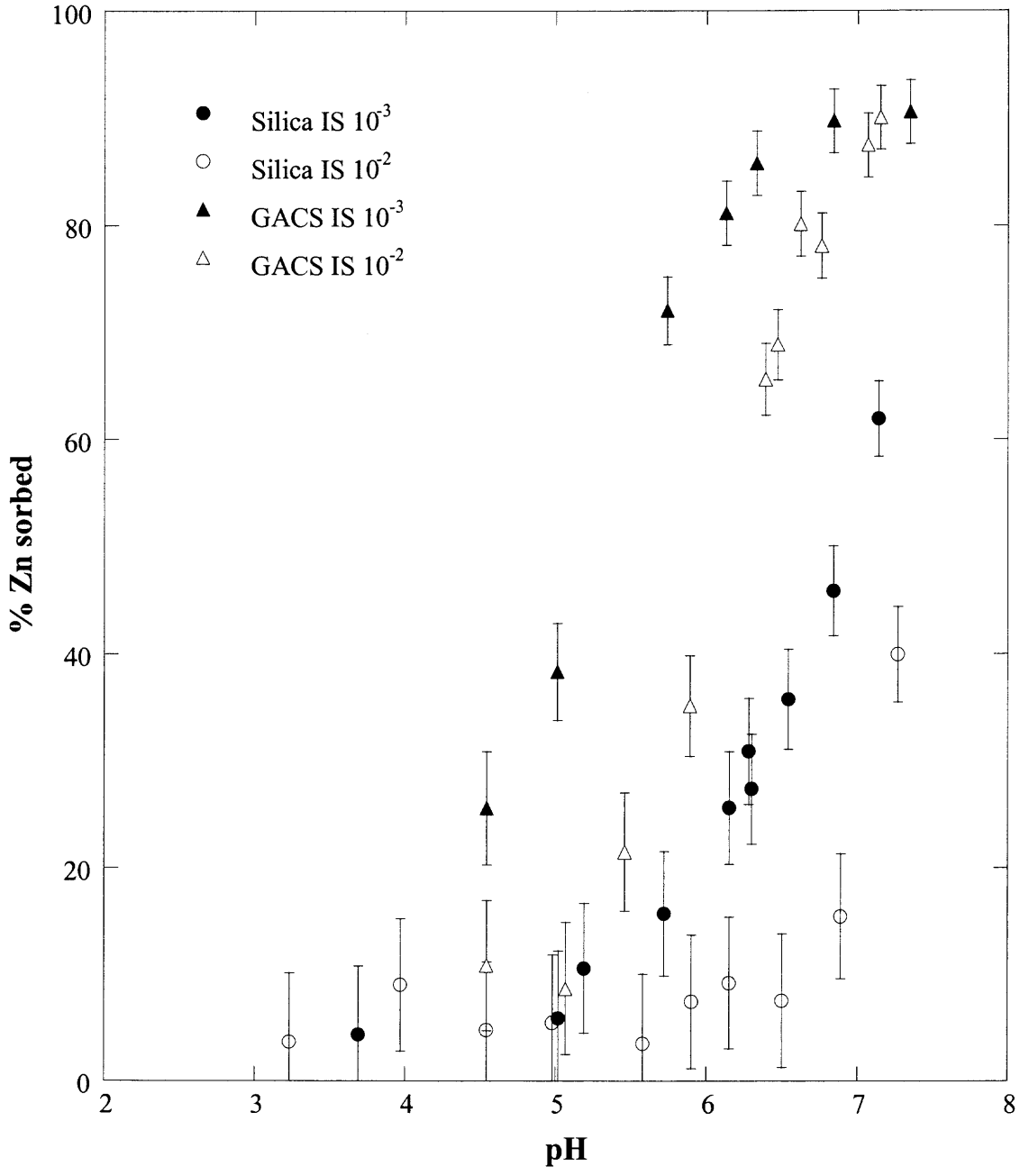

Figure 10.2 Zn adsorption edges on 5 g L^{-1} silica and goethite-coated silica (GACS, 4.01 mg Fe g^{-1} solid) with $[Zn]_0 = 2\times10^{-8}$ M as a function of ionic strength (IS).

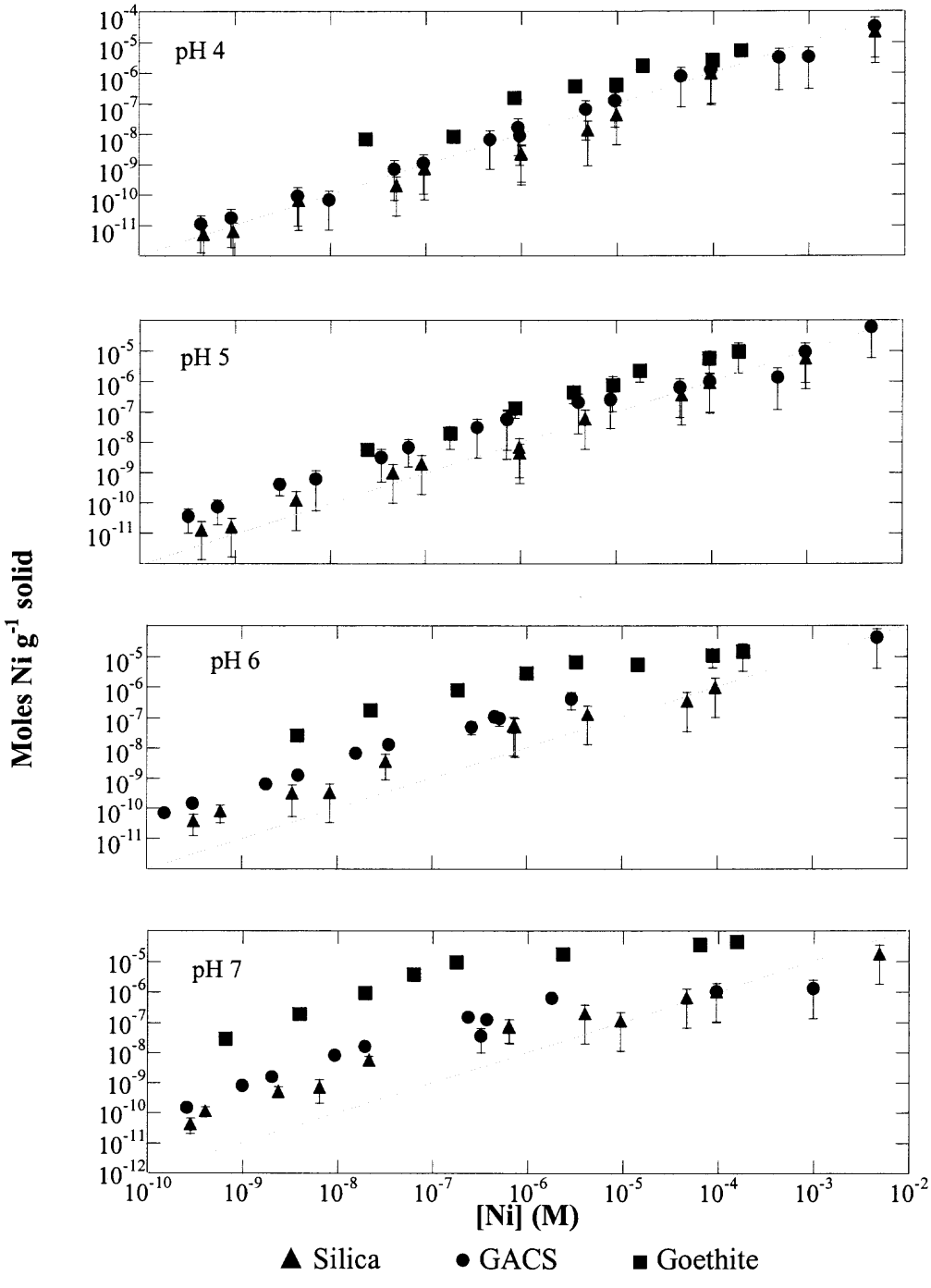

Figure 10.3 Comparison of Ni adsorption isotherms on 5 g L^{-1} silica and goethite-coated silica (GACS, 4.01 mg Fe g^{-1} solid) and 1 g L^{-1} goethite at ionic strength (IS) 10^{-3} as a function of pH.

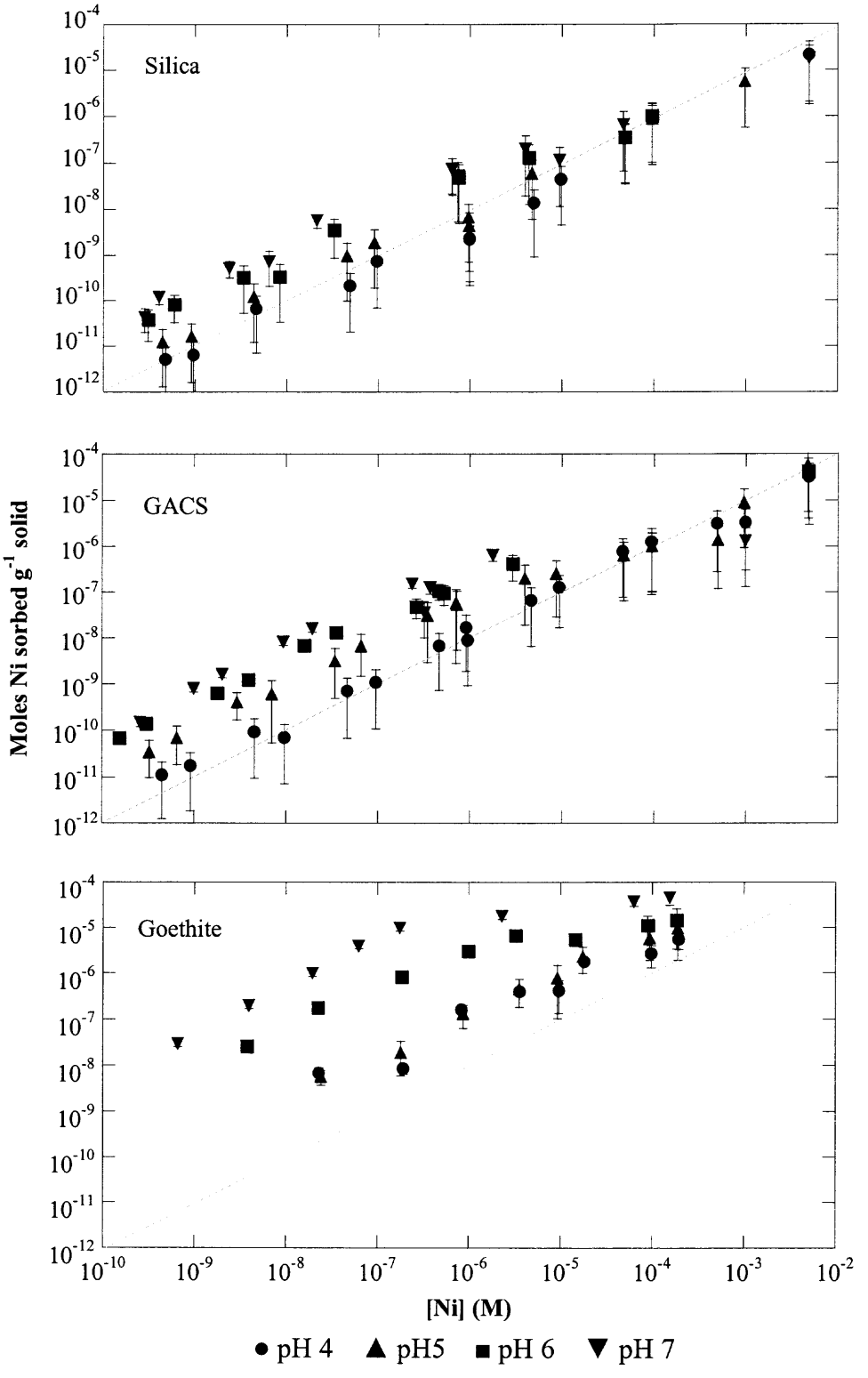

Figure 10.4 Ni adsorption isotherms on 5 g L^{-1} silica and goethite-coated silica (GACS, 4.01 mg Fe g^{-1} solid) and 1 g L^{-1} goethite at ionic strength (IS) 10^{-3} as a function of pH.

sites in the pH 6 and 7 isotherms. For these two conditions, the isotherm appears approach saturation (approximately 5×10^{-7} mole Ni g^{-1} silica) for Ni concentrations greater than 10^{-6} M and less than 10^{-4} M. Interestingly, using a non-electrostatic model, Delolme et al. (2004) obtained an optimized SiOH site concentration of 8×10^{-7} mole g^{-1} for a natural sand with a diameter of 0.3 to 2 mm, similar to that used in this study. The silica isotherms overlap at Ni concentrations greater than 10^{-4} M; this may suggest formation of Ni polymers instead of a lower affinity site. The Ni/silica adsorption isotherm seems to reveal more information than the adsorption edges about surface sites suggesting more than one mechanism. Coupled with electrophoretic information, Kuan et al. (2004) modeled Al(III) adsorption to an amorphous silica reasonably well with a surface complexation/precipitation model over Al(III) concentrations ranging from $10^{-4.5}$ to 10^{-2} M. The authors proposed $Al(H_2O)_6^{3+}$ complex at low pH (<3) and low concentration (up to $10^{-3.75}$ mole Al g^{-1} silica), a hydrolyzed $Al(OH)(H_2O)_6^{2+}$ complex at loadings of $10^{-3.75}$ to $10^{-3.25}$ mole Al g^{-1} silica, and surface-induced precipitation at loadings greater than $10^{-3.25}$ mole Al g^{-1} silica. Also, Cu adsorption on silica can only be modeled by inclusion of surface polymerization and precipitation at higher loadings as well (Subramaniam et al. 2003).

Consistent with the edge studies, Ni isotherms suggest GACS sorbs more Ni than silica at the same pH (Figure 10.3). However, the slopes for all isotherms on GACS (Figure 10.4b) are approximately equal to one up to a Ni concentration of 10^{-6} M. The heterogeneous surface appears to act as one averaged surface; this may be due to the influence of goethite. At Ni concentrations between 10^{-6} and 10^{-3} M, site saturation approaches $\sim2\times10^{-6}$ mole Ni g^{-1} solid. This site density is consistent with the estimated

one for GACS (2.77×10^{-6} mole sites g^{-1} solid) based on the degree of coating and site concentrations of goethite (3.09×10^{-4} mole g^{-1} goethite, Chapter 9) and silica (8×10^{-7} mole g^{-1}, Delolme et al. 2004). At Ni concentrations greater than 10^{-3} M, the increased slope in the isotherms may be due to polymerization. Overall, GACS exhibits one type of site over a large range of Ni concentrations (10^{-10} to 10^{-3} M). Polymers may form on GACS at Ni concentrations greater than 10^{-3} M in contrast to that observed for silica where polymerization may occur at concentrations greater than 10^{-4} M. Although a low affinity site was not reflected in the GACS isotherms, the surface is heterogeneous by nature. Metal sorption mechanisms therefore need to be investigated with other techniques including XAS.

Zn adsorption isotherms were performed on silica, GACS, and goethite at pH 5 and 6 and ionic strength 10^{-3} (Figure 10.5). Adsorption on coated silica is less than that on goethite and slightly greater than silica due to the presence of goethite. The Zn isotherms with silica and GACS are similar over the concentration of 10^{-10} to 10^{-5} M (Figure 10.5) with slopes approximately equal to one below 10^{-7} M and less than one at greater concentrations up to $\sim5\times10^{-6}$ M (Figure 10.6a and b). Site saturation may be approached at approximately 10^{-7} mole Zn g^{-1} solid for both systems at pH 5 and 6. The abrupt increase in adsorption near 10^{-5} M may suggest precipitation of a new phase. In an EXAFS analysis of Zn complexation on an amorphous silica, Roberts et al. (2003) observed inner-sphere adsorption complexes for pH 5.1 to 7.45, a loading 6.3×10^{-6} to 2.63×10^{-4} mole Zn g^{-1} solid, and a reaction time of 24 hours to 18 months. They found amorphous $Zn(OH)_2$ precipitation occurring at the highest pH 7.51. Overall, isotherms with silica and GACS suggest one type of site over a Zn concentration of 10^{-10} to 5×10^{-6}

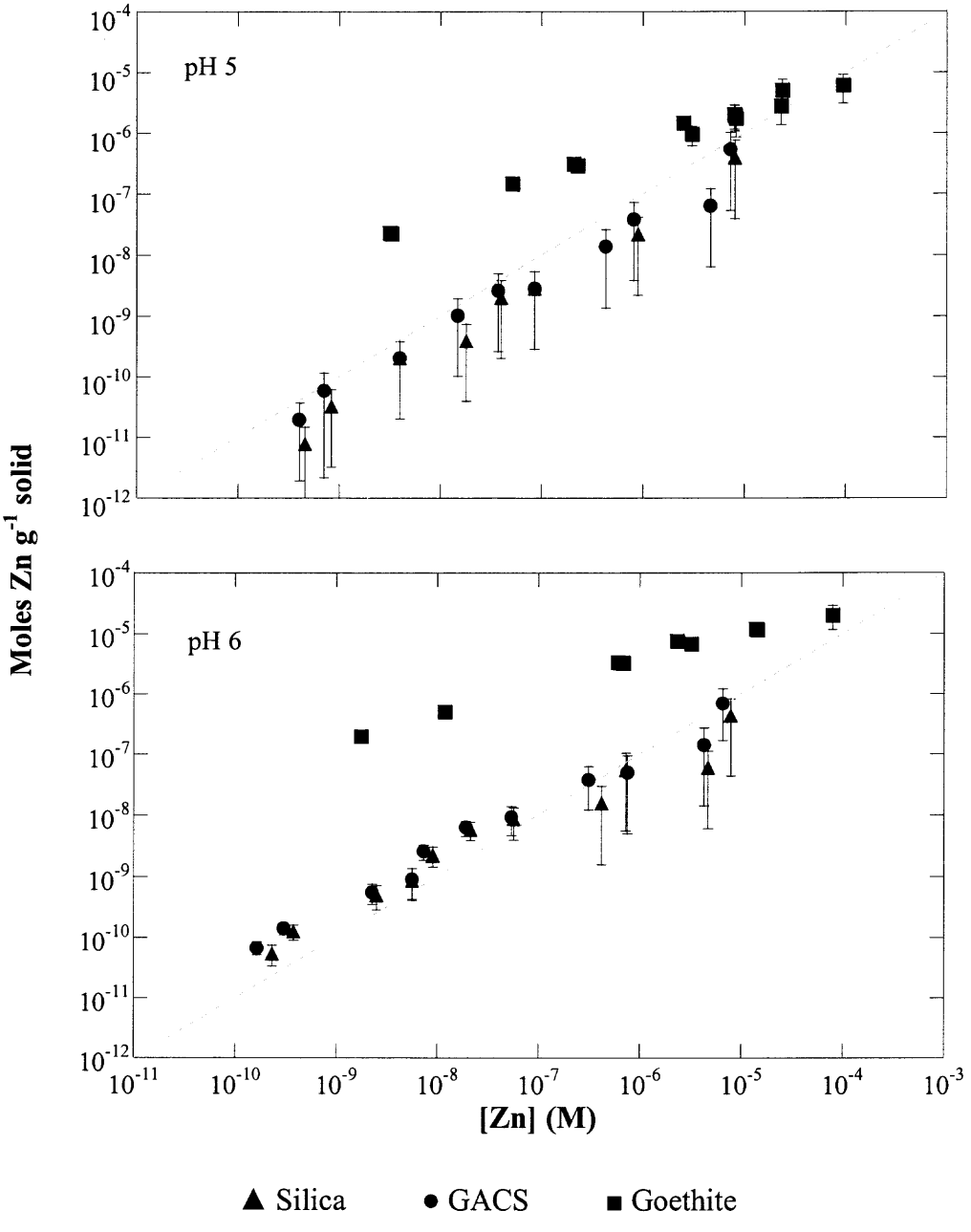

Figure 10.5 Comparison of Zn adsorption isotherms on 5 g L^{-1} silica and goethite-coated silica (GACS, 4.01 mg Fe g^{-1} solid) at ionic strength (IS) 10^{-3} as a function of pH.

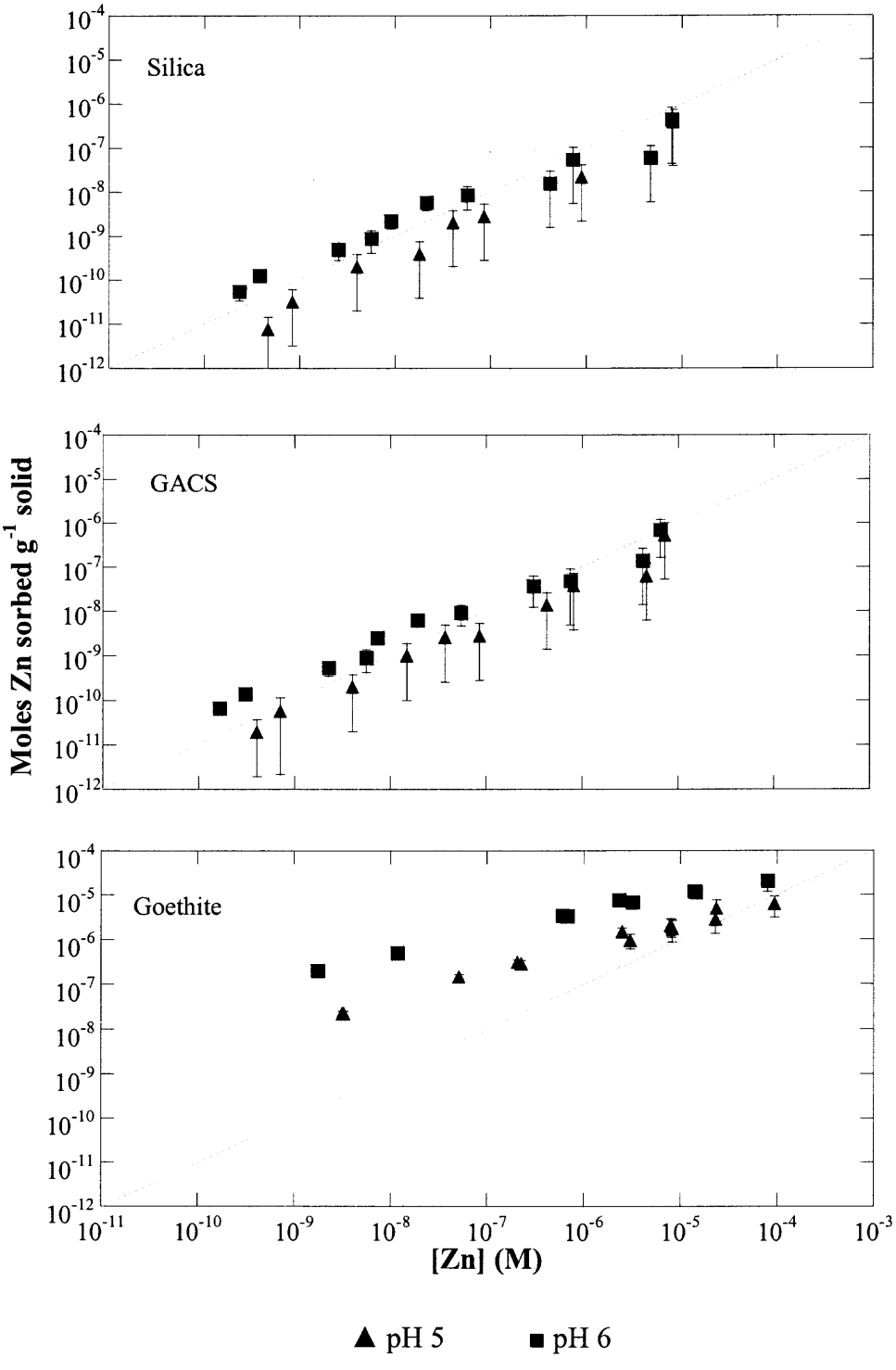

Figure 10.6 Zn adsorption isotherms on 5 g L^{-1} silica and goethite-coated silica (GACS, 4.01 mg Fe g^{-1} solid) and 1 g L^{-1} goethite at ionic strength (IS) 10^{-3} as a function of pH.

M. Polymerization may occur at concentrations greater than 5×10^{-6} M. Similar to Ni, Zn adsorption mechanisms need to be investigated further with techniques including spectroscopic ones.

10.3 Summary

Overall, GACS has a higher affinity for Ni and Zn than silica due to the presence of goethite. However, the electrostatic effect is controlled by silica. Both surfaces are needed for successfully describing adsorption on this heterogeneous sorbent. Although edge studies potentially suggest outer-sphere adsorption for silica and GACS, Ni and Zn adsorption isotherms reveal more than one sorption mechanism. Silica exhibits high- and low-affinity sites for Ni at low pH (4 and 5), but one type of site for Ni at high pH (6 and 7) and for Zn at all pH values (4-7). GACS is composed of two types of surfaces, however, only one type of adsorption site was reflected in Ni and Zn isotherms up to 10^{-6} M. Although Ni and Zn adsorption on goethite were successfully modeled without inclusion of polymer formation, it may be needed for modeling silica and GACS system. Depicting accurate adsorption mechanisms under various conditions need to be addressed using techniques including EXAFS. This work is challenging because metal loadings are low (Figure 10.3 and Figure 10.5). Amorphous silica is a high surface area analogue for quartz (Manceau et al. 1999; Elzinga and Sparks, 2002), which may be a good substrate for studying metal adsorption. Overall, sorption on iron oxide-coated silica has not yet come to the same level as discrete iron oxide, and therefore more work is needed in this area.

CHAPTER 11

CONCLUSIONS AND FUTURE WORK

Sorption of trace elements onto iron oxide is an important process regulating contaminant mobility and bioavailability in natural systems. The purpose of this research is to understand the effect of iron oxides, as discrete particles and coatings, on contaminant adsorption and develop surface complexation models to predict heavy metal adsorption and competition.

A model system for soils and sediments, iron oxide-coated silica, was synthesized using adsorption and precipitation methods. The degree of coating was highly sensitive to the particle size of silica and ranged between 0.59 and 21.36 mg Fe g^{-1} solid. The interaction between goethite and silica potentially involves chemical forces. Iron oxide coatings on the silica surface are non-uniform increasing surface area and introducing small pores. The pH_{PZC} of coated silica is between that of pure silica and iron oxide suggesting both silica and goethite surfaces are important for adsorption. Ni adsorption on the coated silica is greater than that for pure silica and the sub-micrometer goethite coatings exhibit a larger capacity than discrete goethite impacting interactions at the aqueous interface.

EXAFS analysis of Pb(II)-sorbed to freshly precipitated HFO suggest that Pb(II) ions form mononuclear bidentate edge-sharing surface complexes on FeO_6 octahedra. This mechanism appears to be invariant of pH, ionic strength, Pb loading, and reaction time. The internal sites on micropore walls appear to be no different than the external ones. Intraparticle surface diffusion modeling described the two-step Pb/HFO sorption process reasonably well. The rate-limiting diffusion process may occur for decades

accounting for approximately 46% of total Pb uptake. XAS also revealed that the freshly precipitated HFO exhibits short-range order possibly forming edge and face-sharing polymers. By binding to the edges of octahedra polymers, Pb(II) ions inhibit crystallization of HFO which is stable up to 21 months of aging, thus maintaining its large capacity for heavy metals.

Similarly, Ni(II) forms mononuclear bidentate edge-sharing surface complexes upon adsorption to HFO. This mechanism was observed as a function of ionic strength 2.8×10^{-3} to 10^{-1}, pH 6 to 7, loading 8×10^{-4} to 8.1×10^{-3} mole Ni g^{-1} HFO, and reaction time 4 hours to 8 months. The presence of Ni(II) potentially inhibited HFO transformation into a more crystalline iron oxide; therefore the large sorption capacity of HFO was maintained. Metastable α-$Ni(OH)_2$ appears to have formed when coprecipitated with HFO. Ni^{2+} was not found to substitute for Fe^{3+} up to 8 months at room temperature possibly because HFO did not undergo phase transformation into a more crystalline form.

Constrained with spectroscopic information, the 2-pK TLM can successfully predict Ni or Zn adsorption in single adsorbate systems. The curvature in adsorption isotherms was accurately described using two types of sites – high affinity and low affinity ones. A unique set of parameters was found for each metal ion that can successfully describe adsorption over a large range of experimental conditions, covering six to seven orders of magnitude in concentration, ionic strength from 10^{-3} to 10^{-2}, and an environmentally relevant pH range. Competition was also predicted quantitatively with parameters calibrated using single adsorbate data.

GACS has a higher affinity for Ni and Zn than silica due to the presence of goethite. However, the electrostatic effect is controlled by silica. Therefore, both

surfaces are needed for successfully describing adsorption on this heterogeneous sorbent. Ni and Zn adsorption isotherms reveal more than one sorption mechanism on silica and coated silica. Although GACS is composed of two types of surfaces, only one type of adsorption site was reflected in Ni and Zn isotherms up to 10^{-6} M. Polymer formation may be needed for modeling silica and GACS system. Depicting accurate adsorption mechanisms under various conditions need to be addressed using techniques including spectroscopic ones.

Therefore, future work associated with this research should include addressing adsorption mechanisms on silica and iron oxide-coated silica under various conditions using techniques including XAS. Amorphous silica can be used in this regard because of its high surface area. Speciation results can then be used to constrain surface complexation modeling for adsorption to coated silica. Additionally, heavy metal distribution is regulated by microorganisms in the environment as well. Metal ions may be involved in metabolic activities and/or sorbed to biotic coatings. This interaction is not well understood yet and needs to be addressed for better description of natural systems. Models developed for biotically and/or abiotically coated heterogeneous systems can then be incorporated into environmental management programs to predict the bioavailability of heavy metals and evaluate the potential ecological risk.

APPENDIX A

SOLUBILITY AND SPECIATION DIAGRAM FOR NI, PB, AND ZN

The solubility and speciation diagrams of Ni, Pb, and Zn are presented below.

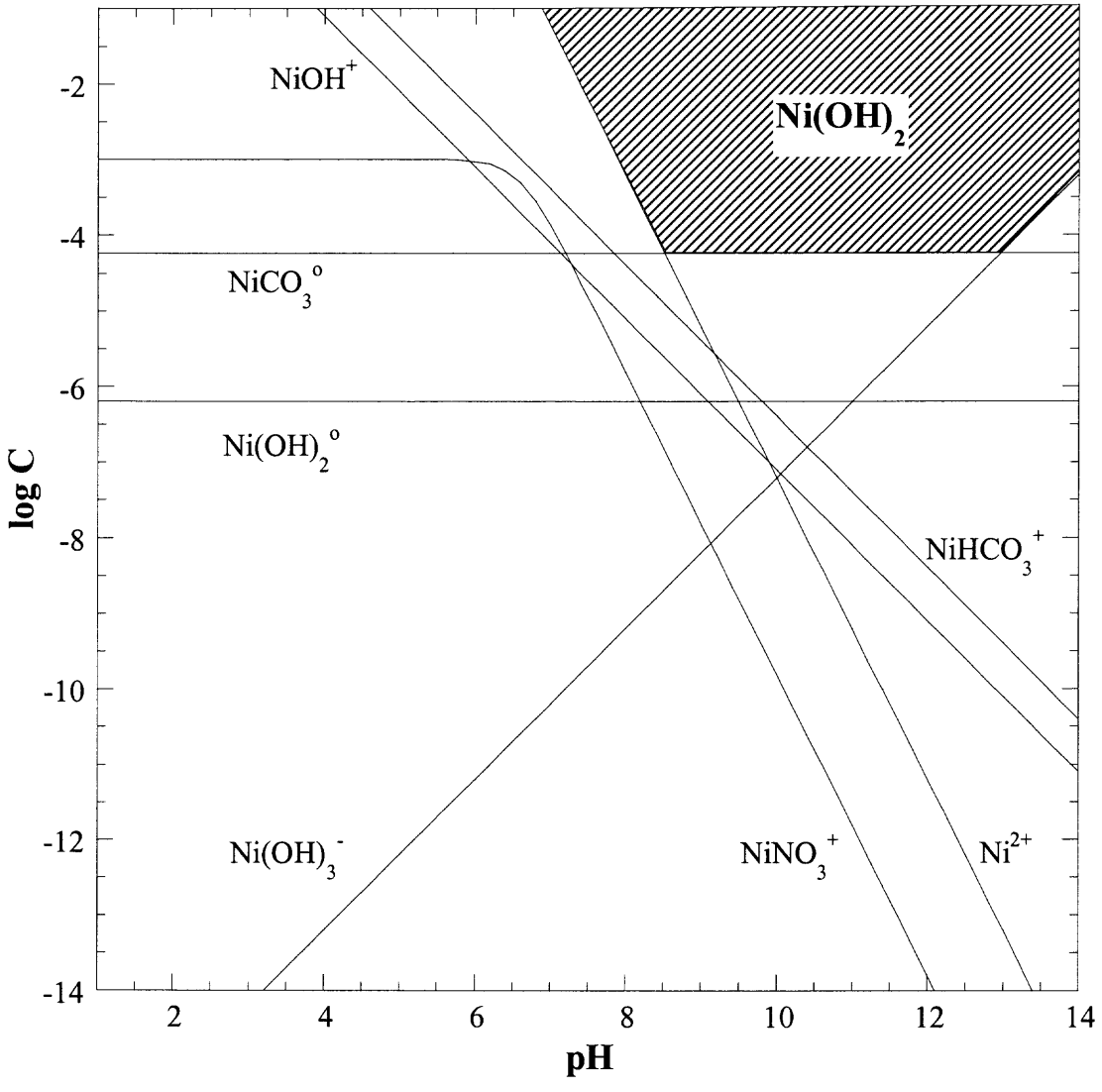

Figure A.1 Ni solubility in open system at 298 K (in 10^{-3} M $NaNO_3$, $P_{CO2}=10^{-3.46}$ atm).

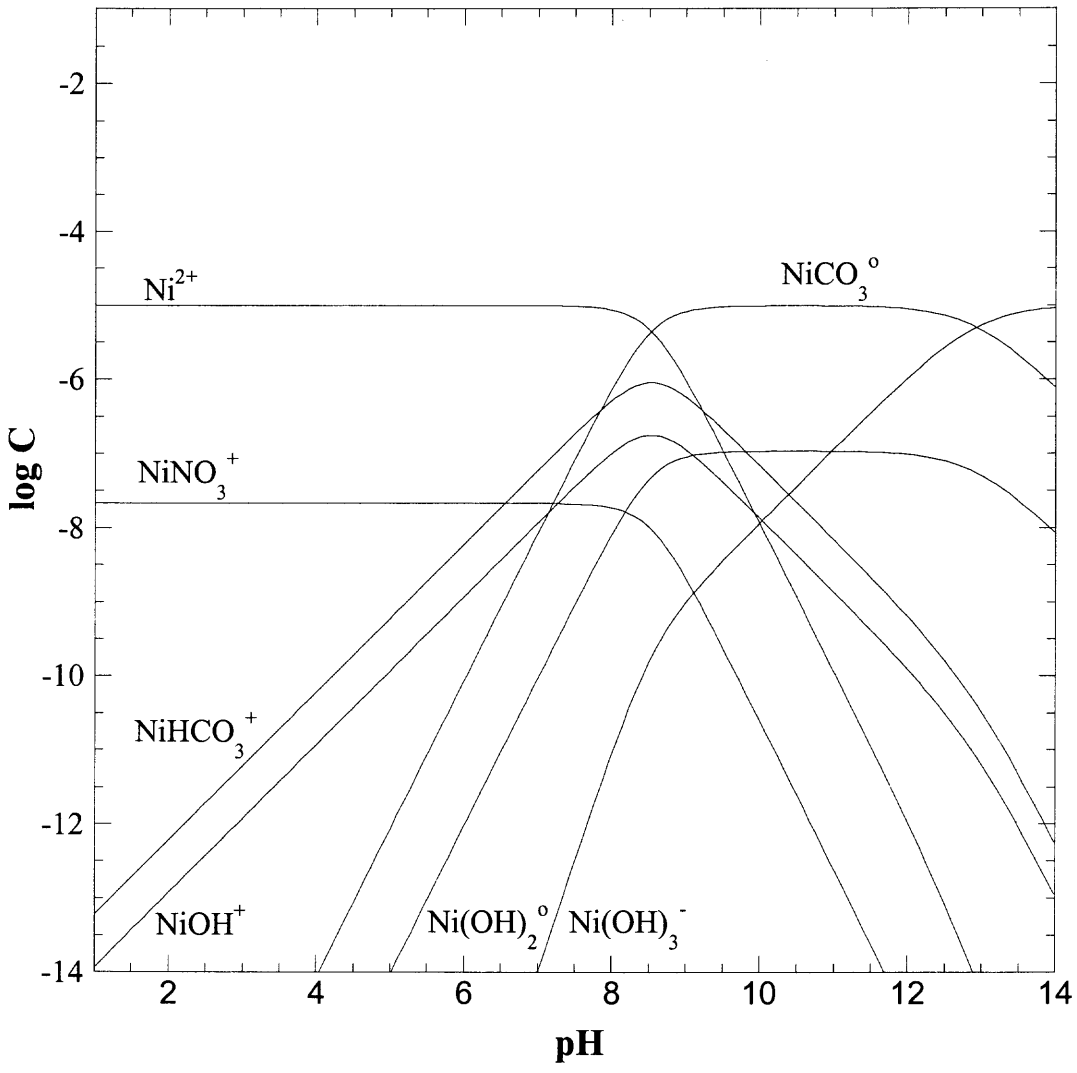

Figure A.2 Ni speciation in 1×10^{-5} M $Ni(NO_3)_2$ in open system at 298 K (ionic strength 10^{-3} $NaNO_3$, $P_{CO2}=10^{-3.46}$ atm).

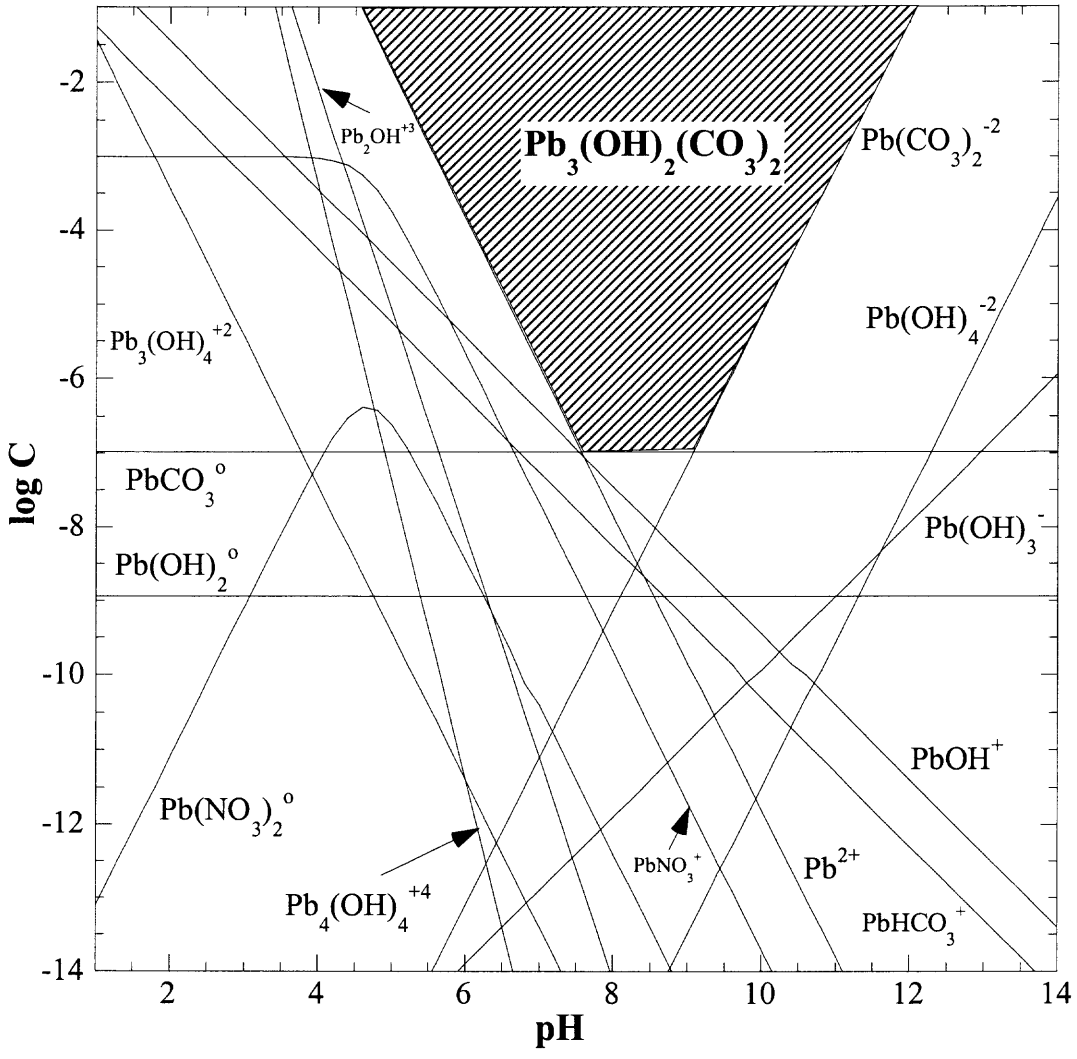

Figure A.3 Pb solubility in open system at 298 K (ionic strength 10^{-3} $NaNO_3$, $P_{CO2}=10^{-3.46}$ atm).

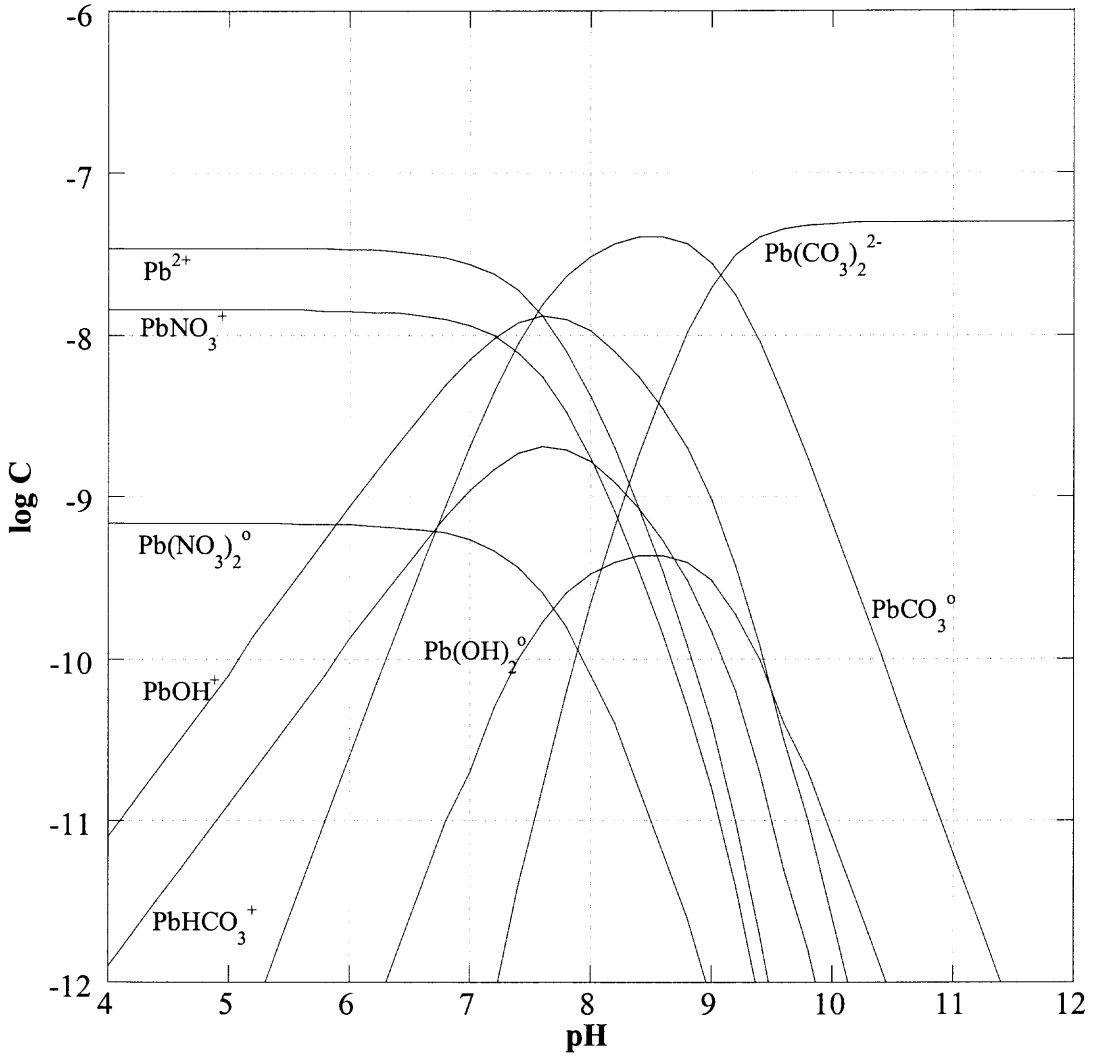

Figure A.4 Pb speciation in 5×10^{-8} M $Pb(NO_3)_2$ in open system at 298 K (ionic strength 10^{-3} $NaNO_3$, $P_{CO2}=10^{-3.46}$ atm).

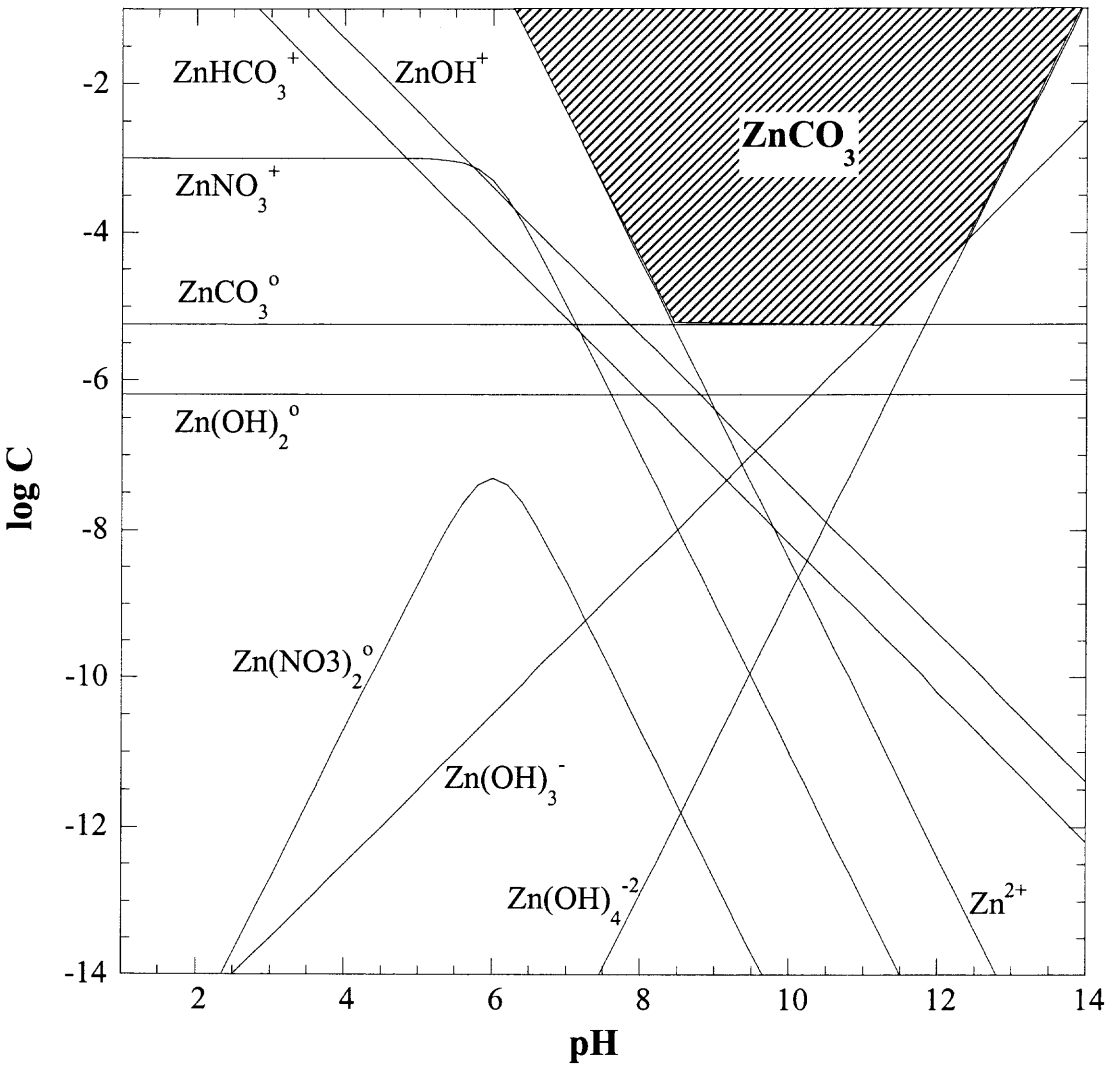

Figure A.5 Zn solubility in open system at 298 K (ionic strength 10^{-3} $NaNO_3$, $P_{CO2}=10^{-3.46}$ atm).

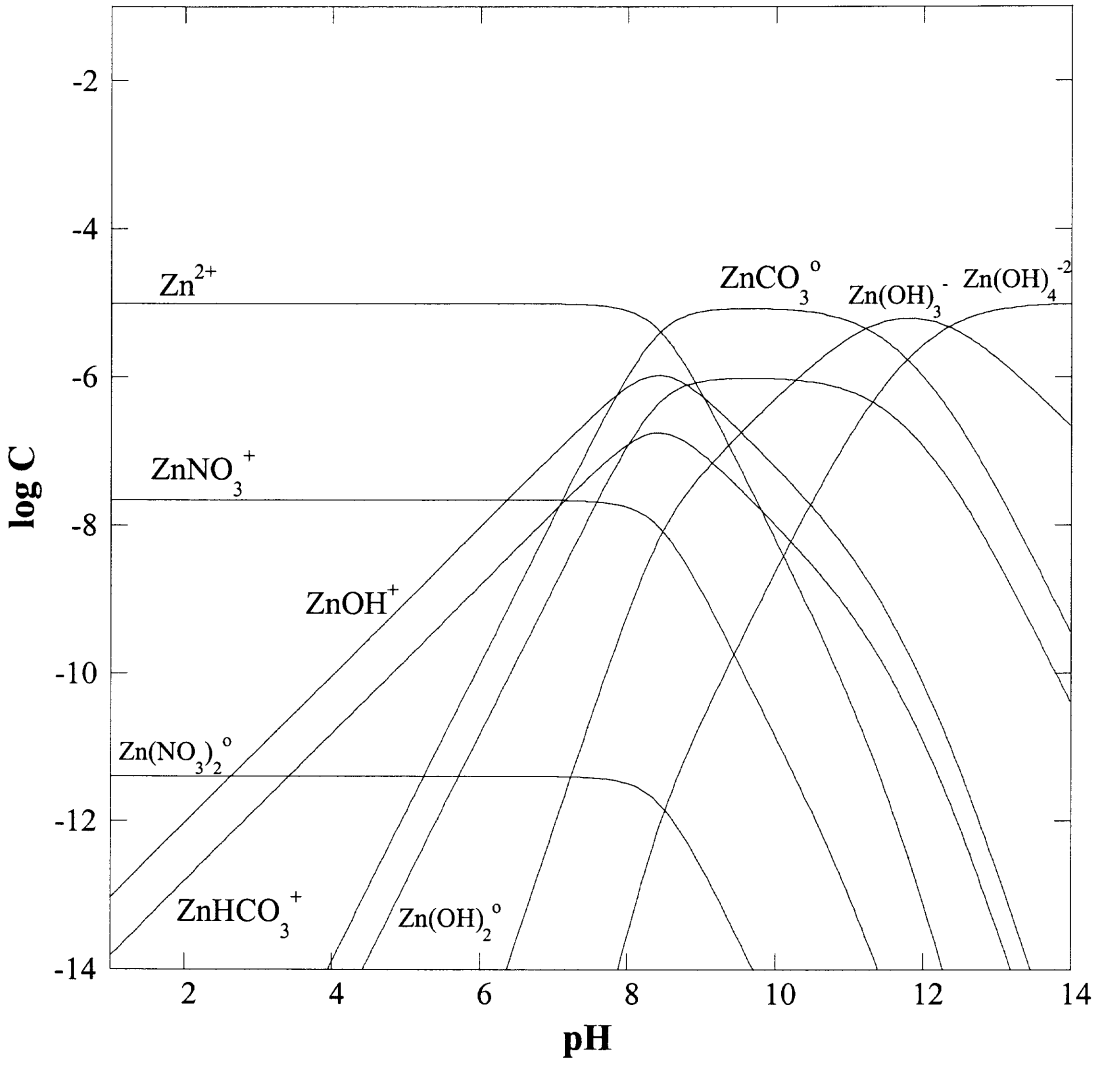

Figure A.6 Zn speciation in 1×10^{-5} M $Zn(NO_3)_2$ in open system at 298 K (ionic strength 10^{-3} $NaNO_3$, $P_{CO2}=10^{-3.46}$ atm).

APPENDIX B

POTENTIOMETRIC TITRATION DATA

Potentiometric titration results of coated silica, silica, and goethite are presented below. Titrations were conducted under a N_2 pressure of 35 psi and room temperature. Surface charge density is represented by σ in meq g^{-1}.

Table B.1 Potentiometric Titration of 1 g L^{-1} Goethite Adsorption-Coated Silica

pH	σ (IS 10^{-3})	pH	σ (IS 10^{-2})	pH	σ (IS 10^{-1})
1.97	2.575	1.99	2.754	1.99	2.859
2.02	2.143	2.05	2.410	2.05	2.504
2.08	1.746	2.18	1.555	2.19	1.696
2.25	1.071	2.27	1.170	2.40	0.898
2.54	0.419	2.40	0.861	2.57	0.527
2.83	0.111	2.56	0.471	2.86	0.166
2.93	0.062	2.86	0.155	2.96	0.105
3.05	0.002	2.96	0.096	3.09	0.045
3.24	-0.042	3.09	0.037	3.27	-0.020
3.37	-0.068	3.28	-0.019	3.60	-0.080
3.56	-0.094	3.63	-0.074	3.65	-0.087
3.61	-0.099	3.68	-0.082	3.71	-0.093
3.67	-0.103	3.75	-0.086	3.78	-0.098
3.73	-0.110	3.82	-0.093	3.86	-0.105
3.81	-0.114	3.92	-0.098	3.96	-0.111
3.91	-0.118	4.04	-0.103	4.09	-0.117
3.97	-0.120	4.11	-0.106	4.17	-0.120
4.04	-0.122	4.20	-0.109	4.27	-0.123
4.12	-0.125	4.32	-0.111	4.40	-0.127
4.21	-0.128	4.48	-0.114	4.60	-0.129
4.34	-0.130	4.74	-0.117	4.96	-0.132
4.52	-0.132	5.41	-0.120	8.06	-0.147
4.84	-0.134	9.00	-0.123	9.21	-0.150
6.53	-0.137	9.47	-0.123	9.53	-0.151
9.21	-0.139	9.70	-0.123	9.71	-0.152
9.55	-0.140	9.85	-0.122	9.84	-0.153
9.74	-0.140	9.97	-0.121	9.95	-0.153
9.88	-0.139	10.06	-0.120	10.02	-0.156
9.98	-0.140				
10.06	-0.140				

Table B.2 Potentiometric Titration of 1 g L^{-1} Goethite Precipitation Coated-Silica

pH	σ (IS 10^{-3})	pH	σ (IS 10^{-2})	pH	σ (IS 10^{-1})
1.68	2.518	1.65	1.784	2.00	3.002
1.71	2.213	1.68	1.527	2.05	2.537
1.83	1.561	1.76	1.280	2.12	2.194
2.00	0.952	1.86	1.063	2.29	1.408
2.17	0.569	1.98	0.723	2.42	1.065
2.48	0.292	2.18	0.654	2.60	0.703
2.78	0.116	2.50	0.371	2.90	0.322
2.83	0.106	2.83	0.210	2.95	0.290
2.89	0.102	2.94	0.175	3.00	0.250
2.95	0.085	3.08	0.132	3.07	0.224
3.03	0.079	3.17	0.110	3.14	0.187
3.11	0.057	3.29	0.091	3.22	0.147
3.22	0.044	3.44	0.065	3.33	0.114
3.37	0.032	3.68	0.042	3.48	0.082
3.43	0.030	3.74	0.035	3.69	0.044
3.49	0.024	3.82	0.031	3.75	0.038
3.56	0.018	3.91	0.025	3.82	0.031
3.62	0.015	4.01	0.017	3.91	0.025
3.69	0.013	4.15	0.010	4.01	0.017
3.73	0.012	4.23	0.006	4.14	0.010
3.77	0.010	4.34	0.003	4.23	0.006
3.82	0.010	4.48	-0.001	4.33	0.002
3.87	0.008	4.66	-0.005	4.47	-0.001
4.00	0.005	4.94	-0.010	4.68	-0.005
4.08	0.004	5.21	-0.018	5.05	-0.009
4.19	0.003	5.95	-0.025	8.15	-0.014
4.32	0.001	9.18	-0.027	9.23	-0.016
4.50	-0.001	9.56	-0.027	9.55	-0.017
4.83	-0.002	9.77	-0.025	9.74	-0.017
5.42	-0.007	9.91	-0.024	9.87	-0.018
8.31	-0.014	10.02	-0.022	9.97	-0.018
9.25	-0.016			10.06	-0.017
9.55	-0.017				
9.71	-0.019				
9.85	-0.020				
9.96	-0.019				
10.05	-0.019				
10.13	-0.018				

Table B.3 Potentiometric Titration of 2 g L^{-1} Silica

pH	σ (IS 10^{-3})	pH	σ (IS 10^{-2})	pH	σ (IS 10^{-1})	pH	σ (IS 10^{-3})
1.55	10.259	1.87	0.999	1.62	5.868	1.68	5.230
1.56	9.585	1.93	0.869	1.64	5.398	1.71	4.924
1.59	8.511	2.08	0.585	1.72	4.304	1.76	3.975
1.65	7.179	2.19	0.515	1.82	3.243	1.91	2.499
1.74	5.287	2.32	0.350	1.96	2.310	2.15	1.098
1.87	3.653	2.50	0.162	2.16	1.314	2.53	0.153
2.06	2.054	2.84	0.020	2.25	0.955	2.55	0.119
2.14	1.788	2.90	0.014	2.28	0.840	2.58	0.113
2.22	1.400	2.95	-0.018	2.33	0.723	2.90	-0.204
2.31	0.967	3.02	-0.034	2.49	0.439	3.02	-0.252
2.44	0.603	3.10	-0.054	2.73	0.119	3.28	-0.338
2.63	0.249	3.20	-0.072	2.76	0.081	3.63	-0.393
2.65	0.202	3.32	-0.096	2.80	0.057	4.06	-0.420
2.77	0.073	3.48	-0.122	2.84	0.026	4.13	-0.423
2.93	-0.064	3.74	-0.148	2.88	-0.011	4.22	-0.427
3.27	-0.244	3.79	-0.150	2.93	-0.040	4.34	-0.429
3.56	-0.312	3.83	-0.153	3.05	-0.100	4.50	-0.432
3.85	-0.345	3.88	-0.155	3.12	-0.134	4.72	-0.436
5.06	-0.379	3.92	-0.159	3.21	-0.163	5.17	-0.440
8.31	-0.383	3.98	-0.161	3.32	-0.195	8.73	-0.444
9.33	-0.384	4.03	-0.166	3.48	-0.222	9.48	-0.441
9.63	-0.383	4.10	-0.169	3.49	-0.228	9.76	-0.438
9.54	-0.397	4.18	-0.172	3.55	-0.238	9.93	-0.434
9.74	-0.397	4.27	-0.176	3.61	-0.250	10.05	-0.430
9.87	-0.397	4.39	-0.179	3.65	-0.259		
9.98	-0.396	4.54	-0.183	3.68	-0.262		
		4.77	-0.187	3.71	-0.265		
		5.22	-0.192	3.74	-0.268		
		8.44	-0.198	3.78	-0.270		
		9.34	-0.198	3.89	-0.282		
		9.62	-0.198	3.99	-0.289		
		9.78	-0.199	4.05	-0.292		
		9.90	-0.199	4.13	-0.295		
		9.99	-0.200	4.22	-0.298		
		10.06	-0.202	4.33	-0.301		
				4.48	-0.304		
				4.71	-0.308		
				5.20	-0.311		
				8.83	-0.315		
				9.46	-0.314		
				9.72	-0.312		
				9.89	-0.309		
				10.01	-0.307		
				10.10	-0.305		

Table B.4 Potentiometric Titration of 1 g L^{-1} Goethite

pH	σ (IS 10^{-3})	pH	σ (IS 10^{-2})	pH	σ (IS 10^{-1})
10.01	-0.028	10.00	-0.070	10.00	-0.079
9.97	-0.027	9.97	-0.067	9.98	-0.075
9.93	-0.025	9.95	-0.061	9.95	-0.071
9.89	-0.022	9.91	-0.059	9.92	-0.067
9.85	-0.019	9.88	-0.054	9.88	-0.063
9.79	-0.018	9.84	-0.051	9.85	-0.059
9.72	-0.018	9.80	-0.047	9.81	-0.055
9.67	-0.013	9.76	-0.042	9.77	-0.051
9.58	-0.012	9.71	-0.039	9.73	-0.046
9.49	-0.009	9.67	-0.033	9.68	-0.042
9.36	-0.007	9.60	-0.030	9.63	-0.037
9.21	-0.004	9.54	-0.025	9.57	-0.033
8.99	0.000	9.47	-0.020	9.50	-0.028
8.64	0.004	9.38	-0.016	9.42	-0.023
8.07	0.011	9.28	-0.011	9.34	-0.018
7.53	0.020	9.16	-0.006	9.22	-0.013
7.19	0.030	9.01	0.000	9.08	-0.008
6.89	0.040	8.82	0.007	8.89	-0.002
6.60	0.050	8.57	0.014	8.61	0.004
6.19	0.059	8.26	0.022	8.20	0.012
5.64	0.068	7.91	0.031	7.72	0.020
5.24	0.074	7.63	0.040	7.32	0.030
4.97	0.079	7.37	0.050	7.04	0.040
4.78	0.083	7.14	0.060	6.77	0.050
4.64	0.087	6.92	0.070	6.52	0.059
4.53	0.090	6.70	0.080	6.27	0.069
4.45	0.095	6.44	0.090	5.96	0.079
4.36	0.096	6.16	0.099	5.64	0.087
4.30	0.100	5.85	0.108	5.34	0.095
4.24	0.102	5.56	0.117	5.08	0.101
4.19	0.105	5.32	0.125	4.88	0.106
4.14	0.108	5.10	0.132	4.71	0.110
4.09	0.109	4.93	0.138	4.58	0.113
4.07	0.115	4.79	0.144	4.47	0.115
4.02	0.114	4.67	0.148	4.38	0.118
3.99	0.118	4.58	0.153	4.30	0.119
		4.50	0.158	4.23	0.121
		4.43	0.163	4.17	0.122
		4.36	0.166	4.12	0.124
		4.31	0.171	4.07	0.125
		4.26	0.175	4.03	0.126
		4.21	0.178	3.99	0.127
		4.17	0.182		
		4.13	0.186		
		4.10	0.190		
		4.07	0.195		

APPENDIX C

ADSORPTION STUDIES ON GOETHITE

Ni and Zn adsorption on goethite data are presented below. All adsorption studies were conducted open to the atmosphere at room temperature.

Table C.1 Ni Adsorption Edges on 1 g L^{-1} Goethite

$[Ni]_0=5\times10^{-10}$ M IS 10^{-2}		$[Ni]_0=3\times10^{-8}$ M IS 10^{-3}		$[Ni]_0=10^{-4}$ M IS 10^{-3}	
pH	% Ni_{sorbed}	pH	% Ni_{sorbed}	pH	% Ni_{sorbed}
3.15	2.6	4.4	18.0	4.0	2.7
4.42	1.4	5.0	19.6	4.5	4.2
5.15	12.3	5.8	53.4	5.0	5.9
5.82	38.0	6.0	87.3	5.5	6.1
6.6	96.3	6.4	97.4	5.9	11.1
6.75	99.1	6.9	97.8	6.4	15.9
7.18	99.7			6.9	37.2
7.54	99.8				
7.73	99.8				

Table C.2 Ni Adsorption Isotherms on 1 g L^{-1} Goethite at Ionic Strength 10^{-3}

pH 4		pH 4.5		pH 5		pH 5.5	
[Ni] (M)	Ni_{ads} (mol/g)	[Ni] (M)	Ni_{ads} (mol/g)	[Ni] (M)	Ni_{ads} (mol/g)	[Ni] (M)	Ni_{ads} (mol/g)
2.30E-08	6.99E-09	2.46E-08	5.39E-09	2.41E-08	5.87E-09	1.43E-07	5.66E-08
1.91E-07	8.65E-09	1.86E-07	1.40E-08	1.80E-07	1.98E-08	7.53E-07	2.47E-07
8.38E-07	1.62E-07	8.83E-07	1.17E-07	8.67E-07	1.33E-07	3.03E-06	9.65E-07
3.61E-06	3.91E-07	3.62E-06	3.82E-07	3.54E-06	4.57E-07	7.86E-06	2.14E-06
9.59E-06	4.09E-07	9.52E-06	4.81E-07	9.21E-06	7.91E-07	1.67E-05	3.25E-06
1.82E-05	1.76E-06	1.81E-05	1.87E-06	1.77E-05	2.34E-06	9.39E-05	6.11E-06
9.73E-05	2.67E-06	9.58E-05	4.20E-06	9.41E-05	5.87E-06	0.00019	1.21E-05
0.00019	5.50E-06	0.00019	6.97E-06	0.00019	9.86E-06		

pH 6		pH 6.5		pH 7	
[Ni] (M)	Ni_{ads} (mol/g)	[Ni] (M)	Ni_{ads} (mol/g)	[Ni] (M)	Ni_{ads} (mol/g)
3.80E-09	2.62E-08	7.91E-10	2.92E-08	6.54E-10	2.93E-08
2.23E-08	1.78E-07	6.06E-09	1.94E-07	3.94E-09	1.96E-07
1.84E-07	8.16E-07	3.78E-08	9.62E-07	1.94E-08	9.81E-07
9.88E-07	3.01E-06	1.59E-07	3.84E-06	6.20E-08	3.94E-06
3.24E-06	6.76E-06	6.29E-07	9.37E-06	1.75E-07	9.82E-06
1.45E-05	5.54E-06	8.60E-06	1.14E-05	2.30E-06	1.77E-05
8.89E-05	1.11E-05	8.41E-05	1.59E-05	6.28E-05	3.72E-05
0.00019	1.46E-05	0.00018	2.30E-05	0.00015	4.53E-05

Table C.3 Zn Adsorption Edges on 1 g L^{-1} Goethite

$[Zn]_0=5.2\times10^{-7}$ M IS 10^{-3}		$[Zn]_0=10^{-5}$ M IS 10^{-3}		$[Zn]_0=10^{-5}$ M IS 10^{-2}	
pH	% Zn_{sorbed}	pH	% Zn_{sorbed}	pH	% Zn_{sorbed}
4.04	5.2	4.52	7.23	4.53	13.4
4.48	18.9	4.93	17.55	5.11	19.2
5.01	56.1	4.96	19.62	5.45	28.3
5.02	59.8	5.02	20.45	6.01	52.6
5.50	89.7	5.57	35.43	6.49	81.3
5.98	97.7	5.84	68.01	6.71	91.6
6.46	99.6	6.07	76.56	6.96	96.8
6.92	99.8	6.60	93.96		

Table C.4 Zn Adsorption Isotherms on 1 g L^{-1} Goethite at Ionic Strength 10^{-3}

pH 4		pH 4.5		pH 5		pH 5.5	
[Zn] (M)	Zn_{ads} (mol/g)	[Zn] (M)	Zn_{ads} (mol/g)	[Zn] (M)	Zn_{ads} (mol/g)	[Zn] (M)	Zn_{ads} (mol/g)
2.35E-08	2.45E-09	1.52E-07	4.83E-08	3.17E-09	2.28E-08	5.88E-10	2.54E-08
4.93E-07	2.68E-08	4.22E-07	9.84E-08	3.32E-09	2.27E-08	5.35E-08	4.66E-07
2.57E-05	3.26E-07	9.28E-06	7.23E-07	5.16E-08	1.48E-07	1.81E-06	2.19E-06
9.82E-05	1.85E-06	2.48E-05	1.24E-06	2.09E-07	3.11E-07	6.46E-06	3.54E-06
				2.28E-07	2.92E-07	1.88E-05	7.25E-06
				2.52E-06	1.48E-06		
				3.04E-06	9.57E-07		
				7.96E-06	2.04E-06		
				8.04E-06	1.96E-06		
				8.25E-06	1.75E-06		
				2.32E-05	2.77E-06		
				2.35E-05	2.51E-06		
				9.38E-05	6.18E-06		
pH 6		pH 6.5		pH 7			
[Zn] (M)	Zn_{ads} (mol/g)	[Zn] (M)	Zn_{ads} (mol/g)	[Zn] (M)	Zn_{ads} (mol/g)		
1.77E-09	1.98E-07	2.06E-09	5.18E-07	3.15E-11	2.60E-08		
1.19E-08	5.08E-07	6.04E-07	9.40E-06	1.22E-09	5.19E-07		
6.11E-07	3.39E-06			7.34E-08	3.93E-06		
6.77E-07	3.32E-06			8.93E-07	2.51E-05		
6.81E-07	3.32E-06			4.99E-05	5.01E-05		
2.34E-06	7.66E-06						
3.20E-06	6.80E-06						
1.40E-05	1.20E-05						
1.44E-05	1.16E-05						
7.96E-05	2.04E-05						

Table C.5 Ni Adsorption in Ni-Zn Bisolute Systems on 1 g L^{-1} Goethite at pH 6 and Ionic Strength 10^{-3}

Ni, Zn binary system		Ni single system	
[Ni] (M)	Ni_{ads} (mol/g)	[Ni] (M)	Ni_{ads} (mol/g)
1.40E-05	6.00E-06	1.05E-05	9.55E-06
2.33E-05	6.71E-06	1.98E-05	1.02E-05
3.17E-05	8.28E-06	2.77E-05	1.23E-05
4.06E-05	9.42E-06	3.63E-05	1.37E-05
5.06E-05	9.43E-06	4.63E-05	1.37E-05
5.86E-05	1.14E-05	5.46E-05	1.54E-05
6.90E-05	1.10E-05	5.48E-05	1.52E-05
7.76E-05	1.24E-05	6.37E-05	1.63E-05
8.76E-05	1.24E-05	7.35E-05	1.65E-05
9.60E-05	1.40E-05	8.28E-05	1.72E-05
1.06E-04	1.39E-05	9.16E-05	1.84E-05
		1.02E-04	1.81E-05

APPENDIX D

ADSORPTION STUDIES ON SILICA AND COATED-SILICA

Ni and Zn adsorption on silica and coated-silica data are presented below. All adsorption studies were conducted open to the atmosphere at room temperature.

Table D.1 Ni Adsorption Edges on 5 g L^{-1} Silica and Goethite-Coated Silica (4.01 mg Fe g^{-1} Solid) at $[Ni]_0=5\times10^{-10}$ M

Silica				Goethite-coated silica					
IS 10^{-3}		IS 10^{-2}		IS 10^{-3}		IS 10^{-2}		IS 10^{-2}	
pH	% Ni_{sorbed}	pH	% Ni_{sorbed}	pH	% Ni_{sorbed}	pH	% Ni_{sorbed}	pH	% Ni_{sorbed}
2.88	3	3.1	1.6	3	4.7312	3.34	1.5514	3.25	0.4
3.54	6.7	3.89	2.5	3.53	12.05	4.08	3.8598	4.04	3.9
4.08	8.1	4.48	3.8	4.03	14.969	4.62	5.2465	4.51	8
4.53	9	4.99	6.9	4.64	36.173	5.23	12.09	5.06	8
5.01	16.8	5.8	4.9	5.21	65.073	5.8	12.39	5.48	10.9
5.52	30.3	6.3	10.1	5.76	70.287	6.35	12.828	5.95	11.6
5.7	33.9	6.44	11.9	5.9	75.367	6.48	22.835	6.13	18.4
6.02	41.8	6.81	13.5	6.05	74.803	7.07	37.055	6.42	22.7
6.25	48.1	7.06	23.9	6.65	91.082	7.31	72.84	6.81	37.1
6.8	58.1	7.46	41.3	7.11	95.598	7.59	94.488	7.09	55.6

Table D.2 Ni Adsorption Isotherms on 5 g L^{-1} Silica at Ionic Strength 10^{-3}

pH 4		pH 5		pH 6		pH 7	
[Ni] (M)	Ni_{ads} (mol/g)	[Ni] (M)	Ni_{ads} (mol/g)	[Ni] (M)	Ni_{ads} (mol/g)	[Ni] (M)	Ni_{ads} (mol/g)
4.74E-10	5.12E-12	4.39E-10	1.23E-11	3.10E-10	3.79E-11	2.82E-10	4.35E-11
9.68E-10	6.38E-12	9.19E-10	1.63E-11	5.93E-10	8.18E-11	4.03E-10	1.20E-10
4.66E-09	6.70E-11	4.38E-09	1.23E-10	3.37E-09	3.25E-10	2.36E-09	5.27E-10
4.90E-08	2.11E-10	4.52E-08	9.78E-10	8.34E-09	3.37E-10	6.43E-09	7.27E-10
9.63E-08	7.51E-10	9.04E-08	1.92E-09	3.27E-08	3.51E-09	2.14E-08	5.81E-09
9.88E-07	2.36E-09	9.78E-07	4.46E-09	7.32E-07	5.40E-08	6.33E-07	7.38E-08
9.89E-07	2.22E-09	9.66E-07	6.96E-09	7.55E-07	4.96E-08	6.43E-07	7.22E-08
4.93E-06	1.39E-08	4.70E-06	6.05E-08	4.34E-06	1.32E-07	4.00E-06	2.00E-07
9.78E-06	4.46E-08	4.81E-05	3.72E-07	4.82E-05	3.58E-07	9.42E-06	1.14E-07
9.51E-05	9.94E-07	9.54E-05	9.22E-07	9.49E-05	1.03E-06	4.66E-05	6.72E-07
0.00489	2.21E-05	0.00097	5.77E-06			9.48E-05	1.04E-06
						0.00491	1.81E-05

Table D.3 Ni Adsorption Isotherms on 5 g L^{-1} Goethite-Coated Silica (4.01 mg Fe g^{-1} Solid) at Ionic Strength 10^{-3}

PH 4		pH 5		pH 6		pH 7	
[Ni] (M)	Ni_{ads} (mol/g)	[Ni] (M)	Ni_{ads} (mol/g)	[Ni] (M)	Ni_{ads} (mol/g)	[Ni] (M)	Ni_{ads} (mol/g)
4.44E-10	1.13E-11	3.22E-10	3.58E-11	1.54E-10	6.98E-11	2.59E-10	1.50E-10
9.12E-10	1.79E-11	6.47E-10	7.15E-11	3.00E-10	1.42E-10	9.82E-10	8.04E-10
4.53E-09	9.46E-11	2.94E-09	4.11E-10	1.79E-09	6.43E-10	2.02E-09	1.63E-09
9.66E-09	7.02E-11	6.98E-09	6.15E-10	3.88E-09	1.25E-09	9.24E-09	8.17E-09
4.65E-08	7.09E-10	3.41E-08	3.20E-09	1.57E-08	6.87E-09	1.93E-08	1.61E-08
9.46E-08	1.09E-09	6.60E-08	6.80E-09	3.51E-08	1.30E-08	3.22E-07	3.63E-08
4.67E-07	6.72E-09	3.48E-07	3.10E-08	2.60E-07	4.88E-08	3.68E-07	1.26E-07
9.55E-07	8.93E-09	7.05E-07	5.88E-08	4.60E-07	1.08E-07	2.35E-07	1.53E-07
9.15E-07	1.69E-08	7.22E-07	5.55E-08	5.19E-07	9.62E-08	1.79E-06	6.54E-07
4.67E-06	6.76E-08	3.97E-06	2.09E-07	2.94E-06	4.20E-07	9.48E-05	1.06E-06
9.36E-06	1.27E-07	8.70E-06	2.59E-07	0.00479	4.21E-05	0.00099	1.34E-06
4.61E-05	7.89E-07	4.67E-05	6.56E-07				
9.36E-05	1.29E-06	9.49E-05	1.03E-06				
0.00048	3.18E-06	0.00049	1.42E-06				
0.00098	3.40E-06	0.00095	9.43E-06				
0.00483	3.30E-05	0.00471	5.88E-05				

Table D.4 Zn Adsorption Edges on 5 g L^{-1} Silica and Goethite-Coated Silica (4.01 mg Fe g^{-1} Solid) at $[Zn]_0=2\times10^{-8}$ M

Silica				Goethite-coated silica			
IS 10^{-3}		IS 10^{-2}		IS 10^{-3}		IS 10^{-2}	
pH	% Zn_{sorbed}	pH	% Zn_{sorbed}	pH	% Zn_{sorbed}	pH	% Zn_{sorbed}
3.69	4.356	3.23	3.6703	4.54	25.55	4.54	10.847
5.02	5.8829	3.97	9.0337	5.01	38.323	6.47	68.873
5.19	10.607	4.54	4.7916	5.74	72.062	5.07	8.6819
5.72	15.709	4.98	5.4557	6.13	81.168	5.46	21.469
6.15	25.563	5.58	3.5112	6.33	85.817	5.89	35.099
6.3	27.324	6.15	9.2311	6.84	89.752	6.39	65.628
6.28	30.863	5.9	7.4398	7.35	90.606	6.62	80.169
6.54	35.721	6.5	7.5594			6.76	78.127
6.84	45.879	6.89	15.487			7.07	87.511
7.14	61.932	7.27	39.935			7.15	90.073

Table D.5 Zn Adsorption Isotherms on 5 g L^{-1} Silica and Goethite-Coated Silica (4.01 mg Fe g^{-1} Solid) at Ionic Strength 10^{-3}

Silica				Goethite-coated silica			
pH 5		pH 6		pH 5		pH 6	
[Zn] (M)	Zn_{ads} (mol/g)	[Zn] (M)	Zn_{ads} (mol/g)	[Zn] (M)	Zn_{ads} (mol/g)	[Zn] (M)	Zn_{ads} (mol/g)
4.62E-10	7.75E-12	2.32E-10	5.45E-11	4.04E-10	1.96E-11	1.66E-10	6.78E-11
8.40E-10	3.26E-11	3.78E-10	1.26E-10	7.07E-10	5.87E-11	3.03E-10	1.41E-10
3.99E-09	2.02E-10	2.53E-09	4.99E-10	4.01E-09	2.01E-10	2.27E-09	5.55E-10
1.81E-08	3.89E-10	5.61E-09	8.76E-10	1.50E-08	1.02E-09	5.59E-09	8.97E-10
4.02E-08	2.01E-09	8.99E-09	2.23E-09	3.71E-08	2.61E-09	7.36E-09	2.55E-09
8.59E-08	2.83E-09	2.14E-08	5.76E-09	8.59E-08	2.85E-09	1.92E-08	6.24E-09
8.89E-07	2.23E-08	5.73E-08	8.65E-09	8.11E-07	3.87E-08	5.46E-08	9.23E-09
8.03E-06	3.95E-07	4.21E-07	1.57E-08	4.68E-06	6.40E-08	7.55E-07	4.96E-08
		7.29E-07	5.49E-08	4.31E-07	1.40E-08	4.30E-06	1.42E-07
		4.70E-06	5.95E-08	7.31E-06	5.42E-07	3.13E-07	3.77E-08
		7.83E-06	4.36E-07			6.54E-06	6.98E-07

APPENDIX E

ADSORPTION STUDIES ON HFO

Ni and Pb adsorption on HFO data are presented below. All adsorption studies were conducted open to the atmosphere at room temperature.

Table E.1 Ni Adsorption Edges on 1 g L^{-1} HFO

$[Ni]_0=5\times10^{-9}$ M			
IS 2.8×10^{-2}		IS 10^{-1}	
pH	% Ni_{sorbed}	pH	% Ni_{sorbed}
4	0.1	4.0	4.4
5	14.8	5.0	3.5
5.5	17.9	5.5	16.3
6	40.6	6.0	49.2
6.5	82.5	6.5	88.7
7	96.6	7.0	97.0
7	95.8	7.0	95.3
7.5	99.4	7.5	99.253
8	99.8	8	99.798
9	99.981	9	100

Table E.2 Ni Adsorption Isotherms on 1 g L^{-1} HFO at Ionic Strength 2.8×10^{-2}

pH 5		pH 6		pH 7	
[Ni] (M)	Ni_{ads} (mol/g)	[Ni] (M)	Ni_{ads} (mol/g)	[Ni] (M)	Ni_{ads} (mol/g)
4.43E-10	5.67E-11	3.17E-10	1.83E-10	1.93E-11	4.81E-10
8.97E-10	1.03E-10	5.96E-10	4.04E-10	5.27E-11	9.47E-10
9.18E-09	8.19E-10	5.76E-09	4.24E-09	5.64E-10	9.44E-09
8.89E-08	1.11E-08	6.14E-08	3.86E-08	6.00E-09	9.40E-08
9.32E-07	6.77E-08	6.30E-07	3.70E-07	4.80E-08	9.52E-07
9.33E-06	6.73E-07	6.73E-06	3.27E-06	6.62E-07	9.34E-06
9.60E-05	4.05E-06	8.16E-05	1.84E-05	6.25E-06	4.38E-05
0.000296	4.15E-06	0.00028	2.42E-05	1.82E-05	8.18E-05
0.000296	4.30E-06	0.00027	2.92E-05	2.08E-05	7.92E-05
0.000481	1.91E-05	0.00044	6.26E-05	0.000108	1.92E-04

Table E.3 Pb CBC Study on 0.3 g L^{-1} HFO at Ionic Strength 1.4×10^{-2}, pH 5, And $[Pb]_e=10^{-4}M$

time ($day^{0.5}$)	Pb_{ads} (mol/g)	[Pb] (M)
0.14434	0.00132	0.0001
0.20412	0.00133	0.0001
0.28868	0.00132	0.0001
0.35355	0.00136	9.29E-05
0.40825	0.00135	9.54E-05
0.51031	0.00134	9.78E-05
0.61237	0.00137	9.48E-05
0.94648	0.00139	9.36E-05
1.0508	0.00142	8.87E-05
1.1456	0.00148	8.24E-05
1.3844	0.00151	9.28E-05
1.4965	0.00152	9.56E-05
1.7678	0.00152	9.96E-05
2.0104	0.00152	0.0001
2.25	0.00154	9.63E-05
2.5062	0.00159	8.61E-05
2.8468	0.0016	9.60E-05
3.0104	0.00168	7.57E-05
3.4851	0.0017	9.31E-05
3.7583	0.00172	9.30E-05
4.0156	0.00176	8.80E-05
4.4861	0.00175	0.0001
4.8164	0.00173	0.00011
5.1174	0.00177	9.66E-05
5.4801	0.00178	9.86E-05
5.8523	0.00175	0.00011
6.5535	0.00174	0.00011
6.9963	0.00179	9.65E-05
7.8229	0.00176	0.00011
8.498	0.00175	0.00011
9.4846	0.00177	0.0001
10.488	0.0018	9.71E-05
11.832	0.00177	0.00011
13.191	0.00177	0.00011
14.9	0.00176	0.00011
16.062	0.00175	0.00011
16.31	0.00172	0.00012
18.466	0.00173	0.00012
19.799	0.00177	0.00011

APPENDIX F

GOETHITE COATING RESULTS

Results for the goethite coating processes are presented below. Abrasion was conducted by shaking coated silica ($Re > 10^4$) in DI for 4 hours. Samples 1 through 9 are based on the adsorption coating method and 10 through 18 the precipitation method.

Table F.1 Iron Concentration of the Coated Silica Before and After Abrasion

Sample	Fe concentration before abrasion (mg Fe g^{-1})			Fe concentration after abrasion (mg Fe g^{-1})		
	Fe_{tot}	Fe_{am}	Fe_{cry}	Fe_{tot}	Fe_{am}	Fe_{cry}
1	6.58	0.56	6.03	5.46	0.14	5.32
2	2.43	0.30	2.13	1.83	0.05	1.78
3	1.42	0.31	1.11	0.87	0.03	0.84
4	25.75	1.82	23.93	21.36	0.25	21.12
5	2.17	0.57	1.60	1.17	0.05	1.12
6	2.56	0.52	2.04	1.09	0.03	1.06
7	4.46	1.06	3.40	1.99	0.10	1.90
8	4.62	0.78	3.84	2.84	0.06	2.77
9	1.77	0.55	1.22	0.59	0.03	0.56
10	7.41	7.27	0.14	4.13	4.17	0.00
11	3.93	0.72	3.21	1.47	0.17	1.30
12	3.84	0.49	3.35	0.67	0.10	0.57
13	20.39	10.06	10.33	8.50	5.85	2.65
14	5.71	1.13	4.58	1.64	0.48	1.16
15	2.30	0.81	1.49	0.88	0.19	0.69
16	7.79	3.94	3.85	6.23	3.69	2.54
17	2.39	0.99	1.40	1.14	0.19	0.95
18	4.70	0.72	3.98	1.58	0.18	1.40

APPENDIX G

INTRAPARTICLE DIFFUSION MODELING

VBA code in Excel for estimating experimental surface diffusivity is listed below.

```
Option Explicit
Option Base 1

Function IntraDiff(rng1 As Range, rng2 As Range) As Integer

Const fPi As Double = 3.14159265358979
Const fDay2Hour As Double = 24#
Const fMum2Cm As Double = 0.0001
Const fTol As Double = 0.0001

IntraDiff = 0
If rng1.Columns.Count <> 2 Or rng1.Rows.Count < 2 Then
   MsgBox "Wrong Pore size distribution data!"
   IntraDiff = 1
   Exit Function
End If
If rng2.Columns.Count <> 2 Or rng2.Rows.Count < 2 Then
   MsgBox "Wrong CBC data!"
   IntraDiff = 2
   Exit Function
End If

Dim i As Integer, j As Integer, iCs As Integer

Dim nPSD As Integer, nCBC As Integer
Dim fRad() As Double, fVol() As Double, fMass() As Double
Dim fTime() As Double, fSorbExp() As Double
Dim fSorbPred() As Double

nPSD = rng1.Rows.Count
nCBC = rng2.Rows.Count

ReDim fRad(nPSD), fVol(nPSD), fMass(nPSD)
ReDim fTime(nCBC), fSorbExp(nCBC)
ReDim fSorbPred(nCBC)

For i = 1 To nPSD
   fRad(i) = rng1.Cells(i, 1) * 0.5 * fMum2Cm
   fVol(i) = rng1.Cells(i, 2) / 100#
```

```
Next i

For i = 1 To nCBC
   fTime(i) = rng2.Cells(i, 1) * fDay2Hour
   fSorbExp(i) = rng2.Cells(i, 2)
Next i

Dim fE As Double
Dim fS As Double
Dim fKd As Double
Dim fDen As Double
Dim fDs0 As Double

fE = Range("C5")
fDen = Range("C6")
fS = Range("C7")
fKd = Range("C8")
fDs0 = Range("C9") * 3600#

Dim fKi As Double, fD As Double, fA As Double, fCs As Double, fDs As Double
Dim fSum1 As Double, fSum2 As Double, fInfSeries As Double
Dim fDiff1 As Double, fDiff2 As Double, fPct As Double, fPerSum As Double
Dim fVar As Double, fAveEr As Double
Dim fMinVar As Double
Dim fIter As Double

fMinVar = 1#

fKi = fE * fKd / (1# - fE)
fCs = fS * fKd

For iCs = 0 To 89

   fDs = fDs0 * (1 + iCs / 10#)
   fD = fDs / (1# + fE / (fDen * 1000# * fKi))

   fSum1 = 0#
   fSum2 = 0#
   fPerSum = 0#
   For i = 1 To nCBC

      fSorbPred(i) = 0#
      For j = 1 To nPSD

         fInfSeries = 0#
         fIter = 1#
```

```
        Do
          fA = fIter ^ 2
          fA = Exp(-fD * fA * fPi ^ 2 * fTime(i) / fRad(j) ^ 2) / fA
          fInfSeries = fInfSeries + fA
          fIter = fIter + 1#
        Loop Until fA < fTol * fInfSeries Or fA = 0#

        fMass(j) = (fCs * fDen) * (1# - 6# / fPi ^ 2 * fInfSeries)
        fMass(j) = fMass(j) * fVol(j)

        fSorbPred(i) = fSorbPred(i) + fMass(j)

    Next j
    fSorbPred(i) = (fSorbPred(i) + fCs * fDen) / fDen

    fDiff1 = Abs(fSorbExp(i) - fSorbPred(i))
    fDiff2 = fDiff1 ^ 2
    fPct = (fDiff1 / fSorbExp(i)) * 100#

    fSum1 = fSum1 + fDiff1
    fSum2 = fSum2 + fDiff2
    fPerSum = fPerSum + fPct

Next i

fVar = (fSum2 - fSum1 ^ 2 / CDbl(nCBC)) / CDbl(nCBC - 1)
fAveEr = fPerSum / CDbl(nCBC)

Cells(14 + iCs, 8) = fVar
Cells(14 + iCs, 9) = fAveEr

If fVar < fMinVar Then

    For i = 1 To nCBC
      Cells(13 + i, 6) = fSorbPred(i)
      Cells(13 + i, 7) = Abs(fSorbExp(i) - fSorbPred(i))
    Next i
    fMinVar = fVar

    Cells(5, 7) = fVar
    Cells(6, 7) = fAveEr
    Cells(7, 7) = fDs / 3600#
    Cells(8, 7) = iCs

End If
```

```
Next iCs

Dim fSorbCalc As Double, fSorbCalc0 As Double
Dim fHours As Double

fHours = fTime(nCBC) + 24#
fSorbCalc0 = fSorbPred(nCBC)
Do
   fSorbCalc = 0#
   For j = 1 To nPSD
      fInfSeries = 0#
      fIter = 1#
      Do
         fA = fIter ^ 2
         fA = Exp(-fD * fA * fPi ^ 2 * fHours / fRad(j) ^ 2) / fA
         fInfSeries = fInfSeries + fA
         fIter = fIter + 1#
      Loop Until fA < fTol * fInfSeries Or fA = 0#

      fMass(j) = (fCs * fDen) * (1# - 6# / fPi ^ 2 * fInfSeries)
      fMass(j) = fMass(j) * fVol(j)
      fSorbCalc = fSorbCalc + fMass(j)
   Next j
   fSorbCalc = (fSorbCalc + fCs * fDen) / fDen

   If Abs(fSorbCalc - fSorbCalc0) / fSorbCalc < fTol / 10# Then
      Exit Do
   Else
      fSorbCalc0 = fSorbCalc
      fHours = fHours + 24#
   End If
Loop
Cells(9, 7) = fHours / 24# / 365#
Cells(10, 7) = fSorbCalc

End Function
```

REFERENCES

1. Adamson A. W. (1982) *Physical Chemistry of Surfaces*. 4th ed. John Wiley & Sons, New York.

2. Ainsworth C. C., Girvin D. C., Zachara J. M. and Smith S. C. (1989) Chromate adsorption on goethite: effects of aluminum substitution. *Soil Sci. Soc. Am. J.* 53, 418-428.

3. Ainsworth C. C., Pilon J. L., Gassman P. L. and Van DerSluys W. G. (1994) Cobalt, cadmium, and lead sorption to hydrous iron oxide: residence time effect. *Soil Sci. Soc. Am. J.* 58, 1615-1623.

4. Ali M. A. and Dzombak D. A. (1996) Competitive sorption of simple organic acids and sulfate on goethite. *Environ. Sci. Technol.* 30, 1061-1071.

5. Anderson P. R. and Benjamin M. M. (1985) Effects of silicon on the crystallization and adsorption properties of ferric oxides. *Environ. Sci. Technol.* 19, 1048-1053.

6. Anderson P. R. and Christensen T. H. (1988) Distribution coefficients of Cadmium, cobalt, nickel, and zinc in soils. *J. Soil Sci.* 39(1), 15-22.

7. Anderson P. R. and Benjamin M. M. (1990) Surface and bulk characteristics of binary oxide suspensions. *Environ. Sci. Technol.* 24(5), 692-698.

8. Anderson V. L. and Mclean R. A. (1974) *Design of Experiments: A Realistic Approach*. Marcel Dekker, Inc., New York.

9. Atkinson R. J., Posner A. M. and Quirk J. P. (1967) Adsorption of potential-determining ions at the ferric oxide-aqueous electrolyte interface. *J. Phys. Chem.* 71(3), 550-558.

10. Axe L. and Anderson P. R. (1995) Sr diffusion and reaction within Fe oxides: evaluation of the rate-limiting mechanism for sorption. *J. Colloid Interface Sci.* 175, 157-165.

11. Axe L. and Anderson P. R. (1997) Experimental and theoretical diffusivities of Cd and Sr in hydrous ferric oxide. *J. Colloid Interface Sci.* 185, 436-448.

12. Axe L., Bunker G. B., Anderson P. R. and Tyson T. A. (1998) An XAFS analysis of strontium at the hydrous ferric oxide surface. *J. Colloid Interface Sci.* 199, 44-52.

13. Baccini P., Grieder E., Stierli R. and Goldberg S. (1982) The influence of natural organic matter on the adsorption properties of mineral particles in lake water. *Schweiz. Z. Hydrol.* 44, 99-116.

14. Baes C. F. Jr. and Mesmer R. E. (1976) *The hydrolysis of Cations*. John Wiley and Sons, Inc.

15. Bailey R. P., Bennett T. and Benjamin M. M. (1992) Sorption onto and recovery of Cr(VI) using iron-oxide-coated sand. *Wat. Sci. Tech.* 26(5-6), 1239-1244.

16. Balistrieri L. S. and Murray J. W. (1982) The adsorption of copper, lead, zinc, and cadmium on goethite from major ion seawater. *Geochim. Cosmochim. Acta* 46, 1253-1265.

17. Bargar J. R., Brown G. E. Jr. and Parks G. A. (1997a) Surface complexation of Pb(II) at oxide-water interfaces: I. XAFS and bond-valence determination of mononuclear and polynuclear Pb(II) sorption products on aluminum oxides. *Geochim. Cosmochim. Acta* 61, 2617-2638.

18. Bargar J. R., Brown G. E. Jr. and Parks G. A. (1997b) Surface complexation of Pb(II) at oxide-water interfaces: II. XAFS and bond-valence determination of mononuclear Pb(II) sorption products and surface functional groups on iron oxides. *Geochim. Cosmochim. Acta* 61, 2639-2652.

19. Bargar J. R., Brown G. E. Jr. and Parks G. A. (1998) Surface complexation of Pb(II) at oxide-water interfaces: III. XAFS determination of Pb(II) and Pb(II)-chloro adsorption complexes on goethite and alumina. *Geochim. Cosmochim. Acta* 62, 193-207.

20. Barnett M. O., Jardine P. M. and Brooks S. C. (2002) U(VI) adsorption to heterogeneous subsurface media: application of a surface complexation model. *Environ. Sci. Technol.* 36, 937-942.

21. Barrow N. J., Gerth J. and Brümmer G. W. (1989) Reaction kinetics of the adsorption and desorption of nickel, zinc and cadmium by goethite. II. Modeling the extent and rate of reaction. *J. Soil Sci.* 40, 437-450.

22. Bar-Tal A., Bar-Yosef B. and Chen Y. (1988) Effects of fulvic acid and pH on zinc sorption on montmorillonite, *J. Soil Sci.* 146, 367-373.

23. Benjamin M. M. and Leckie J. O. (1980) Adsorption of metals at oxide interfaces: Effects of the concentrations of adsorbate and competing metals. In *Contaminants and Sediments* (ed. Baker R. A.), 2, 305-322, Ann Arbor Science Pub.

24. Benjamin M. M. and Leckie J. O. (1981a) Multiple-site adsorption of Cd, Cu, Zn and Pb on amorphous iron oxyhydroxide. *J. Colloid Interface Sci.* 79, 209-221.

25. Benjamin M. M. and Leckie J. O. (1981b) Competitive adsorption of cadmium, copper, zinc, and lead on amorphous iron oxyhydroxide. *J. Coll. Interface Sci.* 83, 410-419.

26. Blake R. L., Hessevick R. E., Zoltai T. and Finger L. W. (1966) *American Mineralogist* 51, 123-129.

27. Bode H., Dehmelt K. and Witte J. (1966) Nickel hydroxide electrodes. I. Nickel(II) hydroxide hydrate. *Electrochimica Acta* 11, 1079-1087.

28. Bolt G. H. (1957) Determination of the charge density of silica sols. *J. Phys. Chem.* 61, 1166-1169.

29. Borggaard O. K. (1981) Selective extraction of amorphous iron oxides by EDTA from soils from Denmark and Tanzania. *J. Soil Sci.* 32, 427-432.

30. Bottero J. Y., Arnaud M., Villieras F., Michot L. J., De Donato P. and Francois M. (1993) Surface and textural heterogeneity of fresh hydrous ferric oxides in water and in the dry state. *J. Colloid Interface Sci.* 159, 45-52.

31. Bradl H. B. (2004) Adsorption of heavy metal ions on soils and soils constituents. *J. Colloid Interface Sci.* 277, 1-18.

32. Brooks S. C. and Herman J. S. (1998) Rate and extent of cobalt sorption to representative aquifer minerals in the presence of a moderately strong organic ligand. *Applied Geochemistry* 13, 77-88.

33. Brown G. E. (1990) Spectroscopic studies of chemisorption reaction mechanisms at oxide-water interfaces in Mineral-Water Interface Geochemistry, *Review in Mineralogy* 23 (ed. M. F. Hochella and A. F. White), p. 309-363. Mineralogical Society of America.

34. Brown G. E. Jr. and Sturchio N. C. (2002) An overview of Synchrotron radiation applications to low temperature geochemistry and environmental science. In *Applications of Synchrotron Radiation in Low-Temperature Geochemistry and Environmental Science* (Ed. Fenter P. A., Rivers N. C., Sturchio S. R. and Sutton S. R.). Reviews in Mineralogy & Geochemistry 49, 1-115, Mineralogical Scciety of America.

35. Buerge-Weirich D., Hari R., Xue H., Behra P. and Sigg L. (2002) Adsorption of Cu, Cd, and Ni on goethite in the presence of natural groundwater ligands. *Environ. Sci. Technol.* 36, 328-336.

36. Bunker B. and Sayers D. (1988) In *X-ray Absorption: Principles, Applications, Techniques of EXAFS, SEXAFS, and XAFS*, Koningsberger, D. C., Prins, R., Eds., Wiley: New York, 1988.

37. Carvalho-E-Silva M. L., Ramos A. Y., Tolentino H. C. N., Enzweiler J., Netto S. M. and Alves M. D. C. M. (2003) Incorporation of Ni into natural goethite: An investigation by X-ray absorption spectroscopy. *American Mineralogist* 88, 876–882.

38. Chao T. T. and Zhou L. (1983) Extraction techniques for selective dissolution of amorphous iron oxides from soils and sediments. *Soil Sci. Soc. Am. J.* 47, 225-232.

39. Charlet L. and Manceau A. A. (1992) X-ray absorption spectroscopic study of the sorption of Cr(III) at the oxide-water interface. *J. Colloid Interface Sci.* 148, 443-458.

40. Charlet L. and Manceau A. A. (1993) Structure, formation, and reactivity of hydrous oxide particles: insights from X-ray absorption spectroscopy. In *Environmental particles* (eds. J. Buffle and H. P. van Leeuwen). *Environmental Analytical and Physical Chemistry Series Vol. 2*, p.117-164. Lewis Publishers.

41. Chisholm-Brause C. J., Hayes K. F., Roe L. A., Brown G. E. Jr., Parks G. A. and Leckie J. O. (1990) Spectroscopic investigation of Pb(II) complexes at the γ-Al_2O_3/water interface. *Geochim. Cosmochim. Acta* 54, 1897-1909.

42. Chisholm-Brause C. J., Roe A. L., Hayes K. F., Brown G. E. Jr., Parks G. A. and Leckie J. O. (1989) XANES and EXAFS study of aqueous lead(II) adsorbed on oxide surfaces. *Physica B: Condensed Matter* (Amsterdam, Netherlands) 158(1-3), 674-675.

43. Chisholm-Brause C. J., Hayes K. F., Roe L. A., Brown G. E. Jr., Parks G. A. and Leckie J. O. (1990) Spectroscopic investigation of Pb(II) complexes at the γ-Al_2O_3/water interface. *Geochim. Cosmochim. Acta.* 54, 1897-1909.

44. Christensen P. R., Bandfield J. L., Hamilton V. E., Howard D. A., Lane M. D., Piatek J. L., Ruff S. W. and Stefanov W. L. (2000) A thermal emission spectral library of rock-forming minerals. *J. of Geophysical Research* 105(E4), 9735-9739.

45. Christl I. and Kretzschmar R. (1999) Competitive sorption of copper and lead at the oxide-water interface, implications for surface site density. *Geochim. Cosmochim. Acta* 63, 2929-2938.

46. Christophi C. A. (1998) Competition of copper, lead, and cadmium adsorption to goethite. Master thesis. Department of Chemical Engineering, Chemistry, and Environmental Science, New Jersey Institute of Technology. Aug. 1998.

47. Christophi C. A. and Axe L. (2000) Competition of Cd, Cu, and Pb adsorption on goethite. *Journal of Environmental Engineering* 126, 66-74.

48. Clause O., Kermarec M., Bonneviot L., Villain R. and Che M. (1992) Nickel(II) ion-support ionteractions as a function of preparation method of silica-supported nickel materials. *J. Am. Chem. Soc.* 114, 4709-4717.

49. Combes J. M., Manceau A., Calas G. and Bottero J. Y. (1989) Formation of ferric oxides from aqueous solutions: A polyhedral approach by x-ray absorption spectroscopy: I. Hydrolysis and formation of ferric gels. *Geochim. Cosmochim. Acta* 53, 583-594.

50. Combes J. M., Manceau A. and Calas G. (1990) Formation of ferric oxides from aqueous solutions: A polyhedral approach by x-ray absorption spectroscopy: II. Hematite formation from ferric gels. *Geochim. Cosmochim. Acta* 54(4), 1083-1091.

51. Cornell R. M. (1987) Z. Pflanzenernaehr. Bodenkd. 150, 304-307.

52. Cornell R. M., Giovanoli R. and Schindler P. W. (1987) Effect of silicate species on the transformation of ferrihydrite into goethite and hematite in alkaline media. *Clays Clay Miner.* 35, 21-28.

53. Cornell R. M. and Giovanoli R. (1988) The influence of copper on the transformation of ferrihydrite (5Fe2O3·9H2O) into crystalline products in alkaline media. *Polyhedron* 7, 385-391.

54. Cornell R. M., Giovanoli R. and Schneider W. (1992) The effect of nickel on the conversion of amorphous iron(III) hydroxide into more crystalline iron oxides in alkaline media. *J. Chem. Technol. Biotechnol.* 53, 73-79.

55. Cornell R. M. and Schwertmann U. (1996) The Iron Oxides: Structure, Properties, Reactions, Occurrence and Uses. VCH: Weinheim.

56. Coston J. A., Fuller C. C. and Davis J. A. (1995) Pb^{2+} and Zn^{2+} adsorption by a natural aluminum- and iron-bearing surface coating on an aquifer sand. *Geochim. Cosmochim. Acta* 59, 3535-3547.

57. Coughlin B. R. and Stone A. T. (1995) Nonreversible adsorption of divalent metal ions (Mn^{II}, Co^{II}, Ni^{II}, Cu^{II}, and Pb^{II}) onto goethite. Effects of acidification, Fe^{II} addition, and picolinic acid addition. *Environ. Sci. Technol.* 29, 2445-2455.

58. Cowan C. E., Zachara J. M. and Resch, C. T. (1991) Cadmium adsorption on iron oxides in the presence of alkaline earth elements. *Environ. Sci. Technol.* 25, 437-446.

59. Crawford R. J., Harding I. H. and Mainwaring D. E. (1993) Adsorption and coprecipitation of single heavy metal ions onto the hydrated oxides of iron and chromium. *Langmuir* 9, 3050-3056.

60. Davies C. W. (1962) *Ion association.* Butterworths, London.

61. Davis J. A. and Leckie J. O. (1978) Surface ionization and complexation at the oxide/water interface II. Surface properties of amorphous iron oxyhydroxide and adsorption of metal ions. *J. Colloid Interface Sci.* 67(1), 90-107.

62. Davis J. A., Coston J. A., Kent D. B. and Fuller C. C. (1998) Application of the surface complexation concept to complex mineral assemblages. *Environ. Sci. Technol.* 32, 2820-2828.

63. De Kimpe C. R. (1993) *Chaper 68 Sand analysis. Soil Sampling and Methods of Analysis*, M. R. Carter, Ed., Canadian Society of Soil Science, Lewis Publishers.

64. Delolme C., Hébrard-Labit C., Spadini L. and Gaudet J. (2004) Experimental study and modeling of the transfer of zinc in a low reactive sand column in the presence of acetate. *J. Contaminant Hydrology* 70, 205-224.

65. Dixit S. and Hering J. G. (2003) Comparison of arsenic(V) and arsenic(III) sorption onto iron oxide mineralsi for arsenic mobility. *Environ. Sci. Technol.* 37, 4182-4189.

66. Dong D., Nelson Y. M., Lion L. W., Shuler M. L. and Ghiorse W. C. (2000) Adsorption of Pb and Cd onto metal oxides and organic material in natural surface coatings as determined by selective extractions: new Evidence for the importance of Mn and Fe oxides. *Wat. Res.* 34(2), 427-436.

67. Dong D., Li Y. and Hua X. (2001) Investigation of Fe, Mn oxides and organic material in surface coatings and Pb, Cd adsorption to surface coatings developed in different natural waters. *Microchemical Journal* 70, 25-33.

68. Dong D., Hua X., Li Y. and Li Z. (2002) Lead adsorption to metal oxides and organic material of freshwater surface coatings determined using a novel selective extraction method. *Environmental Pollution* 119(3), 317-321.

69. Dube A., Zbytniewski R., Kowalkowski T., Cukrowska E. and Buszewski B. (2001) Adsorption and migration of heavy metals in soil. *Polish Journal of Environmental Studies* 10, 1-10.

70. Düker A., Ledin A., Karlsson S. and Allard B. (1995) Adsorption of zinc on colloidal (hydr)oxides of Si, Al and Fe in the presence of a fulvic acid. *Applied Geochemistry* 10, 197-205.

71. Dyer J. A., Trivedi P., Scrivner N. C. and Sparks D. L. (2003) Lead sorption onto ferrihydrite. 2. Surface complexation modeling. *Environ. Sci. Technol.* 37, 915-922.

72. Dyer J. A., Trivedi P., Scrivner N. C. and Sparks D. L. (2004) Surface complexation modeling of zinc sorption onto ferrihydrite. *J. Colloid Interface Sci.* 270, 56-65.

73. Dzombak D. A. and Morel F. M. M. (1986) Sorption of cadmium on hydrous ferric oxide at high sorbate/sorbent ratios: equilibrium, kinetics, and modeling. *J. Colloid Interface Sci.* 112, 588-598.

74. Dzombak D. A. and Morel F. M. M. (1990) *Surface Complexation Modeling. Hydrous ferric oxide*. John Wiley & Sons

75. Edwards M. and Benjamin M. M. (1989) Adsorptive filtration using coated sand: A new approach for treatment of metal-bearing wastes. *J. Water Pollution Control Fedn.* 61(9), 1523-1533.

76. Elzinga E. J. and Sparks D. L. (2002) X-ray absorption spectroscopy study of the effects of pH and ionic strength on Pb(II) sorption to amorphous silica. *Environ. Sci. Technol.* 36, 4352-4357.

77. Elzinga E. J., Peak D. and Sparks D. L. (2001) Spectroscopic studies of Pb(II)-sulfate interactions at the goethite-water interface. *Geochim. Cosmochim. Acta* 65, 2219-2230.

78. Elzinga E. J. and Sparks D. L. (1999) Nickel sorption mechanisms in a pyrophyllite-montmorillonite mixture. *J. Colloid Interface Sci.* 213, 506-512.

79. Ephraim J., Xu H., Ledin A. and Allard B. (1991) The uptake of zinc, cadmium and mercury by geological media in the presence of a fulvic acid. *Finnish Humus News* 3, 109-114.

80. Evans T. D., Leal J. R. and Arnold P. W. (1979) The interfacial electrochemistry of goethite (α-FeOOH) especially the effect of carbon dioxide contamination. *J. Electroanal. Chem.* 105, 161-167.

81. Fabian D., Henning T., Jager C., Mutschke H., Dorschner J. and Wehrhan O. (2001) Steps toward interstellar silicate mineralogy. Part 6. Dependence of crystalline olivine IR spectra on iron content and particle shape. *Astronomy and Astrophysics* 378(1), 228-238.

82. Fan M., Boonfueng T., Xu Y., Axe L. and Tyson T.A. (2005) Modeling Pb sorption to microporous amorphous oxides as discrete particles and coatings. *J. Colloid Interface Sci.* 281, 39-48.

83. Fan H-J. (1996) Removal and recovery of Cu(II) and Cd(II) by Mn oxide-coated composite adsorbent. Ph.D. dissertation. Illinois Institute of Technology, Chicago Illinois, May 1996.

84. Fendorf S., Eick M., Grossl P. and Sparks D. L. (1997) Arsenate and chromate retention mechanisms on goethite. 1. Surface structure. *Environ. Sci. Technol.* 31(2).

85. Forbes E. A., Posner A. M. and Quirk J. P. (1974) The specific adsorption of inorganic Hg(II) species and Co(III) complex ions on goethite. *J. Colloid Interface Sci.* 49(3), 403-409.

86. Forbes E. A., Posner A. M. and Quirk J. P. (1976) The specific adsorption of divalent cadmium, cobalt, copper, lead, and zinc on goethite. *J. Soil Sci.* 27, 154-166.

87. Ford R. G., Scheinost A. C., Scheckel K. G. and Sparks D. L. (1999) The link between clay mineral weathering and the stabilization of Ni surface precipitates. *Environ. Sci. Technol.* 33, 3140-3144.

88. Fuller C. C., Davis J. A., Coston J. A. and Dixon E. (1996) Characterization of metal adsorption variability in a sand and gravel aquifer, Cape Cod, Massachusetts, U.S.A. *Journal of Contaminant Hydrology* 22, 165-187.

89. Furrer G., Scheidegger A., Plötze M., Kahr G., Studer B., Lothenbach B. and Schulin R. (2001) *Mitt. Dtsch. Bodenkundl. Ges.* 96, 181-182.

90. Furtado A., Madeira M. and Jeanroy E. (1990) Mineralogy of soils from Madeira Island (Portugal), solubility of the iron oxides. *Sci. Geol., Bull.* 43(2-4), 139-149.

91. Gadde R. R. and Laitinen H. A. (1974) Studies of heavy metal adsorption by hydrous iron and manganese oxides. *Analytical Chemistry* 46(13), 2022-2026.

92. Gadsden J. A. (1975) Infrared Spectra of Minerals and Related Inorganic Compounds. Butterworth.

93. Gao Y. and Mucci A. (2001) Acid base reactions, phosphate and arsenate complexation, and their competitive adsorption at the surface of goethite in 0.7 M NaCl solution. *Geochim. Cosmochim. Acta* 65, 2361-2378.

94. Geiger S. C. and Leoppert R. H. (1986) Correlation of DTPA extractable Fe with indigenous properties of selected calcareous soils. *Journal of Plant Nutrition* 9(3-7), 229-240.

95. Goldberg S. (1991) Sensitivity of surface complexation modeling to the surface site density parameter. *J. Colloid Interface Sci.* 145, 1-9.

96. Gomes P. C., Rontes M. P. F., da Silva A. G., Mendonca E. D. and Netto A. R. (2001) Selectivity sequence and competitive adsorption of heavy metals by Brazilian soils. *Soil Sci. Soc. Am. J.* 65(4), 1115-1121.

97. Clesceri L. S., Greenberg A. E. and Eaton A. D. (1998) Standard methods for the examination of water and wastewater, 20th edition. APHA, AWWA, WEF, Washington D. C.

98. Green-Pedersen H., Jensen B. T. and Pind N. (1997) Nickel adsorption on MnO2, Fe(OH)3, montmorillonite, humic acid, and calcite, a comparative study. *Environ. Technol.* 18, 807-815.

99. GTI (2002) Gas Technology Institute, Sample analysis report. Chicago, IL.

100. Gualtieri A. and Venturelli P. (1999) In situ study of the goethite-hematite phase transformation by real time synchrotron powder diffraction. *American Mineralogist* 84, 895-904.

101. Gunneriusson L., Lövgren L. and Sjöberg S. (1994) Complexation of Pb(II) at the goethite (α-GeOOH)/water interface: The influence of chloride. *Geochim. Cosmochim. Acta* 58, 4973-4983.

102. Gupta V. K. (1998) Equilibrium uptake, sorption dynamics, process development, and column operations for the removal of copper and nickel from aqueous solution and wastewater using activated clay, a low-cost adsorbent. *Ind. Eng. Chem. Res.* 37, 192-202.

103. Hayes K. F. (1987) Equilibrium, spectroscopic, and kinetic studies of ion adsorption at the oxide/aqueous interface. PhD dissertation, Stanford Univ., Palo Alto, CA.

104. Hayes K. F. and Leckie J. O. (1986) Mechanism of lead ion adsorption at the goethite-water interface. In *Geochemical Processes at Mineral Surfaces, ACS Symposium series 323* (ed. J. A. Davis and K. F. Hayes), pp. 114-141. American Chemical Society.

105. Hayes K. F. and Leckie J. O. (1987) Modeling ionic strength effects on cation adsorption at hydrous oxide/solution interfaces. *J. Colloid Interface Sci.* 115, 564-572.

106. Hayes K. F., Redden G., Ela W. and Leckie J. O. (1991) Surface complexation models: An evaluation of model parameter estimation using FITEQL and oxide mineral titration data. *J. Colloid Interface Sci.* 142, 448-469.

107. Hayes K. F. and Katz L. E. (1996) Application of x-ray absorption spectroscopy for surface complexation modeling of metal ion sorption. In *Physics and Chemistry of Mineral Surfaces* (ed. Patrick V. Brady), CRC Press.

108. Hayes K. F., Papelis C. and Leckie J. O. (1988) Modeling ionic strength effects on anion adsorption at hydrous oxide/solution interfaces. *J. Colloid Interface Sci.* 125, 717-726.

109. Heidmann I., Christl I., Leu C. and Kretzschmar R. (2005) Competitive sorption of protons and metal cations onto kaolinite: experiments and modeling. *J. Colloid Interface Sci.* 282, 270-282.

110. Herbelin A. and Westall J. (1999) FITEQL: A computer Program for determination of chemical equilibrium constants from experimental data. Version 4.0. Department of Chemistry, Oregon State University. Corvallis, OR.

111. Hiemstra T. and van Riemsdijk W. H. (1996) A surface structural approach to ion adsorption: the charge distribution (CD) model. *J. Colloid Interface Sci.* 179, 488-508.

112. Hiemstra T., de Wit J. C. M. and van Riemsdijk W. H. (1989) Multisite proton adsorption modeling at the solid/solution interface of (hydr)oxides: A new approach. II. Application to various important (hydr)oxides. *J. Colloid Interface Sci.* 133, 105-117.

113. Hiemstra T. and van Riemsdijk W. H. (1999) Surface structural ion adsorption modeling of competitive binding of oxyanions by metal (hydr)oxides. *J. Colloid Interface Sci.* 210, 182-193.

114. Hiemstra T., van Riemsdijk W. H. and Bolt G. H. (1989) Multisite proton adsorption modeling at the solid/solution interface of (hydr)oxides: A new approach. I. Model description and evaluation of intrinsic reaction constants. *J. Colloid Interface Sci.* 133, 91-104.

115. Hill R. J. (1985) *Acta Cryst.* C41, 1281-1284.

116. Hingston F. J., Posner A. M. and Quirk J. P. (1972) *J. Soil Sci.* 23, 177.

117. Honeyman B. D. (1984) Cation and anion adsorption at the oxide/solution interface in systems containing binary mixtures of adsorbents: an investigation of the concept on adsorptive additivity; Ph.D. thesis, Stanford University; Stanford, CA, 1984.

118. Hsi C. K. D. and Langmuir D. (1985) Adsorption of uranyl onto ferric oxyhydroxides: application of the surface complexation site-binding model. *Geochim. Cosmochim. Acta* 49(9), 1931-1941.

119. Jackson R. E. and Inch K. J. (1989) The in-situ adsorption of strontium-90 in a sand aquifer at the Chalk River Nuclear Laboratories. *Journal of Contaminant Hydrology* 4(1), 27-50.

120. Jackson M. L., Lim C. H. and Zelazny L. W. (1986) Oxides, hydroxides, and aluminosilicates. Part 1 Physical and mineralogical methods. Methods of soil analysis. Number 9 in the series *AGRONOMY*. Dinauer, Richard C. Ed. American Society of Agronomy, Inc. and Soil Science Society of America, Inc. 1986.

121. JCPDS (1998) *Handbook for diffraction data* (PCPDFWIN ver. 2.00).

122. Jenne E. A. (1998) Adsorption of metals by Geomedia: data analysis, modeling, controlling factors, and related issues. In *Adsorption of Metal by Geomedia Variables, Mechanisms, and Model Applications* (ed. E. A. Jenne) Chapter 1, 1-73, Academic Press, San Diego, CA.

123. Jeon B-H., Dempsey B. A., Burgos W. D. and Royer R. A. (2003) Sorption kinetics of Fe(II), Zn(II), Co(II), Ni(II), Cd(II), and Fe(II)/Me(II) onto hematite. *Water Research* 37, 4135-4142.

124. Jeon B-H., Dempsey B. A., Burgos W. D., Royer R. A. and Roden E. E. (2004) Modeling the sorption kinetics of divalent metal ions to hematite. *Water Research* 38, 2499-2504.

125. Johnson B. B. (1990) Effect of pH, Temperature, and concentration on the adsorption of cadmium on goethite. *Environ. Sci. Technol.* 24, 112-118.

126. Joshi A. and Chaudhuri M. (1996) Removal of arsenic from ground water by iron oxide-coated sand. *Journal of Environmental Engineering* 122(8), 769-771.

127. Juang R-S. and Chung J-Y. (2004) Equilibrium sorption of heavy metals and phosphate from single-and binary-sorbate solutions on goethite. *J. Colloid Interface Sci.* 275, 53-60.

128. Kanungo S. B. (1994) Adsorption of cations on hydrous oxides of iron I. Interfacial behavior of amorphous FeOOH and β-FeOOH (akaganeite) in different electrolyte solutions. *J. Colloid Interface Sci.* 162, 86-92.

129. Kanungo S. B., Tripathy S. S. and Rajeev. (2004) Adsorption of Co, Ni, Cu, and Zn on hydrous manganese dioxide from complex electrolyte solutions resembling sea water in major ion content. *J. Colloid Interface Sci.* 269, 1-10.

130. Katz L. E. and Hayes K. F. (1995a) Surface complexation modeling. I. Strategy for modeling monomer complex formation at moderate surface coverage. *J. Colloid Interface Sci.* 170, 477-490.

131. Katz L. E. and Hayes K. F. (1995b) Surface complexation modeling. II. Strategy for modeling polymer and precipitation reactions at high surface coverage. *J. Colloid Interface Sci.* 170, 491-501.

132. Khaodhiar R., Azizian M. F., Osathaphan K. and Nelson P. O. (2000) Copper, chromium, and arsenic adsorption and equilibrium modeling in an iron-oxide-coated sand, background electrolyte system. *Water, Air, and Soil Pollution* 119(1-4), 105-120.

133. Kinniburgh D. G. and Jackson M. L. (1982) Concentration and pH dependence of calcium and zinc adsorption by iron hydrous oxide gel. *Soil Sci. Soc. Amer. J.* 46, 56-61.

134. Kooner Z. S. (1993) Comparative study of adsorption behavior of copper, lead, and zinc onto goethite in aqueous systems. *Environmental Geology* 21, 242-250.

135. Kooner Z. S., Cox C. D. and Smoot J. L. (1995) Prediction of adsorption of divalent heavy metals at the goethite/water interface by surface complexation modeling. *Environ. Toxicol. Chem.* 14, 2077-2083.

136. Koopal L. K., van Riemsdijk W. H. and Roffey M. G. (1987) Surface ionization and complexation models: a comparison of methods for determining model parameters. *J. Colloid Interface Sci.* 118, 117-136.

137. Kosmulski M. (1996) Adsorption of cadmium on alumina and silica: analysis of the values of stability constants of surface complexes calculated for different parameters of triple layer model. *Colloids and Surfaces A: Physicochemical and Engineering Aspects* 117, 201-214.

138. Kosmulski M. (1997) Standard enthalpies of adsorption of di- and trivalent cations on alumina. *J. Colloid Interface Sci.* 192, 215-227

139. Kuan W-H., Lo S-L., Wang M-K. and Lin C-F. (1998) Removal of Se(IV) and Se(VI) from water by aluminum-oxide-coated sand. *Wat. Res.* 32(3), 915-923.

140. Kuan W-H., Lo S-L. and Wang M-K. (2004) Modeling and electrokinetic evidences on the process of the Al(III) sorption continuum in $SiO_{2(s)}$ suspension. *J. Colloid and Interface Sci.* 272, 489-497.

141. Kunze G. W. and DiXon J. B. (1986) Pretreatment for mineralogical analysis. Part 1 Physical and mineralogical methods. Methods of Soil Analysis. Number 9 in the series *AGRONOMY.* Dinauer, Richard C. Ed. American Society of Agronomy, Inc. and Soil Science Society of America, Inc. 1986.

142. Lai C-H., Lo S-L. and Chiang H-L. (2000) Adsorption/desorption properties of copper ions on the surface of iron-coated sand using BET and EDAX analyses. *Chemosphere* 41, 1249-1255.

143. Larsen F. and Postma D. (1997) Nickel mobilization in a groundwater well field: release by pyrite oxidation and desorption from manganese oxides. *Environ. Sci. Technol.* 31, 2589-2595.

144. Ledin A., Karisson S., Düker A. and Allard B. (1994) The adsorption of europium to colloidal iron oxyhydroxides and quartz-the impact of pH and an aquatic fulvic acid. *Radiochimica Acta.* 66/67, 213-220.

145. Lee S-Z., Allen H. E., Huang C. P., Sparks D. L., Sanders P. F. and Peijnenburg W. J. G. M. (1996) Predicting Soil-Water Partition Coefficients for Cadmium. *Environ. Sci. Technol.* 30(12), 3418-3424.

146. Lee S-Z., Chang L., Yang H-H., Chen C-M. and Liu M-C. (1998) Adsorption characteristics of lead onto soils. *Journal of Hazardous Materials A* 63, 37-49.

147. Leoppert R. H. and Inskeep W. P. (1996) Chapter 23 Iron, Part 3 Chemical Methods. Mothods of Soil Analysis. Number 5 in the *Soil Science Society of America Book Series*. Bartels, J. M. Ed. Published by Soil Science Society of America, Inc. and American Society of Agronomy, Inc.

148. Liang L., Hofmann A. and Gu B. (2000) Ligand-induced dissolution and release of ferrihydrite colloids. *Geochim. Cosmochim. Acta* 64(12), 2027-2037.

149. Lion L. W., Altmann R. S. and Leckie J. O. (1982) Trace metal adsorption characteristics of estuarine particulate matter: evaluation of contributions of Fe/Mn oxide and organic surface coatings. *Environ. Sci. Technol.* 16, 660-666.

150. Liu C. and Huang P. M. (2001) Pressure-jump relaxation studies on kinetics of lead sorption by iron oxides formed under the influence of citric acid. *Geoderma* 102, 1-25.

151. Lo S-L. and Chen T-Y. (1997) Adsorption of Se(IV) and Se(VI) on an iron-coated sand from water. *Chemosphere* 35(5), 919-930.

152. Lo S-L., Jeng H-T. and Lai C-H. (1997) Characteristics and adsorption properties of iron-coated sand. *Water Science and Technology* 35 (7), 63-70.

153. Lövgren L., Sjöberg S. and Schindler P.W. (1990) Acid/base reactions and Al(III) complexation at the surface of goethite. *Geochim. Cosmochim. Acta* 54, 1301–1306.

154. Lumsdon D. G. and Evans L. J. (1994) Surface complexation model parameters for goethite (α-FeOOH). *J. Colloid Interface Sci.* 164, 119-125.

155. Lützenkirchen J. and Behra P. (1994) Comment on the Article "On the nature of the Energetic Surface Heterogeneity in Ion Adsorption at a Water/Oxide Interface: Theoretical Studies of Some Special Features of Ion Adsorption at Low Ion Concentrations". *Langmuir* 10, 3916-3917.

156. Lützenkirchen J. (2002) Surface complexation models of adsorption. A critical survey in the context of experimental data. *Surfactant Science Series*, 107(Adsorption), 631-710.

157. Manceau A. and Combes J. M. (1988) Structure of manganese and iron oxides and oxyhydroxides: A topological approach by EXAFS. *Physics and Chemistry of Minerals* 15(3), 283-295.

158. Manceau A., Charlet L., Boisset M. C., Didier B. and Spadini L. (1992) Sorption and speciation of heavy metals on hydrous Fe and Mn oxides. From microscopic to macroscopic. *Applied Clay Science*, 7, 201-223.

159. Manceau A. and Drits V. (1993) Local structure of ferrihydrite and feroxyhite by EXAFS spectroscopy. *Clay Minerals* 28, 165-184.

160. Manceau A. and Charlet L. (1994) The mechanism of selenate adsorption on goethite and hydrous ferric oxide. *J. Colloid Interface Sci.* 168, 87-93.

161. Manceau A., Schlegel M., Nagy K. L. and Charlet L. (1999) Evidence for the formation of trioctahedral clay upon sorption of Co^{2+} on quartz. *J. Colloid Interface Sci.* 220, 181-197.

162. Manceau A., Schlegel M. L., Musso M., Sole V. A., Gauthier C., Petit P. E. and Trolard F. (2000) Crystal chemistry of trace elements in natural and synthetic goethite. *Geochim. Cosmochim. Acta* 64, 3643-3661.

163. Manceau A., Tamura N., Celestre R. S., Macdowell A. A., Geoffroy N., Sposito G. and Padmore H. A. (2003) Molecular-scale speciation of Zn and Ni in soil ferromanganese nodules from loess soils of the Mississippi basin. *Environ. Sci. Technol.* 37, 75-80.

164. Manning B. A., Fendorf S. E. and Goldberg S. (1998) Surface structures and stability of arsenic(III) on goethite: spectroscopic evidence for inner-sphere complexes. *Environ. Sci. Technol.* 32(16), 2383-2388.

165. Marchetti S. G., Cagnoli M. V., Alvarez A. M., Gallegos N. G., Bengoa J. F., Yeramian A. A. and Mercader R. C. (1997) Dependence of the oxide-support interaction on the size and nature of iron oxide particles on SiO2. *J. Phys. Chem. Solids.* 58(2), 2119-2125.

166. Martin T. A. and Kempton J. H. (2000) In situ stabilization of metal-contaminated groundwater by hydrous ferric oxide: an experimental and modeling investigation. *Environ. Sci. Technol.* 34, 3229-3234.

167. Martínez C. E. and McBride M. B. (1998) Coprecipitates of Cd, Cu, Pb and Zn in iron oxides: solid phase transformation and metal solubility after aging and thermal treatment. *Clays and Clay Minerals*, 46, 537-545.

168. Meng X. and Letterman R. D. (1993a) Effect of component oxide interaction on the adsorption properties of mixed oxides. *Environ. Sci. Technol.* 27(5), 970-975.

169. Meng X. and Letterman R. D. (1993b) Modeling ion adsorption on aluminum hydroxide modified silica. *Environ. Sci. Technol.* 27(9), 1924-1929.

170. Miller D. M., Sumner M. E. and Miller W. P. (1989) A comparison of batch- and flow-generated anion adsorption isotherms. *Soil Sci. Soc. Am. J.* 53, 373-380.

171. Misak N. Z., Ghoneimy H. F. and Morcos T. N. (1996) Adsorption of Co^{2+} and Zn^{2+} ions on hydrous Fe(III), Sn(IV), and Fe(III)/Sn(IV) oxides. II. Thermal behavior of loaded oxides, isotopic exchange equilibria, and percentage adsorption-pH curves. *J. Colloid Interface Sci.* 184, 31-43.

172. Mishra S. P., Singh V. K. and Tiwary D. (1997) Inorganic particulates in removal of toxic heavy metal ions, efficient removal of cadmium ions from aqueous solutions by hydrous zirconium oxide. *Radiochimica Acta* 76, 97.

173. Mishra S. P. and Tiwary D. (1995) Inorganic particulates in removal of toxic heavy metal ions. Efficient removal of strontium ions from aqueous solutions by hydrous manganese oxide. *Radiochimica Acta* 69, 121.

174. Mishra S. P and Tiwary D. (1998) Inorganic particulates in removal of toxic heavy metal ions, efficient removal of cadmium ions from aqueous solutions by hydrous manganese oxide. *Radiochimica Acta* 80, 213.

175. Müller B. and Sigg L. (1992) Adsorption of lead (II) on the goethite: voltametric evaluation of surface complexation parameters. *J. Colloid Interface Sci.* 148, 517-531.

176. Nachtegaal M. and Sparks D. L. (2003) Nickel sequestration in a kaolinite-humic acid complex. *Environ. Sci. Technol.* 37, 529-534.

177. Nakahara O. (1996) Reconsideration of theoretical basis of Freundlich adsorption isotherm equation. 1. The Problem. *Soil Science and Plant Nutrition* 42(1), 41-49.

178. Nilsson N., Persson P., Loevgren L. and Sjoeberg S. (1996) Competitive surface complexation of o-phthalate and phosphate on goethite (α-FeOOH) particles. *Geochim. Cosmochim. Acta* 60(22), 4385-4395.

179. Nolan, A. L.; Mclaughlin, M. J.; and Mason, S. D. (2003) Chemical speciation of Zn, Cd, Cu, and Pb in pore waters of agricultural and contaminated soils using Donnan dialysis. *Environ. Sci. Technol.* 37(1), 90-98.

180. Nowack B., Lützenkirchen J., Behra P. and Sigg L. (1996) Modeling the adsorption of metal-EDTA complexes onto oxides. *Environ. Sci. Technol.* 30, 2397-2405.

181. Nowok J. W., Hurley J. P. and Stanley D. C. (1993) Local structure of a lignitic coal ash slag and its effect on viscosity. *Energy & Fuels* 7(6), 1135-40.

182. O'Day P. A., Carroll S. A. and Waychunas G. A. (1998) Rock-water interactions controlling zinc, cadmium, and lead concentrations in surface waters and sediments, U.S. tri-state mining district. 1. Molecular identification using X-ray absorption spectroscopy. *Environ. Sci. Technol.* 32, 943-955.

183. O'Day P. A., Brown G. E. Jr. and Parks G. A. (1994) X-ray absorption spectroscopy of cobalt(II) multinuclear surface complexes and surface precipitates on kaolinite. *J. Colloid Interface Sci.* 165, 269-289.

184. O'Reilly S. E. and Hochella M. F. Jr. (2003) Lead sorption efficiencies of natural and synthetic Mn and Fe-oxides. *Geochim. Cosmochim. Acta* 67(23), 4471-4487.

185. Ostergren J. D., Bargar J. B., Brown G. E. Jr. and Parks, G. A. (1999a) *J. Synch. Rad.* 6, 645-647.

186. Ostergren J. D., Brown G. E. Jr., Parks G. A. and Tingle T. N. (1999b) Quantitative speciation of lead in selected mine tailings from leadville, CO. *Environ. Sci. Technol.* 33, 1627-1636.

187. Ostergren J. D., Trainor T. P., Bargar J. R., Brown G. E. Jr. and Parks G. A. (2000a) Inorganic ligand effects on Pb(II) sorption to goethite (α-FeOOH). I. Carbonate. *J. Colloid Interface Sci.* 225, 466-482.

188. Ostergren J. D., Brown G. E. Jr., Parks G. A. and Persson P. (2000b) Inorganic ligand effects on Pb(II) sorption to goethite (α-FeOOH), II. Sulfate. *J. Colloid Interface Sci.* 225, 483-493.

189. Padmanabham M. (1983) Comparative study of the adsorption-desorption behavior of copper(II), zinc(II), cobalt(II), and lead(II) at the goethite-solution interface. *Australian J. Soil Res.* 21, 515-525.

190. Paige C. R., Snodgrass W. J., Nicholson R. V., Scharer J. M. and He Q. H. (1997) The effect of phosphate on the transformation of ferrihydrite into crystalline products in alkaline. *Water, Air, and Soil Pollution*, 97, 397-412.

191. Palmqvist U., Ahlberg E., Lövgren L. and Sjöberg S. (1997) In situ voltammetric determinations of metal ions in goethite suspensions: single metal ion systems. *J. Colloid Interface Sci.* 196, 254-266.

192. Palmqvist U., Ahlberg E., Lövgren L. and Sjöberg S. (1999) Competitive metal ion adsorption in goethite systems using in situ voltammetric methods and potentiometry. *J. Colloid Interface Sci.* 218, 388-396.

193. Pandya K. I., O'Grady W. E., Corrigan D. A., McBreen J. and Hoffman R. W. (1990) Extended X-ray absorption fine structure investigation of nickel hydroxides. *J. Phys. Chem.* 94, 21-26.

194. Papelis C., Roberts P. V. and Leckie J. O. (1995) Modeling the rate of cadmium and selenite adsorption on micro-and mesoporous transition aluminas. *Environ. Sci. Technol.* 29, 1099-1108.

195. Parks G. A. (1965) The isoelectric points of solid oxides, solid hydroxides, and aqueous hydroxo complex systems. *Chem. Rev.* 65, 177-198.

196. Parks G. A. (1967) Aqueous surface chemistry of oxides and complex oxide minerals-isoelectric point and zero point of charge. Equilibrium Concepts in Natural Water Systems. Edited by Werner Stumm, *Advances in Chemistry Series 67*, ACS, Washington, D. C.

197. Paulhiac J. L. and Clause O. (1993) Surface coprecipitation of Co(II), Ni(II), or Zn(II) with Al(III) ions during impregnation of γ-alumina at neutral pH. *J. Am. Chem. Soc.* 115, 11602-11603.

198. Peacock C. L. and Sherman D. M. (2004) Vanadium (V) adsorption onto goethite (alpha-FeOOH) at pH 1.5 to 12: A surface complexation model based on ab initio molecular geometries and EXAFS spectroscopy. *Geochim. Cosmochim. Acta* 68, 1723-1733.

199. Peak D. and Sparks D. L. (2002) Mechanisms of selenate adsorption on iron oxides and hydroxides. *Environ. Sci. Technol.* 36, 1460-1466.

200. Perry R. H. and Green D. W. (1984) *Perry's Chemical Engineers' Handbook*, 6th edition, McGraw-Hill international editions, Chemical engineering series.

201. Pertlik F. (1986) Structures of hydrothermally synthesized cobalt(II) and nickel(II) carbonate. *Acta Crsytallogr.* C42, 4-5.

202. Pieper A. P., Ryan J. N., Harvey R. W., Amy G. L., Illangasekare R. H. and Metge D. W. (1997) Transport and recovery of bacteriophage PRD1 in a sand and gravel aquifer: effect of sewage-derived organic matter. *Environ. Sci. Technol.* 31, 1163-1170.

203. Pierce M. L. and Moore C. B. (1980) Adsorption of arsenite on amorphous iron hydroxide from dilute aqueous solution. *Environ. Sci. Technol.* 14(2), 214-216.

204. Ressler T. (1998) WinXAS: a program for X-ray absorpotion spectroscopy data analysis under MS-Windows. *J. Synchrotron Radiation* 5, 118-122.

205. Reyes I. and Torrent J. (1997) Citrate-ascorbate as a highly selective extractant for poorly crystalline iron oxides. *Soil Sci. Soc. Am. J.* 61, 1647-1654.

206. Richens D. T. (1997) *The Chemistry of Aqua Ions.* John Wiley & Sons, Chichester, UK.

207. Roberts D. R., Scheidegger A. M. and Sparks D. L. (1999) Kinetics of mixed Ni-Al precipitate formation on a soil clay fraction. *Environ. Sci. Technol.* 33, 3749-3754.

208. Roberts D. R., Ford R. G. and Sparks D. L. (2003) Kinetics and mechanisms of Zn complexation on metal oxides using EXAFS spectroscopy. *J. colloid Interface Sci.* 263, 364-376.

209. Robertson A. P. and Leckie J. O (1997) Cation binding predictions of surface complexation models: effects of pH, ionic strength, cation loading, surface complex, and model fit. *J. Colloid Interface Sci.* 188, 444-472.

210. Robertson A. P. and Leckie J. O. (1998) Acid/Base, copper binding, and Cu2+/H+ exchange properties of goethite, an experimental and modeling study. *Environ. Sci. Technol.* 32, 2519-2530.

211. Rodda D. P., Johnson B. B. and Wells J. D. (1993) The effect of temperature and pH on the adsorption of copper(II), lead(II), and zinc(II) onto goethite. *J. Colloid Interface Sci.* 161, 57-62.

212. Roe A. L., Hayes K. F., Chisholm-Brause C., Brown G. E. Jr., Parks G. A., Hodgson K. O. and Leckie J. O. (1991) In situ X-ray absorption study of lead ion surface complexes at the goethite-water interface. *Langmuir* 7, 367–373.

213. Ross G. J. and Wang C. (1993) Extractable Al, Fe, Mn and Si. Soil Sampling and Methods of Analysis, M. R. Carter, Ed., *Canadian society of Soil Science*, Lewis Publishers.

214. Rustad J. R., Felmy A. R. and Hay B. P. (1996) Molecular statics calculations of proton binding to goethite surfaces: a new approach to estimation of stability constants for multistie surface complexation models. *Geochim. Cosmochim. Acta* 60, 1563-1576.

215. Ryan J. N. and Gschwend P. M. (1991) Extraction of iron oxides from sediments using reduction dissolution by titanium(III). *Clays and Clay Minerals* 39(5), 509-518.

216. Ryan J. N. and Gschwend P. M. (1994) Effect of solution chemistry on clay coilloid release from an iron oxide-coated aquifer sand. *Environ. Sci. Technol.* 28(9), 1717-1726.

217. Sahai N. and Sverjensky D. A. (1997) Evaluation of internally consistent parameters for the triple-layer model by the systematic analysis of oxide surface titration data. *Geochim. Cosmochim. Acta* 61, 2801-2826.

218. Sahai N., Carroll S. A., Roberts S. and O'Day P. A. (2000) X-ray absorption spectroscopy of strontium(II) coordination. II. Sorption and precipitation at kaolinite, amorphous silica, and goethite surfaces. *J. Colloid Interface Sci.* 222, 198-212.

219. Sahl K.Z. (1974) *Kristallographie* 139, 215-222.

220. Sauvé S, Hendershot W. and Allen H. E. (2000) Solid-Solution Partitioning of Metals in Contaminated Soils: Dependence on pH, Total Metal Burden, and Organic matter. *Environ. Sci. Technol.* 34(7), 1125-1131.

221. Scheidegger A. M., Borkovec M. and Sticher H. (1993) Coating of silica sand with goethite: preparation and analytical identification. *Geoderma* 58(1-2), 43-65.

222. Scheidegger A. M., Lamble G. M. and Sparks D. L. (1996) Investigation of Ni sorption on pyrophyllite an XAFS study. *Environ. Sci. Technol.* 30, 548-554.

223. Scheidegger A. M., Strawn D. G., Lamble G. M., and Sparks D. L. (1998) The kinetics of mixed Ni-Al hydroxide formation on clay and aluminum oxide minerals: A time-resolved XAFS study. *Geochim. Cosmochim. Acta* 62(13), 2233-2245.

224. Scheinost A. C., Ford R. G. and Sparks D. L. (1999) The role of Al in the formation of secondary Ni precipitates on pyrophyllite, gibbsite, talc, and amorphous silica: a DRS study. *Geochim. Cosmochim. Acta* 63, 3193-3203.

225. Scheinost A. C., Abend S., Pandya K. I. and Sparks D. L. (2001) Kinetic controls on Cu and Pb sorption by ferrihydrite. *Environ. Sci. Technol.* 35, 1090-1096.

226. Scheinost A. C., Kretzschmar R. and Pfister S. (2002) Combining selective sequential extractions, X-ray absorption spectroscopy, and principal component analysis for quantitative zinc speciation in soil. *Environ. Sci. Technol.* 36(23), 5021-5028.

227. Schlegel M. L., Manceau A. and Charlet L. (1997) EXAFS study of Zn and ZnEDTA sorption at the goethite (α-FeOOH)/water interface. *J. Phys. IV France* 7 *Colloque C2, Supplément au Journal de Physique IIId'avril.*

228. Schulthess C. P. and Sparks D. L. (1991) Equilibrium-based modeling of chemical sorption on soils and soil constituents. *Advances in Soil Science* 16, 121-63.

229. Schwarz J. A., Driscoll C. T. and Bhanot A. K. (1984) The zero point of charge of silica-alumina oxide suspensions. *J. Colloid Interface Sci.* 97(1).

230. Schwertmann U. and Thalmann H. (1976) The influence of [iron(II)], [silicon], and pH on the formation of lepidocrocite and ferrihydrite during oxidation of aqueous iron(II) chloride solutions. *Clay Minerals* 11, 189-200.

231. Schwertmann, U. and Murad, E. (1983) Effect of pH on the formation of goethite and hematite from ferrihydrite. *Clays Clay Min.* 31, 277-284.

232. Schwertmann U., Cambier P. and Murad E. (1985) Properties of goethites of varying crystallinity. *Clays and Clay Minerals.* 33(5), 369-378.

233. Schwertman U. and Taylor R. M. (1989) Iron Oxides Minerals in Soil Environments, second edition, SSSA Book Series no.1 WI USA, *Soil Science of America* 379-427.

234. Schwertmann U. and Cornell R. M. (1991) *Iron Oxides in the Laboratory, Preparation and Characterization.* VCH Verlagsgesellschaft mbH, Weinheim (Federal Republic of Germany) and VCH Publishers, Inc., New York, NY (USA).

235. Sen T. K., Mahajan S. P. and Khilar K. C. (2002) Adsorption of Cu^{2+} and Ni^{2+} on iron oxide and kaolin and its importance on Ni^{2+} transport in porous media. *Colloids and Surfaces A: Physicochem. Eng. Aspects* 211, 91-102.

236. Sequi P., De Nobili M. and Pardini G. (1983) Ageing of iron oxides during peroxidation. *Agrochimica* 27(2-3), 158-164.

237. Shuman L. M. (1982) Separating soil iron-and manganese-oxide fractions for microelement analysis. *Soil Sci. Soc. Am. J.* 46(5), 1099-1102.

238. Siegel M. D., Tripathi V. S., Rao M. G. and Ward D. B. (1992) Development and validation of a multi-site model for adsorption of metals by mixtures of minerals: 1 Overviw and preliminary results. *Water-Rock Interat., Proc. Int. Symp.,* 7th, 63-67.

239. Singh B., Sherman D. M., Gilkes R. J., Wells M. and Mosselmans J. F. W. (2000) Structural chemistry of Fe, Mn, and Ni in synthetic hematites as determined by extended X-ray absorption fine structure spectroscopy. *Clays and Clay Minerals*, 48(5), 521-527.

240. Small T. D., Warren L. A. and Ferris F. G. (2001) Influence of ionic strength on strontium sorption to bacteria, Fe (III) oxide, and composite bacteria-Fe(III) oxide surfaces. *Applied Geochemistry* 16, 939-946.

241. Spadini L., Schindler P. W., Charlet L., Manceau A. and Vala Ragnarsdottir K. (2003) Hydrous ferric oxide: evaluation of Cd-HFO surface complexation models combining Cd_k EXAFS data, potentiometric titration results, and surface site structures identified from mineralogical knowledge. *J. Colloid Interface Sci.* 266, 1-18.

242. Sposito G. (1989) Surface reactions in natural aqueous colloidal systems. *Chimia* 43(6), 169-176.

243. Stahl R. S. and James, B. R. (1991a) Zinc Sorption by Iron-Oxide-Coated Sand as a Function of pH. *Soil Sci. Soc. Am. J.* 55, 1287-1290.

244. Stahl R. S. and James, B. R. (1991b) Zinc Sorption by Manganese-Oxide-Coated Sand as a Function of pH. *Soil Sci. Soc. Am. J.* 55, 1291-1294.

245. Stefanova R. Y. (2001) Removal of metal ions from water solutions by iron/cobalt oxide coated keramzite. *Journal of Environmental Science and Health, Part A: Toxidc/Hazardous Substances & Environmental Engineering.* A36(7), 1287-1302.

246. Stenkamp V. S. and Benjamin M. M. (1994) Effect of iron oxide coating on sand filtration. *Journal AWWA* 37-50.

247. Strathmann T. J. and Myneni S. C. B. (2005) Effect of Soil Fulvic Acid on Nickel(II) Sorption and Bonding at the Aqueous-Boehmite (γ-AlOOH) Interface. *Environ. Sci. Technol.* 39, 4027-4034.

248. Strawn D. G., Scheidegger A. M. and Sparks D. L. (1998) Kinetics and mechanisms of Pb(II) sorption and desorption at the aluminum oxide-water interface. *Environ. Sci. Technol.* 32(17) 2596-2601.

249. Stumm W. and Morgan J. J. (1996) *Aquatic Chemistry, Chemical Equilibria and Rates in Natural Waters.* 3rd edition, John Wiley & Sons Inc.

250. Subramaniam K., Vithayaveroj V., Yiacoumi S. and Tsouris C. (2003) Copper uptake by silica and iron oxide under high surface coverage conditions: surface charge and sorption equilibrium modeling. *J. Colloid Interface Sci.* 268, 12-22.

251. Sverjensky D. A. (2005) Prediction of surface charge on oxides in salt solutions: revisions for 1:1 (M^+L^-) electrolytes. *Geochim. Cosmochim. Acta* 69, 225-257.

252. Swallow C. K., Hume D. N. and Morel F. M. M. (1980) Sorption of copper and lead by hydrous ferric oxide. *Environ. Sci. Technol.* 14, 1326-1331.

253. Szecsody J. E., Zachara J. M., and Bruckhart P. L. (1994) Adsorption-dissolution reactions affecting the distribution and stability of CoII EDTA in iron oxide-coated sand. *Environ. Sci. Technol.* 28(9), 1706-1716.

254. Szytula A., Burewicz A., Dimitrijevic Z., Krasnicki S., Rzany H., Todorovic J., Wanic A. and Wolski W. (1968) Neutron diffraction studies of α-FeOOH. *Physica Status Solidi* 26(2), 429-434.

255. Tadanier C. J. and Eick M. J. (2002) Formulating the charge-distribution multisite surface complexation model using FITEQL. *Soil Sci. Soc. Am. J.* 66, 1505-1517.

256. Templeton A. S., Spormann A. M. and Brown G. E. Jr. (2003) Speciation of Pb (II) sorbed by Burkholderia cepacia/goethite composites. *Environ. Sci. Technol.* 37(10), 2166-2172.

257. Theis T. L., Lyer R. and Ellis S. K. (1994) Parameter estimation for trace element sorption on a new granular iron oxide. *Environmental Progress* 13(1), 72-77.

258. Thirunavukkarasu O. S., Viraraghavan T. and Subramanian K. S. (2003) Arsenic removal from drinking water using iron oxide-coated sand. *Water, Air, and Soil Pollution* 142(1-4), 95-111.

259. Tiller K. G., Gerth J. and Brümmer G. (1984) The relative affinities of Cd, Ni, and Zn for different soil clay fractions and goethite. *Geoderma* 34, 17-35.

260. Trainor T. P., Brown G. E. Jr. and Parks G. A. (2000) Adsorption and precipitation of aqueous Zn(II) on alumina powders. *J. Colloid Interface Sci.* 231, 359-372.

261. Trapnell B. M. W. (1955) *Chemisorption.* Academic Press, New York.

262. Trivedi P. and Axe L. (2000) Modeling Cd and Zn sorption to hydrous metal oxides. *Environ. Sci. Technol.* 34(11), 2215-2223.

263. Trivedi P. and Axe L. (2001a) Predicting divalent metal sorption to hydrous Al, Fe, and Mn oxides. *Environ. Sci. Technol.* 35, 1779-1784.

264. Trivedi P. and Axe L. (2001b) Ni and Zn sorption to amorphous versus crystalline iron oxides: macroscopic studies. *J. Colloid Interface Sci.* 244, 221-229.

265. Trivedi P., Axe L. and Tyson T. A. (2001a) An analysis of zinc sorption to amorphous versus crystalline iron oxides using XAS. *J. Colloid Interface Sci.* 244, 230-238.

266. Trivedi P., Axe L. and Dyer J. (2001b) Adsorption of metal ions onto goethite: single-adsorbate and competitive systems. *Colloids and Surfaces A: Physicochemical and Engineering Aspects* 191,107-121.

267. Trivedi P. (2001) Predicting thermodynamic and transport parameters for metal contaminant sorption to hydrated metal oxides in aquatic systems. Ph.D dissertation. Department of Civil and Environmental Engineering. New Jersey Institute of Technology. May 2001.

268. Trivedi P., Dyer J. A. and Sparks D. L. (2003) Lead sorption onto ferrihydrite. 1. A macroscopic and spectroscopic assessment. *Environ. Sci. Technol.* 37(5), 908-914.

269. Trivedi P., Dyer J. A., Sparks D. L. and Pandya K. (2004) Mechanistic and thermodynamic interpretations of zinc sorption onto ferrihydrite. *J. Colloid Interface Sci.* 270, 77-85.

270. Tröger L., Arvanitis D., Baberschke K., Michaelis H., Brimm U. and Zachech E. (1992) Full correction of the self-absorption in soft-fluorescence4 extended x-ray-absoroption fine structure. *Physical Review B* 46(6), 3283-3289.

271. Uygur V. and Rimmer D. L. (2000) Reactions of zinc with iron-oxide coated calcite surfaces at alkaline pH. *European Journal of Soil Science* 51(3), 511-516.

272. Vaishya R. C. and Gupta S. K. (2002) Modelling arsenic(III) adsorption from water by sulfate-modified iron oxide-coated sand (SMIOCS). *Journal of Chemical Technology and Biotechnology* 78, 73-80.

273. Vaishya R. C. and Gupta S. K. (2004) Modeling arsenic(V) removal from water by sulfate modified iron-oxide coated sand (SMIOCS). *SEPARATION SCIENCE AND TECHNOLOGY* 39(3), 645-666.

274. van Riemsdijk W. H. and Hiemstra T. (1998) From molecular structure to ion adsorption modeling. *ACS Symposium Series, 715* (Mineral-Water Interfacial Reactions), 68-87.

275. Venema P., Hiemstra T. and van Riemsdijk W. H. (1996) Comparison of different site binding models for cation sorption: description of pH dependency, salt dependency, and cation-proton exchange. *J. Colloid Interface Sci.* 181, 45-59.

276. Venema P., Hiemstra T., Weidler P. G. and van Riemsdijk W. H. (1998) Intrinsic proton affinity of reactive surface groups of metal (hydr)oxides: application to iron (hydr)oxides. *J. Colloid Interface Sci.* 198, 282-295.

277. Villalobos M., Trotz M. A. and Leckie J. O. (2001) Surface complexation modeling of carbonate effects on the adsorption of Cr(VI), Pb(II), and U(VI) on goethite. *Environ. Sci. Technol.* 35, 3849-3856.

278. Villalobos M., Trotz M. A. and Leckie J. O. (2003) Variability in goethite surface site density: evidence from proton and carbonate sorption. *J. Colloid Interface Sci.* 268, 273-287.

279. Voegelin A. and Kretzschmar R. (2005) Formation and Dissolution of Single and Mixed Zn and Ni Precipitates in Soil: Evidence from Column Experiments and Extended X-ray Absorption Fine Structure Spectroscopy. *Environ. Sci. Technol.* 39, 5311-5318.

280. Voegelin A., Vulava V. M. and Kretzschmar R. (2001) Reaction-based model describing competitive sorption and transport of Cd, Zn, and Ni, in an acidic soil. *Environ. Sci. Technol.* 35, 1651-1657.

281. Vulava V. M, Kretzschmar R., Rusch U., Grolimund D., Westall J. C. and Borkovec M. (2000) Cation competition in a natural subsurface material: modeling of sorption equilibria. *Environ. Sci. Technol.* 34(11), 2149-2155.

282. Waite T. D., Davis J. A., Payne T. E., Waychunas G. A. and Xu N. (1994) Uranium(IV) adsorption to ferrihydrite: application of a surface complexation model. *Geochim. Cosmochim. Acta* 58, 5465-5478.

283. Wallner H. and Gatterer K. (2002) Growth of pure $Ni(OH)_2$ single crystals from solution – control of the crystal size. *Z. Anorg. Allg. Chem.* 628, 2818-2820.

284. Wang H. D., White G. N., Turner F. T. and Dixon J. B. (1993) Ferrihydrite, Lepidocrocite, and goethite in coating from East Texas Vertic Soils. *Soil Sci. Soc. Am. J.* 57, 1381-1386.

285. Wang T. (1995) Copper (II) and cadmium (II) removal and recovery by iron oxide-coated granular activated carbon. Ph.D dissertation, Illinois Institute of Technology, Chicago, Illinois, Dec. 1995.

286. Waychunas G. A., Rea B. A., Feller C. C. and Davis J. A. (1993) Surface chemistry of ferrihydrite: Part 1. EXAFS studies of the geometry of coprecipitated and adsorbed arsenate. *Geochim. Cosmochim. Acta* 57, 2251-2269.

287. Waychunas G. A., Fuller C. C. and Davis J. A. (2002) Surface complexation and precipitate geometry for aqueous Zn(II) sorption on ferrihydrite I: X-ray absorption extended fine structure spectroscopy analysis. *Geochim. Cosmochim. Acta* 66, 1119-1137.

288. Waychunas G. A., Fuller C. C., Davis J. A. and Rehr J. J. (2003) Surface complexation and precipitate geometry for aqueous Zn(II) sorption on ferrihydrite: II XANES analysis and simulation. *Geochim. Cosmochim. Acta* 67, 1031-1043.

289. Wazne M, Korfiatis G. P., and Meng X. (2003) Carbonate effects on hexavalent uranium adsorption by iron oxyhydroxide. *Environ. Sci. Technol.* 37, 3619-3624.

290. Webster J. G., Swedlund P. J. and Webster K. S. (1998) Trace metal adsorption onto an acid mine drainage iron(III) oxy hydroxy sulfate. *Environ. Sci. Technol.* 32(10), 1361-1368.

291. Weesner F. J. and Bleam W. F. (1998) Binding characteristics of Pb2+ on anion-modified and pristine hydrous oxide surfaces studied by electrophoretic mobility and X-ray absorption spectroscopy. *J. Colloid Interface Sci.* 205, 380-389.

292. Weng L., Temminghoff E. J. M., Lofts S., Tipping E. and van Riemsdijk W. H. (2002) Complexation with dissolved organic matter and solubility control of heavy metals in a sandy soil. *Environ. Sci. Technol.* 36, 4804-4810.

293. Westall J. C., Zachary J. L. and Morel F. M. M. (1976) *Mineql-A computer program for the calculation of chemical equilibrium composition of aqueous systems.* Massachusetts Institute of Technology, Cambridge.

294. Westall J. and Hohl H. (1980) A comparison of electrostatic models for the oxide/solution interface. *Adv. Colloid Interface Sci.* 12, 265-294.

295. Wyckoff R. W. G. (1988) *Crystal Structure* 1, III, Interscience Publishers.

296. Yates D. E. (1975) The structure of the oxide / aqueous electrolyte interface. Ph. D dissertation, University of Melbourne, Jan. 1975.

297. Yates D. E. and Healy T. W. (1975) *J. Colloid Interface Sci.* 52, 222.

298. Yee N. and Fein J. B. (2001) Cd adsorption onto bacterial surfaces: a universal adsorption edge. *Geochim. Cosmochim. Acta* 65(13), 2037-2042.

299. Yee N. and Fein J. B. (2003) Quantifying metal adsorption onto bacteria mixtures: a test and application of the surface complexation model. *Geomicrobiology Journal* 20, 43-60.

300. Yoon R. M., Salman T. and Donnay G. (1979) *J. Colloid Interface Sci.* 70, 483.

301. Zabinsky S. I., Rehr J. J., Ankudinov A., Albers R. C. and Eller M. J. (1995) Multiple-scattering calculations of x-ray-absorption spectra. *J. Physical Review B: Condensed Matter* 52(4), 2995-3009.

302. Zachara J. M., Gassman P. L., Smith S. C. and Taylor D. (1995) Oxidation and adsorption of Co(II)EDTA2- complexes in subsurface materials with iron and manganese oxide grain coatings. *Geochim. Cosmochim. Acta* 59(21), 4449-4463.

303. Zeltner W. A. and Anderson M. A. (1988) Surface charge development at the goethite/aqueous solution interface: effects of CO2 adsorption. *Langmuir* 4, 469-474.

304. Zhong Z. Y., Prozorov T., Felner I. and Gedanken A. (1999) Sonochemical synthesis and characterization of iron oxide coated on submicrospherical alumina: a direct observation of interaction between iron oxide and alumina. *J. Phys. Chem. B* 103, 947-956.